TWO-FLUID INTERFACE MOTION IN POROUS MEDIA

A Dissertation

Presented to the Faculty

of the New Mexico Institute of

Mining and Technology

by

Donald W. Beaver

In Partial Fulfillment

of the Requirements for the Degree of

Doctor of Philosophy

in Geoscience

May, 1973

ABSTRACT

A computer technique is presented for simulating the two-dimensional motion of a two-fluid interface through a porous medium. The technique is based on expressing the stream function as the sum of two auxiliary functions, $\Psi = \Psi_1 + \Psi_2$. Under the assumptions that the fluids are incompressible and differ only in their densities, and the porous medium is nondeformable, Ψ_1 satisfies a Poisson equation throughout the Cartesian plane. The solutions for Ψ_1 and the specific discharge components are expressed as line integrals over the length of the interface. Ψ_2 satisfies a Laplace equation, as well as the physical boundary conditions.

Using this approach, the interface is treated as a line of vortices which generates the fluid motion, rather than as a moving boundary between two separate flow regimes.

The interface is approximated by a sequence of connected line segments, which facilitates the evaluation of the line integrals for Ψ_1 and the specific discharge components. Ψ_2 is determined numerically by the point successive over-relaxation method. Values of Ψ_2 and the specific discharge components at interface points are determined by an interpolation scheme. The boundary conditions are treated, in part, by introducing image

interfaces reflected in the impermeable boundaries.

A computer program has been written for simulating the rotation of an initially vertical interface. The results of the computer simulation are compared with published results of analytical and parallel-plate model studies of the same problem. The results of all three lines of investigation generally agree quite well, with the computer simulation following the analytical results more closely than it follows the model results. The computer model allows for simulation of the transient behavior of the interface, while the exact analytical solution can only be obtained at the initial instant.

The basic treatment presented here can, in principle, be extended to include radial flow, storage effects due to compressibility of the fluids and the porous medium, and the motion of a gradual transition zone between the fluids. Phenomena such as anisotropy of the porous medium and viscosity differences between the fluids cannot be treated by the vortex theory of interface motion.

ACKNOWLEDGEMENTS

The guidance of Prof. G. de Josselin de Jong, who first suggested the vortex theory as a basis for a computer model of interface motion, and who served as dissertation advisor during most of this study, is gratefully acknowledged. The assistance of Prof. Jacob Bear, who served as dissertation advisor during the early part of this study, must also be recognized. Thanks are extended to Drs. G. W. Gross, F. B. Titus, Jr., and Merle Hanson for their constant advice and encouragement while serving as members of the faculty advisory committee for this dissertation.

The final copy of this report was produced with the very able assistance of Miss Jamie Ward, who typed the manuscript; Miss Linda Jo Riggin and Mr. Dave Bollschweiler, who prepared the original drawings; and Mrs. Jackie Trujillo and Mr. Charles Treseder, who prepared the final illustrations.

Part of the research leading to this dissertation was supported by a National Science Foundation Traineeship. The computer expenses incurred during this study were funded by the New Mexico Tech Computing Center, through its account for unsponsored research.

TABLE OF CONTENTS

LIST OF FIGURES

LIST OF TABLES

LIST OF PRINCIPAL SYMBOLS

c	Half-width of the parallel-plate model, L
$\vec{g}$	Acceleration due to gravity
I	Maximum number of finite-difference mesh subdivisions in the x-direction,
J	Maximum number of finite-difference mesh subdivisions in the y-direction
k	Permeability of porous medium, L^2
N	Maximum number of interface points
p	Fluid pressure, F/L^2
$\vec{q}$	Specific discharge vector, L/T
q_x	x-component of specific discharge, L/T
q_y	y-component of specific discharge, L/T
$q_x)_1$, $q_y)_1$	Coordinates of specific discharge due to vortex distribution along the interface, L/T
$q_x)_2$, $q_y)_2$	Coordinates of specific discharge due to boundary conditions, L/T
r	Distance between two points in the x, y-plane, L
$R_{i,j}^{k}$	k^{th} residual at mesh point (i, j)
x, y	Coordinates of a general point in the plane, L
x_o, y_o	Coordinates of a point on the interface, L
x_o^n, y_o^n	Coordinates of an interface point, L
x_1^n , y_1^n	Coordinates of lower endpoint of tangent line segment, L

x_2^n, y_2^n	Coordinates of upper endpoint of tangent line segment, L
α	Inclination of the interface
γ	Specific weight of fluid, F/L^3
γ_1	Specific weight of lighter fluid, F/L^3
γ_2	Specific weight of heavier fluid, F/L^3
δ	Half-length of tangent line segment, L
ϵ	Porosity of the medium
μ	Viscosity of fluid, FT/L^2
ν	Direction normal to boundary of flow region
ρ	Density of fluid, M/L^3
σ_n	Slope of tangent line segment
τ_n	Slope of connecting line segment
Ψ	Stream function, L^2/T
Ψ_1	Stream function due to distribution of vortices along the interface, L^2/T
Ψ_2	Stream function due to boundary conditions, L^2/T
ω	Relaxation parameter of the point successive over-relaxation iterative scheme

TWO-FLUID INTERFACE MOTION IN POROUS MEDIA

CHAPTER 1. INTRODUCTION

1.1 General Considerations

The phenomenon of the simultaneous flow of two miscible fluids through a porous medium occurs in many important problems of groundwater hydrology. Examples of such problems are sea-water intrusion into a coastal fresh-water aquifer, and salt-water coning toward a well producing from a fresh-water zone underlain by salt water. Sea-water intrusion can occur wherever a coastal aquifer encounters the sea. Fresh water flows to the sea, and sea water invades the aquifer in the general form of a wedge at the base of the aquifer (Fig. 1.1). As water is produced from the aquifer, the seaward flow of fresh water is decreased, and the salt water intrudes further into the aquifer. Similarly, where a body of fresh water is underlain by salt water, and production of fresh water is taking place, the salt water will tend to rise toward the producing well in the general form of a cone (Fig. 1.2).

Salt water and fresh water are completely miscible at the microscopic scale of the pore space of the medium. Thus, at the macroscopic scale where Darcy's law holds, the contact between fresh and salt water in an aquifer will be a transition zone across which the relative salinity varies between zero and unity. For

this reason, a detailed description of flow phenomena involving fresh and saline water often must be made in terms of the theory of hydrodynamic dispersion. However, in many cases the width of the transition zone is relatively small with respect to the overall dimensions of the flow problem, so that it can be assumed, at least as a first approximation, to be a sharp interface between two fluids of different properties. According to this interface approximation, the interface can be treated as a material surface within the macroscopic flow regime, such that all fluid particles originally on the interface remain on the interface for all time (Muskat, 1937; Bear et al., 1968). This interface approximation will be adopted in the present work.

Figure 1.1. Diagrammatic sketch of an intruded sea-water wedge.

Figure 1.2. Diagrammatic sketch of salt-water coning toward a producing well.

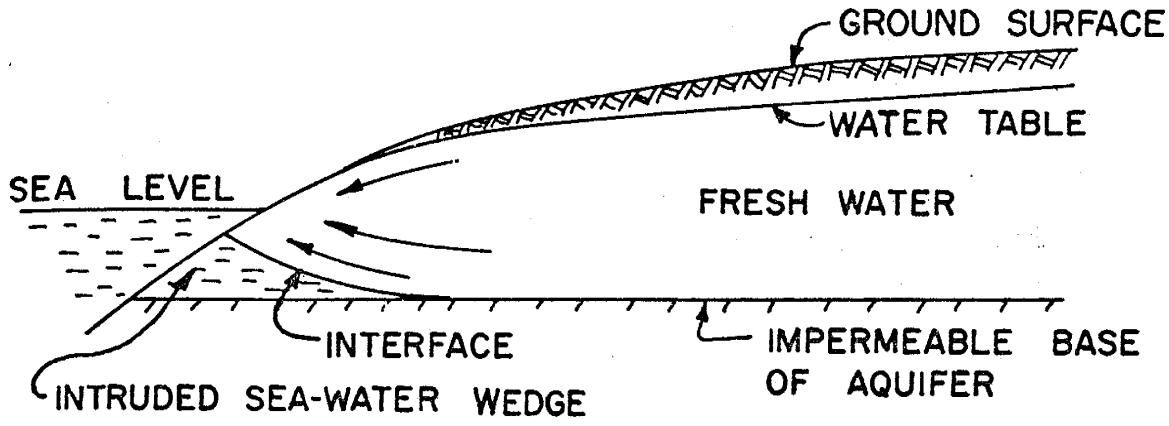
GROUND SURFACE
WATER TABLE
SEA LEVEL
FRESH WATER
INTERFACE
IMPERMEABLE BASE
OF AQUIFER
INTRUDED SEA-WATER WEDGE

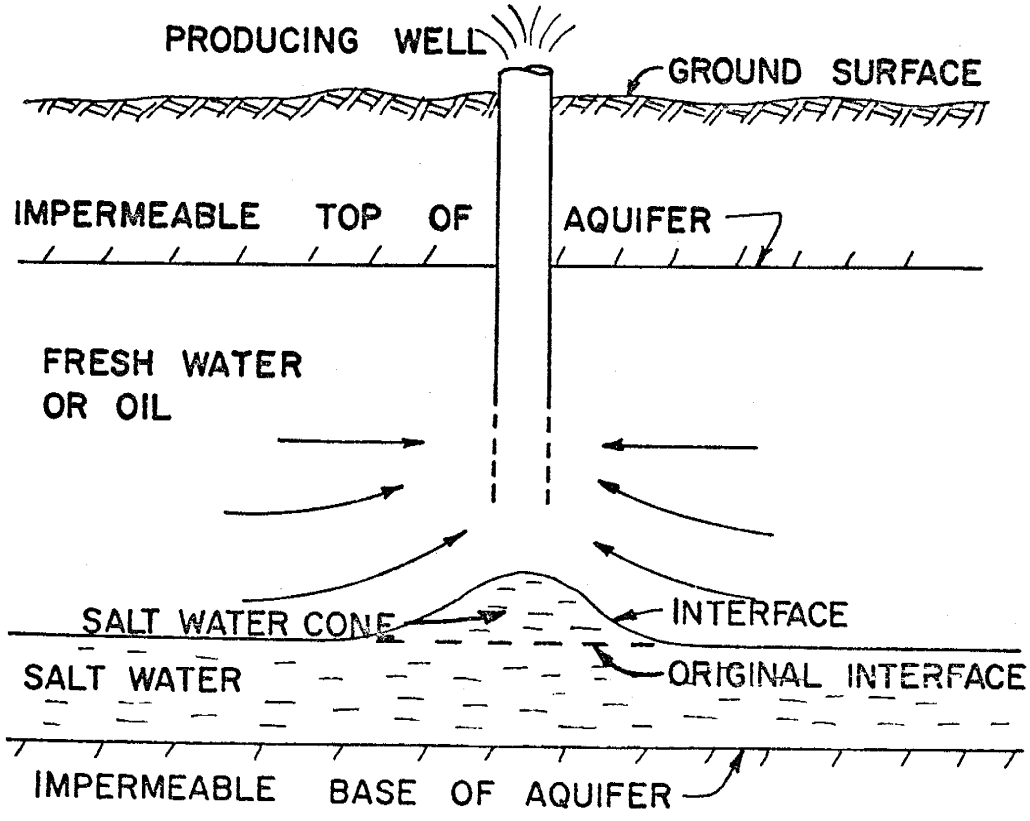
PRODUCING WELL
GROUND SURFACE
IMPERMEABLE TOP OF AQUIFER
FRESH WATER
OR OIL
SALT WATER CONE
INTERFACE
SALT WATER
ORIGINAL INTERFACE
IMPERMEABLE BASE OF AQUIFER

1.2 Previous Investigations

General Theories of Two-Fluid Interfaces in Porous Media. Probably the first attempts at the theoretical description of a two-fluid interface in a porous medium were those of Ghyben and Herzberg, who independently investigated the sea-water intrusion problem around the turn of the century. Their work resulted in the now-familiar Ghyben-Herzberg principle (Todd, 1959; De Wiest, 1965), which relates the shape of the interface to the shape of the water table or piezometric surface through a simple hydrostatic balance. This principle is limited by the fact that it assumes a static condition, with no seaward flow of fresh water.

Muskat (1937) analyzed the conditions necessary for interface motion, based on the assumption that the interface can be treated as a material surface within a continuum. He also presented some solutions to simple problems, which will be considered below.

Hubbert (1940) presented a general theory of the interface between two homogeneous fluids. His theory allows for flow within each fluid region and gives the height and slope of the interface in terms of the potentials within the two fluid regions. This theory, which treats the interface as a boundary between two regions in which the fluid properties are different, is the one which has been most widely applied to the study of interface problems.

De Josselin de Jong (1960) presented a theory of interface motion somewhat different from the basic theories of Muskat and Hubbert. Rather than considering separate potential and stream functions for each of the fluids present, he defined a single stream function and a single quasi-potential function defined throughout the entire flow field; in essence, he assumed a single hypothetical fluid with discontinuities in its properties at the interface. The flow in both the fresh and salt water regions was then generated by singularities, such as vortices, sources, and sinks, distributed along the interface. Mathematically, the flow was described by a Poisson equation for the stream function. Yih (1961) developed the same Poisson equation for the stream function that de Josselin de Jong had obtained, while Knudsen (1962) showed that the pressure function obeys a similar Poisson equation.

Lusczynski (1961) suggested several definitions of head functions applicable to multiple fluid flow. One of these functions, the "point water head", is directly related to de Josselin de Jong's quasi-potential function.

Some basic considerations of the presence of fresh-water -- salt-water interfaces in porous media are given in the standard textbooks by Todd (1959) and De Wiest (1965). More detailed examinations of interface problems, and the more general subject of multiple-fluid flow problems, are given by Muskat (1937), Scheidegger (1960), Polubarinova-Kochina (1962), Bear et al. (1968),

and Bear (1972). The books by Scheidegger (1960) and Bear (1972) are especially useful for their treatments of the flow of miscible fluids by the theory of hydrodynamic dispersion, and the flow of immiscible fluids by the multi-phase flow theory based on the concepts of saturation, capillary pressure, and relative permeability.

Steady-State Flow of Fresh Water in the Presence of a Static Salt-Water Body. Many of the interface problems that have been studied in the past have involved the steady-state flow of fresh water over a static body of salt water. This is due largely to the fact that such problems can be much more easily analyzed than problems involving motion of the interface between fresh water and salt water. Most of this work has been done on the problems of salt-water coning and sea-water intrusion mentioned in Section 1.1.

A. The Salt-Water Coning Problem

Muskat (1937) presented a graphical method for determining the shape of a static salt-water cone beneath a steadily-producing oil well. His coning model is based on the assumption that the presence of the cone does not affect the pressure distribution within the oil zone, and thus must be limited to cases of rather small cone rises.

Meyer and Garder (1954) applied Hubbert's theory to the coning problem, assuming that the fluid within the cone was static. They gave maximum rates of oil production for no gas or

water production, but did not give shapes of the gas or salt-water cones.

Kidder (1956a) presented a hodograph solution to the related problem of the fingering of an oil-water interface toward a well in an inclined reservoir. The hodograph is a specialized technique of conformal mapping which is ideally suited to the study of two-dimensional problems involving stationary interfaces.

Bear and Dagan (1962, 1963, 1964a) carried out a very extensive examination of many aspects of the sea-water intrusion and coning problems. They presented many analytical and model studies of the basic intrusion problem, interface motion, and upconing of the interface toward collector wells. Some of their results were also given in Bear and Dagan (1964b), where they considered the solutions to some intrusion and coning problems obtained by the hodograph method.

De Josselin de Jong (1965) extended some of the hodograph solutions of Bear and Dagan (1964b). He analyzed the problem of sea-water intrusion with a drain withdrawing water from the aquifer, again with steady flow of the fresh water over a static salt-water wedge. His work included a consideration of mapping a double-sheeted hodograph by means of the Schwarz-Christoffel transformation.

Wang (1965) presented an approximate theory of salt-water

coning toward a well partially penetrating an unconfined aquifer. Her theory assumed static salt water, and applied the Ghyben-Herzberg principle. The results of her study gave the maximum rate of fresh-water production which can be maintained with no salt water entering the well, with the fresh water assumed to be flowing under steady-state conditions.

Bennett et al. (1968) reported on some electric-analog model studies of salt-water coning, based on the graphical procedure presented by Muskat (1937). Their work was limited to static salt water and steady flow of fresh water, but they found that by using electric analog models, it was not necessary to employ Muskat's assumption that the fresh-water potential was unaffected by the presence of the salt-water cone.

Strack (1972) presented a very complete examination of the application of conformal mapping techniques to the solution of interface problems. Of special interest is his extension of the Schwarz-Christoffel integral to allow the treatment of multi-sheeted mappings. This allows conformal mapping techniques to be applied to problems of interface upconing toward multiple points of fresh-water discharge.

B. The Sea-Water Intrusion Problem

Todd (1953) presented abstracts of a great many papers dealing with the problem of sea-water intrusion, published through

1952. Most of the papers abstracted cover field observations, laboratory studies, and simple analytical solutions (mainly based on the Ghyben-Herzberg Principle).

Henry (1959) applied the hodograph method to the solution of the sea-water intrusion problem, assuming steady-state flow of fresh water and static salt water.

Glover (1959) examined the steady-state flow of fresh water over a static intruded salt-water wedge. He used the theory of complex variables to study the fresh-water flow, and showed that there must be a gap between the interface and the water-table outcrop at the beach, in contrast to the Ghyben-Herzberg result that the interface and the water table meet in a knife-edge at the beach.

Cooper (1959) recognized the possibility that the salt water within an intruded sea-water wedge could be in motion. He hypothesized that the presence of a transition zone at the interface could lead to a cyclic flow of salt water from the sea into the transition zone and then back to the sea, and that this flow would tend to lessen the extent of sea-water intrusion into the aquifer. Kohout (1960) presented field observations from the Biscayne aquifer in Florida supporting Cooper's hypothesis, and showed that the interface had an inflection point and was concave downward near its toe (Fig. 1.3).

Figure 1.3. Observed shape of intruded sea-water wedge.

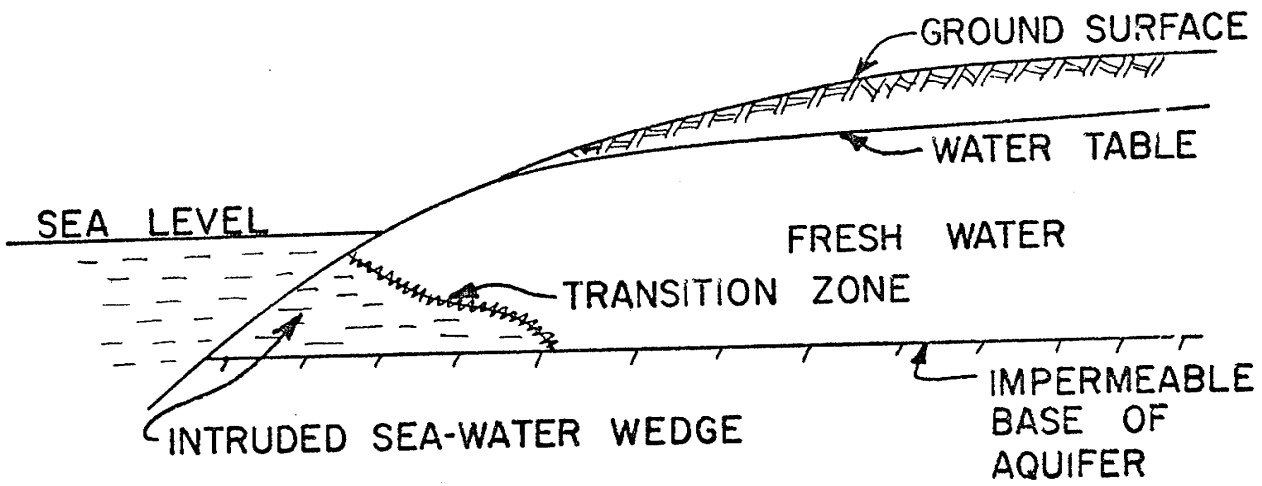
GROUND SURFACE
WATER TABLE
SEA LEVEL
FRESH WATER
TRANSITION ZONE
IMPERMEABLE
BASE OF
AQUIFER
INTRUDED SEA-WATER WEDGE

As mentioned above, Bear and Dagan (1962, 1963, 1964a) studied many aspects of the intrusion problem, including upconing of the intruded sea-water wedge toward collector wells. Bear and Dagan (1964b) also analyzed some intrusion problems by the hodograph method, and their work was extended by de Josselin de Jong (1965).

Columbus (1965) carried out a viscous model study of steady-state sea-water intrusion. His analysis of the results was based on the Ghyben-Herzberg principle and the Dupuit assumptions that the flow is purely horizontal and uniform across a vertical section. He concluded that the Ghyben-Herzberg principle gives a fairly good prediction of the shape and position of the interface, although he did notice some circulation within the salt-water zone.

Kashef (1968) presented a graphical method for determining the steady interface in the sea-water intrusion problem, as well as the influence of fresh-water pumpage on the interface. His method was based on the work of Kashef and McDonald (1968), who analyzed free-surface shapes under steady flow conditions by considering the hydraulic forces acting within the system. Their results compared favorably with those of other approaches to steady free-surface problems, such as the hodograph method or the numerical solution to Laplace's equation by relaxation, but they found their method to be faster and easier to use than other approaches. Their method also eliminated the need to rely on

the Dupuit assumptions.

The conformal mapping techniques developed by Strack (1972) can also be applied to certain intrusion problems. His extension of the Schwarz-Christoffel integral is especially useful in analyzing problems in which the shape of the intruded interface is influenced by pumpage from the fresh-water zone.

Motion of the Interface Between Fresh Water and Salt Water. Relatively little work has been done on problems involving motion of two-fluid interfaces in porous media, largely because of the mathematical difficulties involved in treating such problems. In most of the studies that have been carried out, separate potential functions have been defined in the fresh water and salt water regions, and the interface has been treated as a moving boundary between the two regions. In such a formulation, the boundary conditions at the interface must be expressed as rather complex nonlinear functions of the two potentials (Bear et al., 1968; Bear, 1972), thus limiting the mathematical tools available for treating the problem. Nevertheless, some work has been done on moving-interface problems.

Muskat (1937) analyzed the conditions necessary for interface motion, based on the assumption that the interface is a material surface within a continuum. He also presented analytical solutions to some simple problems, such as the horizontal motion of a vertical oil-water interface in linear and radial geometries.

Kidder (1956b) presented an approximate method for determining general interface motion, similar to the approach used in the linear theory of water waves. However, his method is only valid if the initial interface has low slope and small curvature.

As mentioned above, de Josselin de Jong (1960), Yih (1961), and Knudsen (1962) independently developed the equations necessary to describe interface motion in porous media. Their work was based on postulating a single hypothetical fluid with discontinuities in its properties at the interface. By this theory, the interface no longer had to be treated as a moving boundary. De Josselin de Jong (1960) applied this theory to the problem of an initially vertical interface rotating to a horizontal position under the influence of gravity, and obtained good agreement between theoretical predictions and the results of a parallel-plate model experiment.

Bear and Dagan (1964c) presented an approximate solution for the motion of the interface in an intrusion problem. Their solution was based on applying the Dupuit assumptions and assuming a distribution of discharge along the interface.

Dagan and Bear (1968) obtained an approximate solution to the problem of interface upconing by applying the method of small perturbations, in which the solution is presented as a power series in some appropriate small parameter. Their method has the advantage that it takes into account the flow of the salt water as well as

the fresh water, but, by comparison with sandbox model studies, they found that the theory was accurate only for small interface rises.

Hantush (1968) obtained an approximate solution for the motion of the interface between fresh and salt water in an unconfined aquifer. His method was based on averaging the hydraulic head over a vertical line between the water table and the interface. He gave a detailed analysis of the growth of a fresh-water lens under vertical percolation and well injection, and he also briefly considered the application of his theory to the problems of sea-water intrusion, decay of a fresh-water lens, and pumpage from a fresh-water lens.

Very recently, as digital computers have become quite widely used in analyzing problems of groundwater hydrology, numerical methods have been applied to problems of interface motion. Shamir and Dagan (1970, 1971) presented a numerical solution for the motion of the interface in sea-water intrusion problems. Their technique was based on applying the Dupuit assumptions, so that they considered the essentially one-dimensional problem of determining the interface height as a function of horizontal distance. They employed fairly standard finite-difference techniques, although they obtained a more precise solution by redefining the grid spacing for each time

step. Kleinecke (1971) described a computer model for simulating problems of intrusion and coning on a regional basis, in which the interface was assumed to be a transition zone of parallel salinity contours. Each salinity contour was treated as a Ghyben-Herzberg interface, with their positions adjusted to account for dispersion. He concluded that the technique appeared to be feasible, but was not fast enough to be used for operational simulation for aquifer management. Prickett and Lonnquist (1972) described a similar computer model for simulating the problem of salt-water coning in the vicinity of a single pumping well, in which the salinity contours were treated as grid lines in a Lagrangian mesh. They reported difficulties in treating the flow near the well face because of distortions of the mesh.

1.3 Purpose and Scope

The present work is a report on the development of a computer code for the analysis of two-fluid interface motion in porous media. The techniques used in this code are based on the theory of interface motion developed by de Josselin de Jong (1959, 1960). This theory was adopted because it does not require the interface to be treated as a moving boundary. In most previous studies of two-fluid interface motion, separate potential functions were defined for each of the two fluids, with each function satisfying a Laplace equation within the region occupied by the corresponding fluid. The interface thus had to be treated as a moving boundary between the two flow regions, with the boundary conditions being rather complex nonlinear relations between the two potential functions (Bear et al., 1968; Bear, 1972). The nonlinearity of these boundary conditions made any treatment, whether analytical or numerical, quite difficult. On the other hand, the postulation of a single hypothetical fluid with discontinuities in its properties at the interface allows the flow of both fluids to be described by a single Poisson equation. After the Poisson equation has been solved, the motion of the interface is given by the local average velocity. This is a much simpler procedure than the simultaneous solution of two Laplace equations coupled by nonlinear boundary equations.

This computer code is designed to treat two-dimensional interface motion without relying on some of the simplifying assumptions which have been made in the past. Thus, the code is applicable to problems involving a moving interface between two fluids, each of which is allowed to flow. Furthermore, vertical components of flow are allowed, so that the Dupuit assumptions need not to be made. Nevertheless, a number of assumptions are necessary regarding the nature of the fluids and the porous medium involved. Throughout most of this paper, the following assumptions will be made:

1) The porous medium is homogeneous, isotropic, and non-deformable. This last assumption means that the storage capacity of the medium is neglected.

2) Two homogeneous fluids are present in the porous medium, and they are separated on the macroscopic scale by a sharp interface, which is treated as a material surface. The transition zone at the interface is neglected.

3) The fluids have the same viscosity. Thus the results of this study can only be applied to problems involving fresh water and sea water, and certain laboratory models, where the differences in viscosity of the fluids can usually be neglected.

4) The motion of the fluids through the porous medium obeys Darcy's law.

Some of these assumptions, such as assuming a homogeneous medium, neglecting the viscosity difference of the fluids, and neglecting the transition zone at the interface, are not inherent in the theory of de Josselin de Jong, and can be relaxed somewhat. This subject will be considered in greater detail in a later chapter.

Most of the work carried out here involves the study of a specific problem of limited practical interest, which will be called the basic check problem. This problem is the rotation of an initially vertical interface between two fluids of different densities but equal viscosity. This has been chosen as the basic check problem because the analytical solution exists for the initial distribution of specific discharge in the system. This problem has also been studied by means of a parallel plate model, and an approximate analytical solution has been determined for the rate of rotation of the interface. The results of the computer model can be checked against the results of this previous work, and the degree of mass conservation maintained by the code can also be easily determined for this simple problem. The application of the model to problems of more practical interest will be considered in a later chapter.

REFERENCES

Bear, J., Dynamics of Fluids in Porous Media, 764 pp., American Elsevier, New York, 1972.

Bear, J., and G. Dagan, The steady interface between two immiscible fluids in two-dimensional flow, The Transition Zone Between Fresh and Salt Waters in Coastal Aquifers, Progress Report No. 1, P. N. 3/62, 124 pp., Hydraulic Laboratory, Technion - Israel Institute of Technology, Haifa, 1962.

Bear, J., and G. Dagan, A. Steady flow to an array of wells above the interface (immiscible fluids) B. Approximate solution for a moving interface, The Transition Zone Between Fresh and Salt Waters in Coastal Aquifers, Progress Report No. 2, P. N. 1/63, 46 pp., Hydraulic Laboratory, Technion - Israel Institute of Technology, Haifa, 1963.

Bear, J., and G. Dagan, The unsteady interface below a coastal collector, The Transition Zone Between Fresh and Salt Waters in Coastal Aquifers, Progress Report No. 3, P. N. 3/64, 122 pp., Hydraulic Laboratory, Technion - Israel Institute of Technology, Haifa, 1964a.

Bear, J., and G. Dagan, Some exact solutions of interface problems by means of the hodograph method, Journal of Geophysical Research, 69, 1563, 1964b.

Bear, J., and G. Dagan, Moving interface in coastal aquifers, ASCE Proceedings, 90, HY4, 193, 1964c.

Bear, J., D. Zaslavsky, and S. Irmay, Physical Principles of Water Percolation and Seepage, 465 pp., UNESCO, Paris, 1968.

Bennett, G. D., M. J. Mundorff, and S. Amjad Hussain, Electri.-analog studies of brine coning beneath fresh-water wells in the Punjab Region, West Pakistan, USGS Water-Supply Paper 1608-J, 31 pp., 1968.

Columbus, N., Viscous model study of sea water intrusion in water table aquifers, Water Resources Research, 1, 313, 1965.

Cooper, H. H., Jr., A hypothesis concerning the dynamic balance of fresh water and salt water in a coastal aquifer, Journal of Geophysical Research, 64, 461, 1959.

Dagan, G., and J. Bear, Solving the problem of local interface upconing in a coastal aquifer by the method of small perturbations, Journal of Hydraulic Research, 6, 15, 1968.

de Josselin de Jong, G., Vortex theory for multiple phase flow through porous media, Water Resources Center Contribution 23, 80 pp., Hydraulic Laboratory, University of California, Berkeley, 1959.

de Josselin de Jong, G., Singularity distributions for the analysis of multiple-fluid flow through porous media, Journal of Geophysical Research, 65, 3739, 1960.

de Josselin de Jong, G., A many-valued hodograph in an interface problem, Water Resources Research, 1, 543, 1965.

De Wiest, R. J. M., Geohydrology, 366 pp., John Wiley, New York, 1965.

Glover, R. E., The pattern of fresh-water flow in a coastal aquifer, Journal of Geophysical Research, 64, 457, 1959.

Hantush, M. S., Unsteady movement of fresh water in thick unconfined saline aquifers, IASH Bulletin, 13, 40, 1968.

Henry, H. R., Salt intrusion into fresh-water aquifers, Journal of Geophysical Research, 64, 1911, 1959.

Hubbert, M. K., The theory of ground-water motion, Journal of Geology, 48, 785, 1940.

Kashef, A. I., Salt water intrusion in coastal well fields, Proceedings of the Symposium on Ground-Water Hydrology, San Francisco, Series No. 4, 235-258, American Water Resources Association, Urbana, Illinois, 1968.

Kidder, R. E., Flow of immiscible fluids in porous media: exact solution of a free boundary problem, Journal of Applied Physics, 27, 867, 1956a.

Kidder, R. E., Motion of the interface between two immiscible liquids of unequal density in a porous solid, Journal of Applied Physics, 27, 1546, 1956b.

Kleinecke, David, Mathematical modeling of fresh-water aquifers having salt-water bottoms, 71 TMP-47, 68 pp., General Electric Company -- Tempo, Santa Barbara, California, 1971.

Knudsen, W. C., Equations of fluid flow through porous media -- incompressible fluid of varying density, Journal of Geophysical Research, 67, 733-737, 1962.

Kohout, F. A., Cyclic flow of salt water in the Biscayne aquifer of southeastern Florida, Journal of Geophysical Research, 65, 2133, 1960.

Lusczynski, Norbert J., Head and flow of ground water of variable density, Journal of Geophysical Research, 66, 4247 - 4256, 1961.

Meyer, H. I., and A. O. Garder, Mechanics of two immiscible fluids in porous media, Journal of Applied Physics, 25, 1400, 1954.

Muskat, M., The Flow of Homogeneous Fluids Through Porous Media, 763 pp., McGraw-Hill, New York, 1937 (reprinted by J. W. Edwards, Ann Arbor, Michigan, 1946).

Polubarinova-Kochina, P. Ya., Theory of Ground Water Movement, translated from Russian by R. J. M. De Wiest, 613 pp., Princeton University Press, Princeton, New Jersey, 1962.

Prickett, T. A., and C. G. Lonnquist, Digital model for dynamic ground water quality predictions, Illinois State Water Survey unpublished report, 1972.

Scheidegger, A. E., The Physics of Flow Through Porous Media, second edition, 313 pp., University of Toronto Press, Toronto, 1960.

Shamir, U., and G. Dagan, Motion of the sea-water interface in a coastal aquifer: a numerical solution, R. N. 6/70, 54 pp., Water Resources Laboratories, Hydrodynamics and Hydraulic Engineering Laboratory, Technion - Israel Institute of Technology, Haifa, 1970.

Shamir, U., and G. Dagan, Motion of the sea-water interface in coastal aquifers: a numerical solution, Water Resources Research, 7, 644, 1971.

Strack, O. D. L., Some cases of interface flow towards drains, Journal of Engineering Mathematics, 6, 175-191, 1972.

Todd, D. K., An abstract of literature pertaining to sea-water intrusion and its control, Technical Bulletin No. 10, I. E. R., Series 37, Sanitary Engineering Research Project, 72 pp., University of California, Berkeley, 1953.

Todd, D. K., Ground Water Hydrology, 366 pp., John Wiley, New York, 1965.

Wang, Flora Chu, Approximate theory for skimming well formulation in the Indus Plain of West Pakistan, Journal of Geophysical Research, 70, 5055, 1965.

Yih, C. S., Flow of a nonhomogeneous fluid in a porous medium, Journal of Fluid Mechanics, 10, 133-141, 1961.

CHAPTER 2. VORTEX THEORY OF INTERFACE MOTION

2.1 Introduction

De Josselin de Jong (1959, 1960, 1969) has presented a very complete theory of the motion of the interface between miscible fluids through porous media. His theory is based on representing the interface by a region of singularities, such as vortices, sources, and sinks, which generate the flow in the two different fluid regions, and hence the motion of the interface itself.

The general theory of de Josselin de Jong takes into consideration variations in the density and viscosity of the fluids present, as well as variations in the permeability of the medium. The general theory can also be applied to a transition zone of finite width between the two fluids, as well as to a sharp interface. For the development of the basic computer code for interface motion, a simplified form of the theory will be used. Thus, we will assume that the two fluids have different densities, but the same viscosity. We will also assume that the porous medium is homogeneous and isotropic, and that a sharp interface is maintained between the two fluids. We will also restrict our attention to two-dimensional flows. Modifications of the code which will be necessary to apply the more general theory will be discussed in

a later chapter. In the present chapter, we will briefly consider the basic theory as restricted by the assumptions stated above.

2.2 Fundamental Theory

We begin by assuming that the specific discharge $\vec{q} = \hat{\imath} q_x + \hat{\jmath} q_y$ is given by Darcy's law. Under the assumptions that the viscosity μ of the fluid and the permeability k of the porous medium are constant, while the density ρ of the fluid is variable, Darcy's law is written in two dimensions as

$$(\mu/k)\, q_x = -\partial p/\partial x \qquad (2.2.1a)$$

$$(\mu/k)\, q_y = -\partial p/\partial y - \gamma, \qquad (2.2.1b)$$

where p is the fluid pressure, $\gamma = \rho g$ is the specific weight of the fluid, and the force of gravity acts in the negative y direction. In addition to Darcy's law, the flow must satisfy the continuity equation:

$$\nabla \cdot \vec{q} = \partial q_x/\partial x + \partial q_y/\partial y = 0. \qquad (2.2.2)$$

Equation (2.2.2) results from assuming that the fluid is incompressible and that the porous medium is nondeformable.

In order to study the motion of a two-fluid interface, we must examine the specific discharge vector $\vec{q}$. This is done most conveniently by introducing the stream function Ψ, which is defined by

$$\partial \Psi/\partial x = q_y \qquad (2.2.3a)$$

$$\partial \Psi / \partial y = - q_x \qquad (2.2.3b)$$

Substituting equations (2.2.3) into equation (2.2.2), we get

$$\nabla \cdot \vec{q} = - \frac{\partial^2 \Psi}{\partial x \, \partial y} + \frac{\partial^2 \Psi}{\partial y \, \partial x} = 0 \, .$$

By Young's Theorem, this implies that Ψ is a continuous, single-valued function throughout the xy-plane. Substituting equation (2.2.1a) into equation (2.2.3b), and differentiating with respect to y, we get

$$\frac{\mu}{k} \left(\frac{\partial^2 \Psi}{\partial y^2} \right) = \frac{\partial^2 p}{\partial y \, \partial x} \qquad (2.2.4a)$$

Similarly, from equations (2.2.1b) and (2.2.3a), we get (differentiating with respect to x),

$$\frac{\mu}{k} \left(\frac{\partial^2 \Psi}{\partial x^2} \right) = - \frac{\partial^2 p}{\partial x \, \partial y} - \frac{\partial \gamma}{\partial x} \, . \qquad (2.2.4b)$$

p is a physical scalar quantity, and the fluids are miscible so there is no capillary pressure. Thus p must be single-valued and continuous, so

$$\frac{\partial^2 p}{\partial y \, \partial x} - \frac{\partial^2 p}{\partial x \, \partial y} = 0 .$$

Then, adding equations (2.2.4a) and (2.2.4b), we get

$$\nabla^2 \Psi = - (k/\mu)(\partial \gamma / \partial x) \, . \qquad (2.2.5)$$

Equation (2.2.5) is a Poisson equation, which, from potential theory, has the integral solution

$$\Psi = -(k/\mu)\int\int_A (1/2\pi) \ln r \, (\partial\gamma/\partial x) \, dA \qquad (2.2.6)$$

in two dimensions. The integration in equation (2.2.6) actually extends over the entire plane, but only has a contribution from the region A in which $\partial\gamma/\partial x$ does not vanish. r is the distance between the point at which Ψ is to be evaluated and a point in the region A.

We should note here that equation (2.2.6) defines Ψ at every point in the xy-plane, both inside and outside the region A. In general, however, a problem of physical interest will be defined within a bounded region containing A, and the value of Ψ given by equation (2.2.6) may not satisfy the appropriate conditions on the boundary of that region. Thus Ψ must be modified to account for the boundary conditions, as will be discussed in Section 2.4.

In addition to giving the value of Ψ at all points in the xy-plane, equation (2.2.6) also allows a physical interpretation of the region A in which $\partial\gamma/\partial x$ does not vaniah. The stream function due to a potential point vortex of strength Γ located

at the origin of a two-dimensional Cartesian coordinate system is $\Psi = (\Gamma/2\pi) \ln r$, where $r^2 = x^2 + y^2$. The vortex motion is counter-clockwise for $\Gamma > 0$. Similarly, for potential vortices of strength Γ located within a differential area dA, the stream function is

$$d\Psi = (\Gamma \, dA / 2\pi) \ln r \text{ , or}$$

$$\Psi = (1/2\pi) \int_A \int \Gamma \ln r \quad dA \; ; \qquad (2.2.7)$$

Ψ satisfies

$$\nabla^2 \Psi = \Gamma \quad \text{within A} \qquad (2.2.8a)$$

$$\nabla^2 \Psi = 0 \quad \text{outside A} \qquad (2.2.8b)$$

Thus, from equation (2.2.6), we see that the region A can be interpreted as a region containing potential vortices of strength $-(k/\mu)(\partial\gamma/\partial x)$. The direction of the vortex at any point in A is determined by the sign of $\partial\gamma/\partial x$ at that point. This view of equation (2.2.6) will prove to be quite useful in interpreting some of the results of later chapters. For the case in which A reduces to a sharp interface between the fluids, the vortices distributed along the interface produce a shear discontinuity in the specific discharge at the inferface. This is discussed in more detail in Section 3.3 and Appendix D.

2.3 Solution for an Abrupt Interface

As seen in the preceding section, the stream function Ψ has an integral representation, given by equation (2.2.6), whenever the flow region has an area in which the horizontal density gradient $\partial\gamma/\partial x$ does not vanish. In general, this area could consist of a transition zone between two miscible fluids of different densities. However, this area could also be an abrupt interface between two such fluids; the stream function for this case can be determined by applying equation (2.2.6), and considering the behavior of $\partial\gamma/\partial x$ at an abrupt interface.

Consider a point $P(x_o, y_o)$ on an abrupt interface between two fluids of different densities (Fig. 2.3.1). Let the inclination of the interface at P be α. Furthermore, let us introduce at P an orthogonal coordinate system (s, n), with the s-axis tangent to the interface and the n-axis normal to it. The transformation equations relating the (x, y) and (s, n) coordinate systems are

$$s = (x - x_o)\cos\alpha + (y - y_o)\sin\alpha$$

$$n = (y - y_o)\cos\alpha - (x - x_o)\sin\alpha$$

Then

$$\frac{\partial\gamma}{\partial x} = \frac{\partial\gamma}{\partial s}\frac{\partial s}{\partial x} + \frac{\partial\gamma}{\partial n}\frac{\partial n}{\partial x} = -\sin\alpha\,\frac{\partial\gamma}{\partial n},$$

since $\partial\gamma/\partial s = 0$. Now consider the interface to be the degeneration of a transition zone between two fluids of specific weights $\gamma_2 > \gamma_1$.

Let the thickness of the zone be dn. As $dn \to 0$, $\partial\gamma/\partial n \to \infty$ in such a way that

$$\lim_{dn\to 0} \frac{\partial \gamma}{\partial n}\, dn = -(\gamma_2 - \gamma_1).$$

That is, for a very narrow transition zone we can assume that the density gradient across the zone is linear, so that

$$\frac{\partial \gamma}{\partial n}\, dn = -\frac{\gamma_2 - \gamma_1}{dn}\, dn = -(\gamma_2 - \gamma_1),$$

which ratio also holds in the limit as $dn \to 0$. Then

$$\begin{aligned} d\Psi &= -(k/2\pi\mu) \ln r\, (\partial\gamma/\partial x)\, dA \\ &= \lim_{dn\to 0} \left[(-k/2\pi\mu) \ln r \left(-\frac{\partial \gamma}{\partial n} \sin\alpha\right) dn\, ds\right] \\ &= (k/2\pi\mu) \ln r \cdot \sin\alpha\, ds \left[\lim_{dn\to 0} (\partial\gamma/\partial n)\, dn\right] \\ &= -(k/2\pi\mu)(\gamma_2 - \gamma_1) \sin\alpha \ln r\, ds \end{aligned}$$

Hence

$$\Psi = -\frac{k(\gamma_2 - \gamma_1)}{2\pi\mu} \int_S \sin\alpha \cdot \ln r \cdot ds \qquad (2.3.1)$$

The integration extends over the length S of the interface. Finally, since $\sin\alpha = dy_o/ds$ (Fig. 2.3.2), equation (2.3.1) can be written

$$\Psi(x,y) = -\frac{k(\gamma_2 - \gamma_1)}{2\pi\mu} \int_{y_{o_1}}^{y_{o_2}} \ln r\, dy_o, \qquad (2.3.2)$$

where

$$r^2 = (x - x_o)^2 + (y - y_o)^2$$

and y_{o1} and y_{o2} denote the endpoints of the interface.

Figure 2.3.1. Definition sketch for the (s, n) coordinate system.

Figure 2.3.2. Definition sketch for r and dy_o.

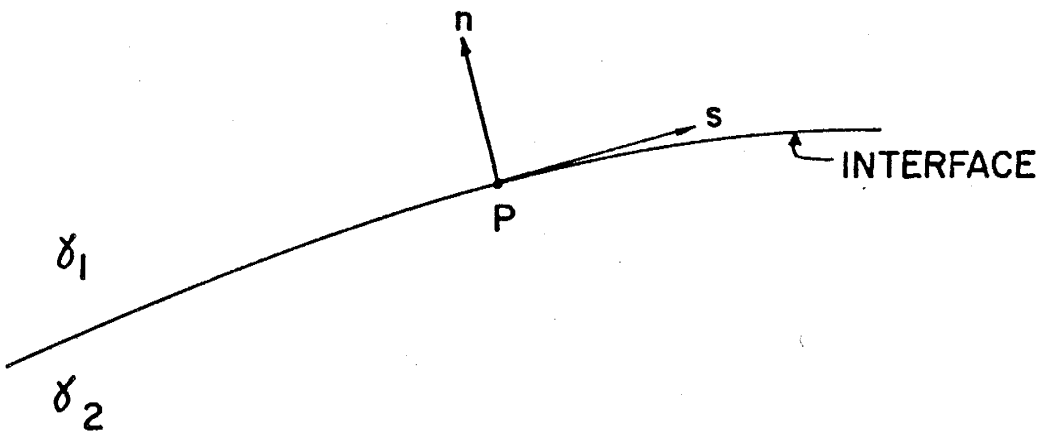
n
s
INTERFACE
P
γ_1
γ_2

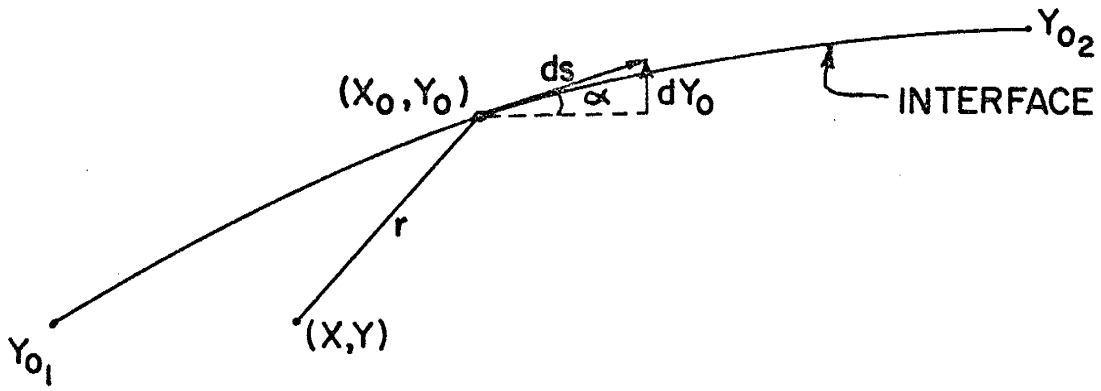
Y_{O_2}
ds
(X_O, Y_O)
α
dY_O
INTERFACE
r
Y_{O_1}
(X,Y)

Equations (2.3.1) and (2.3.2) are line integrals which must be integrated over the length of the interface. Equation (2.3.1) shows that the interface can be interpreted as a line of potential vortices of strength $-k(\gamma_2-\gamma_1)\sin\alpha/\mu$. The direction of motion of the vortex located at a point P of the interface depends upon the sign of $\sin\alpha$ at that point. For $\gamma_2>\gamma_1$, and $-\pi/2 < \alpha < \pi/2$, the vortex motion is clockwise for $\alpha > 0$ and counter-clockwise for $\alpha < 0$. Equation (2.3.2), which is equivalent to equation (2.3.1), is more convenient for numerical calculation.

2.4 Solution of a Boundary-Value Problem

As noted in Section 2.2, the values of Ψ given by equation (2.3.1) will not in general satisfy the appropriate conditions at the boundaries of a physical problem. Thus, we can let $\Psi = \Psi_1 + \Psi_2$, where Ψ_2 satisfies Laplace's equation within the region of physical interest. Then

$$\begin{aligned} \nabla^2 \Psi &= \nabla^2 (\Psi_1 + \Psi_2) \\ &= \nabla^2 \Psi_1 + \nabla^2 \Psi_2 \\ &= \nabla^2 \Psi_1 + 0 = -(k/\mu)(\partial\gamma/\partial x). \end{aligned}$$

Hence Ψ_1 is given by equation (2.3.1) within the region of physical interest (and on its boundaries), and represents the contribution to Ψ due to the distribution of vortices along the interface curve S. Boundary conditions on Ψ_2 must be chosen so that the function $\Psi = \Psi_1 + \Psi_2$ satisfies the appropriate conditions at the boundaries of the flow region. Ψ_2 thus represents the contribution to Ψ due to the boundary conditions.

In general, then, we have the following problem: Ψ obeys the equation

$$\nabla^2 \Psi = -(k/\mu)(\partial\gamma/\partial x)$$

in a region R of the xy-plane, and satisfies the conditions

$$A\Psi + B(\partial\Psi/\partial\nu) = C$$

on the boundary L of R, where ν is the direction normal to L.

Let $\Psi = \Psi_1 + \Psi_2$ where

$$\nabla^2 \Psi_1 = -(k/\mu)(\partial\gamma/\partial x) \qquad \text{in the xy-plane,}$$

and $$\nabla^2 \Psi_2 = 0 \qquad \text{in R.}$$

From equation (2.3.1), we can determine Ψ_1 and $\partial\Psi_1/\partial\nu$ on L, as well as Ψ_1 in R. Then the boundary conditions on Ψ_2 are given by

$$A\Psi_2 + B(\partial\Psi_2/\partial\nu) = C - A\Psi_1 - B(\partial\Psi_1/\partial\nu) \qquad (2.4.1)$$

on L. Finally, Ψ_2 can be determined throughout R by some appropriate technique. For some problems, Ψ_2 can be determined analytically. In the present work, with a view toward making the computer code as general as possible, Ψ_2 will be determined by a standard numerical technique, such as successive over-relaxation. Ψ is then given throughout R by

$$\Psi = \Psi_1 + \Psi_2 \qquad (2.4.2)$$

2.5 Interface Motion

Equation (2.3.1), plus the solution for Ψ_2 described above, gives the stream function Ψ throughout the flow region. From this, it is possible to determine the actual interface motion. The interface will move with the local average velocity $\vec{q}/\epsilon$, where $\vec{q}$ is the specific discharge, and ϵ is the (constant) porosity of the medium. Given the stream function Ψ, we can determine the specific discharge at any point in the medium by applying equations (2.2.3). The specific discharge at a point on the interface can also be determined by means of equations (2.2.3), or by means of the following equations:

$$\partial\Psi/\partial n = -q_s \qquad (2.5.1a)$$

$$\partial\Psi/\partial s = q_n \qquad (2.5.1b)$$

where n denotes the direction normal to the interface and s denotes the direction tangential to the interface. The choice between equations (2.2.3) and equations (2.5.1) will depend upon the manner in which the interface is represented, and the algorithms used to evaluate equation (2.3.2) and the derivatives of Ψ.

The specific discharge at a point on the interface has three distinct components:

(a) a component q_n normal to the interface, which must be continuous in order to preserve the continuity of the fluid in the fluid region; if this component were discontinuous, there could

be gaps in the fluid at the interface;

(b) a shear discontinuity tangent to the interface, produced by the vortex at that point on the interface; and

(c) a continuous component tangent to the interface, produced by the vortices at all other points of the interface.

We will see in a later chapter that the shear discontinuity can be isolated in the expressions we will obtain for the specific discharge at the interface, and the interface motion can then be given by the other two components, which give a continuous but not necessarily normal velocity at the interface.

REFERENCES

de Josselin de Jong, G., Vortex theory for multiple phase flow through porous media, Water Resources Center Contribution 23, 80 pp., Hydraulic Laboratory, University of California, Berkeley, 1959.

de Josselin de Jong, G., Singularity distributions for the analysis of multiple-fluid flow through porous media, Journal of Geophysical Research, 65, 3739, 1960.

de Josselin de Jong, G., Generating functions in the theory of flow through porous media, in Flow Through Porous Media, edited by R. J. M. De Wiest, p. 377, Academic Press, New York, 1969.

CHAPTER 3. DISCUSSION OF THE COMPUTER MODEL OF INTERFACE MOTION

3.1 Introduction

The computer model which we will consider in this chapter follows the general procedure for solving a boundary-value problem outlined in Chapter 2. It consists essentially of four parts:

(a) determination of an appropriate curve fit for the interface;

(b) determination of Ψ_1 and its derivatives by evaluating line integrals along the interface fit;

(c) determination of Ψ_2 and its derivatives by appropriate finite-difference techniques; and

(d) movement of interface points.

The first two parts of this approach must be considered together. Some of the interface fitting techniques which we will consider must be rejected because they produce difficulties in evaluating the line integrals, particularly those for the derivatives of Ψ_1. From equation (2.3.2)

$$\Psi_1(x,y) = -\left[k(\gamma_2-\gamma_1)/4\pi\right]\int_{Y_0'}^{Y_0''} \ln\left[(x-x_0)^2+(y-y_0)^2\right]\, dy_0 \qquad (3.1.1a)$$

The integration in equation (3.1.1a) extends over the interface curve $f(x_0, y_0) = 0$. The interface is represented basically by a

finite number of points, referred to as interface points and denoted by their coordinates (x_o^n, y_o^n), $n = 1, 2, \ldots, N$ (see Fig. 3.1.1). The line integral in equation (3.1.1a) can thus be expressed as a sum of line integrals evaluated along the segments of the interface connecting successive interface points. That is,

$$\Psi_1(x,y) = -\left[k(\gamma_2-\gamma_1)/4\pi\mu\right] \sum_{n=1}^{N-1} \int_{y_o^n}^{y_o^{n+1}} \ln\left[(x-x_o)^2+(y-y_o)^2\right] dy_o \qquad (3.1.1b)$$

The derivatives of Ψ_1 with respect to the general coordinates x and y can be determined by merely differentiating under the integral sign in equations (3.1.1). Thus

$$\frac{\partial \Psi_1}{\partial x} = -\frac{k(\gamma_2-\gamma_1)}{2\pi\mu} \int_{y_o^1}^{y_o^N} \frac{(x-x_o)\, dy_o}{(x-x_o)^2+(y-y_o)^2} \qquad (3.1.2a)$$

$$= -\frac{k(\gamma_2-\gamma_1)}{2\pi\mu} \sum_{n=1}^{N-1} \int_{y_o^n}^{y_o^{n+1}} \frac{(x-x_o)\, dy_o}{(x-x_o)^2+(y-y_o)^2} \qquad (3.1.2b)$$

and

$$\frac{\partial \Psi_1}{\partial y} = -\frac{k(\gamma_2-\gamma_1)}{2\pi\mu} \int_{y_o^1}^{y_o^N} \frac{(y-y_o)\, dy_o}{(x-x_o)^2+(y-y_o)^2} \qquad (3.1.3a)$$

$$= -\frac{k(\gamma_2-\gamma_1)}{2\pi\mu} \sum_{n=1}^{N-1} \int_{y_o^n}^{y_o^{n+1}} \frac{(y-y_o)\, dy_o}{(x-x_o)^2+(y-y_o)^2} \qquad (3.1.3b)$$

The evaluation of the integrals in equations (3.1.1) through (3.1.3) will be considered in detail later.

In order to make the computer code as general as possible, we will determine Ψ_2 and its derivatives by finite-difference methods. Thus we will have to define a finite-difference mesh by means of orthogonal grid lines overlain on the physical flow region. It will be most convenient for us to take the grid lines as being parallel to the x and y coordinate axes (Fig. 3.1.1). A general point P can be defined in terms of its x and y coordinates in the physical plane, or its i and j "coordinates" in the finite-difference mesh. An interface point can be defined in terms of its coordinates x_o^n and y_o^n in the physical plane, or by an index n along the interface.

The general solution scheme then proceeds along the following steps:

(a) Determine Ψ_1, $\partial\Psi_1/\partial x$, and $\partial\Psi_1/\partial y$ at each mesh point (i, j), and at each interface point (n). These calculations are carried out by evaluating the line integrals in equations (3.1.1) through (3.1.3) along the interface.

(b) Determine appropriate expressions for the boundary conditions on Ψ_2 by applying equation (2.4.1) at the boundary mesh points.

(c) Calculate Ψ_2 at each mesh point by an appropriate finite-difference technique.

Figure 3.1.1. Finite-difference mesh and interface points.

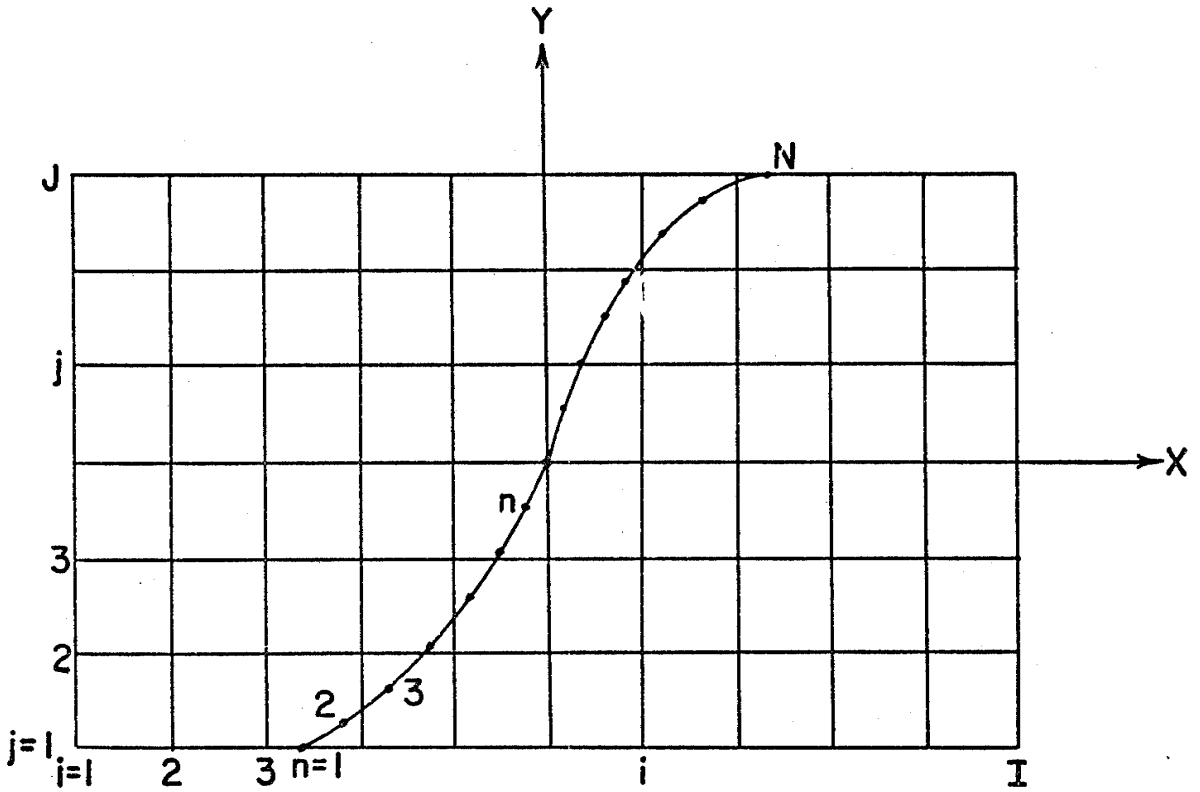
Y
X
J
j
3
2
j=1
N
n
2
3
i=1
2
3
n=1
i
I

(d) Calculate finite-difference approximations to $\partial\Psi_2/\partial x$ and $\partial\Psi_2/\partial y$ at each mesh point.

(e) Calculate Ψ_2, $\partial\Psi_2/\partial x$, and $\partial\Psi_2/\partial y$ at each interface point by means of an interpolation scheme.

The derivatives of Ψ_1 and Ψ_2 are needed to determine the specific discharge at each mesh point and each interface point. By equations (2.4.2) and (2.2.3), the components of the specific discharge are

$$q_x = -\partial\Psi/\partial y = -\partial\Psi_1/\partial y - \partial\Psi_2/\partial y \tag{3.1.4}$$

$$q_y = \partial\Psi/\partial x = \partial\Psi_1/\partial x + \partial\Psi_2/\partial x \tag{3.1.5}$$

In the subsequent work, we will occasionally use the notations

$$q_x)_1 = -\partial\Psi_1/\partial y \tag{3.1.6a}$$

$$= +\frac{k(\gamma_2-\gamma_1)}{2\pi\mu}\int_{Y_0'}^{Y_0^N}\frac{(y-y_0)\,dy_0}{(x-x_0)^2+(y-y_0)^2} \tag{3.1.6b}$$

$$= +\frac{k(\gamma_2-\gamma_1)}{2\pi\mu}\sum_{n=1}^{N-1}\int_{Y_0^n}^{Y_0^{n+1}}\frac{(y-y_0)\,dy_0}{(x-x_0)^2+(y-y_0)^2} \tag{3.1.6c}$$

$$q_y)_1 = \partial\Psi_1/\partial x \tag{3.1.7a}$$

$$= -\frac{k(\gamma_2-\gamma_1)}{2\pi\mu}\int_{Y_0'}^{Y_0^N}\frac{(x-x_0)\,dy_0}{(x-x_0)^2+(y-y_0)^2} \tag{3.1.7b}$$

$$= -\frac{k(\gamma_2-\gamma_1)}{2\pi\mu}\sum_{n=1}^{N-1}\int_{Y_0^n}^{Y_0^{n+1}}\frac{(x-x_0)\,dy_0}{(x-x_0)^2+(y-y_0)^2} \tag{3.1.7c}$$

$$q_x)_2 = - \partial \Psi_2 / \partial y \qquad (3.1.8)$$

$$q_y)_2 = \partial \Psi_2 / \partial x \qquad (3.1.9)$$

In this chapter we will consider the techniques used for the computation of the various parts of the computer model, as well as some approaches which were rejected for various reasons. Greater detail of some of the analyses are given in the appendices.

3.2 Interface Fitting Technique

As noted in Section 3.1, the interface is represented basically by a finite number of interface points (x_o^n, y_o^n), $n = 1, 2, \ldots N$. These points are chosen somewhat arbitrarily, although they must lie on the initial configuration of the interface. At the end of each time step in the calculations, each interface point is moved to a new position according to the local average velocity at that point. Subject to the limitations of the truncation and roundoff errors inherent in any computational scheme, the new positions of these interface points lie on the true interface at the new time. In order to proceed to the next time step in the calculations, we must fit an appropriate curve through the new positions of the interface points. The curve fit must be a reasonably accurate representation of the true interface, but it must also be simple enough to allow the line integrals to be calculated quickly and easily.

The simplest way to fit the interface would be to connect the interface points by straight line segments. As shown in Figure 3.2.1, the resulting interface fit is a polygonal curve with corners at the interface points. As we will see below, this leads to infinite logarithmic singularities in the expressions for the specific discharge components $q_x)_1$ and $q_y)_1$ at the interface points.

Figure 3.2.1. Line segment interface fit.

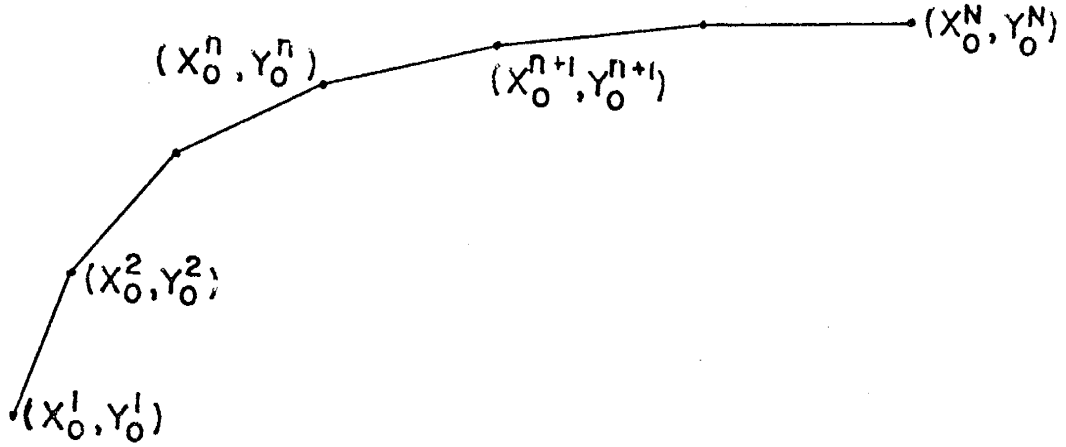
(X_0^n, Y_0^n)
(X_0^{n+1}, Y_0^{n+1})
(X_0^N, Y_0^N)
(X_0^2, Y_0^2)
(X_0^1, Y_0^1)

A line integral along this interface fit can be expressed as the sum of integrals along each straight line segment, as in equations (3.1.1b), (3.1.2b), and (3.1.3b). Applying the notation of Appendix A to equations (3.1.2b) and (3.1.3b), we can write

$$q_x)_1 = -\partial\Psi_1/\partial y = [k(\gamma_2-\gamma_1)/2\pi\mu] \sum_{n=1}^{N-1} I_2^n \qquad (3.2.1a)$$

$$q_y)_1 = \partial\Psi_1/\partial x = -[k(\gamma_2-\gamma_1)/2\pi\mu] \sum_{n=1}^{N-1} I_3^n \qquad (3.2.1b)$$

We need consider only the integrals along one of these line segments in order to demonstrate the infinite logarithmic singularities in $q_x)_1$ and $q_y)_1$.

The slope of the line segment connecting points (x_o^n, y_o^n) and (x_o^{n+1}, y_o^{n+1}) is

$$\sigma_n = (y_o^{n+1} - y_o^n)/(x_o^{n+1} - x_o^n) \qquad (3.2.2)$$

Furthermore, this line segment passes through the point (x_o^n, y_o^n). Thus the results of Appendix A apply to this case, with

$$m = \sigma_n \qquad (3.2.3a)$$

$$(x_n, y_n) = (x_o^n, y_o^n) \qquad (3.2.3b)$$

$$(x_1, y_1) = (x_o^n, y_o^n) \qquad (3.2.3c)$$

$$(x_2, y_2) = (x_o^{n+1}, y_o^{n+1}) \qquad (3.2.3d)$$

Applying equations (3.2.3) to equation (A.3.9), we get

$$I_2^n \equiv \int_{Y_o^n}^{Y_o^{n+1}} \{ (Y-Y_o) / [(X-X_o)^2 + (Y-Y_o)^2] \} \, dY_o$$

$$= -\frac{\sigma_n^2}{2(1+\sigma_n^2)} \ln \left\{ \frac{(X-X_o^{n+1})^2 + [(Y-Y_o^n) - \sigma_n (X-X_o^n) + \sigma_n (X-X_o^{n+1})]^2}{(X-X_o^n)^2 + (Y-Y_o^n)^2} \right\} +$$

$$+ \frac{\sigma_n}{1+\sigma_n^2} \left\{ \tan^{-1} \frac{(1+\sigma_n^2)(X_o^{n+1}-X) - \sigma_n [(Y-Y_o^n) - \sigma_n (X-X_o^n)]}{(Y-Y_o^n) - \sigma_n (X-X_o^n)} - \right.$$

$$\left. - \tan^{-1} \frac{(1+\sigma_n^2)(X_o^n-X) - \sigma_n [(Y-Y_o^n) - \sigma_n (X-X_o^n)]}{(Y-Y_o^n) - \sigma_n (X-X_o^n)} \right\} \qquad (3.2.4)$$

Applying equations (3.2.3) to equation (A.4.5), we get

$$I_3^n \equiv \int_{Y_o^n}^{Y_o^{n+1}} \{ (X-X_o) / [(X-X_o)^2 + (Y-Y_o)^2] \} \, dY_o$$

$$= -\frac{\sigma_n}{2(1+\sigma_n^2)} \ln \left\{ \frac{(X-X_o^{n+1})^2 + [(Y-Y_o^n) - \sigma_n (X-X_o^n) + \sigma_n (X-X_o^{n+1})]^2}{(X-X_o^n)^2 + (Y-Y_o^n)^2} \right\} -$$

$$- \frac{\sigma_n^2}{1+\sigma_n^2} \left\{ \tan^{-1} \frac{(1+\sigma_n^2)(X_o^{n+1}-X) - \sigma_n [(Y-Y_o^n) - \sigma_n (X-X_o^n)]}{(Y-Y_o^n) - \sigma_n (X-X_o^n)} - \right.$$

$$\left. - \tan^{-1} \frac{(1+\sigma_n^2)(X_o^n-X) - \sigma_n [(Y-Y_o^n) - \sigma_n (X-X_o^n)]}{(Y-Y_o^n) - \sigma_n (X-X_o^n)} \right\} \qquad (3.2.5)$$

Substituting equations (3.2.4) and (3.2.5) into equation (3.2.1), we obtain $q_x)_1$ and $q_y)_1$, which are contributions to the discharge components q_x and q_y. We see from these equations that the argument of the logarithm term becomes infinite at $(x, y) = (x_o^n, y_o^n)$. Thus the specific discharge has an infinite logarithmic singularity at that interface point and we must reject this interface fitting scheme.

We can more thoroughly examine the nature of the infinite logarithmic singularity in the specific discharge at (x_o^n, y_o^n)

by considering the effect of integrating along both line segments which meet at that point. For (x, y) lying on the n^{th} line segment, we have $y - y_o^n - \sigma_n (x - x_o^n) = 0$ (since this is the equation of that line segment), so the logarithm term in equation (3.2.4) becomes

$$L_2^n = -\frac{\sigma_n^2}{2(1+\sigma_n^2)} \ln\left\{\frac{(1+\sigma_n^2)(x-x_o^{n+1})^2}{(1+\sigma_n^2)(x-x_o^n)^2}\right\} = -\frac{\sigma_n^2}{2(1+\sigma_n^2)} \ln\left\{\frac{(x-x_o^{n+1})^2}{(x-x_o^n)^2}\right\} \quad (3.2.6)$$

For the $(n-1)^{th}$ line segment, we can let n = n-1 in equation (3.2.6) to get

$$L_2^{n-1} = -\frac{\sigma_{n-1}^2}{2(1+\sigma_{n-1}^2)} \ln\left\{\frac{(x-x_o^n)^2}{(x-x_o^{n-1})^2}\right\} \quad (3.2.7)$$

Summing equations (3.2.6) and (3.2.7), we get

$$L_2 = L_2^{n-1} + L_2^n = -\frac{\sigma_{n-1}^2}{2(1+\sigma_{n-1}^2)} \ln\left\{\frac{(x-x_o^n)^2}{(x-x_o^{n-1})^2}\right\} - \frac{\sigma_n^2}{2(1+\sigma_n^2)} \ln\left\{\frac{(x-x_o^{n+1})^2}{(x-x_o^n)^2}\right\}$$

$$= \frac{1}{2}\left[\frac{\sigma_n^2}{1+\sigma_n^2} - \frac{\sigma_{n-1}^2}{1+\sigma_{n-1}^2}\right] \ln(x-x_o^n)^2 + \frac{\sigma_{n-1}^2}{2(1+\sigma_{n-1}^2)} \ln(x-x_o^{n-1})^2 -$$

$$- \frac{\sigma_n^2}{2(1+\sigma_n^2)} \ln(x-x_o^{n+1})^2 \quad (3.2.8)$$

Similarly, the logarithm terms for I_3 are

$$L_3 = \frac{1}{2}\left[\frac{\sigma_n}{1+\sigma_n^2} - \frac{\sigma_{n-1}}{1+\sigma_{n-1}^2}\right] \ln(x-x_o^n)^2 + \frac{\sigma_{n-1}}{2(1+\sigma_{n-1}^2)} \ln(x-x_o^{n-1})^2 -$$

$$- \frac{\sigma_n}{2(1+\sigma_n^2)} \ln(x-x_o^{n+1})^2 \quad (3.2.9)$$

At $x = x_o^n$, both L_2 and L_3 exhibit infinite logarithmic singularities. However, we can see from equations (3.2.8) and (3.2.9) that these singularities would not occur if $\sigma_n = \sigma_{n-1}$, because then the term $\ln(x - x_o^n)^2$ would not appear. Thus it would seem that the

logarithmic singularity in the specific discharge at (x_o^n, y_o^n) might be due to the fact that this interface fit does not have continuous slope at that point.

A polynomial spline fit to the interface points will result in an interface representation which exhibits continuity of slope at the interface points. A cubic spline fit to a set of points is discussed in most standard textbooks on numerical analysis. A parabolic spline fit to the interface points is considered in Appendix B, and the evaluation, along a parabolic arc, of the line integrals in equations (3.1.1) through (3.1.3) is discussed in Appendix C. However, because of the great deal of algebraic manipulation needed to evaluate equations (C.3.5), (C.4.4), and (C.5.4), we will reject this approach and seek a more convenient interface fit.

A combination of a parabolic spline fit and a line segment fit results in an interface representation along which the line integrals can be readily evaluated. In this approach, a parabolic spline fit is first made to the interface points, according to the procedure given in Appendix B. The parabolic spline fit is then used to determine the slope of the curve at each interface point. A short line segment is then constructed tangent to the parabolic spline at each interface point, with the length of the segment being inversely proportional to the curvature of the parabolic spline at that point. The endpoints of the tangent line segments are

then connected by additional line segments (Fig. 3.2.2). The resulting representation of the interface consists of connected line segments, along which the line integrals can be easily evaluated, and it also exhibits continuity of slope at the interface points. However, after computational experimentation, we must reject this approach because, as time progresses, the resulting interface shape begins to show inflection points due to the parabolic spline fit (Fig. 3.2.3).

The interface fit which we will use in the code is a modification of the simplest approach of just connecting the interface points by linear segments. For interface points which do not lie on the boundary of the flow region, we first take three successive points and connect them directly by two straight line segments (Fig. 3.2.4). We then determine the angles of inclination, α_{n-1} and α_n, of these line segments. We next calculate an average angle of inclination $\beta_n = \frac{1}{2}(\alpha_{n-1} + \alpha_n)$, to be applied at interface point n. We now construct a short line segment, called the n^{th} tangent line segment, passing through point (x_o^n, y_o^n) and having inclination β_n. As can be seen from Figure 3.2.4, this tangent line segment is the bisector of the angle formed by the line segment between points (x_o^n, y_o^n) and (x_o^{n+1}, y_o^{n+1}), and the extension of the line segment between points (x_o^n, y_o^n) and (x_o^{n-1}, y_o^{n-1}). After we have done this for each interior interface point, we join the tangent line segments

by additional connecting line segments (Fig. 3.2.5).

The n^{th} tangent line segment has the length 2δ, and is bisected by the n^{th} interface point. As will be shown in Section 3.3, we cannot allow the endpoints of this line segment to coincide with a mesh point, because the specific discharge calculated at that mesh point would then exhibit infinite logarithmic singularities. Thus δ must be chosen so that neither endpoint of the tangent line segment coincides with a mesh point. The choice of δ will be discussed in more detail in Chapter 4.

At interface points which lie on the boundary of the flow region, we must construct the tangent line segments so that the boundary conditions are satisfied. In this case, at the impermeable boundaries, the tangent line segments are horizontal and half as long as the interior line segments. This point will be discussed in Chapter 4 in more detail.

The interface representation resulting from this procedure exhibits a number of desirable features. It consists entirely of straight line segments, so we can easily calculate the line integrals to be evaluated along the interface. It exhibits continuity of slope at the interface points, so we can readily evaluate the derivatives of Ψ_1 (and hence the specific discharge components) at those points. Finally, computational experimentation shows that this interface representation results in a reasonably smooth curve, the motion of which follows theoretical

and experimental results quite closely. The interface does not exhibit the oscillatory or "zig-zag" shape which sometimes characterizes the results of numerical calculations. The results of the computational experimentation are discussed in more detail in Chapter 5.

Figure 3.2.2. Combined linear-parabolic interface fit.

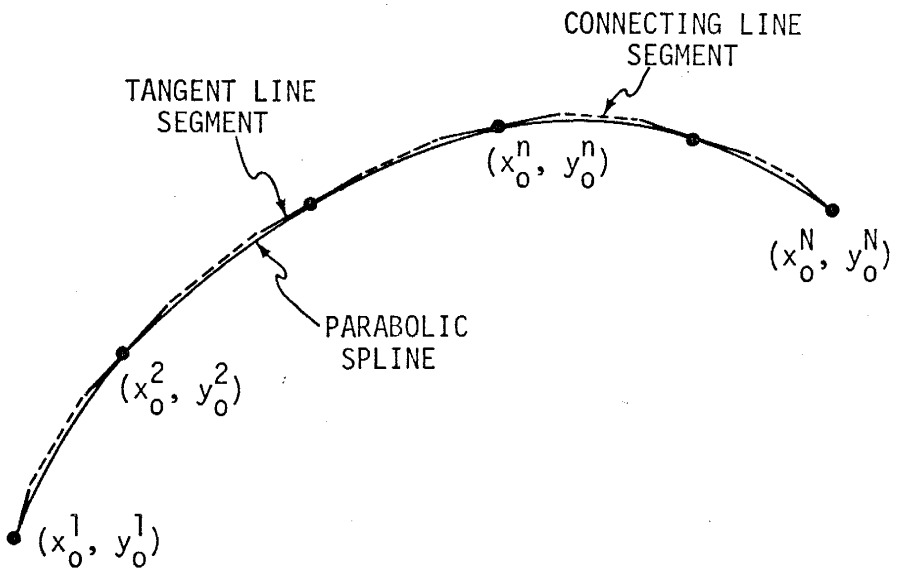
CONNECTING LINE SEGMENT
TANGENT LINE SEGMENT
(x_o^n, y_o^n)
(x_o^N, y_o^N)
PARABOLIC SPLINE
(x_o^2, y_o^2)
(x_o^1, y_o^1)

Figure 3.2.3. Inflection points in the combined linear-parabolic interface fit.

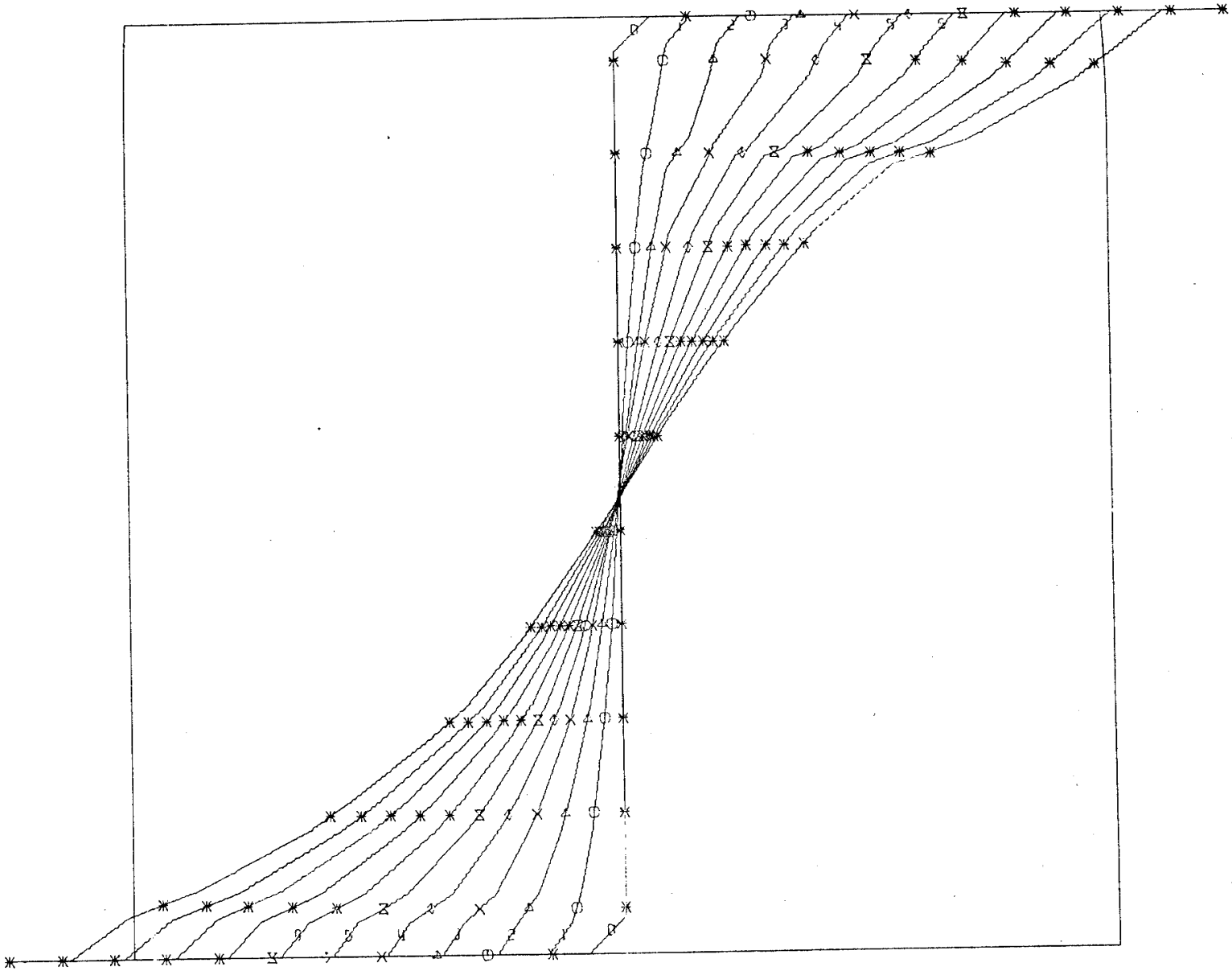

Figure 3.2.4. Definition of tangent line segment for modified line segment interface fit.

Figure 3.2.5. Modified line segment interface fit.

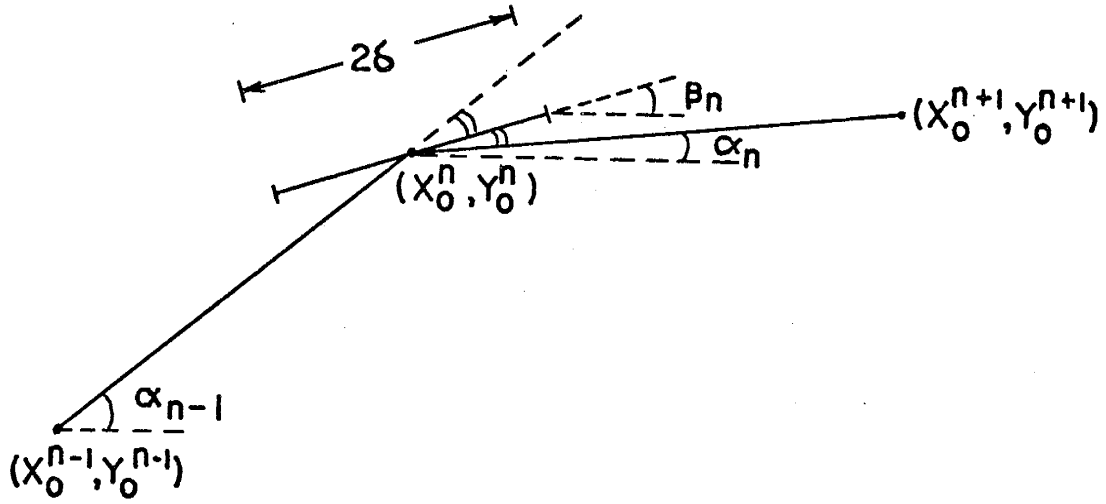
2δ
β_n
α_n
(X_0^{n+1}, Y_0^{n+1})
(X_0^n, Y_0^n)
α_{n-1}
(X_0^{n-1}, Y_0^{n-1})

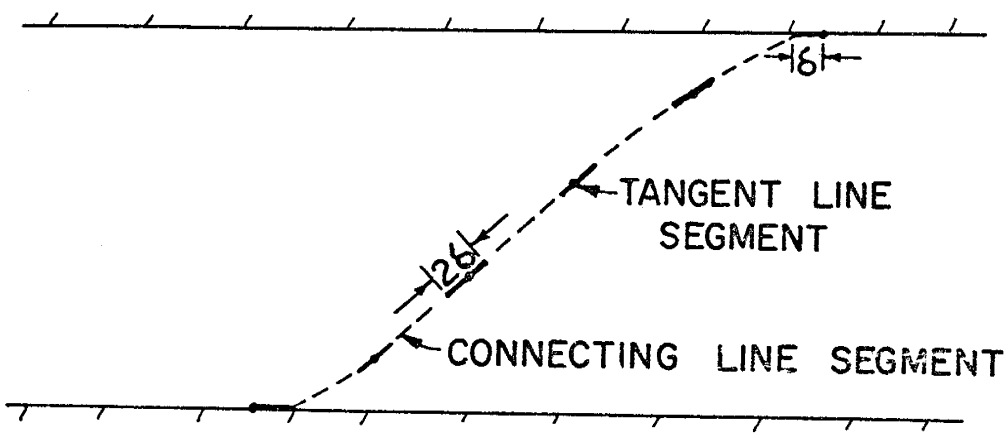
δ
TANGENT LINE SEGMENT
2δ
CONNECTING LINE SEGMENT

3.3 Calculation of Line Integrals

Once we have determined an appropriate representation of the interface, we can proceed to determine the stream function and the specific discharge. We will do this by following the general procedure for solving a boundary-value problem outlined in Chapter 2 and in Section 3.1. In the present section, we will consider only the evaluation of the line integrals needed to determine Ψ_1, $\partial\Psi_1/\partial x$, and $\partial\Psi_1/\partial y$ at the mesh points and interface points.

As noted in Section 3.2, the interface fit consists of a sequence of connected tangent line segments and connecting line segments. Referring to Figure 3.3.1, let (x_o^n, y_o^n) denote the n^{th} interface point, let (x_1^n, y_1^n) denote the lower endpoint of the n^{th} tangent line segment, and let (x_2^n, y_2^n) denote the upper endpoint. Furthermore, let σ_n denote the slope of the n^{th} tangent line segment, and let τ_n denote the slope of the line segment connecting points (x_2^n, y_2^n) and (x_1^{n+1}, y_1^{n+1}). Then equations (3.1.1), (3.1.6), and (3.1.7) can be written

$$\Psi_1(x,y) = -\frac{k(\gamma_2-\gamma_1)}{4\pi\mu}\left\{\sum_{n=1}^{N}\int_{y_1^n}^{y_2^n}\ln\left[(x-x_o)^2+(y-y_o)^2\right]dy_o + \sum_{n=1}^{N-1}\int_{y_2^n}^{y_1^{n+1}}\ln\left[(x-x_o)^2+(y-y_o)^2\right]dy_o\right\} \qquad (3.3.1)$$

$$q_y)_1 = \frac{\partial \Psi_1}{\partial x} = -\frac{k(\gamma_2-\gamma_1)}{2\pi\mu}\left\{\sum_{n=1}^{N}\int_{Y_1^n}^{Y_2^n}\frac{(x-x_0)\,dy_0}{(x-x_0)^2+(y-y_0)^2}+\sum_{n=1}^{N-1}\int_{Y_2^n}^{Y_1^{n+1}}\frac{(x-x_0)\,dy_0}{(x-x_0)^2+(y-y_0)^2}\right\} \quad (3.3.2)$$

$$q_x)_1 = -\frac{\partial \Psi_1}{\partial y} = \frac{k(\gamma_2-\gamma_1)}{2\pi\mu}\left\{\sum_{n=1}^{N}\int_{Y_1^n}^{Y_2^n}\frac{(y-y_0)\,dy_0}{(x-x_0)^2+(y-y_0)^2}+\sum_{n=1}^{N-1}\int\frac{(y-y_0)\,dy_0}{(x-x_0)^2+(y-y_0)^2}\right\} \quad (3.3.3)$$

The integrals in equations (3.3.1) through (3.3.3) can be evaluated according to the formulas in Appendix A. Along a tangent line segment, we have

$$m = \sigma_n \quad (3.3.4a)$$

$$(x_n, y_n) = (x_0^n, y_0^n) \quad (3.3.4b)$$

$$(x_1, y_1) = (x_1^n, y_1^n) \quad (3.3.4c)$$

$$(x_2, y_2) = (x_2^n, y_2^n) \quad (3.3.4d)$$

while along a connecting line segment, we have

$$m = \tau_n \quad (3.3.5a)$$

$$(x_n, y_n) = (x_2^n, y_2^n) \quad (3.3.5b)$$

$$(x_1, y_1) = (x_2^n, y_2^n) \quad (3.3.5c)$$

$$(x_2, y_2) = (x_1^{n+1}, y_1^{n+1}) \quad (3.3.5d)$$

Figure 3.3.1. Definition of parameters in formulas for the evaluation of the line integrals.

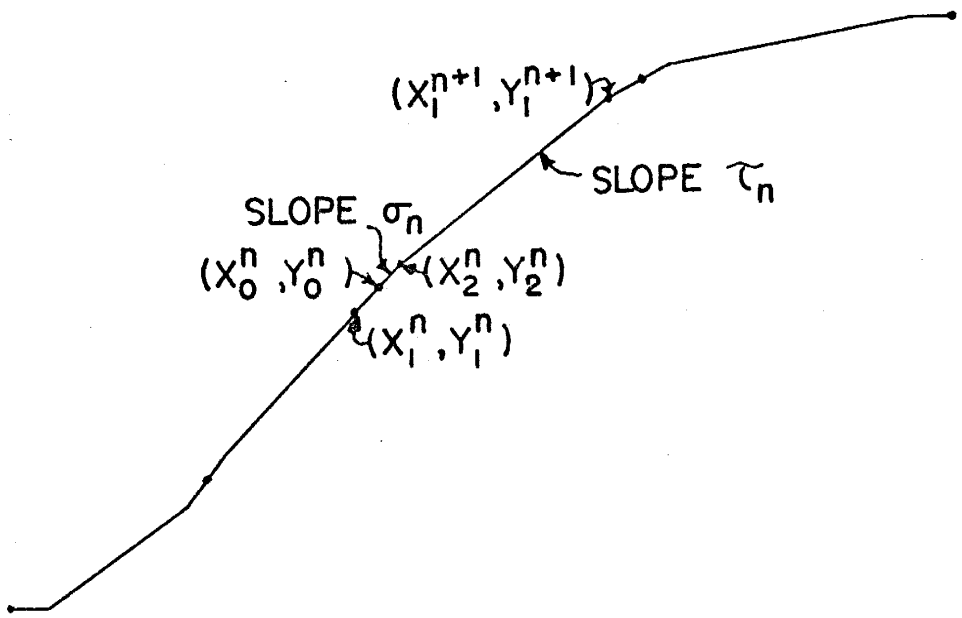
(X_1^{n+1}, Y_1^{n+1})
SLOPE τ_n
SLOPE σ_n
(X_0^n, Y_0^n)
(X_2^n, Y_2^n)
(X_1^n, Y_1^n)

Then, applying equations (3.3.4) and (3.3.5) to the formulas for I_1 in Appendix A, we get

$$\int_{Y_1^n}^{Y_2^n} \ln\left[(x-x_0)^2+(y-y_0)^2\right] dy_0 =$$

$$= \frac{\sigma_n}{1+\sigma_n^2}\left\{(1+\sigma_n^2)(x_2^n-x)-\sigma_n\left[(y-y_0^n)-\sigma_n(x-x_0^n)\right]\right\} \ln\left\{(x-x_2^n)^2+\left[(y-y_0^n)-\right.\right.$$

$$\left.\left.-\sigma_n(x-x_0^n)+\sigma_n(x-x_2^n)\right]^2\right\} - \frac{\sigma_n}{1+\sigma_n^2}\left\{(1+\sigma_n^2)(x_1^n-x)-\sigma_n\left[(y-y_0^n)-\right.\right.$$

$$\left.\left.-\sigma_n(x-x_0^n)\right]\right\} \ln\left\{(x-x_1^n)^2+\left[(y-y_0^n)-\sigma_n(x-x_0^n)+\sigma_n(x-x_1^n)\right]^2\right\} -$$

$$-2(x_2^n-x_1^n)\sigma_n + \frac{2\left[(y-y_0^n)-\sigma_n(x-x_0^n)\right]\sigma_n}{1+\sigma_n^2}\left\{\tan^{-1}\frac{(1+\sigma_n^2)(x_2^n-x)-\sigma_n\left[(y-y_0^n)-\sigma_n(x-x_0^n)\right]}{(y-y_0^n)-\sigma_n(x-x_0^n)}-\right.$$

$$\left.-\tan^{-1}\frac{(1+\sigma_n^2)(x_1^n-x)-\sigma_n\left[(y-y_0^n)-\sigma_n(x-x_0^n)\right]}{(y-y_0^n)-\sigma_n(x-x_0^n)}\right\}, \quad 0<|\sigma_n|<\infty \qquad (3.3.6a)$$

$$= 0, \qquad \sigma_n = 0 \qquad (3.3.6b)$$

$$= -(y-y_2^n)\ln\left[(x-x_0^n)^2+(y-y_2^n)^2\right] + (y-y_1^n)\ln\left[(x-x_0^n)^2+(y-y_1^n)^2\right] -$$

$$-2(y_2^n-y_1^n)-2(x-x_0^n)\left\{\tan^{-1}\left(\frac{y-y_2^n}{x-x_0^n}\right)-\tan^{-1}\left(\frac{y-y_1^n}{x-x_0^n}\right)\right\}, \quad |\sigma_n|=\infty \qquad (3.3.6c)$$

$$\int_{Y_2^n}^{Y_1^{n+1}} \ln\left[(x-x_0)^2+(y-y_0)^2\right] dy_0 =$$

$$= \frac{\tau_n}{1+\tau_n^2}\left\{(1+\tau_n^2)(x_1^{n+1}-x)-\tau_n\left[(y-y_2^n)-\tau_n(x-x_2^n)\right]\right\} \ln\left\{(x-x_1^{n+1})^2+\right.$$

$$\left.+\left[(y-y_2^n)-\tau_n(x-x_2^n)+\tau_n(x-x_1^{n+1})\right]^2\right\} + \frac{\tau_n}{1+\tau_n^2}\left\{(x-x_2^n)+\tau_n(y-y_2^n)\right\} \times$$

$$\times \ln\left\{(x-x_2^n)^2+(y-y_2^n)^2\right\} - 2(x_1^{n+1}-x_2^n)\tau_n + \frac{2\left[(y-y_2^n)-\tau_n(x-x_2^n)\right]\tau_n}{1+\tau_n^2} \times$$

$$\times\left\{\tan^{-1}\frac{(1+\tau_n^2)(x_1^{n+1}-x)-\tau_n\left[(y-y_2^n)-\tau_n(x-x_2^n)\right]}{(y-y_2^n)-\tau_n(x-x_2^n)} + \right.$$

$$\left.+\tan^{-1}\frac{(x-x_2^n)+\tau_n(y-y_2^n)}{(y-y_2^n)-\tau_n(x-x_2^n)}\right\}, \qquad 0<|\tau_n|<\infty \qquad (3.3.7a)$$

$$= 0, \qquad \tau_n = 0 \qquad (3.3.7b)$$

$$\int_{Y_2^n}^{Y_1^{n+1}} \ln\left[(x-x_0)^2+(y-Y_0)^2\right] dY_0 =$$

$$= (y-Y_2^n)\ln\left[(x-X_2^n)^2+(y-Y_2^n)^2\right] - (y-Y_1^{n+1})\ln\left[(x-X_2^n)^2+(y-Y_1^{n+1})^2\right] -$$

$$-2(Y_1^{n+1}-Y_2^n) - 2(x-X_2^n)\left\{\tan^{-1}\left(\frac{y-Y_1^{n+1}}{x-X_2^n}\right) - \tan^{-1}\left(\frac{y-Y_2^n}{x-X_2^n}\right)\right\}, \quad |\tau_n| = \infty \qquad (3.3.7c)$$

We can now determine Ψ_1, from equations (3.3.1), (3.3.6), and (3.3.7), at any mesh point (x, y) = (x_i , y_j) which does not lie on the interface. At such a mesh point, applying the results for I_3 from Appendix A to evaluate the integrals in equation (3.3.2), we get

$$\int_{Y_1^n}^{Y_2^n} \frac{(x-x_0)\,dY_0}{(x-x_0)^2+(y-Y_0)^2} = -\frac{\sigma_n}{2(1+\sigma_n^2)}\ln\left\{\frac{(x-X_2^n)^2+\left[(y-Y_0^n)-\sigma_n(x-X_0^n)+\sigma_n(x-X_2^n)\right]^2}{(x-X_1^n)^2+\left[(y-Y_0^n)-\sigma_n(x-X_0^n)+\sigma_n(x-X_1^n)\right]^2}\right\} -$$

$$-\frac{\sigma_n^2}{1+\sigma_n^2}\left\{\tan^{-1}\frac{(1+\sigma_n^2)(X_2^n-x)-\sigma_n\left[(y-Y_0^n)-\sigma_n(x-X_0^n)\right]}{(y-Y_0^n)-\sigma_n(x-X_0^n)} -\right.$$

$$\left. -\tan^{-1}\frac{(1+\sigma_n^2)(X_1^n-x)-\sigma_n\left[(y-Y_0^n)-\sigma_n(x-X_0^n)\right]}{(y-Y_0^n)-\sigma_n(x-X_0^n)}\right\}, \quad 0<|\sigma_n|<\infty \qquad (3.3.8a)$$

$$= 0, \qquad \sigma_n = 0 \qquad (3.3.8b)$$

$$= \tan^{-1}\left(\frac{y-Y_1^n}{x-X_0^n}\right) - \tan^{-1}\left(\frac{y-Y_2^n}{x-X_0^n}\right), \qquad |\sigma_n| = \infty \qquad (3.3.8c)$$

$$\int_{Y_2^n}^{Y_1^{n+1}} \frac{(x-x_0)\,dY_0}{(x-x_0)^2+(y-Y_0)^2} = -\frac{\tau_n}{2(1+\tau_n^2)}\ln\left\{\frac{(x-X_1^{n+1})^2+\left[(y-Y_2^n)-\tau_n(x-X_2^n)+\tau_n(x-X_1^{n+1})\right]^2}{(x-X_2^n)^2+(y-Y_2^n)^2}\right\} -$$

$$-\frac{\tau_n^2}{1+\tau_n^2}\left\{\tan^{-1}\frac{(1+\tau_n^2)(X_1^{n+1}-x)-\tau_n\left[(y-Y_2^n)-\tau_n(x-X_2^n)\right]}{(y-Y_2^n)-\tau_n(x-X_2^n)} +\right.$$

$$\left. +\tan^{-1}\frac{(x-X_2^n)+\tau_n(y-Y_2^n)}{(y-Y_2^n)-\tau_n(x-X_2^n)}\right\}, \qquad 0<|\tau_n|<\infty \qquad (3.3.9a)$$

$$= 0, \qquad \tau_n = 0 \qquad (3.3.9b)$$

$$= \tan^{-1}\left(\frac{y-Y_2^n}{x-X_2^n}\right) - \tan^{-1}\left(\frac{y-Y_1^{n+1}}{x-X_2^n}\right), \qquad |\tau_n| = \infty \qquad (3.3.9c)$$

Similarly, applying the results for I_2 from Appendix A, we get for the integrals in equation (3.3.3)

$$\int_{Y_1^n}^{Y_2^n} \frac{(Y-Y_0)\,dY_0}{(X-X_0)^2+(Y-Y_0)^2} = -\frac{\sigma_n^2}{2(1+\sigma_n^2)} \ln\left\{\frac{(X-X_2^n)^2+\left[(Y-Y_0^n)-\sigma_n(X-X_0^n)+\sigma_n(X-X_2^n)\right]^2}{(X-X_1^n)^2+\left[(Y-Y_0^n)-\sigma_n(X-X_0^n)+\sigma_n(X-X_1^n)\right]^2}\right\} +$$

$$+\frac{\sigma_n}{1+\sigma_n^2}\left\{\tan^{-1}\frac{(1+\sigma_n^2)(X_2^n-X)-\sigma_n\left[(Y-Y_0^n)-\sigma_n(X-X_0^n)\right]}{(Y-Y_0^n)-\sigma_n(X-X_0^n)} -\right.$$

$$\left.-\tan^{-1}\frac{(1+\sigma_n^2)(X_1^n-X)-\sigma_n\left[(Y-Y_0^n)-\sigma_n(X-X_0^n)\right]}{(Y-Y_0^n)-\sigma_n(X-X_0^n)}\right\}, \quad 0<|\sigma_n|<\infty \qquad (3.3.10a)$$

$$=0, \qquad \sigma_n=0 \qquad (3.3.10b)$$

$$=\frac{1}{2}\ln\left[\frac{(X-X_0^n)^2+(Y-Y_1^n)^2}{(X-X_0^n)^2+(Y-Y_2^n)^2}\right], \qquad |\sigma_n|=\infty \qquad (3.3.10c)$$

$$\int_{Y_2^n}^{Y_1^{n+1}} \frac{(Y-Y_0)\,dY_0}{(X-X_0)^2+(Y-Y_0)^2} = -\frac{\tau_n^2}{2(1+\tau_n^2)} \ln\left\{\frac{(X-X_1^{n+1})^2+\left[(Y-Y_2^n)-\tau_n(X-X_2^n)+\tau_n(X-X_1^{n+1})\right]^2}{(X-X_2^n)^2+(Y-Y_2^n)^2}\right\} +$$

$$+\frac{\tau_n}{1+\tau_n^2}\left\{\tan^{-1}\frac{(1+\tau_n^2)(X_1^{n+1}-X)-\tau_n\left[(Y-Y_2^n)-\tau_n(X-X_2^n)\right]}{(Y-Y_2^n)-\tau_n(X-X_2^n)} +\right.$$

$$\left.+\tan^{-1}\frac{(X-X_2^n)+\tau_n(Y-Y_2^n)}{(Y-Y_2^n)-\tau_n(X-X_2^n)}\right\}, \qquad 0<|\tau_n|<\infty \qquad (3.3.11a)$$

$$=0, \qquad \tau_n=0 \qquad (3.3.11b)$$

$$=\frac{1}{2}\ln\left[\frac{(X-X_2^n)^2+(Y-Y_2^n)^2}{(X-X_2^n)^2+(Y-Y_1^{n+1})^2}\right], \qquad |\tau_n|=\infty \qquad (3.3.11c)$$

Equations (3.3.6) through (3.3.11) can be used to calculate Ψ_1 and its derivatives at any mesh point $(x, y) = (x_i, y_j)$ which does not lie on the interface. These results must be modified slightly in order to calculate the integrals at a mesh point through

which the interface passes. Note here that we cannot allow $(x, y) = (x_1^n, y_1^n)$ or $(x, y) = (x_2^n, y_2^n)$, as these situations give rise to infinite logarithmic singularities in some of the formulas. Thus, in the interface routine, the lengths of the tangent line segments must be chosen so that the endpoints of these segments do not coincide with the mesh points.

Let the point (x, y) lie on the connecting line segment of slope τ_n. The equation of this line segment is $y - y_2^n = \tau_n (x - x_2^n)$, so that we have

$$(y - y_2^n) - \tau_n (x - x_2^n) = 0. \qquad (3.3.12)$$

This quantity does not occur in the integrals evaluated along the tangent line segments, so equations (3.3.6), (3.3.8), and (3.3.10) remain unchanged. Equation (3.3.7a) becomes

$$\int_{y_2^n}^{y_1^{n+1}} \ln\left[(x-x_0)^2 + (y-y_0)^2\right] dy_0 =$$

$$= \tau_n (x_1^{n+1} - x) \ln\left[(1+\tau_n^2)(x-x_1^{n+1})^2\right] + \tau_n (x - x_2^n) \ln\left[(x-x_2^n)^2 + \right.$$

$$\left. + (y-y_2^n)^2\right] - 2\tau_n (x_1^{n+1} - x_2^n), \qquad 0 < |\tau_n| < \infty \qquad (3.3.13)$$

Equations (3.3.7b) and (3.3.7c), which cover the cases $\tau_n = 0$ and $|\tau_n| = \infty$, remain unchanged. Equations (3.3.9) become

$$\int_{y_2^n}^{y_1^{n+1}} \frac{(x-x_0)\, dy_0}{(x-x_0)^2 + (y-y_0)^2} = -\frac{\tau_n}{2(1+\tau_n^2)} \ln\left\{\frac{(x-x_1^{n+1})^2}{(x-x_2^n)^2}\right\} - \frac{\tau_n}{1+\tau_n^2}\left(\pm\pi\right), \quad 0 < |\tau_n| < \infty \qquad (3.3.14a)$$

$$= 0, \qquad \tau_n = 0 \qquad (3.3.14b)$$

$$\int_{Y_2^n}^{Y_1^{n+1}} \frac{(x-x_0)\,dy_0}{(x-x_0)^2+(y-y_0)^2} = \pm\pi, \qquad |\tau_n| = \infty \quad (3.3.14c)$$

Equation (3.3.11a) becomes

$$\int_{Y_2^n}^{Y_1^{n+1}} \frac{(y-y_0)\,dy_0}{(x-x_0)^2+(y-y_0)^2} = -\frac{\tau_n^2}{2(1+\tau_n^2)} \ln\left\{\frac{(x-x_1^{n+1})^2}{(x-x_2^n)^2}\right\} + \frac{\tau_n}{1+\tau_n^2}(\pm\pi) \quad (3.3.15)$$

Equations (3.3.11b) and (3.3.11c) are unchanged. The $\pm\pi$ terms in equations (3.3.14a), (3.3.14c), and (3.3.15) result from a shear discontinuity in the specific discharge at the interface, as discussed in Appendix D. In the present work, the shear discontinuity will be omitted whenever it occurs; thus the $\pm\pi$ terms in equations (3.3.14) and (3.3.15) do not appear in the actual computer program. Omitting the shear discontinuity should not be overly restrictive for two reasons. In the first place, the interface will rarely, if ever, pass through a mesh point. In the second place, we are primarily interested in determining the specific discharge at the interface points, since these values control the interface motion. The specific discharge at a mesh point located on the interface plays no part in determining the discharge at the N interface points unless it coincides with one of these. Omitting the shear term in the discharge at such a mesh point will not affect the interface motion. The values of $q_x)_1$ and $q_y)_1$ at the mesh points are only calculated in order to obtain a picture of the nature of the flow within the areas occupied by

the two different fluids.

The specific discharge components at a mesh point should actually include the inverse tangent terms which produce the $\pm \pi$ terms in equations (3.3.13) and (3.3.14). The shear discontinuity due to the inverse tangent terms occurs only when the specific discharge is evaluated at a mesh point through which the interface passes. However, the inverse tangent terms can also produce difficulties in evaluating the specific discharge at a mesh point which is very near the interface. In such a case, the arguments of the inverse tangent terms can be very large, exceeding the limits for the inverse tangent function included in the library of a given computer system. Thus it might be better to treat these terms by defining some minimum distance of approach. If the distance between the mesh point and the interface is greater than this minimum distance of approach, the inverse tangent terms are evaluated; otherwise, the $\pm \pi$ terms are used, depending on which side of the interface the mesh point lies. If a mesh point lies exactly on the interface (a very rare occurrence), the $+ \pi$ term can be arbitrarily chosen. In the present work, the interface was never so near a mesh point that the inverse tangent terms could not be evaluated. Nevertheless, the refinement in the evaluation of the specific discharge components discussed in this paragraph

will be included in future versions of the computer code.

Equations (3.3.13) through (3.3.15) are for the case in which a connecting line segment passes through a mesh point. A tangent line segment can also pass through a mesh point. Let the point (x, y) lie on the tangent line segment of slope σ_n, but not at the interface point (x_o^n, y_o^n) (the calculations at the interface points will be considered later). The equation of this segment is

$$(y - y_o^n) - \sigma_n (x - x_o^n) = 0 . \qquad (3.3.16)$$

This quantity does not occur in the integrals evaluated along the connecting line segments, so equations (3.3.7), (3.3.9), and (3.3.11) are unchanged for this case. Equations (3.3.6) become

$$\int_{Y_1^n}^{Y_2^n} \ln\left[(x-x_o)^2 + (y-y_o)^2\right] dy_o =$$

$$= \sigma_n (x_2^n - x) \ln\left[(1+\sigma_n^2)(x-x_2^n)^2\right] - \sigma_n (x_1^n - x) \ln\left[(1+\sigma_n^2)(x-x_1^n)^2\right] -$$

$$-2\sigma_n (x_2^n - x_1^n), \qquad 0 < |\sigma_n| < \infty \qquad (3.3.17a)$$

$$= 0, \qquad \sigma_n = 0 \qquad (3.3.17b)$$

$$= -(y-Y_2^n) \ln\left[(y-Y_2^n)^2\right] + (y-Y_1^n) \ln\left[(y-Y_1^n)^2\right] -$$

$$-2(Y_2^n - Y_1^n), \qquad |\sigma_n| = \infty \qquad (3.3.17c)$$

Equations (3.3.8) become

$$\int_{Y_1^n}^{Y_2^n} \frac{(x-x_o)\, dy_o}{(x-x_o)^2 + (y-y_o)^2} =$$

$$= -\frac{\sigma_n}{2(1+\sigma_n^2)} \ln\left\{\frac{(x-x_2^n)^2}{(x-x_1^n)^2}\right\} - \frac{\sigma_n^2}{1+\sigma_n^2}\left(\pm\pi\right), \qquad 0 < |\sigma_n| < \infty \qquad (3.3.18a)$$

$$\int_{Y_1^n}^{Y_2^n} \frac{(x-x_o)\,dy_o}{(x-x_o)^2+(y-y_o)^2} = 0, \qquad \sigma_n = 0 \quad (3.3.18b)$$

$$= \pm\pi, \qquad |\sigma_n| = \infty \quad (3.3.18c)$$

Equations (3.3.10) become

$$\int_{Y_1^n}^{Y_2^n} \frac{(y-y_o)\,dy_o}{(x-x_o)^2+(y-y_o)^2} =$$

$$= -\frac{\sigma_n^2}{2(1+\sigma_n^2)} \ln\left\{\frac{(x-x_2^n)^2}{(x-x_1^n)^2}\right\} + \frac{\sigma_n}{1+\sigma_n^2}(\pm\pi), \quad 0<|\sigma_n|<\infty \quad (3.3.19a)$$

$$= 0, \qquad \sigma_n = 0 \quad (3.3.19b)$$

$$= \frac{1}{2} \ln\left\{\frac{(y-y_1^n)^2}{(y-y_2^n)^2}\right\}, \qquad |\sigma_n| = \infty \quad (3.3.19c)$$

Again, in equations (3.3.18a), (3.3.18c), and (3.3.19a), the $\pm\pi$ terms result from the shear discontinuity in the specific discharge at the mesh point $(x, y) = (x_i, y_j)$. These terms have been omitted in the present version of the computer code.

Equations (3.3.6) through (3.3.19) give us all the formulas we need to calculate Ψ_1 and its derivatives at the mesh points. We must finally determine the values of these quantities at the interface points. Thus, let $(x, y) = (x_o^n, y_o^n)$, or $x = x_o^n$ and $y = y_o^n$. Then, since (x, y) lies on the n^{th} tangent line segment of the interface, equations (3.3.7), (3.3.9), and (3.3.11) are unchanged, while equations (3.3.17) through (3.3.19) apply with $x = x_o^n$ and $y = y_o^n$. However, in this case we must consider further the effects of omitting the $\pm\pi$ terms due to the shear

discontinuity in the specific discharge at the interface point (x_o^n, y_o^n).

As we can see from Appendix D, the arctangent terms which produce the $\pm\pi$ terms in equations (3.3.18a), (3.3.18c), and (3.3.19a) produce a component of the specific discharge which consists of a shear flow tangent to the interface. This shear term, which has been omitted in the computer code, is produced by the vortex located at the interface point (x_o^n, y_o^n), and is proportional to the vortex strength at that point. We eventually seek to determine the total specific discharge at this interface point, so that we can move the point, during a time step Δt, to a new position according to its local average velocity $\vec{q}/\epsilon$ at the beginning of the time step. In omitting the shear term in the discharge, we are only omitting a term which tends to move the interface points along the interface. Thus, the new position of the interface point, determined by omitting the shear term in the discharge, will still lie on the true interface at the end of the time step. Furthermore, since the total specific discharge consists of a summation of terms over all tangent line segments and all connecting line segments, as given in equations (3.3.2) and (3.3.3), the terms which we have omitted should be small in magnitude relative to the total discharge.

3.4 Solution of Laplace's Equation for Ψ_2

Since we have now determined Ψ_1 and its derivatives at each mesh point, and specifically at the boundary mesh points, we can proceed to determine Ψ_2 at each mesh point. Note first that since we have determined $\partial\Psi_1/\partial x$ and $\partial\Psi_1/\partial y$ at each boundary mesh point, we immediately know

$$\text{grad } \Psi_1 = \hat{\imath}\,(\partial\Psi_1/\partial x) + \hat{\jmath}\,(\partial\Psi_1/\partial y)$$

at those points. Thus, assuming we know the geometrical configuration of the boundary, we can readily determine

$$\partial\Psi_1/\partial\nu = \vec{\nu} \cdot \text{grad } \Psi_1 \ ,$$

where $\vec{\nu}$ is a unit vector normal to the boundary. Hence, by applying equation (2.4.1), we can determine boundary values for Ψ_2. Note here that if the boundary conditions require us to specify $\partial\Psi_2/\partial\nu$ at the boundary, it will be convenient to introduce a staggered finite-difference mesh, so that the boundary lies midway between the last two mesh lines. However, we will assume in this section that Ψ_2 satisfies a simple Dirichlet problem (which is the case for the basic check problem to be discussed in Chapter 4), so that the boundary condition results in merely specifying the values of Ψ_2 at the boundary mesh points. Thus our problem reduces to solving

$$\nabla^2 \Psi_2 = 0, \qquad (3.4.1)$$

with Ψ_2 specified at each boundary mesh point.

Equation (3.4.1) can be solved by the point successive over-relaxation (PSOR) iterative scheme described in Appendix F. From equations (F.1.6) and (F.1.7), we have

$$\Psi_2)_{i,j}^{k+1} = \Psi_2)_{i,j}^{k} + \omega \, R_{i,j}^{k} \quad , \tag{3.4.2}$$

where

$$R_{i,j}^{k} = \left\{ \Delta y^2 \left[\Psi_2)_{i-1,j}^{k+1} + \Psi_2)_{i+1,j}^{k} \right] + \Delta x^2 \left[\Psi_2)_{i,j-1}^{k+1} + \right.\right.$$

$$\left.\left. + \Psi_2)_{i,j+1}^{k} \right] - 2(\Delta x^2 + \Delta y^2) \Psi_2)_{i,j}^{k} \right\} / 2(\Delta x^2 + \Delta y^2) \tag{3.4.3}$$

The subscripts (i, j) denote quantities evaluated at the mesh point (x_i , y_j), while the superscript k denotes the k^{th} iterative step. Equation (3.4.2) is applied at each mesh point in succession for a given value of k. Then k is increased by unity and equation (3.4.2) is again applied at each mesh point in succession. This procedure continues until the maximum residual $R_{i,j}^{k}$ is less than some predefined small value. Brief analyses of the accuracy and stability of this scheme, as well as an estimate of the optimum relaxation parameter ω, are given in Appendix F.

3.5 Finite-Difference Approximations for $q_x)_2$ and $q_y)_2$

Having determined the value of Ψ_2 at each mesh point by the PSOR scheme described above, we can now determine approximate values for the specific discharge components at each mesh point by applying equations (3.1.8) and (3.1.9). This is necessary because just as Ψ_1 will in general not satisfy the correct physical boundary conditions, neither will its derivatives. Furthermore, the gradient of Ψ_2 at each mesh point will generate a component of specific discharge at that point, which must be added to the value determined from Ψ_1 in order to give the total specific discharge at that point.

The values of $\partial\Psi_2/\partial x$ and $\partial\Psi_2/\partial y$ in equations (3.1.8) and (3.1.9) are approximated by standard second-order accurate central finite differences at interior mesh points, and by first-order accurate forward or backward differences at boundary mesh points, according to the formulas given in Appendix E. At interior mesh points,

$$q_y)_2 = \partial\Psi_2/\partial x)_{i,j} \approx \left[\Psi_2)_{i+1,j} - \Psi_2)_{i-1,j}\right] / 2\Delta x \qquad (3.5.1a)$$

$$q_x)_2 = -\partial\Psi_2/\partial y)_{i,j} \approx -\left[\Psi_2)_{i,j+1} - \Psi_2)_{i,j-1}\right] / 2\Delta y \qquad (3.5.1b)$$

Along the left-hand boundary i = 1 ,

$$q_y)_2 = \partial \Psi_2/\partial x)_{1,j} \approx [\Psi_2)_{2,j} - \Psi_2)_{1,j}]/\Delta x \qquad (3.5.2a)$$

and along the right-hand boundary i = I,

$$q_y)_2 = \partial \Psi_2/\partial x)_{I,j} \approx [\Psi_2)_{I,j} - \Psi_2)_{I-1,j}]/\Delta x \qquad (3.5.2b)$$

Along the lower boundary j = 1,

$$q_x)_2 = -\partial \Psi_2/\partial y)_{i,1} \approx -[\Psi_2)_{i,2} - \Psi_2)_{i,1}]/\Delta y \qquad (3.5.3a)$$

and along the upper boundary j = J,

$$q_x)_2 = -\partial \Psi_2/\partial y)_{i,J} \approx -[\Psi_2)_{i,J} - \Psi_2)_{i,J-1}]/\Delta y \qquad (3.5.3b)$$

Along the vertical boundaries, equation (3.5.1b) holds, while along the horizontal boundaries, equation (3.5.1a) holds.

Equations (3.5.2) and (3.5.3) are designed for the boundaries of a rectangular flow region, but an appropriate combination of these formulas can be applied at any boundary segment which is horizontal or vertical. More complicated formulas can be derived for the derivatives at a curved boundary segment, but curved boundaries rarely must be used. A flow region with irregular boundaries can usually be adequately represented by a region bounded by horizontal and vertical line segments. An example is shown in Figure 3.5.1. In the basic problem used to check the behavior of the code, the flow region is rectangular,

and the above formulas can be used directly.

Figure 3.5.1. Finite-difference mesh for approximating a flow region with irregular boundaries.

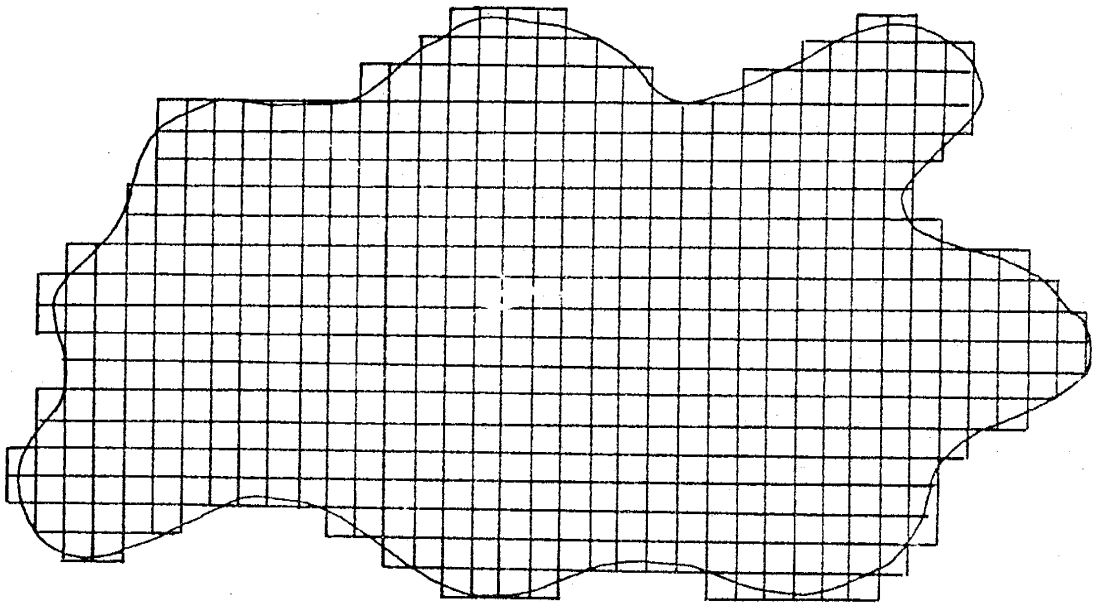

3.6 Interpolation at the Interface Points

In the preceding section, we considered the determination of Ψ_2, $q_x)_2$, and $q_y)_2$ at the mesh points by finite-difference methods. However, since we wish to describe the actual interface motion, we must determine at least $q_x)_2$ and $q_y)_2$ at the interface points. Given the values of Ψ_2, $q_x)_2$, and $q_y)_2$ at the mesh points, we can determine values of these quantities at the interface points by interpolation.

The function Ψ_2 satisfies Laplace's equation at all points within the flow region, with specified values along the boundaries of the region. Furthermore, there are no singularities within the domain of Ψ_2. Thus Ψ_2 and its first derivatives are continuous throughout the flow region. For this reason, determining the values of these quantities at the interface points by interpolating between values at the mesh points should be reasonably accurate.

The interpolating scheme used in this code is based on the Taylor series expansion of $\Psi_2(x, y)$ about the mesh point (x_i, y_j). From equation (E.2) of Appendix E, we have

$$\Psi_2(x,y) = \Psi_2)_{i,j} + (x-x_i)(\partial\Psi_2/\partial x)_{i,j} + (y-y_j)(\partial\Psi_2/\partial y)_{i,j} +$$
$$+ \tfrac{1}{2}(x-x_i)^2(\partial^2\Psi_2/\partial x^2)_{i,j} + (x-x_i)(y-y_j)(\partial^2\Psi_2/\partial x\partial y)_{i,j} +$$
$$+ \tfrac{1}{2}(y-y_j)^2(\partial^2\Psi_2/\partial y^2)_{i,j} + \cdots \qquad (3.6.1)$$

At the interface point (x_o^n, y_o^n), equation (3.6.1) gives us

$$\Psi_2(x_o^n, y_o^n) \approx \Psi_2)_{i,j} + (x_o^n - x_i)(\partial\Psi_2/\partial x)_{i,j} + (y_o^n - y_j)(\partial\Psi_2/\partial y)_{i,j} +$$

$$+ \tfrac{1}{2}(x_o^n - x)^2 (\partial^2\Psi_2/\partial x^2)_{i,j} + (x_o^n - x_i)(y_o^n - y_j)(\partial^2\Psi_2/\partial x\,\partial y)_{i,j} +$$

$$+ \tfrac{1}{2}(y_o^n - y_j)^2 (\partial^2\Psi_2/\partial y^2)_{i,j} \qquad (3.6.2)$$

The mesh point (x_i, y_j) is chosen as the nearest mesh point to the interface point (x_o^n, y_o^n) at which equation (3.6.2) is evaluated. The partial derivatives in equation (3.6.2) are approximated by second-order accurate central finite differences; from Appendix E, we have

$$(\partial\Psi_2/\partial x)_{i,j} \approx \left[\Psi_2)_{i+1,j} - \Psi_2)_{i-1,j}\right] / 2\Delta x \qquad (3.6.3a)$$

$$(\partial\Psi_2/\partial y)_{i,j} \approx \left[\Psi_2)_{i,j+1} - \Psi_2)_{i,j-1}\right] / 2\Delta y \qquad (3.6.3b)$$

$$(\partial^2\Psi_2/\partial x^2)_{i,j} \approx \left[\Psi_2)_{i+1,j} - 2\Psi_2)_{i,j} + \Psi_2)_{i-1,j}\right] / \Delta x^2 \qquad (3.6.3c)$$

$$(\partial^2\Psi_2/\partial y^2)_{i,j} \approx \left[\Psi_2)_{i,j+1} - 2\Psi_2)_{i,j} + \Psi_2)_{i,j-1}\right] / \Delta y^2 \qquad (3.6.3d)$$

$$\left.\frac{\partial^2\Psi_2}{\partial x\,\partial y}\right)_{i,j} \approx \frac{\Psi_2)_{i+1,j+1} - \Psi_2)_{i-1,j+1} - \Psi_2)_{i+1,j-1} + \Psi_2)_{i-1,j-1}}{4\,\Delta x\,\Delta y} \qquad (3.6.3e)$$

If the nearest mesh point (x_i, y_j) happens to be a boundary point, then equations (3.6.3) are centered about the point $(x_{i\pm1}, y_j)$ or $(x_i, y_{j\pm1})$, the first interior mesh point normal to the boundary. If the interface point $(x, y) = (x_o^n, y_o^n)$ lies on the boundary, then simple linear interpolation along the boundary

is used; for example, if (x_o^n, y_o^n) lies between (x_{i+1}, y_1) and (x_i, y_1) along the lower boundary of the flow region, then

$$\Psi_2(x_o^n, y_o^n) \approx \left[(x_{i+1}-x_o^n)\,\Psi_2)_{i,1} + (x_o^n - x_i)\,\Psi_2)_{i+1,1}\right] / \Delta x \qquad (3.6.4)$$

We can use equations (3.6.3) and (3.6.4) to determine Ψ_2 at each interface point. We can now determine the values of $q_x)_2$ and $q_y)_2$ at the interface points in one of two possible ways. In the first place, in the preceding section we determined finite-difference approximations to $q_x)_2$ and $q_y)_2$ at each mesh point. Thus we can treat the values of $q_x)_2$, for example, as constituting a scalar field, so that values of $q_x)_2$ at the interface points can be determined by interpolating between the values of $q_x)_2$ given at the mesh point. Hence, replacing Ψ_2 by $q_x)_2$ in equation (3.6.2), we get

$$\begin{aligned} q_x)_2\,[x_o^n, y_o^n] \approx\ & [q_x)_2]_{i,j} + (x_o^n - x_i)\,[\partial\, q_x)_2/\partial x]_{i,j} + \\ & + (y_o^n - y_i)\,[\partial q_x)_2/\partial y]_{i,j} + \tfrac{1}{2}(x_o^n - x_i)^2\,[\partial^2 q_x)_2/\partial x^2]_{i,j} + \\ & + (x_o^n - x_i)(y_o^n - y_i)\,[\partial^2 q_x)_2/\partial x\,\partial y]_{i,j} + \\ & + \tfrac{1}{2}(y_o^n - y_i)^2\,[\partial^2 q_x)_2/\partial y^2]_{i,j} \end{aligned} \qquad (3.6.5)$$

We can obtain approximations to the partial derivatives of $q_x)_2$ in equation (3.6.5) by replacing Ψ_2 by $q_x)_2$ in equations (3.6.3). Replacing $q_x)_2$ by $q_y)_2$ in equation (3.6.5), we obtain a formula for determining $q_y)_2$ at each interface point by interpolating between the values of $q_y)_2$ which are given at each mesh point.

Recall now that the values of $q_x)_2$ and $q_y)_2$ at each mesh point have been given by finite-difference approximations involving values of Ψ_2 at the mesh points. For example, from equation (3.5.1b), we have

$$q_x)_2]_{i,j} = -\partial \Psi_2 / \partial y)_{i,j}$$

$$\approx [\Psi_2)_{i,j-1} - \Psi_2)_{i,j+1}] / 2\Delta y \qquad (3.6.6)$$

Then, in equation (3.6.5), we get

$$\partial q_x)_2 / \partial x]_{i,j} \approx \{ q_x)_2]_{i+1,j} - q_x)_2]_{i-1,j} \} / 2\Delta x$$

$$\approx \{ [\Psi_2)_{i+1,j-1} - \Psi_2)_{i+1,j+1}] / 2\Delta y -$$

$$- [\Psi_2)_{i-1,j-1} - \Psi_2)_{i-1,j+1}] / 2\Delta y \} / 2\Delta x$$

$$= [\Psi_2)_{i+1,j-1} - \Psi_2)_{i+1,j+1} - \Psi_2)_{i-1,j-1} + \Psi_2)_{i-1,j+1}] / 4\Delta x \Delta y \qquad (3.6.7)$$

We can obtain similar expressions for the other derivatives in equation (3.6.5), so that $q_x)_2[x_o^n, y_o^n]$ can ultimately be expressed entirely in terms of values of Ψ_2 at mesh points.

From equations (3.6.2) and (3.6.3), the value of Ψ_2 at an interface point is defined by its values at the nine nearest mesh points (Fig. 3.6.1). If the value of $q_x)_2$ at an interface point is determined by equation (3.6.5), then $q_x)_2$ is given by the values of Ψ_2 at fifteen neighboring mesh points (Fig. 3.6.2). Similarly, the value of $q_y)_2$ at an interface point is given by the values of Ψ_2 at fifteen neighboring mesh points.

Figure 3.6.1. Mesh points used in interpolating Ψ_2 at the point $(x_o^n,\ y_o^n)$.

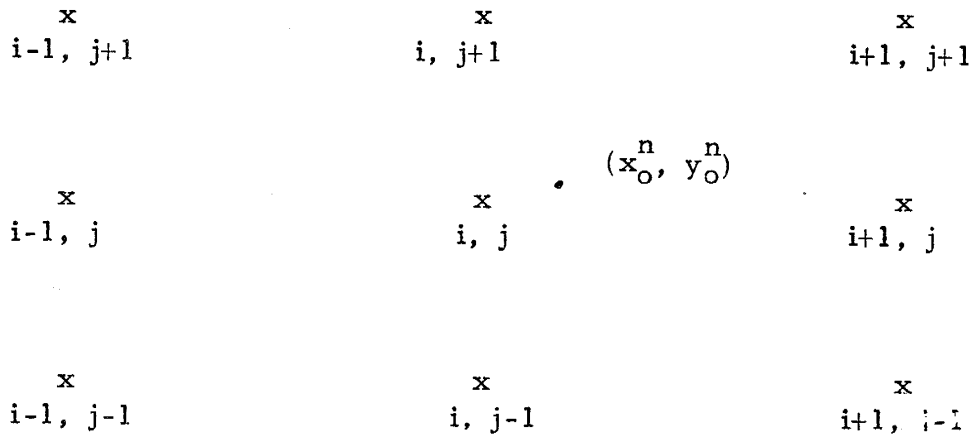
x
i-1, j+1
x
i, j+1
x
i+1, j+1
(x_o^n, y_o^n)
x
i-1, j
x
i, j
x
i+1, j
x
i-1, j-1
x
i, j-1
x
i+1, j-1

Figure 3.6.2. Mesh-point values of Ψ_2 used in interpolating $q(x)_2$ at the point (x_o^n, y_o^n).

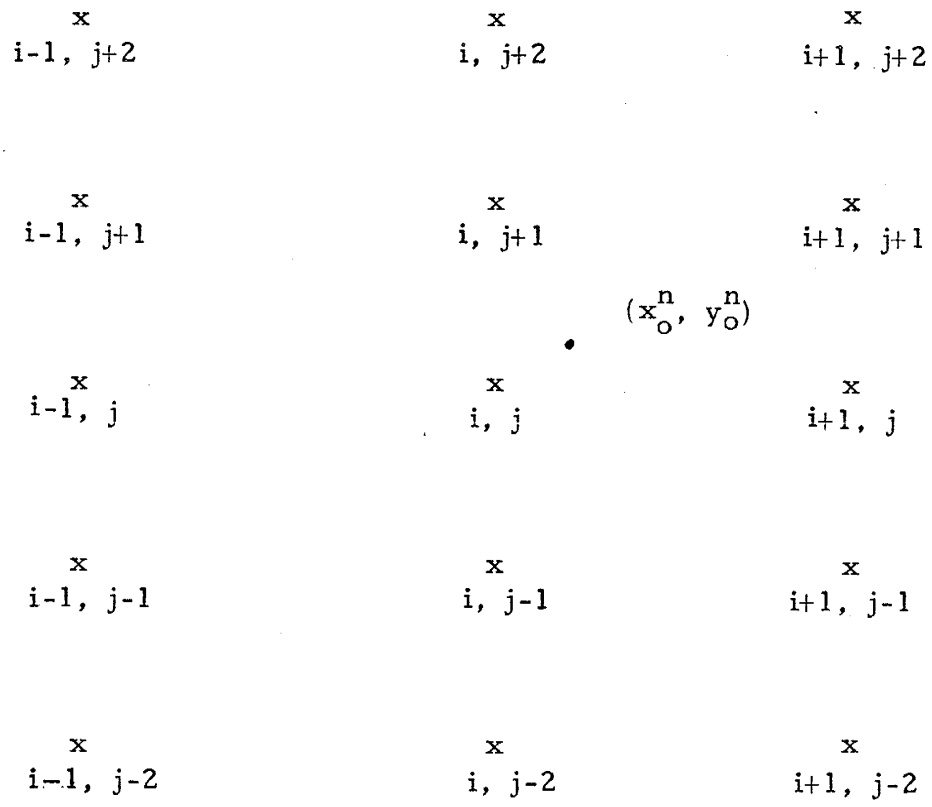
x
i-1, j+2
x
i, j+2
x
i+1, j+2
x
i-1, j+1
x
i, j+1
x
i+1, j+1
(x_o^n, y_o^n)
x
i-1, j
x
i, j
x
i+1, j
x
i-1, j-1
x
i, j-1
x
i+1, j-1
x
i-1, j-2
x
i, j-2
x
i+1, j-2

We can also try a second scheme for determining $q_x)_2$ and $q_y)_2$. This scheme is based on the fact that the interpolation formula (3.6.1) actually defines $\Psi_2(x, y)$ at every point in the flow region, not just the interface points. Thus equation (3.6.1) defines Ψ_2 as a continuous and differentiable function of x and y. Differentiating equation (3.6.1), we get

$$\partial\Psi_2/\partial x \approx (\partial\Psi_2/\partial x)_{i,j} + (x-x_i)(\partial^2\Psi_2/\partial x^2)_{i,j} + (y-y_j)(\partial^2\Psi_2/\partial x\,\partial y)_{i,j} \quad (3.6.8a)$$

and

$$\partial\Psi_2/\partial y \approx (\partial\Psi_2/\partial y)_{i,j} + (x-x_i)(\partial^2\Psi_2/\partial x\,\partial y)_{i,j} + (y-y_j)(\partial^2\Psi_2/\partial y^2)_{i,j} \quad (3.6.8b)$$

Thus, since $q_x)_2 = -\partial\Psi_2/\partial y$ and $q_y)_2 = \partial\Psi_2/\partial x$, we can use equations (3.6.3), with equations (3.6.8) evaluated at $(x, y) = (x_o^n, y_o^n)$, to determine $q_x)_2$ and $q_y)_2$ at the interface points. In this manner, $q_x)_2$ is given in terms of the values of Ψ_2 at only seven neighboring mesh points (Fig. 3.6.3). Similarly, $q_y)_2$ is given by the value of Ψ_2 at seven neighboring mesh points.

Although the alternate interpolation scheme for $q_x)_2$ and $q_y)_2$ given by equations (3.6.8) is somewhat more intuitively appealing than the preceding scheme, we must reject it because the resulting interface shape exhibits an oscillatory of "zig-zag" nature. Referring to Figure 3.6.3, we see that this undesirable

result is probably caused by the fact that this scheme, in calculating $q_x)_2$, does not appropriately take into account the variation of Ψ_2 in the x-direction. Similarly, the calculations for $q_y)_2$ do not appropriately take into account the variation of Ψ_2 in the y-direction.

Figure 3.6.3. Mesh-point values of Ψ_2 used in the alternate interpolation scheme for $q_x)_2$ at the point (x_o^n, y_o^n).

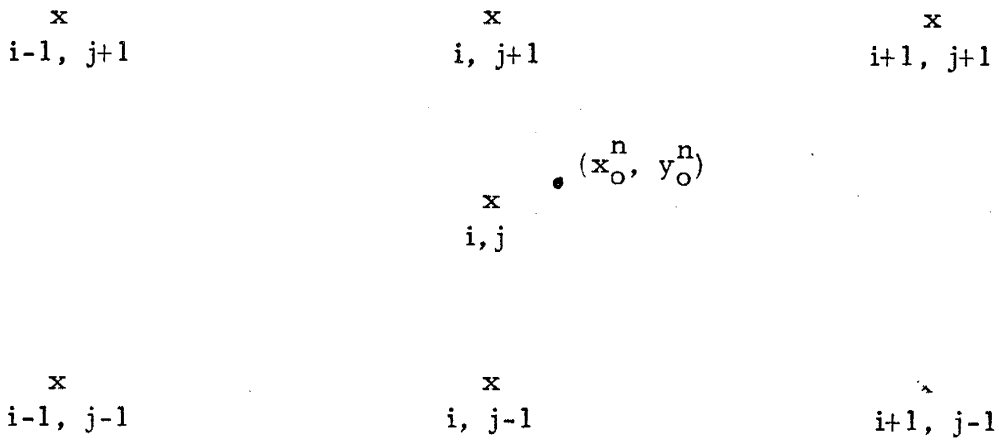
x
i-1, j+1
x
i, j+1
x
i+1, j+1
(x_o^n, y_o^n)
x
i, j
x
i-1, j-1
x
i, j-1
i+1, j-1

3.7 Movement of Interface Points

The final stage in the calculations gives the new position of each interface point. Let (x_n^{ℓ}, y_n^{ℓ}) denote the location of the n^{th} interface point at the end of time step ℓ, with

$$t^{\ell} = t_o + \sum_{m=1}^{\ell} \Delta t^m$$

$$= t^{\ell-1} + \Delta t^{\ell}$$

We wish to determine the location $(x_n^{\ell+1}, y_n^{\ell+1})$ of the n^{th} interface point at time $t^{\ell+1} = t^{\ell} + \Delta t^{\ell+1}$. In the preceding sections, we have described the determination of $(q_x)_1^n$, $(q_y)_1^n$, and $(q_x)_2^n$, $(q_y)_2^n$, where the subscripts 1 and 2 refer, respectively, to values determined from the vortex distribution along the interface and from the boundary conditions on the flow region, and the superscript n refers to the n^{th} interface point. The components of the local average velocity at the interface point (x_n^{ℓ}, y_n^{ℓ}) are then

$$u_n^{\ell} = \left[(q_x)_1^n + (q_x)_2^n \right] / \epsilon$$

$$v_n^{\ell} = \left[(q_y)_1^n + (q_y)_2^n \right] / \epsilon \quad ,$$

where ϵ is the porosity of the medium. Then

$$x_n^{\ell+1} = x_n^{\ell} + u_n^{\ell} \Delta t^{\ell+1}$$

$$y_n^{\ell+1} = y_n^{\ell} + v_n^{\ell} \Delta t^{\ell+1}$$

CHAPTER 4. SPECIAL PROCEDURES NEEDED TO TREAT THE BASIC CHECK PROBLEM

4.1 Introduction

The computer code combines both analytical and numerical methods, so it is difficult to perform a theoretical analysis of the accuracy of its results. Analyses of some of the individual parts of the code are presented in the appendices, but the overall behavior of the code can perhaps be best determined by comparing its results with theoretical and experimental results for a specific problem.

Consider the case of an initially vertical interface between two fluids of different specific weights but the same viscosity in a homogeneous porous medium (Fig. 4.1.1). Such a configuration is unstable, so that as time progresses the lighter fluid will override the heavier fluid, until the interface attains a stable horizontal shape. The results of parallel-plate model experiments (de Josselin de Jong, 1959, 1960) indicate that, at least relatively early in time, the interface has the general form of an S-shaped curve. The present computer model has been initially formulated to treat this problem, using as input data the same values of the physical parameters as were used in the parallel-plate model of de Josselin de Jong. The following sections describe some special features of the computer code

needed to treat this problem, as well as a brief analysis of the degree of mass conservation maintained by the code. Some of the techniques introduced in this chapter were motivated by the results of computational experimentation with the code; these techniques will be discussed in greater detail in Chapter 5.

Figure 4.1.1. Rotation of an initially vertical interface between two fluids of different specific weights.

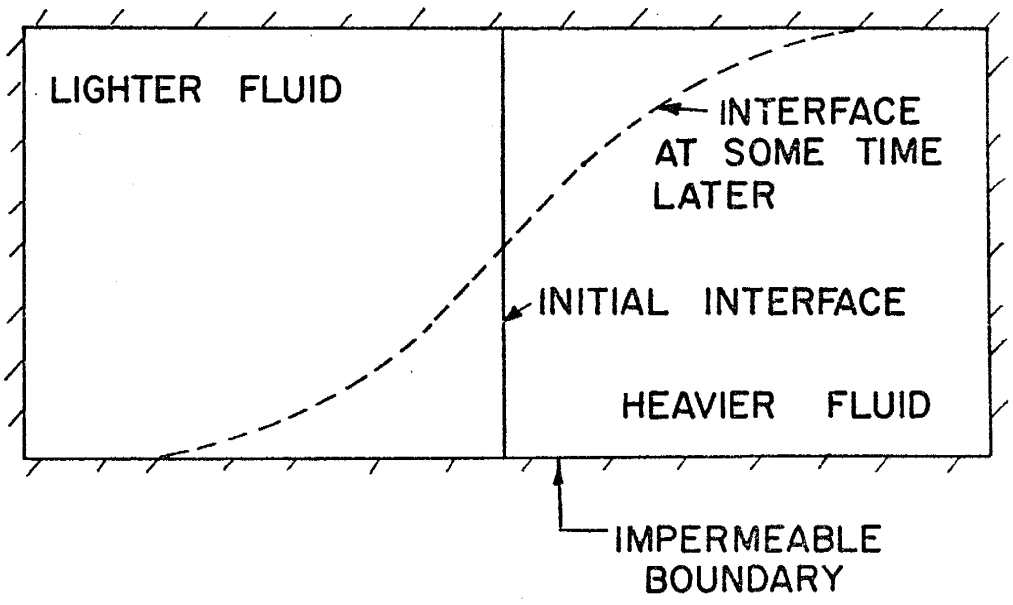
LIGHTER FLUID
INTERFACE AT SOME TIME LATER
INITIAL INTERFACE
HEAVIER FLUID
IMPERMEABLE BOUNDARY

4.2 Boundary Conditions

Boundary conditions, in general, will vary from problem to problem. In the present problem, the flow region is a rectangular area with impermeable boundaries. Continuity requires that the specific discharge be everywhere tangent to these boundaries, so that q_ν, the normal component of the discharge, must be zero at the boundaries. Otherwise, the fluid would flow across the boundary and out of the flow region, or it would flow away from the boundary into the flow region, producing gaps in the fluid at the boundary. Either of these situations is physically impossible. Thus our boundary conditions have the form

$$q_\nu = 0 , \tag{4.2.1}$$

or, applying equation (2.5.1b) and the fact that $\Psi = \Psi_1 + \Psi_2$,

$$\partial \Psi_1 / \partial s + \partial \Psi_2 / \partial s = 0. \tag{4.2.2}$$

Since equation (4.2.2) applies along a portion of the boundary where the normal coordinate is constant, we can integrate it directly to obtain

$$\Psi_1 + \Psi_2 = C . \tag{4.2.3}$$

C is an arbitrary constant of integration; choosing it to be zero, we obtain

$$\Psi_2 = - \Psi_1 . \tag{4.2.4}$$

Once Ψ_1 has been determined at all boundary mesh points, equation (4.2.4) defines values of Ψ_2 at those points, thus giving us a simple Dirichlet problem for Ψ_2. Ψ_2 can then be calculated directly by means of the formulas in Section 3.4.

However, the treatment of the flow at the boundaries proves to be somewhat more complicated than merely specifying boundary values for Ψ_2. In the first place, the interface is of finite length and terminates on the boundary. In order to describe adequately the motion of the interface endpoints, these points should be included in the basic set of interface points used to determine the interface fit. Thus, let (x_o^N, y_o^N) denote the interface point lying on the upper boundary of the flow region, and let the N^{th} tangent line segment have slope σ_N, with $0 < |\sigma_N| \leq \infty$ (Fig. 4.2.1). We seek to determine q_x and q_y at (x_o^N, y_o^N). Since the interface terminates at (x_o^N, y_o^N), the integrals in equations (3.3.18) and (3.3.19) must have y_o^N, rather than y_2^N, as their upper limit. Thus we get

$$q_x)_1^N = -\frac{\partial \Psi_1}{\partial y} \propto \begin{cases} -\frac{\sigma_N^2}{2(1+\sigma_N^2)} \ln\left[\frac{(x-x_o^N)^2}{(x-x_1^N)^2}\right] + \frac{\sigma_N}{1+\sigma_N^2}(\pm\pi), & 0<|\sigma_N|<\infty \quad (4.2.5a) \\ \frac{1}{2}\ln\left[\frac{(y-y_1^N)^2}{(y-y_o^N)^2}\right], & |\sigma_N| = \infty \quad (4.2.5b) \end{cases}$$

Figure 4.2.1. Interface points at the upper end of the interface, n = N.

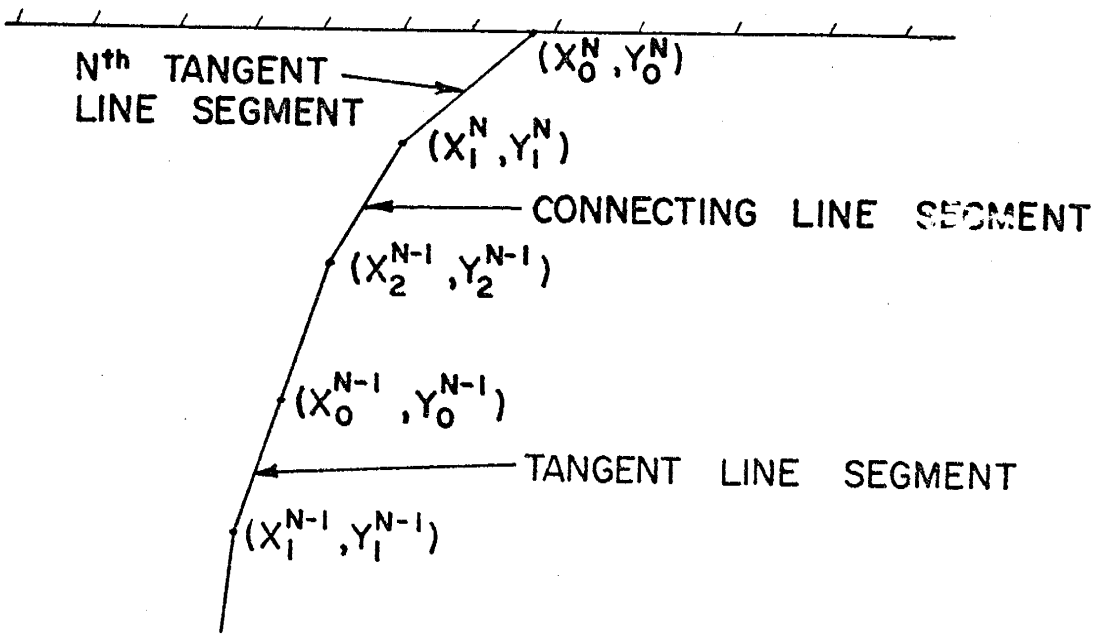
N^{th} TANGENT LINE SEGMENT
(X_0^N, Y_0^N)
(X_1^N, Y_1^N)
CONNECTING LINE SEGMENT
(X_2^{N-1}, Y_2^{N-1})
(X_0^{N-1}, Y_0^{N-1})
TANGENT LINE SEGMENT
(X_1^{N-1}, Y_1^{N-1})

$$q_y)_1^N = \frac{\partial \Psi_1}{\partial x} \propto \begin{cases} -\frac{\sigma_N}{2(1+\sigma_N^2)} \ln\left[\frac{(x-x_o^N)^2}{(x-x_1^N)^2}\right] - \frac{\sigma_N}{1+\sigma_N^2}(\pm\pi), & 0<|\sigma_N|<\infty \quad (4.2.6a) \\ 0, & |\sigma_N| = \infty \quad (4.2.6b) \end{cases}$$

Evaluating equations (4.2.5) and (4.2.6) at $x = x_o^N$ and $y = y_o^N$, we obtain infinite logarithmic singularities in the specific discharge components at this point. However, these logarithmic singularities do not occur if $\sigma_N = 0$, because then, from equations (3.3.18b) and (3.3.19b), $q_x)_1^N$ and $q_y)_1^N$ are both zero. Similar results apply at the interface point (x_o', y_o') lying on the lower boundary.

In order to avoid these logarithmic singularities, the slopes σ_1 and σ_N of the tangent line segments passing through the endpoints of the interface fit are taken to be zero. This is equivalent to assuming that the interface is always horizontal at a boundary of the flow region. This assumption is consistent with the observed S-shaped nature of the interface curve, as well as the fact that the final shape of the interface should be entirely horizontal.

An additional refinement to the treatment at the boundaries is motivated by the results of computational experimentation using the techniques described above. The values of the specific discharge components at the boundary are given by

$$q_x = q_x)_1 + q_x)_2 , \quad (4.2.7a)$$

$$q_y = q_y)_1 + q_y)_2 . \quad (4.2.7b)$$

By equation (4.2.1), on the upper and lower boundaries of the flow region, q_y should be zero. The results of computational experimentation show that this is the case at each boundary mesh point except the two points immediately adjacent to the interface endpoint on each boundary, where the calculated values of q_y are not zero. This discrepancy is probably due to the truncation error involved in the finite-difference approximations used to determine $q_y)_2$. Furthermore, by this approach, the interface curve gradually develops inflection points near the boundaries, so that the expected S-shaped nature of the curve is not seen (Fig. 4.2.2).

Correct specific discharge components can be obtained at all points of the boundary by making two modifications to the basic approach outlined in Section 3.6. The first modification is merely to set

$$q_v)_2 = - q_v)_1$$

at each boundary mesh point, so that $q_v = 0$ everywhere on the boundary. This is done prior to the point in the computer program at which values of Ψ_2, $q_x)_2$, and $q_y)_2$ are interpolated at the interface points, so that the interpolation routine uses correct values of $q_x)_2$ and $q_y)_2$ at the boundary mesh points. In this way, we obtain correct values of q_v at the boundary mesh points. Furthermore, the interface points on the boundary move more

rapidly along the boundary, so that the S-shaped nature of the curve is maintained, although no significant change in shape is seen for about the central third of the curve.

The second modification involves the introduction of image interfaces reflected in the upper and lower boundaries (Fig. 4.2.3). The vortices on the image interfaces have the opposite direction from those on the true interface. The line integrals used to calculate Ψ_1, $q_x)_1$, and $q_y)_1$ are taken over the length of the interface and both images. The algorithms used for calculating Ψ_2, $q_x)_2$, and $q_y)_2$ are not changed by this procedure.

An image vortex outside the flow region will produce a change in the value of Ψ_1 calculated at a point inside the flow region, as well as at each point on the boundary. The resultant change in the boundary conditions for Ψ_2 gives a change in Ψ_2 such that the total stream function $\Psi = \Psi_1 + \Psi_2$ at a point within the flow region is not affected by the presence of vortices along the image interfaces. Similarly, the specific discharge components at points within the flow region are not affected by the image interfaces. The only net effect of the image interfaces is at each boundary interface point, where the opposite directions of the true interface vortices and the image vortices produces specific discharge vectors which are strictly tangent to the boundaries. Thus, it is not necessary that the images be reflections of the entire interface ; only the first four or five interfacial line segments

need be reflected in the lower boundary, and the last four or five segments reflected in the upper boundary.

Figure 4.2.2. Interface shape at later times resulting from unmodified treatment of boundary conditions.

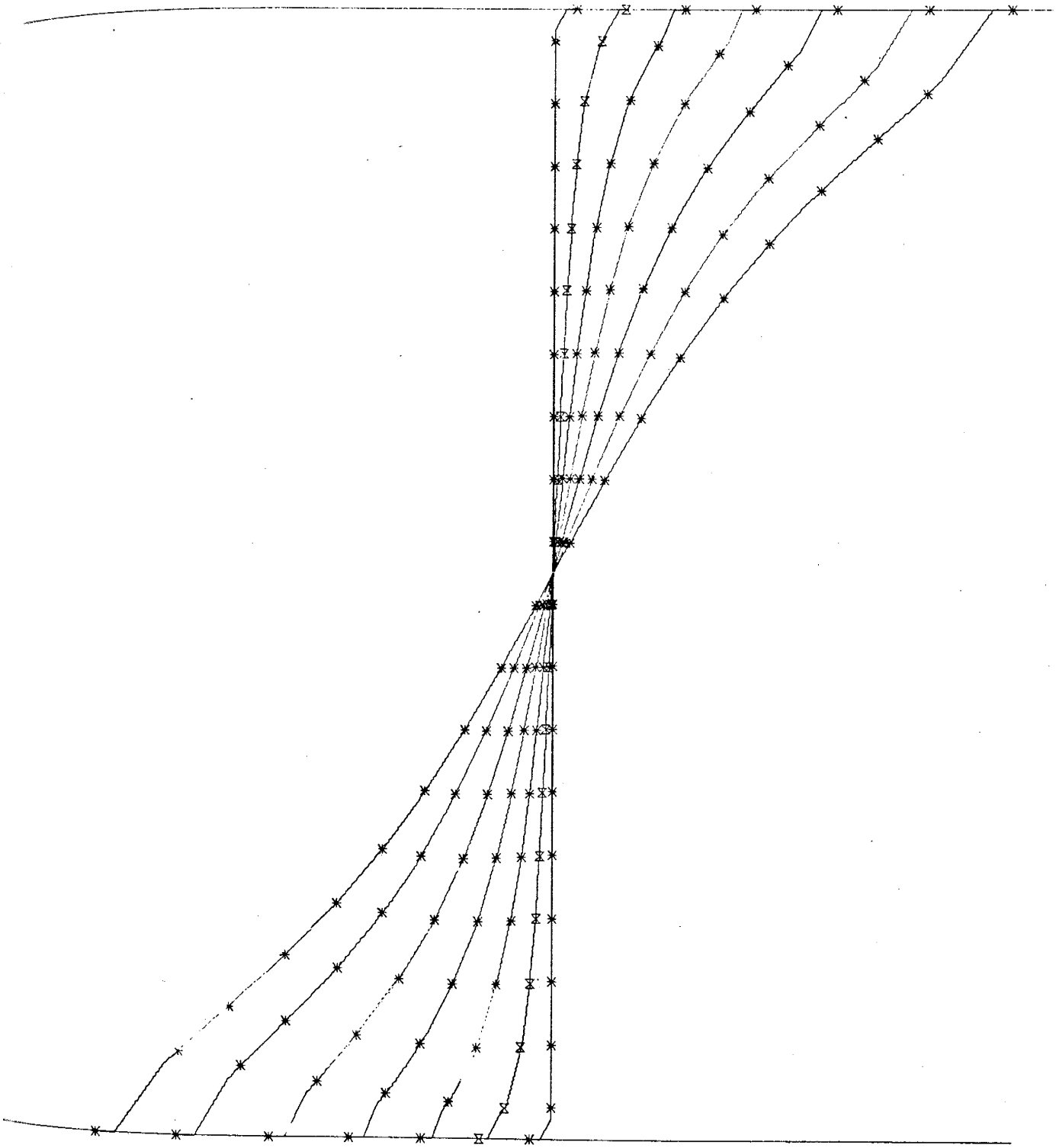

Figure 4.2.3. Definition of image interfaces introduced to produce correct boundary conditions.

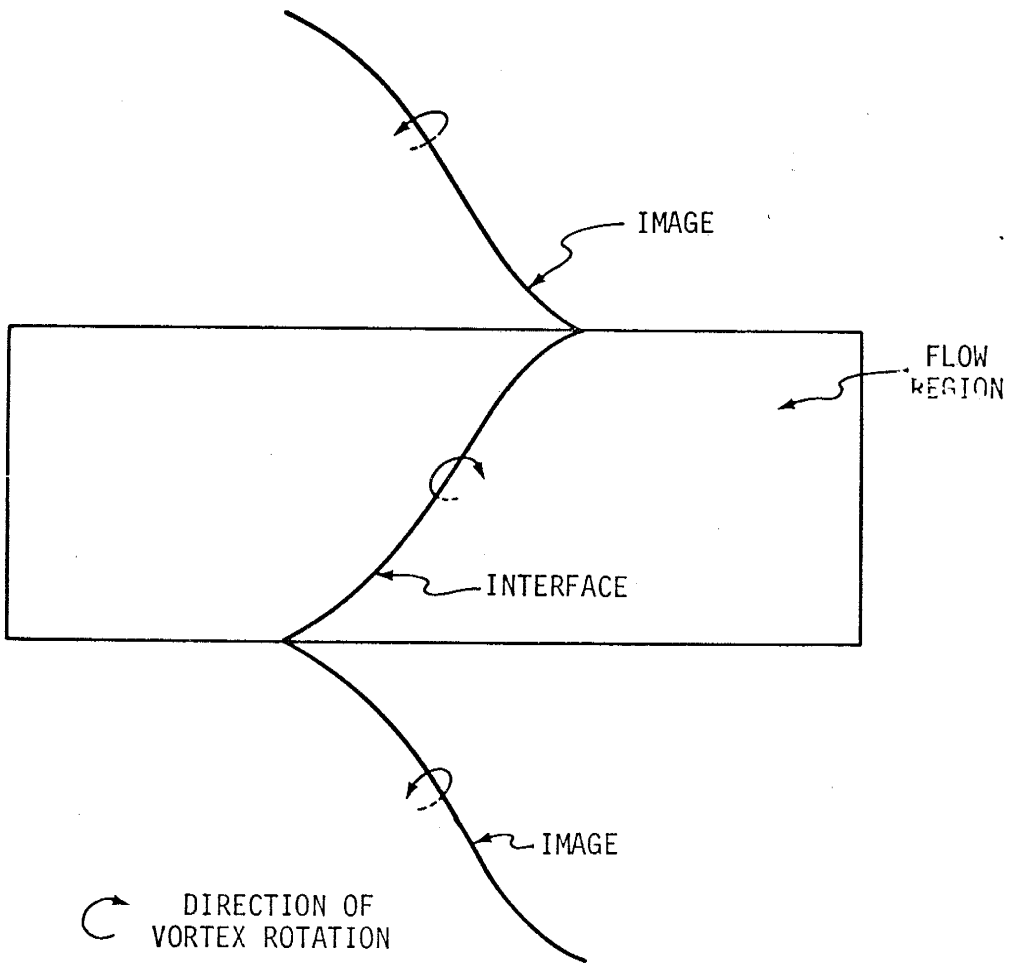
IMAGE
FLOW
REGION
INTERFACE
IMAGE
DIRECTION OF
VORTEX ROTATION

4.3 Initial Conditions

Initially, the interface is a vertical straight line. However, if we take the initial interface curve in the computer model to be a vertical straight line, we cannot calculate the initial specific discharge components at the boundary interface points (x_o^1, y_o^1) and (x_o^N, y_o^N). From equation (4.2.5b), we see that $q_x)_1^N$, and similarly $q_x)_1^1$, have infinite logarithmic singularities in such a case. We can get around this difficulty by starting the computer model at some very small time δt after zero, such that the boundary interface points have moved a very small distance along the boundary, while all the other interface points still lie along the initial vertical interface (Fig. 4.3.1). In this way, we can take the tangent line segments at (x_o^1, y_o^1) and (x_o^N, y_o^N) to be horizontal at the initial time. Then we can apply the formulas of Section 3.4 at the initial time, and we do not obtain the infinite logarithmic singularities in the specific discharge.

Figure 4.3.1. The initial interface configuration used in the computer code.

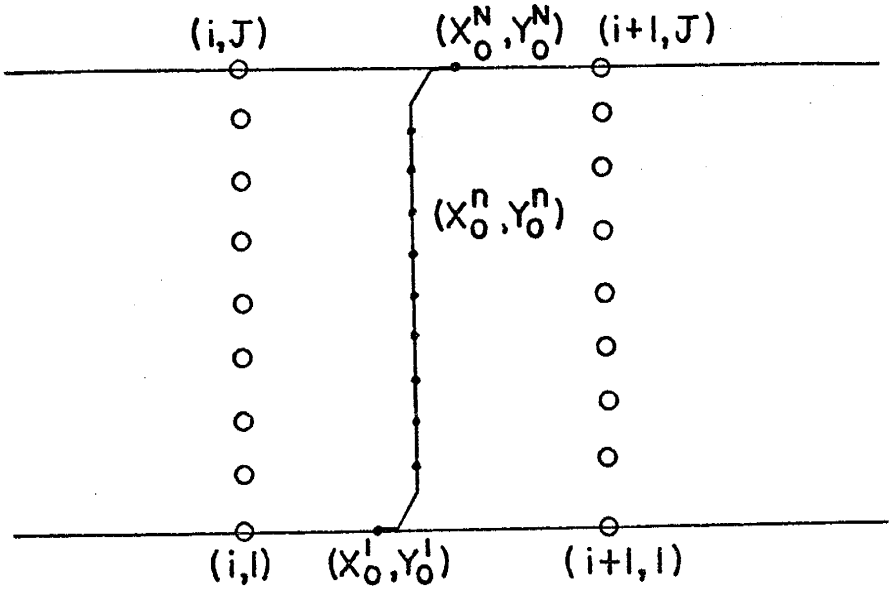
(i,J)
(X_0^N, Y_0^N)
(i+1,J)
(X_0^n, Y_0^n)
(i,1)
(X_0^1, Y_0^1)
(i+1,1)
o MESH POINTS
• INTERFACE POINTS

4.4 Length of the Tangent Interfacial Line Segments

In the present formulation of the computer code, the lengths of all the tangent line segments have been chosen to be equal. Furthermore, the interface points are more closely spaced near the ends of the interface, where the maximum curvature occurs, than near the center. For this formulation, the shape and rate of motion of the interface are rather sensitive to the half-length δ chosen for the tangent interfacial line segments. As discussed in more detail in Chapter 5, computational experimentation indicates that the optimum value of δ is of the order of 0.01 cm, approximately one percent of the mesh spacing $\Delta x = \Delta y = 1.5$ cm. For values of δ significantly less than 0.01 cm, round-off error causes the interface to develop an oscillatory or "zig-zag" shape, which grows with time, although the rate of rotation of the central portion of the interface remains close to the theoretical rate of rotation. For values of δ significantly greater than 0.01 cm, the interface rapidly becomes highly unstable, with the interface points moving in seemingly random directions, some of them actually leaving the flow region. This behavior is caused by the fact that near the ends of the interface, where the interface points are closely spaced, some of the points can move to within 2δ of each other, so that the tangent and connecting line segments overlap. Such a configuration is physically impossible, and is highly unstable.

These problems can be lessened somewhat by making a few changes in the present code. Some of the effects of round-off error can be diminished by reprogramming certain statements in the code. The half-length δ of the tangent line segments can be made a function of the spacing of the interface points, rather than taken as a constant. Nevertheless, as seen in Chapter 5, the present formulation of the code does a reasonably good job of reproducing the interface motion for the basic check problem.

4.5 Mass Conservation

For this basic check problem, we can quite simply determine the degree of mass conservation maintained by the code. Since the flow region is finite, and since there should be no net gain or loss of fluid by the system, the total mass of heavier fluid in the system should remain constant. Furthermore, since the specific weight of the heavier fluid is constant, the fluids are assumed to be incompressible, and the medium is assumed to be nondeformable, the total volume occupied by this fluid should remain constant. Finally, since the porosity of the medium is constant, and because of the two-dimensional symmetry of the problem, the volume occupied by the heavier fluid is directly proportional to the area of the flow region occupied by the fluid. We can readily determine this area by merely integrating the interface curve in order to find the area under the curve. The difference between the initial area of the heavier fluid and the area at any later time is generally less than 0.001%.

We should note, however, that this result only shows that the computed interface exhibits symmetry with respect to a pivot point located at the center of the flow region. Such symmetry is also demonstrated by computer plots of the interface at successive times. This does not prove that the computed interface curve is absolutely correct, but it does show that the code does not generate any abnormal "drift" of any of the interface points.

REFERENCES

de Josselin de Jong, G., Vortex theory for multiple phase flow through porous media, Water Resources Center Contribution 23, 80 pp., Hydraulic Laboratory, University of California, Berkeley, 1959.

de Josselin de Jong, G., Singularity distributions for the analysis of multiple-fluid flow through porous media, Journal of Geophysical Research, 65, 3739, 1960.

CHAPTER 5. SOLUTION OF THE BASIC CHECK PROBLEM

5.1 Introduction

The basic check problem was described briefly in Chapter 4. The flow region is a rectangle in the vertical x, y-plane, with its sides aligned parallel to the x- and y-axes. The boundaries of the flow region are impermeable, and the porous medium within the flow region is isotropic and homogeneous. At the initial instant, a vertical interface at the center of the rectangle separates two fluids of different specific weights, with the lighter fluid to the left of the interface. Because of the difference in the specific weights of the two fluids, gravity causes the interface to rotate in a clockwise direction, until the interface attains a stable horizontal configuration. Parallel-plate model experiments (de Josselin de Jong, 1960) indicate that, at least early in time, the general form of the interface is that of an S-shaped curve.

In the present chapter, we will consider some analytical solutions to this problem, as well as the results of parallel-plate model experiments. We will then consider the solution to this problem by means of the computer technique which has been discussed in previous chapters, and compare the computer solution with the analytical and experimental studies. The discussion of the computer solution will include examination of some of the computational experimentation which led to modifications

of the basic computer model.

5.2 Analytical Solutions

Initial distribution of specific discharge. Analytical solutions have been determined for a modified form of the basic problem (de Josselin de Jong, 1959, 1960). In the modified problem, the flow region is an infinite strip in the x, y-plane (Fig. 5.2.1), rather than a rectangle. The strip has width 2c, and is symmetrical with respect to the x-axis. An analytical solution for the initial specific distribution can be obtained in closed form by applying complex analysis. The x, y-plane can be interpreted as the complex z-plane, with any point in the plane being uniquely determined by its complex coordinate $z = x + iy$, where $i^2 = -1$. By means of the transformation

$$z = (2c/\pi) \ln \zeta , \qquad (5.2.1)$$

the infinite strip in the z-plane is mapped onto the right half of the $\zeta = \xi + i\eta$ plane (Fig. 5.2.2). The boundaries of the flow region in the x-plane are mapped onto the η-axis of the ζ-plane, and the interface is mapped onto the semicircle $|\zeta| = 1$ in the ζ-plane. The components of the specific discharge in the ζ-plane can be readily determined to be (de Josselin de Jong, 1959, 1960)

$$q_x = -\frac{k(\gamma_2-\gamma_1)}{2\pi/\mu} \ln \left[\frac{\xi^2+(\eta-1)^2}{\xi^2+(\eta+1)^2}\right] \qquad (5.2.2a)$$

$$q_y)_1 = \frac{k(\gamma_2-\gamma_1)}{\pi/\mu} (\varphi_1 - \pi) \qquad (5.2.2b)$$

$$q_y)_2 = -\frac{k(\gamma_2-\gamma_1)}{\pi\mu}(2\pi - \psi_2) \qquad (5.2.2c)$$

where $\psi_i = \tan^{-1}[(\eta+1)/\xi] - \tan^{-1}[(\eta-1)/\xi]$,

with $\pi \le \psi_1 \le 3\pi/2$ and $3\pi/2 \le \psi_2 \le 2\pi$.

The subscripts 1 and 2 here refer to the y-components of the specific discharge in the regions ofthe lighter and heavier fluids, respectively. Applying the transformation (5.2.1), the components in the z-plane become

$$q_x = -\frac{k(\gamma_2-\gamma_1)}{2\pi\mu}\ln\left[\frac{\cosh(\pi x/2c) - \sin(\pi y/2c)}{\cosh(\pi x/2c) + \sin(\pi y/2c)}\right] \qquad (5.2.3a)$$

$$q_y)_1 = \frac{k(\gamma_2-\gamma_1)}{\pi\mu}\left\{\tan^{-1}\left[\frac{\sin(\pi y/2c) + e^{-\pi x/2c}}{\cos(\pi y/2c)}\right] - \tan^{-1}\left[\frac{\sin(\pi y/2c) - e^{-\pi x/2c}}{\cos(\pi y/2c)}\right] - \pi\right\} \qquad (5.2.3b)$$

$$q_y)_2 = -\frac{k(\gamma_2-\gamma_1)}{\pi\mu}\left\{2\pi - \tan^{-1}\left[\frac{\sin(\pi y/2c) + e^{-\pi x/2c}}{\cos(\pi y/2c)}\right] + \tan^{-1}\left[\frac{\sin(\pi y/2c) - e^{-\pi x/2c}}{\cos(\pi y/2c)}\right]\right\} \qquad (5.2.3c)$$

The initial specific-discharge vectors given by equations (5.2.3) are shown in Figure 5.2.3.

Initial displacement of the interface. In general, the displacement of the interface can be given by the local average velocity normal to the interface. Since the initial position of the interface is vertical, the velocity normal to the interface is given by q_x/ϵ, where q_x is the x-component of the specific discharge, given by equation (5.2.3a), and ϵ is the porosity of the medium. Evaluating equation (5.2.3a) at x=0, and simplifying, we get

$$\frac{dx_o}{dt} = \frac{k(\gamma_2-\gamma_1)}{\epsilon\pi\mu}\ln\left\{\cot\left[\frac{\pi(c-y_o)}{4c}\right]\right\}, \qquad (5.2.4)$$

where the subscript o indicates a value at the interface. The initial velocity dx_o/dt as a function of y_o is shown in Figure 5.2.4; the S-shaped curve shown there is representative of the shape of the interface at a small time after zero.

Approximate rate of rotation of the interface. An analytical solution cannot be obtained for the shape of the interface at any time greater than zero, so the general motion of the interface cannot be determined exactly. However, an approximate solution for the rate of motion of the interface can be determined under the assumption that the interface maintains a linear shape (Fig. 5.2.5). Let the inclination of the interface at any time $t > 0$ be $\alpha = \cot^{-1} a$, so that the equation of the interface is

$$x_o = y_o \cot\alpha = a\, y_o . \qquad (5.2.5)$$

The rate of rotation of the linear interface is then given implicitly by the equation (de Josselin de Jong, 1959)

$$[k(\gamma_2-\gamma_1)/\epsilon\mu c]\, t = 2\int_{\alpha}^{\pi/2} \{1/[\sin^2\alpha \cdot \sin(2\alpha-\beta)]\}\, d\alpha , \qquad (5.2.6)$$

where $\beta = \cot^{-1}[\sinh(\pi a/2c)]$. A general solution to the integral in equation (5.2.6) cannot be obtained, but numerical step-by-step evaluation of the integral gives the curve shown in Figure 5.2.6 for the inclination α of the interface as a function of time.

Figure 5.2.1. Infinite confined aquifer in the z-plane (de Josselin de Jong, 1959).

Figure 5.2.2. Transformed infinite confined aquifer in the ζ-plane (de Josselin de Jong, 1959).

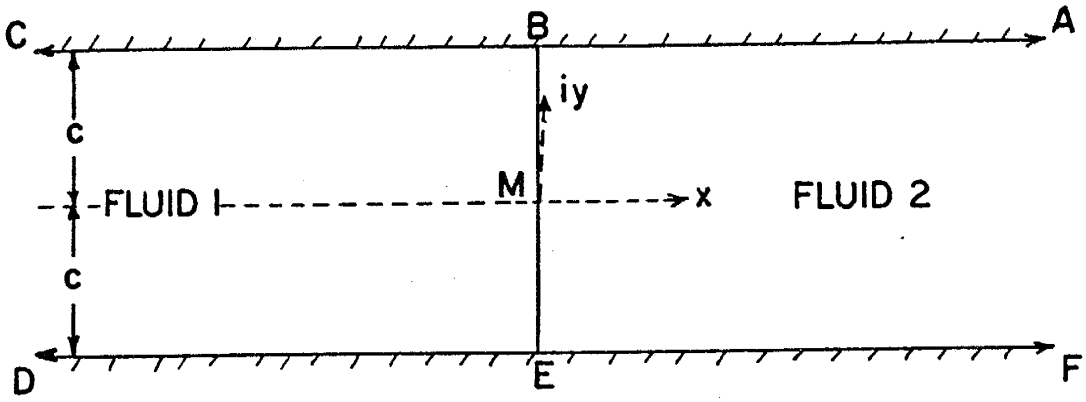
C
B
A
iy
c
FLUID 1
M
x
FLUID 2
c
D
E
F

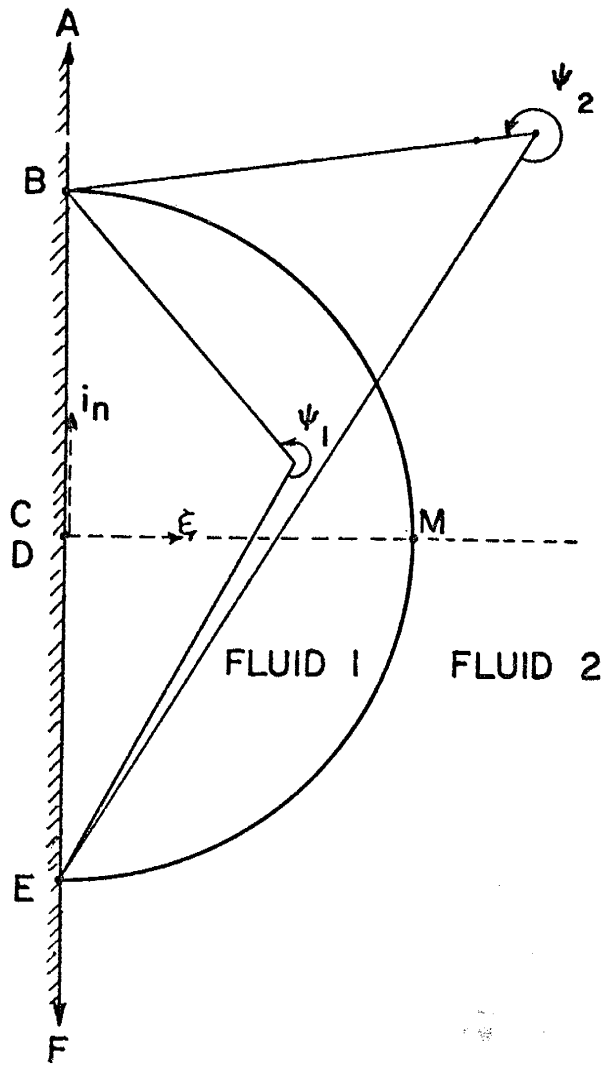
A
ψ2
B
in
ψ1
C
D
ξ
M
FLUID 1
FLUID 2
E
F

Figure 5.2.3. Discharge vectors at time t = 0

(de Josselin de Jong, 1959).

Figure 5.2.4. Distribution of discharge normal to interface

(de Josselin de Jong, 1959).

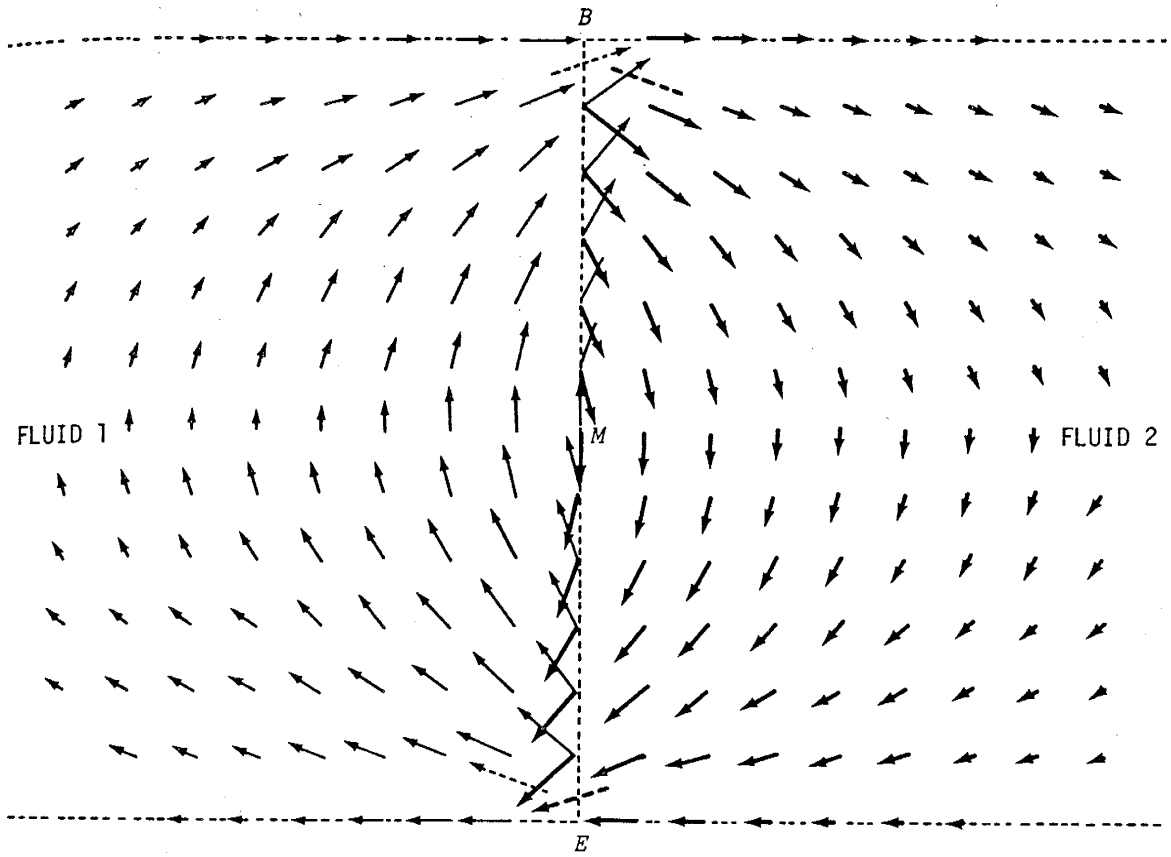
B
FLUID 1
M
FLUID 2
E

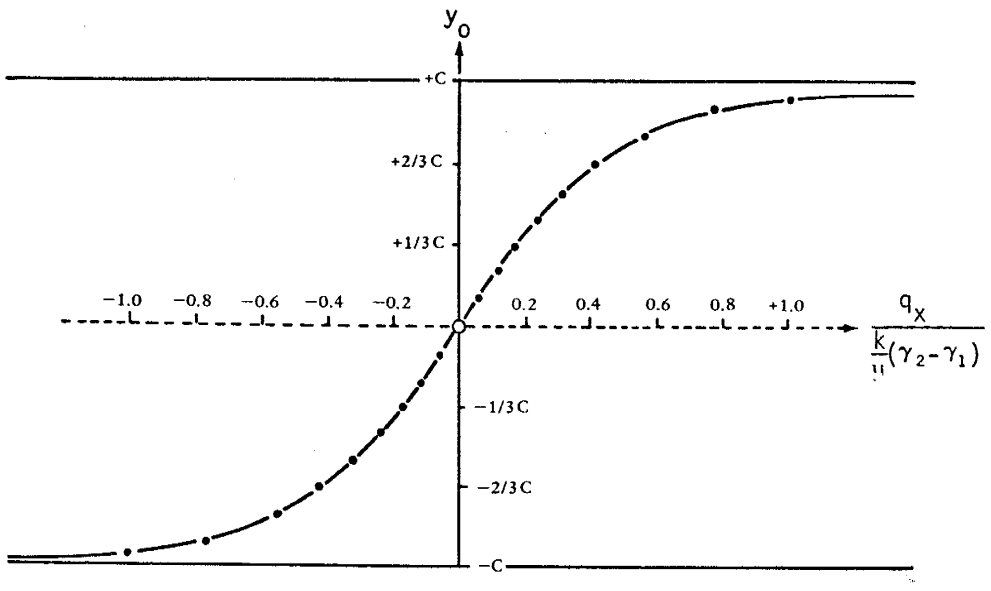
y_0
+C
+2/3 C
+1/3 C
−1.0
−0.8
−0.6
−0.4
−0.2
0.2
0.4
0.6
0.8
+1.0
q_x
$\frac{k}{u}(\gamma_2-\gamma_1)$
−1/3 C
−2/3 C
−C

Figure 5.2.5. Approximate linear interface (de Josselin de Jong, 1959).

Figure 5.2.6. Slope of linear interface as a function of time (de Josselin de Jong, 1959).

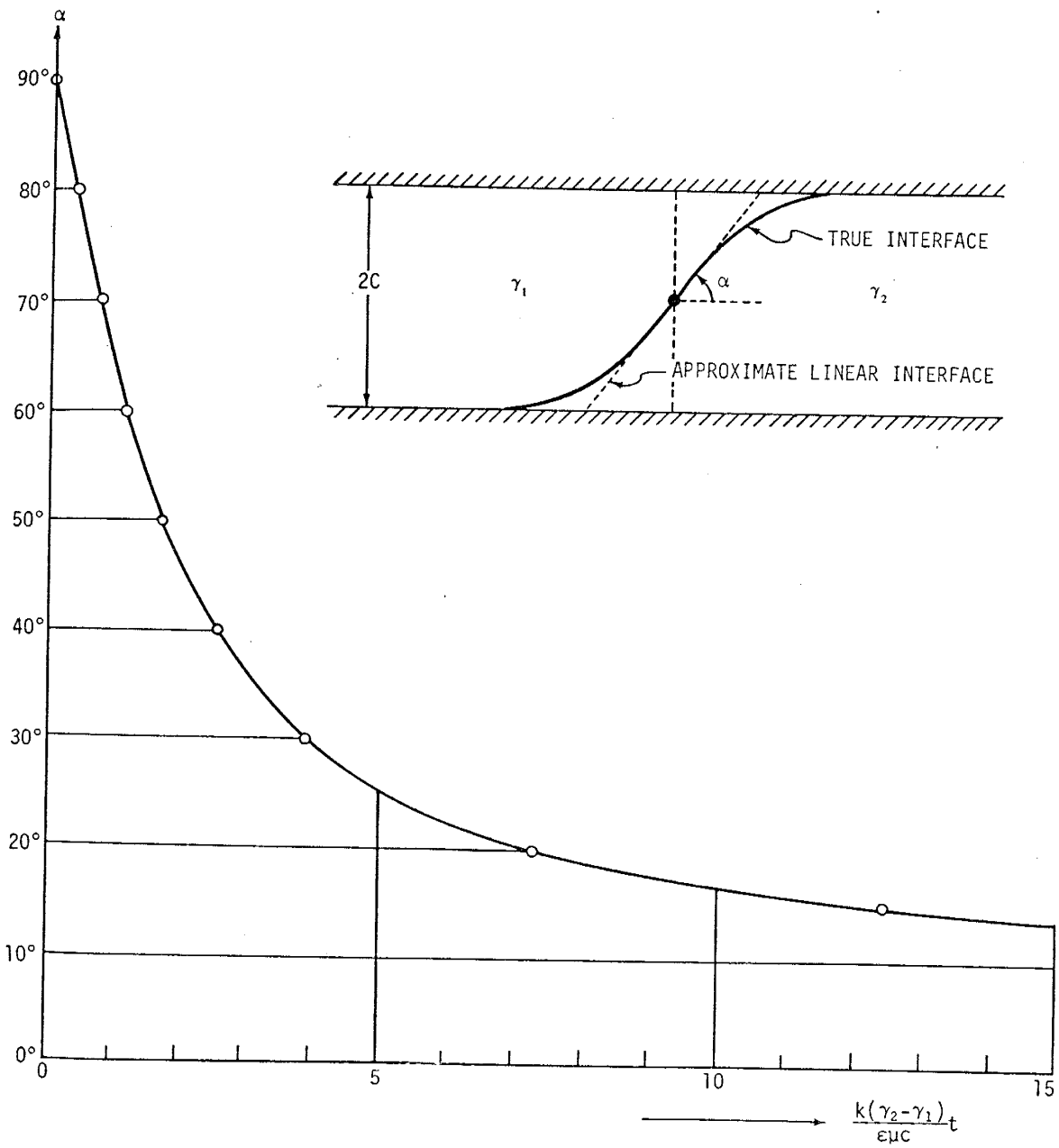
α
90°
80°
70°
60°
50°
40°
30°
20°
10°
0°
0
5
10
15
$\frac{k(\gamma_2-\gamma_1)}{\varepsilon\mu c}t$
2C
γ_1
γ_2
α
TRUE INTERFACE
APPROXIMATE LINEAR INTERFACE

5.3 Parallel-Plate Model Study

The analytical results summarized above were verified by de Josselin de Jong (1960) by means of parallel-plate model experiments. The model was a 15 x 60 cm Lucite rectangle, with a slot width of d = 1 mm. The fluid to the left of the initial interface was glycerine of density 1.23 g/cm^3, or specific weight γ_1 = 1205.4 dynes/cm^3, and the fluid to the right of the interface was a mixture of 60% glycerine and 40% phosphoric acid of density 1.40 g/cm^3, or specific weight γ_2 = 1372.0 dynes/cm^3. The viscosity of each fluid at 24°C was μ =490 centipoises = 4.90 dyne sec/cm^2. The porosity of the parallel-plate model was ϵ = 1, and the permeability was $k = d^2/12 = 8.3 \times 10^{-4}$ cm^2. For these parameters, the coefficient of t in equation (5.2.6) is $k(\gamma_2 - \gamma_1)/\epsilon\mu c = 0.00376$ sec^{-1}.

The fluids in the model contained suspended gold-leaf flakes; because of their large surface-thickness ratio, the flakes had a small settling velocity with respect to the velocity of the fluid itself. The model was photographed for periods of 90 seconds, so that the gold-leaf flakes appear as dark streaks on a lighter background (Fig. 5.4.10). The length and orientation of each streak reflects the average velocity vector in that region during the 90-second period of exposure. In the vicinity of the interface, the streaks cross one another because of the shear flow at the interface; these crossing paths are also shown in Figure 5.2.3.

The crossing paths of the particles lead to a dark band in the photographs, representative of the average position of the interface during the 90-second period of exposure.

Qualitatively, as can be seen from Figure 5.4.10 and the phtographs presented by de Josselin de Jong (1960), the S-shaped interface predicted by equation (5.2.4) is clearly visible in the parallel-plate model. Quantitatively, the results of the model experiment are more difficult to interpret. Since an analytical solution was not obtained for the specific discharge distribution at any time greater than zero, the discharge vectors reflected by the particle streaks in photographs of the model cannot be verified. However, the rate of rotation of the central portion of the model interface can be compared with the theoretical rate of rotation given by equation (5.2.6), as is done in Figure 5.3.1. From that figure, it appears that the model interface rotates more rapidly than would be expected from the theory, although the theoretical slope is only about 10% greater than the observed slope at 165 seconds. This apparent discrepancy will be examined more thoroughly in Section 5.4, where the results of the numerical model can also be considered.

Figure 5.3.1. Interface slope as a function of time.

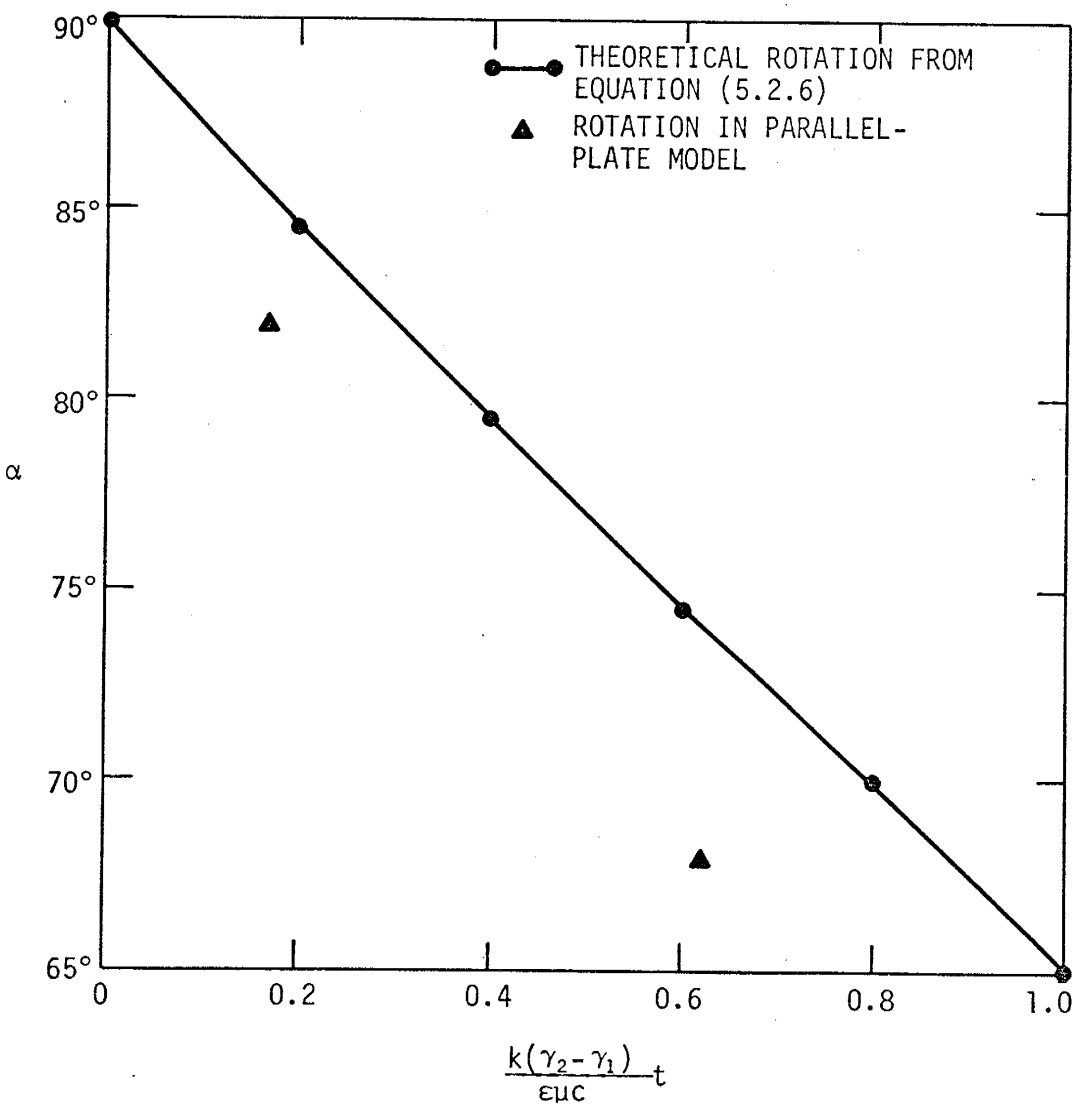
90°
85°
80°
75°
70°
65°
α
0
0.2
0.4
0.6
0.8
1.0
THEORETICAL ROTATION FROM EQUATION (5.2.6)
ROTATION IN PARALLEL-PLATE MODEL
$\frac{k(\gamma_2-\gamma_1)}{\varepsilon\mu c}t$

5.4 Computer Model Study

Introduction. The mathematical procedures for describing interface motion which were discussed in Chapters 3 and 4 have been programmed for numerical calculation by digital computer. Descriptions of the program and its use, including data input and output routines and formats, are given in Appendix G. Appendix H is a listing of the FORTRAN digital computer program.

Table 5.4.1 gives a list of the parameters occuring in the mathematical formulation, their corresponding FORTRAN symbols, and their values used in the computer code. Portions of the computer program, such as the treatment of initial and boundary conditions, are problem-dependent; they are presently formulated so that the program is a direct simulation of the parallel-plate experiment discussed in Section 5.3. The rectangular region simulated is 15 cm in height and 31.5 cm in length. Although this is only about one half the length of the parallel-plate experiment, the numerical model should give a reasonably accurate reproduction of the physical model for early time, before the influence of the lateral boundaries is felt significantly. The numerical values of all other parameters are the same as those for the parallel-plate model. Note here that the values listed for the specific weights γ_1 and γ_2 are actually the values of the densities of the two fluids used in the physical

model, and the value listed for the viscosity is actually μ/g, where g is the acceleration due to gravity. Since these parameters always occur in the ratio $(\gamma_2 - \gamma_1)/\mu$, no problem is caused by this convention. The values used here are those given by de Josselin de Jong (1960).

Computational experimentation. The computational experimentation consisted of running the computer program and observing the results in order to test various parts of the formulation. The results of the computer program were presented as values of the coordinates of the interface points, values of the stream function and specific discharge components at each mesh point and each interface point, and computer-generated plots of the interface shape. These results were computed for various times. The results were interpreted according to the qualitative motion of the plotted interface, as well as the computed rate of rotation of the interface.

Some of the results of the computational experimentation were discussed in Chapter 3. The combined linear-parabolic interface fit was rejected because of the observed motion of the computed interface, which began to show inflection points as time progressed (Sections 3.2 and Fig. 3.2.3). One of the interpolation routines for determining $q_x)_2$ and $q_y)_2$ was tested by computational experimentation and was rejected

because the computed interface shape exhibited an oscillatory or "zig-zag" nature (Section 3.6). In those cases, the computational experimentation resulted in the rejection of proposed techniques, and thus will not be considered further. However, computational experimentation also resulted in some techniques which have become important parts of the computer model, and those results will be considered further in this section.

A. Treatment of Boundary Conditions

The initial formulation of the computer program was based entirely on the techniques outlined in Chapter 3. In particular, the discharge at the boundary of the flow region was given by $\vec{q} = \vec{q}_1 + \vec{q}_2$, where $\vec{q}_1$ is the specific discharge vector arising from the distribution of vortices along the interface, and $\vec{q}_2$ is the discharge vector given by the boundary conditions. According to the boundary condition(4.2.1), the discharge component q_y should be zero at every point on the upper and lower boundaries of the flow region. However, the results of computer runs made with the basic treatment of the boundary conditions indicated that the computed values of q_y were zero at every mesh point except the two mesh points on either side of the interface endpoints (Fig. 5.4.1). This discrepancy can be attributed to the truncation error inherent in the finite-difference approximations used for calculating $q_x)_2$ and $q_y)_2$.

Table 5.4.1. Input values of physical parameters for numerical simulation of the basic check problem.

Math. Symbol	FORTRAN Symbol	Input Value	Description
I	IMX	22	Number of finite-difference nodes in x-direction
J	JMX	11	Number of finite-difference nodes in y-direction
N	NMAX	Variable	Number of interface points
k	PERM	0.0008	Permeability of parallel-plate model, cm^2
γ_1	GAM1	1.23	Normalized specific weight (density) of lighter fluid, g/cm^3
γ_2	GAM2	1.40	Normalized specific weight (density) of heavier fluid, g/cm^3
μ	VIS	0.005	Normalized viscosity of fluids, g sec/cm^2
ω	OMEGA	1.30	Relaxation parameter, nondimensional
t_o	TIME	0.0	Initial time, sec
Δt	DT	5.0	Time increment, sec
c	CBND	7.5	Half-width of model, cm
None	XIN	0.0	x-coordinate of initial vertical interface, cm
x_o^n, y_o^n	XO(N), YO(N)	Variable	Coordinates of interface points, cm

Table 5.4.1. Continued.

Math. Symbol	FORTRAN Symbol	Input Value	Description
x_i, y_j	X(I), Y(J)	Variable	Coordinates of finite-difference mesh points, cm
x_1	X(1)	-15.75	x-coordinate of lower left point of numerical model, cm
y_1	Y(1)	-7.5	y-coordinate of lower left point of numerical model, cm
Δx	DX	1.5	Mesh spacing in x-direction, cm
Δy	DY	1.5	Mesh spacing in y-direction, cm

Figure 5.4.1. Specific discharge components along horizontal boundaries.

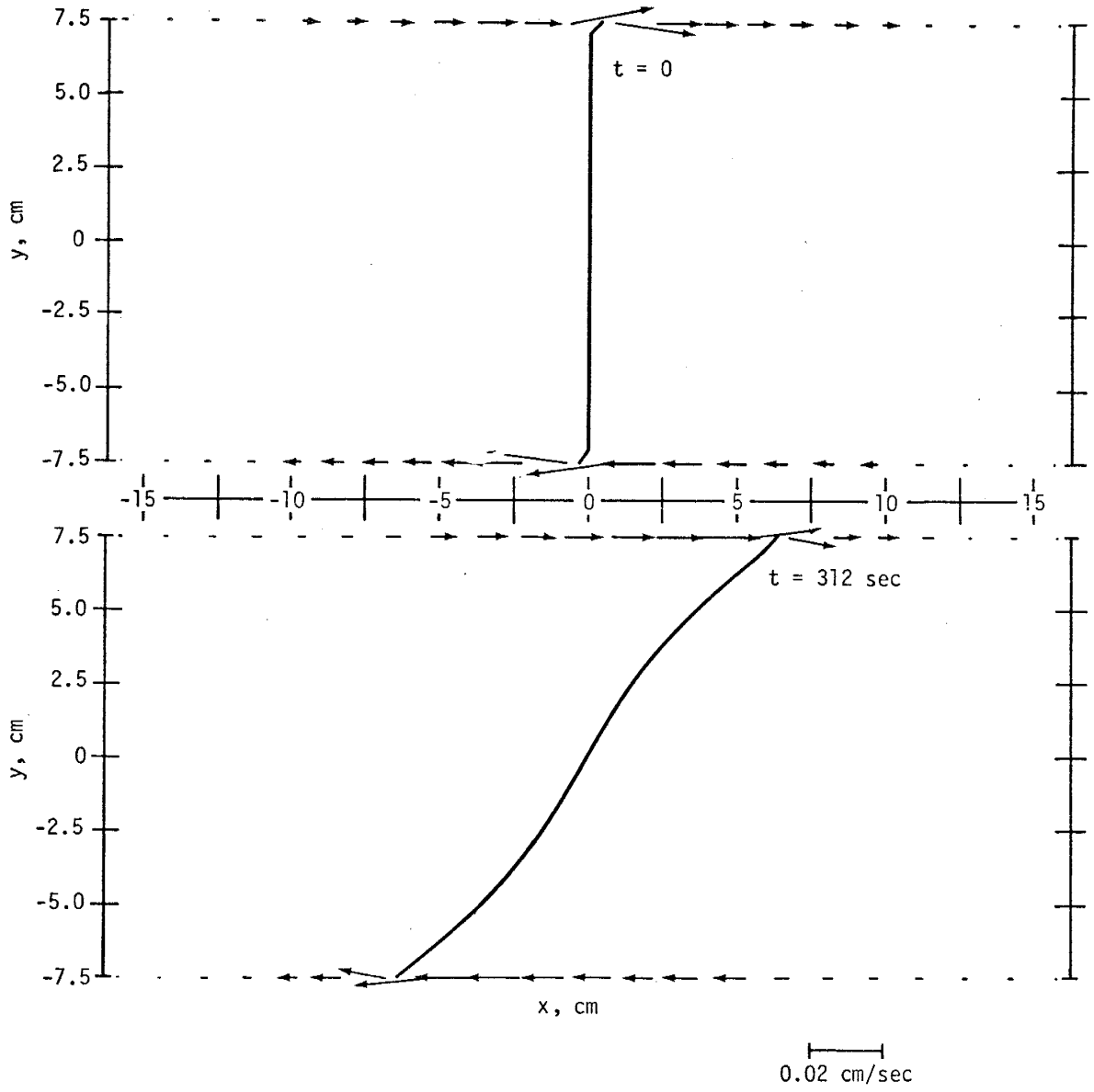
7.5
5.0
2.5
0
-2.5
-5.0
-7.5
y, cm
t = 0
-15
-10
-5
0
5
10
15
t = 312 sec
x, cm
0.02 cm/sec

The first approach used to rectify this problem was a rather artificial one, consisting of merely setting $q_y)_2 = - q_y)_1$ at all boundary mesh points, where q_y denotes the component of the specific discharge normal to the boundary. This was done prior to interpolating values of $q_x)_2$ and $q_y)_2$ at the interface points, so that the interpolation routine made use of correct values of $q_y)_2$ along the boundaries. This approach gave correct values of $q_y = 0$ along the horizontal boundaries of the flow region, while producing no noticeable change in the values of Ψ, q_x, or q_y at interior mesh points. However, since this was a rather artificial solution to the problem, a more realistic approach was sought.

The boundary treatment adopted in the final version of the code makes use of image interfaces, as discussed briefly in Chapter 4. Using the image interfaces, correct values of $q_y = 0$ were again obtained at all mesh points on the upper and lower boundaries of the flow region. However, since this approach is based on physical principles rather than a computational artifice, it can be used with much more confidence. Computational experimentation also indicated that the lengths of the image interfaces had relatively little effect on the interface motion. The values of the stream function and specific discharge components differed by no more than 5% if the entire interface was reflected in the upper and lower boundaries, or if only the first

four or five interfacial line segments were reflected in the boundaries.

B. Choice of Tangent Line Segment Length

In the present version of the computer code, the lengths of all tangent line segments have been chosen to be equal. The half-length of a tangent line segment is denoted by δ. Computational experimentation indicated that the shape and motion of the computed interface were rather sensitive to the value chosen for δ, with the motion becoming unstable for $\delta < 0.01$ cm and $\delta > 0.05$ cm. For $\delta < 0.01$ cm, the interface began to exhibit an oscillatory or "zig-zag" shape which gradually grew as time progressed, but which was symmetrical with respect to the midpoint of the interface (Fig. 5.4.2). For $\delta > 0.05$ cm, the interface rapidly became very ragged, with some interface points moving in seemingly random directions (Fig. 5.4.3). This section presents a summary of analyses used to determine the causes of the observed anomalous behavior of the computed interface.

The behavior of the computed interface for $\delta < 0.01$ cm was determined to have been caused by round-off error resulting from inefficient programming of certain statements in the code. This was determined by examining a simple system consisting of a single tangent line segment and two connecting line segments, as shown in Figure 5.4.4. The velocity at the interface point

(x_2, y_2) has a contribution from the vortices distributed along each of the three line segments:

$$\vec{V} = \vec{V}_1 + \vec{V}_t + \vec{V}_2$$

$$= \hat{\imath}(u_1 + u_t + u_2) + \hat{\jmath}(v_1 + v_t + v_2)$$

$$= K\left[\hat{\imath}(u_1^* + u_t^* + u_2^*) - \hat{\jmath}(v_1^* + v_t^* + v_2^*)\right],$$

where $K = k(\gamma_2 - \gamma_1)/(4\pi\mu\epsilon) = 2.16 \times 10^{-3}$ cm/sec for the simulation of the parallel-plate model experiment. The subscripts 1 and 2 refer to the lower and upper connecting line segments, respectively, and the subscript t refers to the tangent line segment. We confine our attention to the components u_t and v_t since, omitting the shear discontinuity in $\vec{V}$ as was done in the code, u_t and v_t should theoretically be identically zero.

Values of u_t^*, v_t^*, u_t, and v_t were calculated for various values of δ, using the routine from the computer code for interface motion. For small δ, u_t^* and v_t^* were both greater than zero, and decreased as δ increased. After the values of u_t^* and v_t^* had decreased to an order of 10^{-7}, they were computed by the computer as being identically zero. Similarly, the computed values of u_t and v_t were greater than zero for small δ, and decreased as δ increased. The values of u_t and v_t decreased to an order of 10^{-7} for δ approximately equal to 0.01 cm, which is the order of δ for which the computed interface motion is stable.

Figure 5.4.2. Interface motion for δ = 0.005 cm.

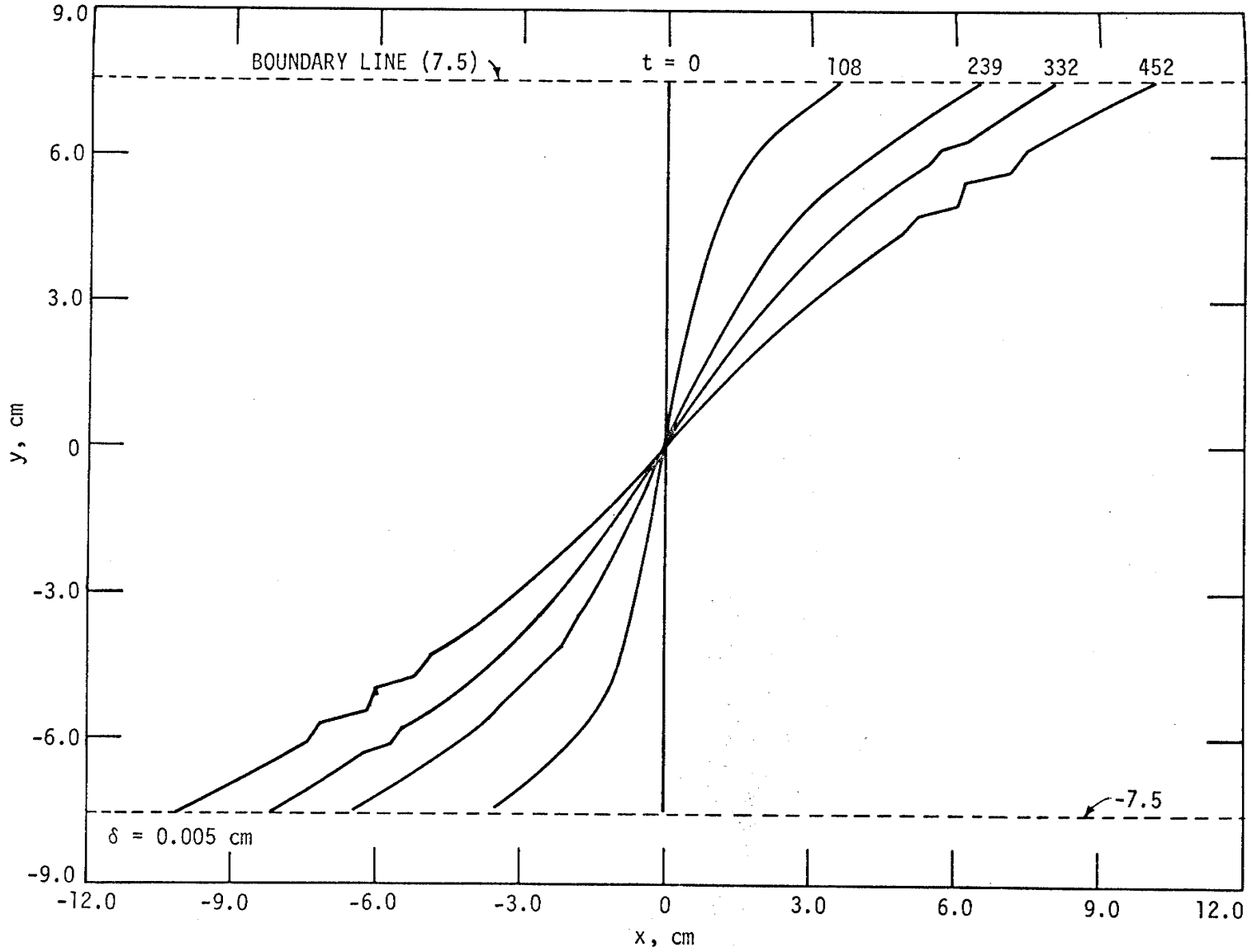
9.0
6.0
3.0
0
-3.0
-6.0
-9.0
BOUNDARY LINE (7.5)
t = 0
108
239
332
452
-7.5
δ = 0.005 cm
-12.0
-9.0
-6.0
-3.0
0
3.0
6.0
9.0
12.0
y, cm
x, cm

Figure 5.4.3. Interface motion for δ = 0.1 cm.

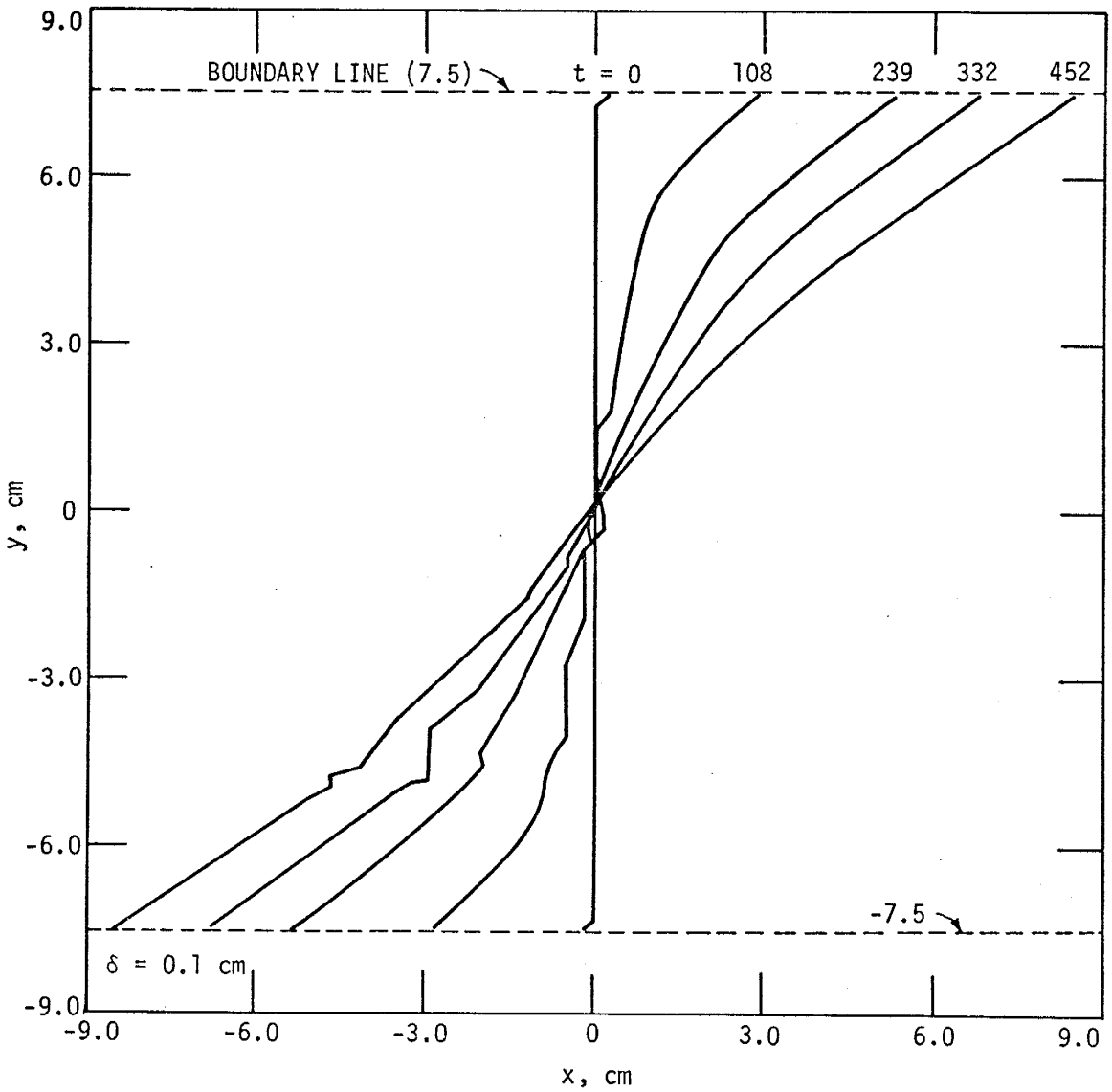
9.0
6.0
3.0
0
-3.0
-6.0
-9.0
BOUNDARY LINE (7.5)
t = 0
108
239
332
452
-7.5
δ = 0.1 cm
-9.0
-6.0
-3.0
0
3.0
6.0
9.0
y, cm
x, cm

Figure 5.4.4. Simple interface fit for analysis of effects of variable δ .

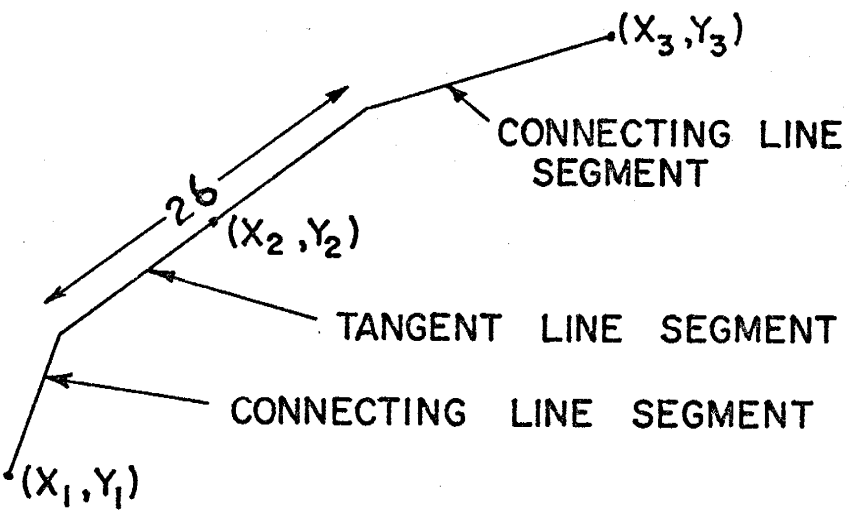
(X_3, Y_3)
CONNECTING LINE SEGMENT
2b
(X_2, Y_2)
TANGENT LINE SEGMENT
CONNECTING LINE SEGMENT
(X_1, Y_1)

The question remains why the computed values of u_t and v_t were not all identically zero. This question can be answered by examining the FORTRAN coding of the statements used to compute those velocity components. Both u_t and v_t are proportional to the quantity

$$\ln\left\{\frac{\left[\left(x_2 + \delta/\sqrt{1+m^2}\right) - x_2\right]^2}{\left[\left(x_2 - \delta/\sqrt{1+m^2}\right) - x_2\right]^2}\right\}, \qquad (5.4.1)$$

where m is the slope of the tangent line segment. In both the numerator and denominator of (5.4.1), the expression is coded so that the operation in parentheses is carried out before the operation in brackets is carried out. When δ is small, the operations within the brackets in (5.4.1) consist of subtracting two numbers which are nearly equal in value. This is the least accurate operation which can be carried out, with regard to round-off error, on the digital computer. The expression (5.4.1) should be identically zero, because the argument of the logarithm should be identically unity. However, when δ is small, the argument of the logarithm deviates slightly from unity because of the round-off error, and thus the logarithm deviates slightly from zero. Apparently, the expression (5.4.1) should have been coded so that the order of the operations was reversed.

The cause of the behavior of the computed interface motion for $\delta > 0.05$ cm was obscured during some of the computational experimentation because of the manner in which the interface

position was plotted. Rather than showing all tangent line segments and all connecting line segments, the plotted interface consisted only of straight line segments connecting the interface points. A more detailed look at the computed interface immediately reveals the problem. Figure 5.4.5 shows the complete interface fit, including tangent line segments and connecting line segments, for the lower four interface points at t = 5 seconds. For δ = 0.01 cm, the interface fit is fairly smooth and approximates the lower end of an S-shaped curve. However, for δ =0.1 cm, the tangent line segments at the second and third interface points are too long, so that their endpoints overlap and the interface fit attains an unstable configuration. For δ = 0.05 cm, the second tangent line segment does not appear to have a large enough slope. The slope of the second tangent line segment was taken as the arithmetic mean of the slopes of lines drawn between the first and second and between the second and third interface points. In the present case, because of the location of the first interface point (dictated by the initial condition, see Section 4.3), the slope of the line between it and the second point is too small; hence the average slope is also too small.

Figure 5.4.6 shows the complete interface fit to four interface points located near the center of the interface. In this case, δ = 0.1 cm and t = 239 seconds. Again, it is apparent that the two central tangent line segments are too long. Furthermore,

Figure 5.4.5. Complete interface fit to four lower interface points at t = 5 seconds.

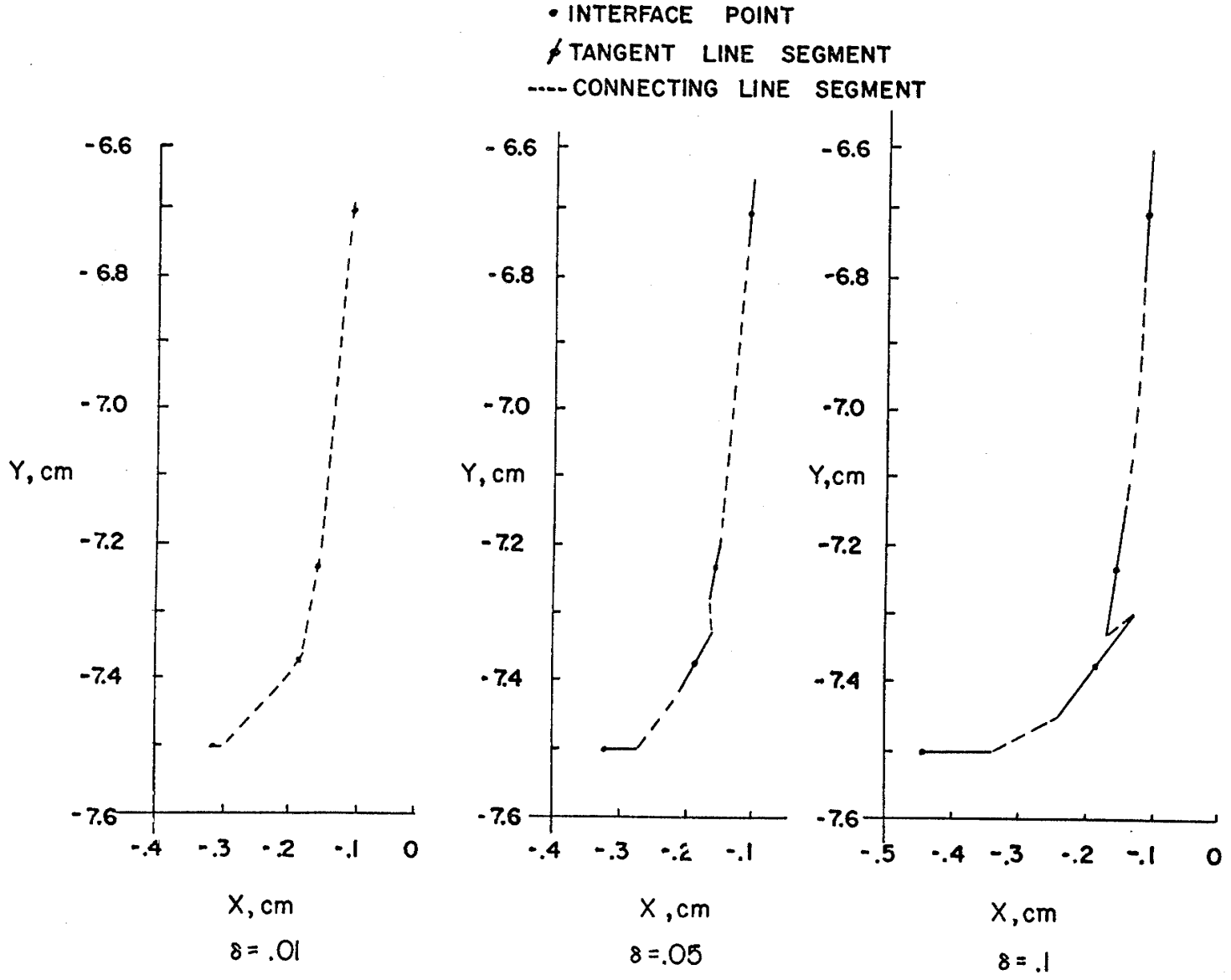
• INTERFACE POINT
TANGENT LINE SEGMENT
---- CONNECTING LINE SEGMENT
-6.6
-6.8
-7.0
-7.2
-7.4
-7.6
Y, cm
-.4
-.3
-.2
-.1
0
X, cm
δ = .01
-.5
X, cm
δ = .05
δ = .1

Figure 5.4.6. Complete interface fit to four central interface points. t = 239 seconds, δ = 0.1 cm

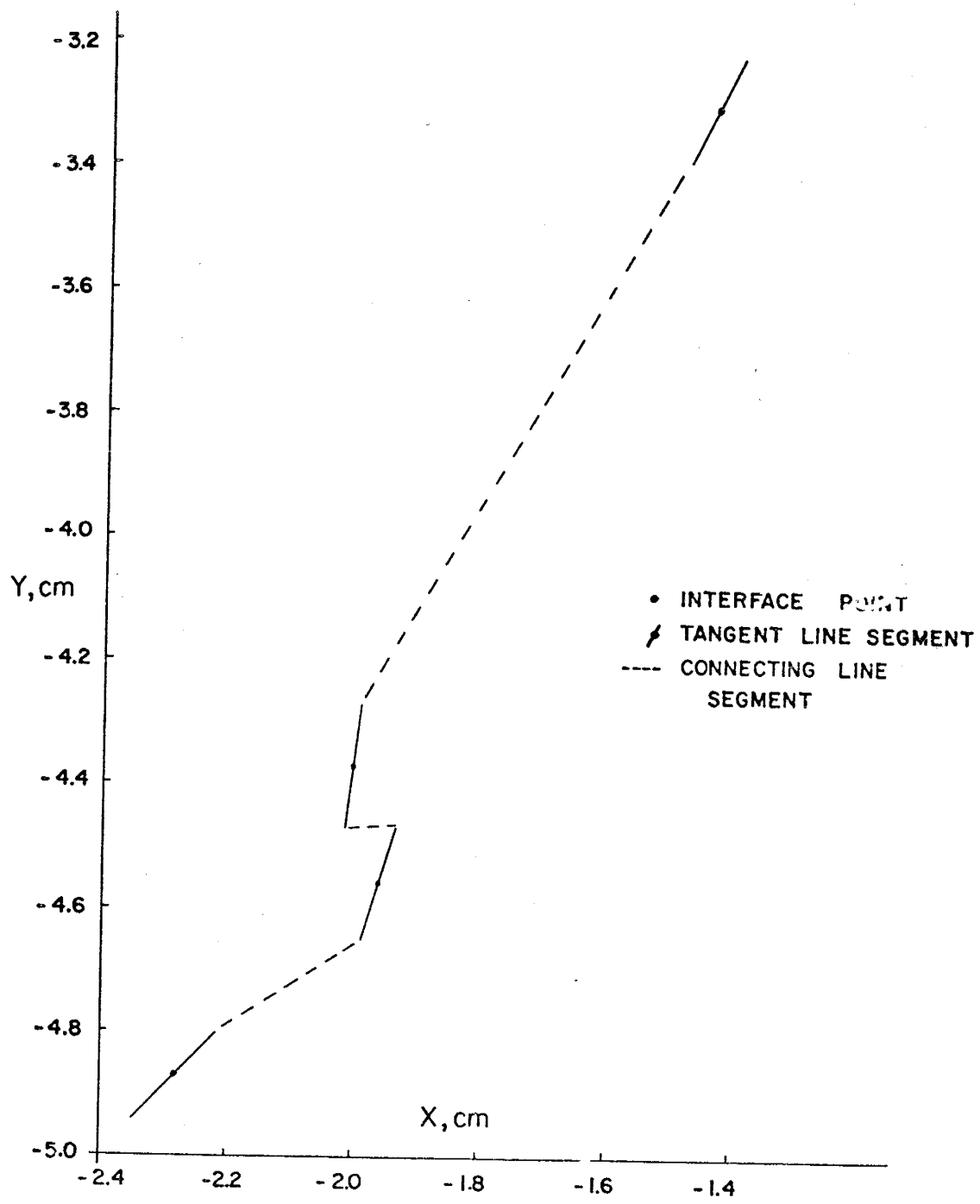
-3.2
-3.4
-3.6
-3.8
-4.0
Y, cm
-4.2
-4.4
-4.6
-4.8
-5.0
-2.4
-2.2
-2.0
-1.8
-1.6
-1.4
X, cm
INTERFACE POINT
TANGENT LINE SEGMENT
CONNECTING LINE SEGMENT

the two central interface points are not in correct positions because of errors produced by the incorrect interface fits at earlier times. From the information gained from this aspect of the computational experimentation, the formulation of the computer code can probably be improved by letting δ be variable, with its value dependent on the spacing of the interface points and the slope of the tangent line segment.

Additional information can be obtained by comparing the rates of interface rotation for various values of δ with the theoretical rate of rotation discussed in Section 5.2. Figure 5.4.7 shows such a comparison. The figure shows that the computed rate of rotation is near the theoretical rate for $\delta \leq 0.05$ cm. However, for $\delta = 0.1$ cm, the computed rate is extremely variable, again reflecting the instability caused by the overlap of the tangent line segments discussed above. Note that for $\delta = 0.005$ cm, the computed rate of rotation appears to be reasonably accurate, although the shape of the computed interface is less accurate than might be desired (Fig. 5.4.2) because of the round-off error examined above. Thus, in this case, the code simulates the motion, if not the shape, of the interface with relative accuracy.

C. Iteration of Interface Position

Before the computer model was actually formulated, it was felt that iteration might be needed to determine the change in

Figure 5.4.7. Inclination of interface, α , as a function of time.

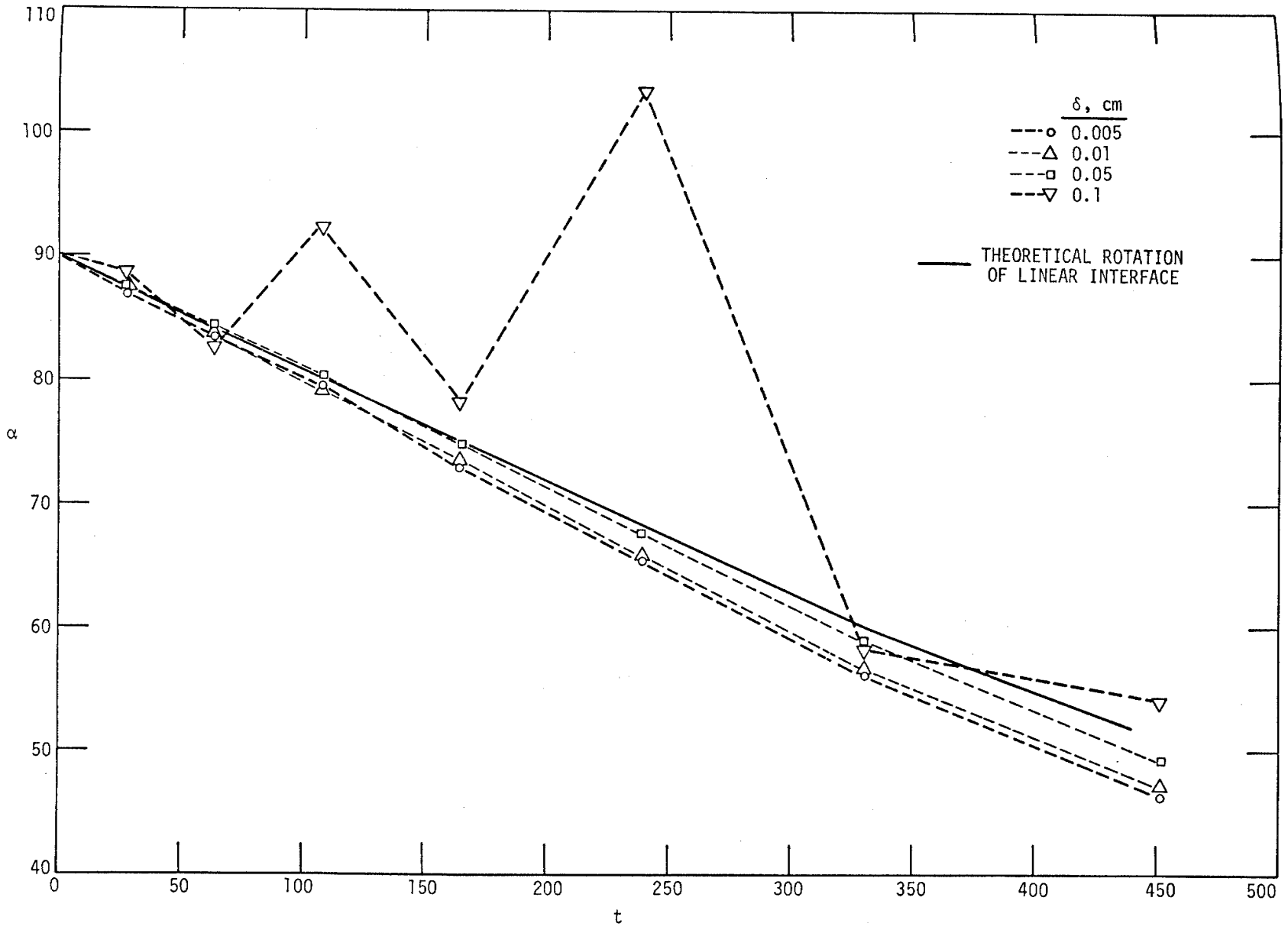
110
100
90
80
70
60
50
40
α
0
50
100
150
200
250
300
350
400
450
500
t
δ, cm
0.005
0.01
0.05
0.1
THEORETICAL ROTATION
OF LINEAR INTERFACE

position of the interface during a given time step. For example, at a given time t, the velocity $\vec{V}_n = \hat{\imath} u_n + \hat{\jmath} v_n$ at each interface point (x_n, y_n) could be determined by the methods of Chapter 3. Each interface point (x_n, y_n) would then be moved to a new position (x_n^*, y_n^*) by

$$x_n^* = x_n + u_n \Delta t$$

$$y_n^* = y_n + v_n \Delta t,$$

and the velocity $\vec{V}_n^*$ could be determined at the new position of each interface point. A second iteration for the new position could be determined by applying the average velocity $\langle \vec{V}_n \rangle = \frac{1}{2} \left[\vec{V}_n + \vec{V}_n^* \right] = \hat{\imath} \langle u_n \rangle + \hat{\jmath} \langle v_n \rangle$ at the average position $(\langle x_n \rangle , \langle y_n \rangle)$, with $\langle x_n \rangle = \frac{1}{2} \left[x_n + x_n^* \right]$ and $\langle y_n \rangle = \frac{1}{2} \left[y_n + y_n^* \right]$. The second iteration (x_n^{**}, y_n^{**}) would be given by

$$x_n^{**} = \langle x_n \rangle + \tfrac{1}{2} \langle u_n \rangle \Delta t$$

$$y_n^{**} = \langle y_n \rangle + \tfrac{1}{2} \langle v_n \rangle \Delta t$$

This iterative procedure could be continued until successive positions of each point coverged. The entire procedure would then be repeated for the next time step, and so on.

However, the basic check problem was first run without using such an iterative procedure. Thus, the position of each

interface point at time $t + \Delta t$ was given merely by

$$x_n^* = x_n + u_n \Delta t$$

$$y_n^* = y_n + v_n \Delta t \ ,$$

and the calculations proceeded immediately to the next time step. This simpler procedure simulated the interface motion quite closely, so it was decided that the use of an iterative technique to determine interface motion was not necessary for the basic check problem. Nevertheless, it may prove necessary to employ such an iterative approach in the simulation of more complex interface problems.

Interface motion for optimum δ. The computational experimentation considered above indicates that the optimum choice for δ is of the order of 0.01 cm. In this section, we will consider in more detail the computed interface motion for δ = 0.01 cm.

A. Initial Distribution of Specific Discharge

Figure 5.4.8 shows the initial distribution of the specific discharge vectors. A comparison of Figure 5.4.8 with Figure 5.2.3, which are both drawn to the same scale, shows that there is no apparent difference between the theoretical and computed values of the specific discharge. A comparison between

Figure 5.4.8. Initial specific discharge vectors given by computer model.

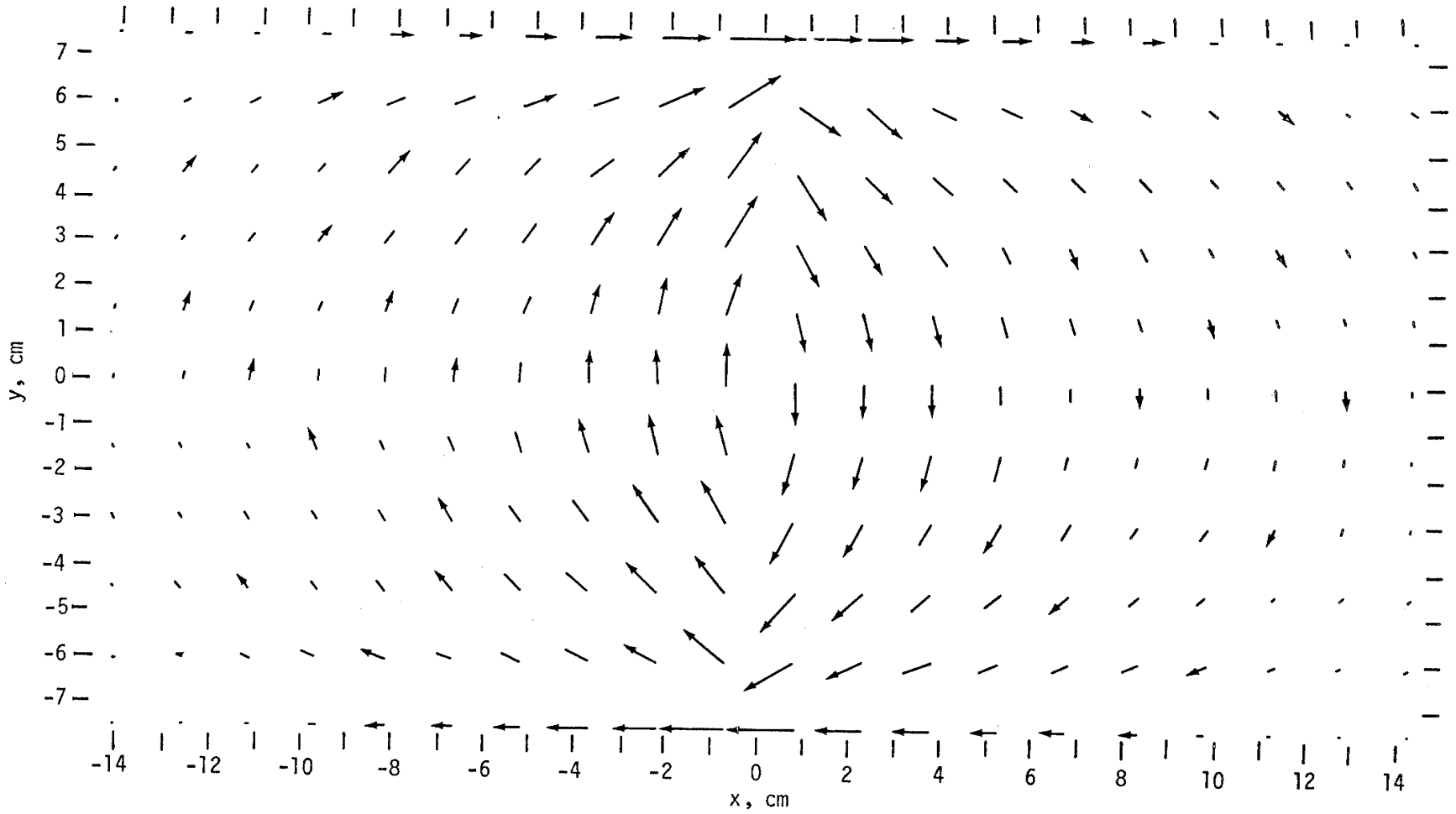
y, cm
7
6
5
4
3
2
1
0
-1
-2
-3
-4
-5
-6
-7
-14
-12
-10
-8
-6
-4
-2
0
2
4
6
8
10
12
14
x, cm

Table 5.4.2. Comparison between theoretical and computer model values of specific discharge at t = 0. All values in cm/sec.

	y = 7.5 cm*		y = -7.5 cm*		y = 0**	
	q_x		q_x		q_y	
x, cm	Theory	Model	Theory	Model	Theory	Model
-14.25	0.0009	0.0005	-0.0009	-0.0005	0.0009	0.0015
-12.75	0.0012	0.0010	-0.0012	-0.0010	0.0012	0.0017
-11.25	0.0017	0.0015	-0.0017	-0.0016	0.0017	0.0020
-9.75	0.0023	0.0023	-0.0023	-0.0023	0.0023	0.0025
-8.25	0.0032	0.0032	-0.0032	-0.0033	0.0032	0.0032
-6.75	0.0045	0.0044	-0.0045	-0.0045	0.0043	0.0043
-5.25	0.0062	0.0062	-0.0062	-0.0063	0.0058	0.0057
-3.75	0.0088	0.0087	-0.0088	-0.0088	0.0077	0.0075
-2.25	0.0131	0.0129	-0.0131	-0.0130	0.0100	0.0097
-0.75	0.0224	0.0223	-0.0224	-0.0224	0.0127	0.0122
0.75	0.0224	0.0223	-0.0224	-0.0223	-0.0127	-0.0123
2.25	0.0131	0.0129	-0.0131	-0.0129	-0.0100	-0.0097
3.75	0.0088	0.0087	-0.0088	-0.0088	-0.0077	-0.0075
5.25	0.0062	0.0061	-0.0062	-0.0062	-0.0058	-0.0057
6.75	0.0045	0.0045	-0.0045	-0.0044	-0.0043	-0.0043
8.25	0.0032	0.0031	-0.0032	-0.0032	-0.0032	-0.0032
9.75	0.0023	0.0022	-0.0023	-0.0022	-0.0023	-0.0025
11.25	0.0017	0.0015	-0.0017	-0.0015	-0.0017	-0.0019
12.75	0.0012	0.0009	-0.0012	-0.0009	-0.0012	-0.0016
14.25	0.0009	0.0005	-0.0009	-0.0005	-0.0009	-0.0014

*q_y (theory) = q_y(model) = 0
**q_x (theory) = q_x(model) = 0

Table 5.4.2. Continued.

	x = 6.75 cm				x = -6.75 cm			
	q_x		q_y		q_x		q_y	
y, cm	Theory	Model	Theory	Model	Theory	Model	Theory	Model
-7.5	-0.0045	-0.0044	0.0000	0.0000	-0.0045	-0.0045	0.0000	0.0000
-6.0	-0.0042	-0.0041	-0.0014	-0.0014	-0.0042	-0.0042	0.0014	0.0014
-4.5	-0.0035	-0.0034	-0.0026	-0.0026	-0.0035	-0.0035	0.0026	0.0026
-3.0	-0.0025	-0.0024	-0.0036	-0.0036	-0.0025	-0.0024	0.0036	0.0035
-1.5	-0.0013	-0.0012	-0.0041	-0.0041	-0.0013	-0.0012	0.0041	0.0041
0.0	0.0000	0.0000	-0.0043	-0.0043	0.0000	0.0000	0.0043	0.0043
1.5	0.0013	0.0013	-0.0041	-0.0041	0.0013	0.0013	0.0041	0.0041
3.0	0.0025	0.0024	-0.0036	-0.0036	0.0025	0.0025	0.0036	0.0035
4.5	0.0035	0.0034	-0.0026	-0.0027	0.0035	0.0034	0.0026	0.0026
6.0	0.0042	0.0040	-0.0014	-0.0014	0.0042	0.0041	0.0014	0.0014
7.5	0.0045	0.0044	0.0000	0.0000	0.0045	0.0044	0.0000	0.0000

theoretical and computed values of the specific discharge components can better be carried out in tabular form. Table 5.4.2 gives values of the discharge components along various representative sections through the flow region. The comparisons in Table 5.4.2 indicate an excellent agreement between theoretical and computed components of specific discharge at time t = 0. The only major differences occur near the lateral boundaries of the computer model, which are at $x = \pm 15.75$ cm. The flow must be tangent to those boundaries, so $q_x = 0$ there in the computer model. However, $|q_x| > 0$ at those lines in the theoretical solution because that solution assumes an infinite flow region. Similarly, the y-component of the specific discharge near those boundaries is slightly larger in magnitude in the computer model than in the theoretical solution. However, these effects of the lateral boundaries are seen only in the immediate vicinity of the bounaries; there is practically no difference between the theoretical and computed specific discharge in the interior of the flow region.

B. Initial Displacement of the Interface

As noted in Section 5.2, the initial displacement of the interface is given by the velocity normal to the interface. Table 5.4.3 gives a comparison between the theoretical initial interface velocity, given by equation (5.2.4), and the initial interface velocity predicted by the computer model. The values given in the table have

Table 5.4.3. Initial velocity normal to the interface.

y_o, cm	dx_o/dt, cm/sec	
	Theory	Model
7.5	$+\infty$	0.0586
7.37	0.0372	0.0372
7.23	0.0322	0.0311
6.70	0.0225	0.0216
6.16	0.0176	0.0171
5.625	0.01455	0.0141
5.09	0.0122	0.0118
4.55	0.0103	0.0100
4.02	0.0088	0.0084
3.48	0.0072	0.0071
2.95	0.0059	0.0058
2.41	0.0042	0.0047
1.875	0.0039	0.0036
1.34	0.0026	0.0025
0.80	0.0015	0.0015
0.27	0.0005	0.0005
-0.27	-0.0005	-0.0005
-0.80	-0.0015	-0.0015
-1.34	-0.0026	-0.0025
-1.875	-0.0039	-0.0035
-2.41	-0.0042	-0.0046
-2.95	-0.0059	-0.0058
-3.48	-0.0072	-0.0070
-4.02	-0.0088	-0.0084
-4.55	-0.0103	-0.0100
-5.09	-0.0122	-0.0119
-5.625	-0.01455	-0.0141
-6.16	-0.0176	-0.0171
-6.70	-0.0225	-0.0216
-7.23	-0.0322	-0.0312
-7.37	-0.0372	-0.0373
-7.50	$-\infty$	-0.0587

been calculated at the initial positions of the interface points. Table 5.4.3 also indicates excellent agreement between the theoretical velocities and the velocities given by the computer model. However, the velocities given by the code are in general slightly less than those given by the theory. This difference is due to the fact that the velocities given by the code are actually those at a very small time δt after zero, as discussed in Chapter 4, and thus would be expected to be slightly less than the velocities at time zero.

C. Comparison Between Computer Model and Parallel-Plate Model for $t > 0$

It is difficult to determine the accuracy of the computer-generated interface motion at times greater than zero because of the lack of an analytical solution at such times. However, the computed interface position can be compared with photographs of the parallel-plate model, and the specific discharge vectors generated by the computer code can be compared with the traces of the gold-leaf flakes in the photograph of the model. Figure 5.4.9 shows the interface position, the specific discharge vectors at the mesh points, and the velocity vectors at the interface points, at $t = 165$ seconds. These quantities can be compared with Figure 5.4.10, which shows a photograph of the parallel-plate model for the exposure interval of 120 seconds to 210 seconds. Both figures are to the same scale, with the

lengths of the vectors plotted in Figure 5.4.9 being given by the velocity at t = 165 seconds multiplied by the time interval Δt = 90 seconds. Thus the vectors in both Figures 5.4.9 and 5.4.10 can be directly compared because the length of a particle streak in Figure 5.4.10 should be approximately equal to the average velocity of the particle during the 90-second exposure period, multiplied by the length of the period. As can be seen by comparing the two figures, the computer-generated velocity vectors reproduce the particle paths quite well. However, the upper end of the model interface has progressed further along the boundary than the upper end of the computed interface. This difference can probably be attributed to experimental procedures which were not accounted for in the computer program. This point will be treated in greater detail below.

D. Rate of Rotation of the Interface

A final test which can be applied to the accuracy of the computer model is based on the rate of rotation of the interface. Figure 5.4.11 shows the theoretical rate of interface rotation based on the assumption that the interface retains its initial (straight line) shape, the rate of interface rotation given by the computer code, and the rate of interface rotation observed in the parallel-plate model. The figure indicates that the computed rate of rotation is slightly faster than the theoretical rate. In contrast, the interface in the parallel-plate model appears to rotate more rapidly than would be predicted

Figure 5.4.9. Computer-generated interface position and specific discharge vectors at t = 165 seconds.

Figure 5.4.10. Photograph of parallel-plate model for $120 < t < 210$ seconds (de Josselin de Jong, 1960).

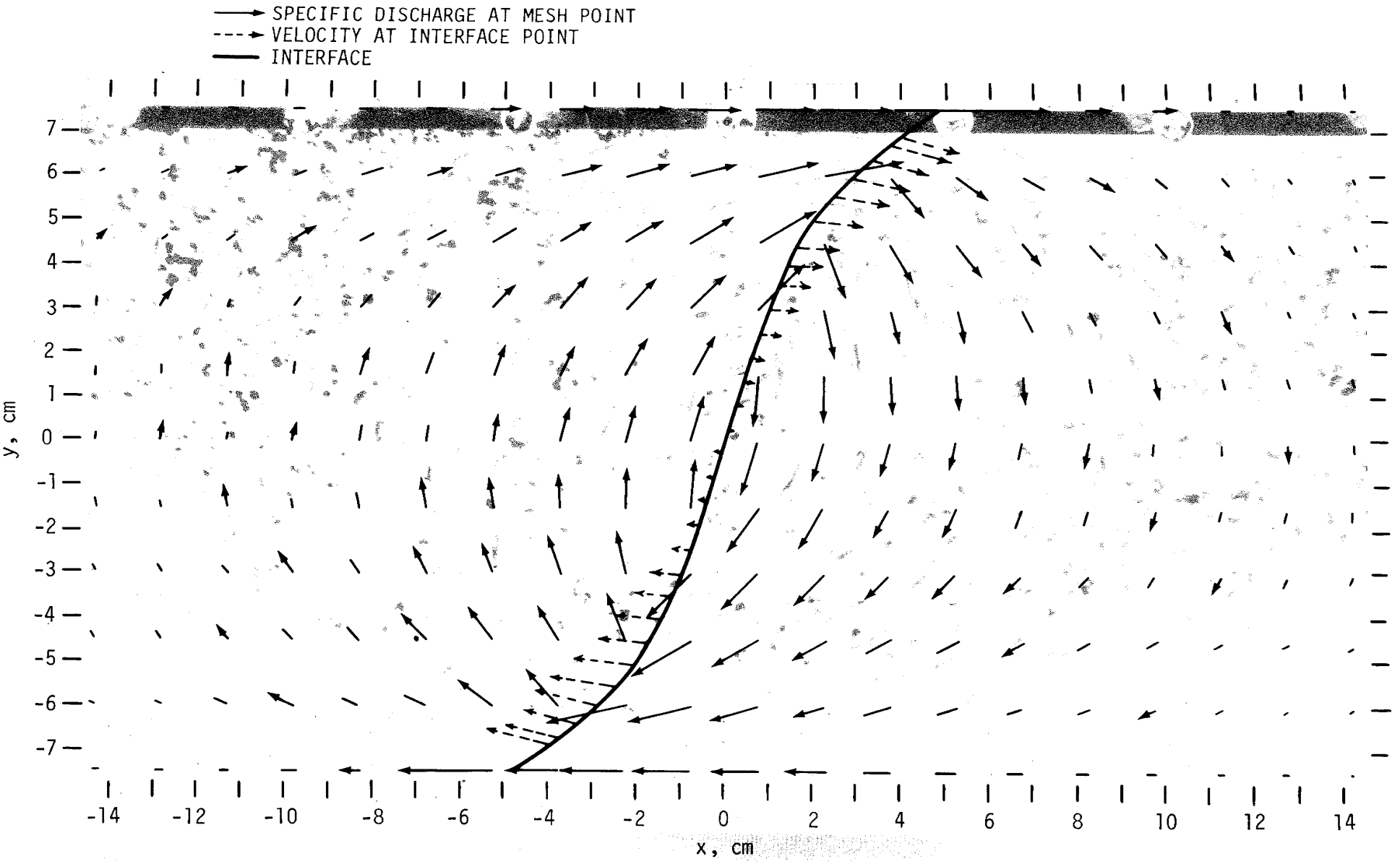
SPECIFIC DISCHARGE AT MESH POINT
VELOCITY AT INTERFACE POINT
INTERFACE
y, cm
7
6
5
4
3
2
1
0
-1
-2
-3
-4
-5
-6
-7
-14
-12
-10
-8
-6
-4
-2
0
2
4
6
8
10
12
14
x, cm

by either the approximate analytical theory or the computer program. The difference could have a number of possible causes:

(1) The theoretical interface might rotate more slowly because the theoretical model is unbounded laterally, while the physical model and the computer model both have lateral boundaries. However, if this were the cause of the observed differences in the rates of rotation, the interface in the computer model should rotate more rapidly than that in the physical model, because the computer model is shorter than the parallel-plate model.

(2) The theoretical rate of rotation might be retarded somewhat by the assumption that the interface is linear. However, the computed interface rotation (where the linear assumption was not made) follows the theoretical rotation more closely than it follows the experimental rotation. Furthermore, as will be seen below, the computed interface gradually approaches a linear shape, and at all times has a significant central linear portion. Thus, the more rapid rate of rotation observed in the parallel-plate model is probably due to some physical effect which appears in the parallel-plate model but which is not accounted for in the theoretical or computer calculations.

Figure 5.4.11. Comparison of rates of interface rotation.

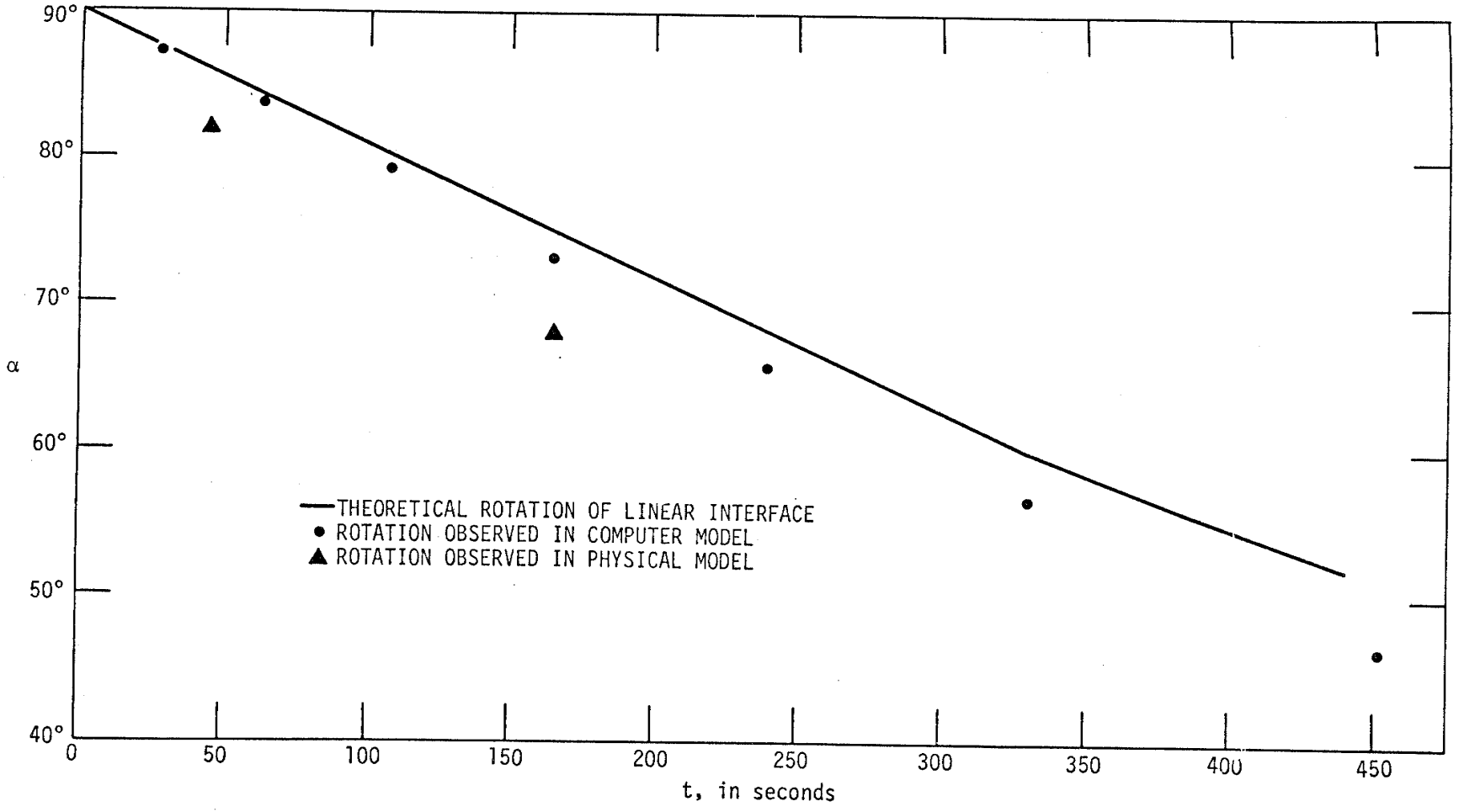
90°
80°
70°
60°
50°
40°
α
0
50
100
150
200
250
300
350
400
450
t, in seconds
THEORETICAL ROTATION OF LINEAR INTERFACE
ROTATION OBSERVED IN COMPUTER MODEL
ROTATION OBSERVED IN PHYSICAL MODEL

(3) The rate of interface rotation in the parallel-plate model might be affected by the miscibility of the fluids involved. Since the two fluids used in the model were glycerine and a mixture of glycerine and phosphoric acid, the fluids are probably miscible to some extent, and the mixing of the two fluids could well affect the observed rate of rotation of the interface between them. Experiments with sand-box models (Kumar and Kimbler, 1970; Gelhar et al., 1972), which dealt in part with the influence of dispersion on interface motion, indicated that mixing of the fluids actually retards the rate of interface rotation in both linear and radial flow systems. In those experiments, however, the flow velocities were much higher than in the present case because those systems included injection of the lighter fluid into a body of heavier fluid. Since the coefficient of dispersion in a porous medium is proportional to the velocity (Bear, 1972), mixing of the fluids would influence the models of Kumar and Kimbler and Gelhar et al. much more strongly than it would influence the present parallel-plate model. Thus the retarding of the interface rotation due to mixing of the fluids is relatively small in the present case, and can probably be neglected. (The effects of dispersion can be included in the computer model, as will be discussed in Chapter 6.)

Two other possibilities exist for the higher rate of rotation observed in the parallel-plate model, both involving the actual set-up and use of the model.

(4) Although the gold-leaf flakes used in the model to trace flow lines were assumed to have negligible settling velocity compared with the actual motion of the fluid, it is possible that their settling velocity was actually significant. If this were the case, the settling of particles in the upper half of the model would tend to indicate an additional clockwise rotation of the upper end of the interface. However, the settling of particles in the lower half of the model would tend to indicate an additional counter-clockwise rotation of the lower end of the interface. Since the lower end of the interface is not clearly visible in the photographs of the model, it is not possible to test this hypothesis, so it must be left as only a suggestion, and by no means the explanation of the observed discrepancy between the theoretical and experimental interface motion.

(5) Another possible suggestion of the observed behavior lies in the manner in which the model was set up to produce the desired initial conditions. The parallel-plate model was first placed on one end, filled halfway with the heavier fluid, and then filled with the lighter fluid. The model was then rotated to a horizontal position so that the initial condition was a vertical interface

between the two fluids (G. de Josselin de Jong, personal communication, 1972). Although this process was carried out very carefully so as to minimize experimental error, it is nevertheless possible that the filling and then the rotation of the model could have imparted an initial motion to the body of fluid, which was not considered in either the theoretical or the computer solution to the problem, but which caused the interface to rotate more rapidly than predicted.

E. Computed Interface Shape and Motion

Figure 5.4.12 shows the computed interface at various times. The predicted S-shaped nature of the curve is clearly evident at early times, and gradually becomes more pronounced at intermediate times. However, at later times the curve gradually approaches a linear shape. This is due to the fact that as the ends of the interface approach the lateral boundaries, the horizontal velocity components approach zero; at those impermeable boundaries, the horizontal velocity must be identically zero. Furthermore, at all times, there is a significant central portion of the interface which remains linear. These observations are consistent with the fact that the final interface configuration should be a horizontal straight line.

Figure 5.4.12. Computed interface position at various times.

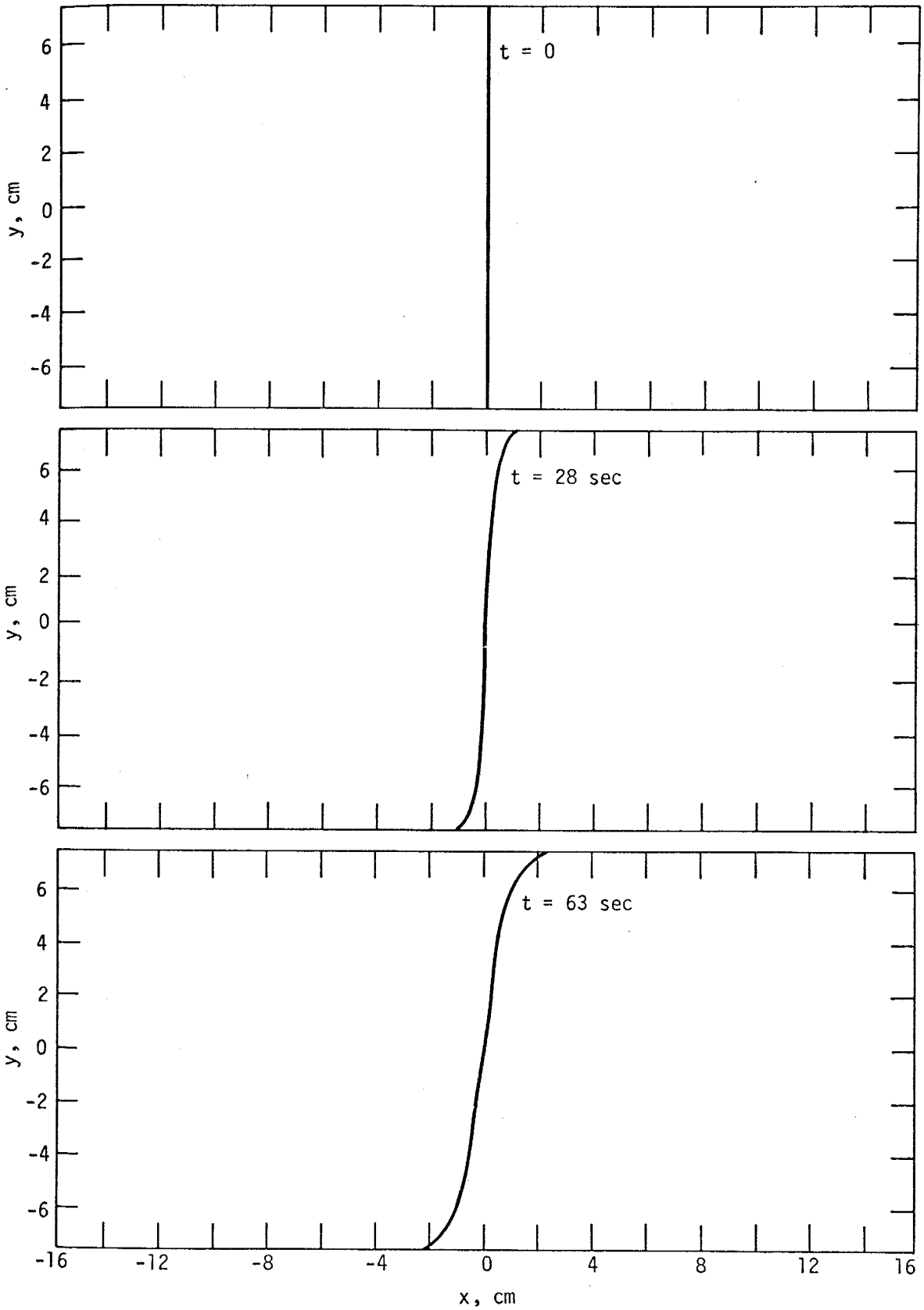
t = 0
t = 28 sec
t = 63 sec
y, cm
x, cm
6
4
2
0
-2
-4
-6
-16
-12
-8
-4
0
4
8
12
16

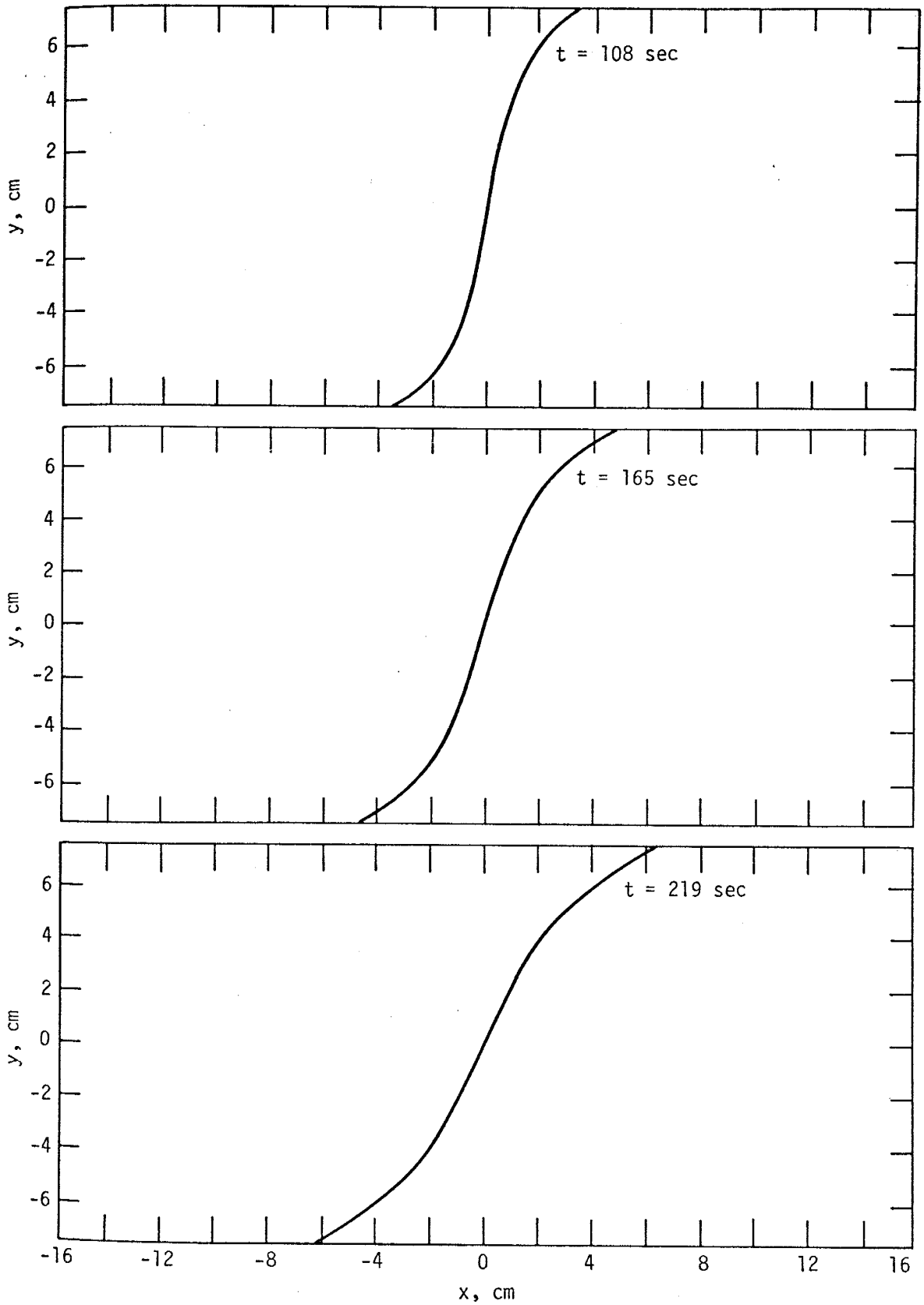
t = 108 sec
t = 165 sec
t = 219 sec
y, cm
x, cm
6
4
2
0
-2
-4
-6
-16
-12
-8
-4
0
4
8
12
16

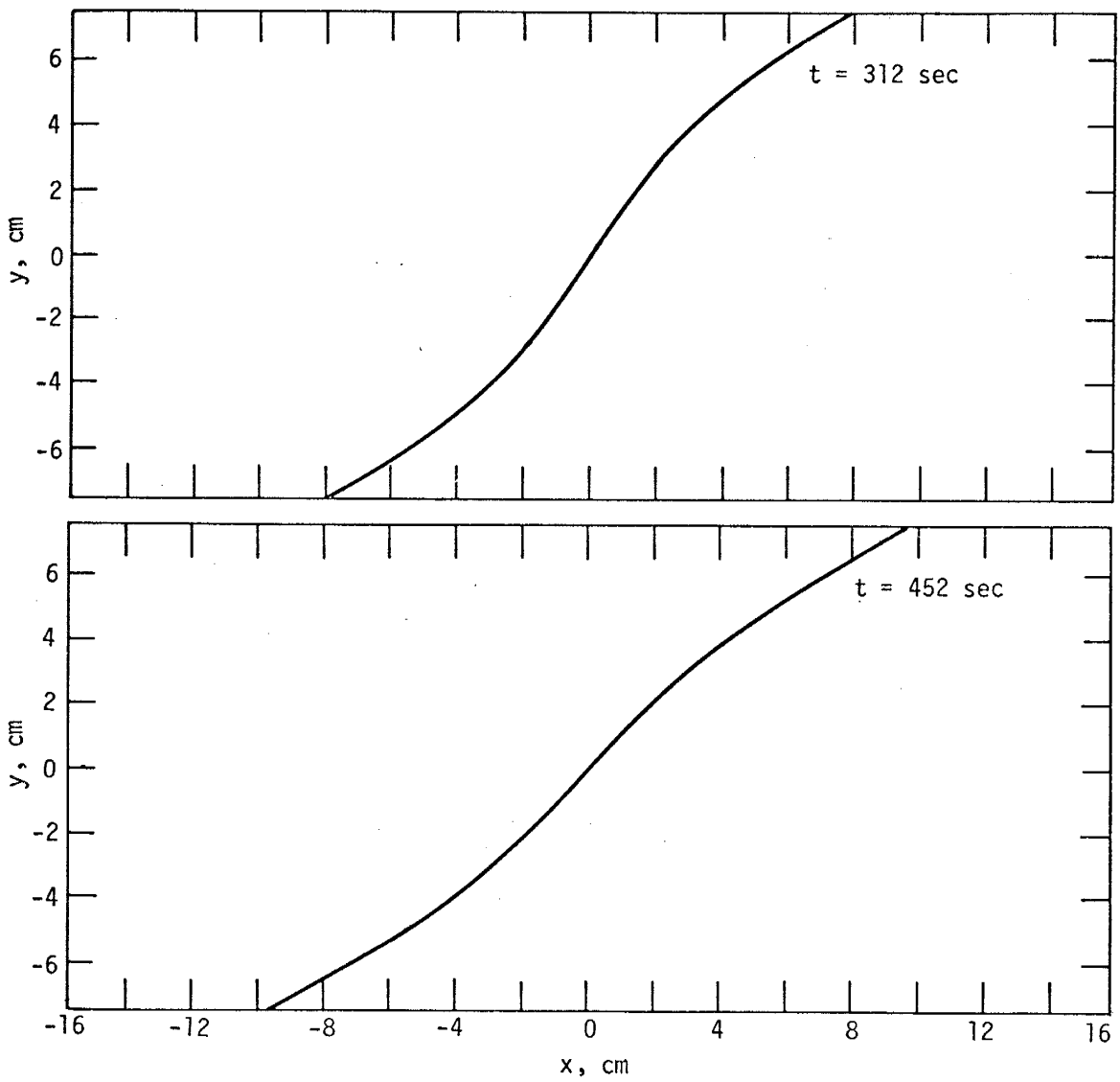
t = 312 sec
t = 452 sec
y, cm
x, cm
6
4
2
0
-2
-4
-6
-16
-12
-8
-4
0
4
8
12
16

5.5 Discussion

The results of the study presented above indicate that there is generally good agreement among the results of the computer model, analytical solutions, and the parallel-plate model experiment for the basic check problem. The differences which do appear among these three lines of investigation can be explained in a satisfactory manner, and many of them could be rectified by means of minor modifications in the computer model. This study has also indicated a few ways in which the computer model could be improved, such as by reprogramming some statements in the FORTRAN code, and letting the lengths of the tangent line segments be dependent upon the spacing of the interface points and the slopes of the tangent line segments. This study shows that the present computer model for interface motion can potentially be a useful tool for the study of practical problems of two-fluid interface motion in porous media.

The motion of the interface shown in Figure 5.4.12 shows that the interface always has a significant central linear portion, and the total interface gradually approaches a linear shape. This indicates that theories of interface motion based on the assumption that the interface always maintains a linear shape, such as those presented by Kumar and Kimbler (1970) and Gardner et al. (1962), should give reasonably accurate representations of the interface motion.

REFERENCES

Bear, Jacob, Dynamics of Fluids in Porous Media, 764 pp., American Elsevier, New York, 1972.

de Josselin de Jong, G., Vortex theory for multiple phase flow through porous media, Water Resources Center Contribution 23, 80 pp., Hydraulic Laboratory, University of California, Berkeley, 1959.

de Josselin de Jong, G., Singularity distributions for the analysis of multiple-fluid flow through porous media, Journal of Geophysical Research, 65, 3739, 1960.

Gardner, G.H.F., J. Downie, and H.A. Kendall, Gravity segregation of miscible fluids in linear models, Society of Petroleum Engineers Journal, 2, 95-104, 1962

Gelhar, Lynn W., John L. Wilson, and John S. Miller, Gravitational and dispersive mixing in aquifers, Proceedings of the American Society of Civil Engineers, 98, HY 12, 2135-2153, 1972.

Kumar, A., and O.K. Kimbler, Effect of dispersion, gravity segregation, and formation stratification on the recovery of freshwater stored in saline aquifers, Water Resources Research, 6, 1689-1700, 1970.

CHAPTER 6. EXTENSIONS OF THE COMPUTER TECHNIQUE FOR STUDYING INTERFACE MOTION

6.1 Introduction

In the previous chapters, we have considered the development of a computer technique for solving a certain class of problems involving the motion of a two-fluid interface through a porous medium. The present computer code is limited to problems involving the flow of incompressible fluids through a nondeformable medium, with the fluids differing only in their densities at a sharp interface between them. However, in practical problems of multiple-fluid flow, a number of additional phenomena can be important. Under the assumption of a sharp interface between the fluids, we can also consider

(1) storage effects produced by compressibility of the fluids and/or deformation of the porous medium;

(2) a difference in the viscosities of the two fluids; and

(3) anisotropy and inhomogeneity of the porous medium.

Furthermore, the assumption of a sharp interface may not apply. Either or both fluids may exhibit continuous variations in density and/or viscosity, caused by hydrodynamic dispersion or natural variations in the properties of the fluids. In this chapter, we will consider some ways in which these phenomena can be incorporated into the present computer code for simulating interface motion.

6.2 Extensions of the Vortex Theory of Interface Motion

The vortex theory of interface motion discussed in Chapter 2 is limited to problems involving only a density difference between the two fluids. However, the theory presented there can be extended somewhat to include storage effects of the fluid-medium system and the effect of a gradual transition zone between the fluids, across which the density varies. In addition, the flow equations can be formulated in terms of the fluid pressure rather than the stream function, and in geometries other than the two-dimensional Cartesian geometry considered previously.

Knudsen's Equation. For some applications, it may be convenient to formulate the flow equations in terms of the fluid pressure rather than the stream function. Such applications would generally include problems of deep subsurface flow, such as disposal of liquid wastes and secondary recovery of petroleum, in which only the fluid pressure at isolated points can be measured economically.

The flow equations can be formulated in terms of the fluid pressure by again applying Darcy's law and the continuity equation. Darcy's law can be written in the form

$$\vec{q} = -(k/\mu)(\nabla p + \rho \vec{g}) , \qquad (6.2.1)$$

where $\vec{g}$ is the gravitational acceleration. Under the assumptions that the fluids are incompressible and the medium is nondeformable,

the continuity equation is

$$\nabla \cdot \vec{q} = 0. \qquad (6.2.2)$$

Combining equations (6.2.1) and (6.2.2), and assuming that the permeability k and viscosity μ are constant, we get

$$\nabla^2 p = -(\partial \gamma / \partial z) . \qquad (6.2.3)$$

Equation (6.2.3), which was first presented by Knudsen (1962), is a Poisson equation with the integral solution

$$p = -(1/2\pi) \iint_{A_o} (\partial \gamma / \partial z)_o \ln R \, dA_o \qquad (6.2.4)$$

in two dimensions. The integration in equation (6.2.4) extends over the entire plane, but only has a contribution from the region A_o in which $\partial \gamma / \partial z$ does not vanish. R is the distance between the point at which p is to be evaluated and a point in the region A_o. The subscript o denotes a quantity evaluated at a point within A_o.

The evaluation of equation (6.2.4), and the incorporation of initial and boundary conditions, can be carried out by techniques quite similar to those presented in Chapters 3 and 4. The specific discharge is given by equation (6.2.1), and can also be evaluated by the procedures of Chapter 3.

Radial Symmetry. Problems of interface motion involving flow in the vicinity of a discharging or recharging well can best be

analyzed in a system of cylindrical geometry exhibiting radial symmetry. Such a system is essentially three-dimensional, so the concept of the stream function is difficult to apply. Thus the flow can most easily be described in terms of the fluid pressure, using the formulas presented above.

The pressure distribution is given by equation (6.2.3), in which the Laplacian of p in cylindrical coordinates (r, θ, z) is

$$\nabla^2 p = (1/r)\,\partial(r\,\partial p/\partial r)/\partial r + (1/r^2)(\partial^2 p/\partial\theta^2) + \partial^2 p/\partial z^2 \tag{6.2.5}$$

The integral solution of the Poisson equation (6.2.3) in cylindrical geometry is

$$p(r,\theta,z) = (1/4\pi)\iiint_{V_o} (1/R)(\partial\gamma/\partial z)_o r_o dr_o d\theta_o dz_o \tag{6.2.6}$$

where the subscript o denotes a quantity evaluated at a point within the region V_o where $\partial\gamma/\partial z$ does not vanish. R is the distance between the point (r, θ, z) at which the pressure is to be evaluated, and a general point (r_o, θ_o, z_o) within the region V_o. Under the assumption of radial symmetry, p is independent of θ and equation (6.2.6) becomes

$$p(r,z) = \tfrac{1}{2}\iint_{A_o} (1/R)(\partial\gamma/\partial z)_o r_o dr_o dz_o \ , \tag{6.2.7}$$

where A_o is the region in the vertical (r, z)-plane in which $\partial\gamma/\partial z$ does not vanish. In equation (6.2.7),

$$R^2 = (r - r_o)^2 + (z - z_o)^2 \quad .$$

Again, the evaluation of equation (6.2.7), the incorporation of initial and boundary conditions, and the determination of the specific discharge distribution, can be carried out by procedures similar to those presented in Chapters 3 and 4.

Storage Effects. When the fluids are slightly compressible liquids and the medium undergoes vertical deformation (e.g., because of the constant load of overburden rocks), the flow equations become rather complex because of the nonlinear terms which arise (Jacob, 1950; Bear, 1972). These effects are usually incorporated into the flow equations by way of the specific storativity, which is an empirically-determined parameter of the fluid-medium system.

An approximate form of the continuity equation which involves the specific storativity has been presented by Holley and Saylor (1973). The general continuity equation for a compressible fluid flowing through a deformable porous medium is

$$\nabla \cdot (\rho \vec{q}) = - \partial (\rho \epsilon) / \partial t \quad . \qquad (6.2.8)$$

In the formulation of Holley and Saylor, the change in density $\partial \rho / \partial t$ is assumed to result from either of two effects:

(1) If spatial density gradients exist, the density at a point can change when fluid of different density is convected to that

point. This change in density is denoted by $(\partial \rho / \partial t)_a$.

(2) If the fluid is compressible, the density changes when the fluid compresses or expands due to pressure changes. This change in density is denoted by $(\partial \rho / \partial t)_c$.

Then, assuming that $\partial \rho / \partial t = (\partial \rho / \partial t)_a + (\partial \rho / \partial t)_c$, the continuity equation (6.2.8) may be written

$$\nabla \cdot (\rho \vec{q}) = - \epsilon (\partial \rho / \partial t)_a - [\epsilon (\partial \rho / \partial t)_c + \rho \, \partial \epsilon / \partial t] \quad . \quad (6.2.9)$$

Introducing the specific storativity S_o (Bear, 1972), we may write the bracketed terms in equation (6.2.9) as

$$\epsilon (\partial \rho / \partial t)_c + \rho \, \partial \epsilon / \partial t = S_o \, \partial p / \partial t, \quad (6.2.10)$$

so that the continuity equation becomes

$$\nabla \cdot (\rho \vec{q}) = - \epsilon (\partial \rho / \partial t)_a - S_o \, \partial p / \partial t. \quad (6.2.11)$$

Since all the effects of compressibility are now included in the specific storativity, the subscript a may be dropped in the first term on the right side of equation (6.2.11).

We may now treat the problem as one involving liquids which are incompressible but of variable density, flowing through a porous medium of specific storativity S_o. The continuity equation for such a system is

$$\nabla \cdot \vec{q} = - (S_o / \rho)(\partial p / \partial t) \, . \quad (6.2.12)$$

Subtracting equation (6.2.12) from equation (6.2.11), we get

$$\vec{q} \cdot \nabla \rho = - \epsilon (\partial \rho / \partial t) \quad . \tag{6.2.13}$$

We may now proceed by taking equation (6.2.12) as the continuity equation, and letting equation (6.2.13) describe the convection of density in the system. In addition to these equations, we must apply Darcy's law, equation (6.2.1). In considering only the motion of a sharp interface through a medium of specific storativity S_o, we may omit equation (6.2.13). If we wish to consider the effects of dispersion, equation (6.2.13) must be replaced by an equation describing the dispersion of tracer concentration, and an equation relating tracer concentration to fluid density.

For the case of a sharp interface, we can combine equations (6.2.12) and (6.2.1) to get

$$\nabla^2 p = - \partial \gamma / \partial z + (S_o \mu / k \rho)(\partial p / \partial t). \tag{6.2.14}$$

A solution to equation (6.2.14) can be attempted by letting $p = p_1 + p_2$, with

$$\nabla^2 p_1 = - \partial \gamma / \partial z. \tag{6.2.15}$$

A solution to equation (6.2.15) can be obtained in integral form, as outlined previously. Subtracting equation (6.2.15) from equation

(6.2.14), we get

$$\nabla^2 p_2 = (S_o \mu / k \rho)(\partial p_2 / \partial t) + (S_o \mu / k \rho)(\partial p_1 / \partial t). \qquad (6.2.16)$$

Equation (6.2.16) can now be interpreted as a diffusion equation for p_2 with a source term $(S_o \mu / k \rho)(\partial p_1 / \partial t)$, for which a numerical solution can be readily obtained by standard methods.

Equation (6.2.14) could also be treated directly as a diffusion equation with a source term $(-\partial \gamma / \partial z)$. However, for the case of interface motion, $\partial \gamma / \partial z$ vanishes throughout the flow region except at the interface. Since the inferface will not in general pass through mesh points of a finite-difference grid, the determination of the pressure and specific discharge at the interface will require some kind of averaging of fluid properties at interface points. Such a procedure is not desirable, because it can lead to numerical "smearing" of the interface position. On the other hand, the numerical solution of equation (6.2.16) does not require any averaging techniques, because the source term is uniquely defined at each mesh point.

Gradual Transition Zone. The interface between two homogeneous fluids can be replaced by a transition zone across which the fluid density varies gradually from that of the first fluid to that of the second. In this case, the stream function or pressure distribution can be obtained by methods considered previously,

but additional equations must be introduced to determine the density distribution within the transition zone. These could be the dispersion equations, discussed in Section 6.3, or equation (6.2.13) if dispersion can be neglected. For problems of this class, it may prove to be quite difficult to solve numerically the equations describing the density distribution, because of their hyperbolic nature.

A. Cartesian Symmetry

In two-dimensional Cartesian symmetry, the stream function is given by the Poisson equation (2.2.5)

$$\nabla^2 \Psi = -(k/\mu)(\partial \gamma / \partial x),$$

which has the integral solution (2.2.6)

$$\Psi = -(k/2\pi\mu) \int_{A_o} \ln R \, (\partial\gamma/\partial x)_o \, dA_o . \quad (6.2.17)$$

In the case of a sharp interface, the integral in equation (6.2.17) reduces to a line integral along the length of the interface, as discussed in Section 2.3. In the present case, the integral in equation (6.2.17) remains a double integral which must be evaluated over the region A_o where $\partial\gamma/\partial x$ does not vanish, which is the transition zone. The integration can be simplified by letting the boundaries of A_o be approximated by linear segments (Fig. 6.2.1). The density distribution within the transition zone could perhaps be determined numerically at mesh points of a

Lagrangian finite-difference grid overlain on the principal grid (Fig. 6.2.2). γ could then be approximated by a piecewise-continuous curve along a horizontal mesh line , so that $\partial\gamma/\partial x$ is constant between adjacent vertical mesh lines (Fig. 6.2.3). The integral in equation (6.2.17) could then be expressed as the sum of integrals evaluated over the polygons delimited by mesh lines of the Lagrangian grid, and the linear segments bounding the transition zone. Within each polygon, $\partial\gamma/\partial x$ could be taken as a constant given by an appropriate average of the values along the bounding horizontal mesh lines.

B. Cylindrical Symmetry

In cylindrical symmetry, the pressure is given by the Poisson equation (6.2.3)

$$\nabla^2 p = - \partial\gamma/\partial z,$$

which has the integral solution (6.2.7)

$$p(r,z) = \tfrac{1}{2} \int_{A_o}\int (1/R)(\partial\gamma/\partial z)_o \, r_o dr_o dz_o \, . \qquad (6.2.18)$$

In the case of a sharp interface, equation (6.2.18) also reduces to a line integral along the length of the interface. In the case of a transition zone between the two fluids, the integral in equation (6.2.18) could be evaluated by techniques similar to those discussed above. In this case, however, γ would have to be

approximated by a piecewise-continuous curve along a vertical mesh line, with $\partial\gamma/\partial z$ constant between adjacent horizontal mesh lines.

We should note that the techniques discussed in this section are merely suggested approaches to the solution of two-fluid motion with a gradual transition zone. These techniques, and alternate approaches to the problem, must be subjected to additional study before they can be used in the computer model for simulating interface motion.

Figure 6.2.1. Approximation of the boundaries of a gradual transition zone by linear segments.

Figure 6.2.2. Values of γ at mesh points of the Lagrangian finite-difference grid.

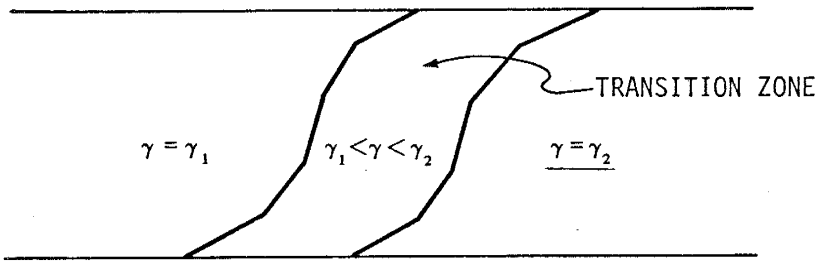
TRANSITION ZONE
$\gamma = \gamma_1$
$\gamma_1 < \gamma < \gamma_2$
$\gamma = \gamma_2$

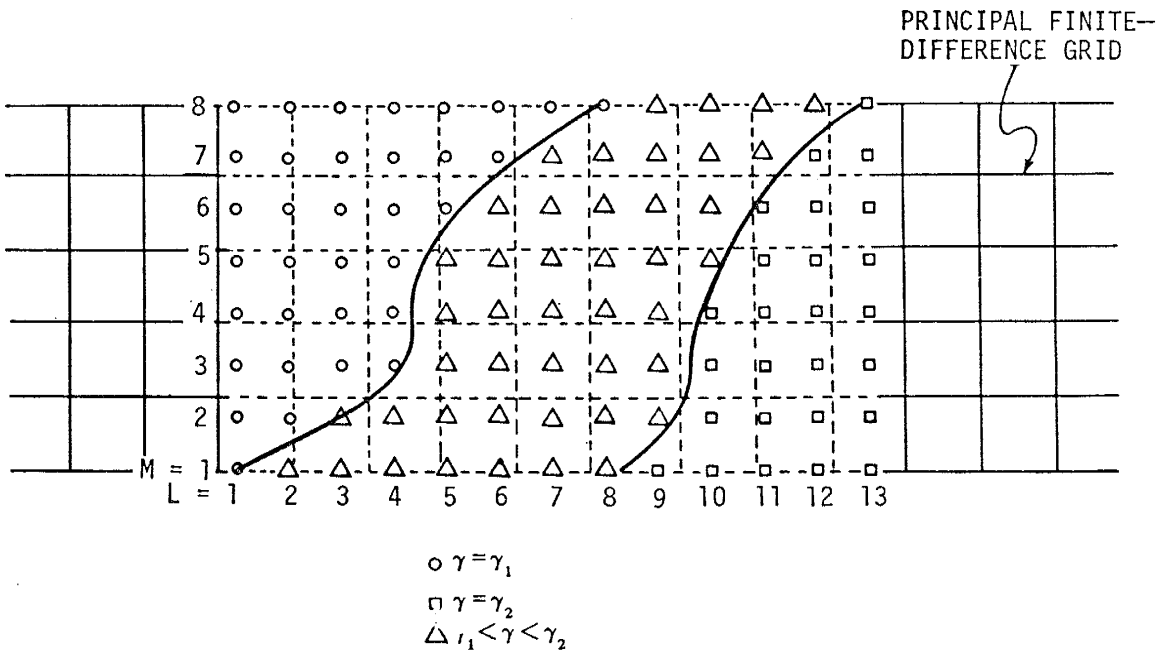
PRINCIPAL FINITE-DIFFERENCE GRID
8
7
6
5
4
3
2
M = 1
L = 1 2 3 4 5 6 7 8 9 10 11 12 13
o $\gamma = \gamma_1$
□ $\gamma = \gamma_2$
△ $\gamma_1 < \gamma < \gamma_2$

Figure 6.2.3. Piecewise-continuous approximation of the density distribution along the mesh line M=5 of Figure 6.2.2.

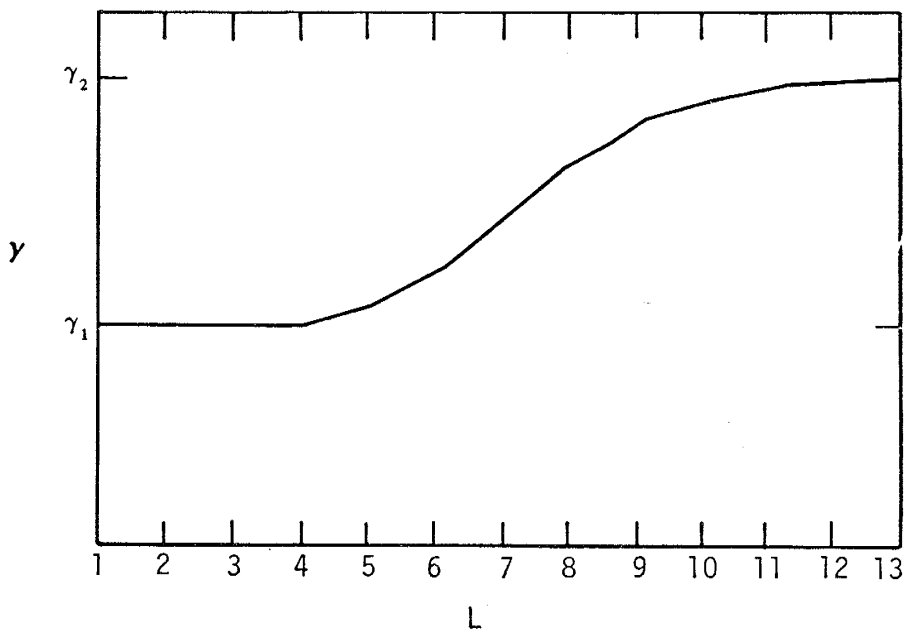
γ_2
γ_1
y
1 2 3 4 5 6 7 8 9 10 11 12 13
L

6.3 Further Extensions

In addition to the phenomena discussed in Section 6.2, we can also consider the effects on interface motion of anisotropy and heterogeneity of the porous medium, viscosity differences between the fluids, and hydrodynamic dispersion. However, when these phenomena are considered, the flow equations can no longer be interpreted according to the vortex theory discussed in previous chapters. Instead, except for very simple problems, the flow equations can only be solved by completely numerical techniques.

Anisotropy of the Porous Medium. When the axes of a Cartesian coordinate system coincide with the principal axes of anisotropy, Darcy's law may be written in two dimensions as

$$q_x = -(k_x/\mu)(\partial p/\partial x), \qquad (6.3.1a)$$

$$q_z = -(k_z/\mu)(\partial p/\partial z + \gamma). \qquad (6.3.1b)$$

Applying the continuity equation $\nabla \cdot \vec{q} = 0$, we get

$$k_x \partial^2 p/\partial x^2 + k_z \partial^2 p/\partial z^2 = -k_z \partial \gamma/\partial z. \qquad (6.3.2)$$

Since equation (6.3.2) is not a Poisson equation, its solution cannot be expressed in integral form as can the solution of Knudsen's equation.

Introducing the stream function Ψ, defined by

$$\partial\Psi/\partial x = q_z \qquad (6.3.3a)$$

$$\partial\Psi/\partial z = -q_x , \qquad (6.3.3b)$$

into equations (6.3.1), we get

$$\partial\Psi/\partial x = -(k_z/\mu)(\partial p/\partial z + \gamma) \text{ and} \qquad (6.3.4a)$$

$$\partial\Psi/\partial z = (k_x/\mu)\,\partial p/\partial x . \qquad (6.3.4b)$$

Differentiating equation (6.3.4a) by x, equation (6.3.4b) by z, and adding, we get

$$\partial^2\Psi/\partial x^2 + \partial^2\Psi/\partial z^2 = -(k_z/\mu)(\partial^2 p/\partial x\partial z + \partial\gamma/\partial x) + (k_x/\mu)\,\partial^2 p/\partial z\,\partial x. \qquad (6.3.5)$$

Although p is again single-valued and continuous, so that

$$\partial^2 p/\partial z\,\partial x - \partial^2 p/\partial x\partial z = 0,$$

p cannot be eliminated from equation (6.3.5). Thus, since p and Ψ are related through equations (6.3.4), equation (6.3.5) cannot be interpreted as a Poisson equation. In fact, for an anisotropic medium, no advantage is gained by introducing the stream function.

Viscosity Variation. In a homogeneous, isotropic medium, Darcy's law is given by

$$\vec{q} = -(k/\mu)(\nabla p + \rho \vec{g}) . \qquad (6.3.6)$$

For incompressible fluids and nondeformable medium, the continuity equation is

$$\nabla \cdot \vec{q} = 0 . \qquad (6.3.7)$$

However, if we assume that the fluids differ in both density and viscosity, then the substitution of equation (6.3.6) into equation (6.3.7) gives us

$$\nabla^2 p = -\partial \gamma / \partial z - \mu \nabla (1/\mu) \cdot (\nabla p + \rho \vec{g}) . \qquad (6.3.8)$$

Introducing the stream function through equations (6.3.3), we get

$$\partial^2 \Psi / \partial x^2 + \partial^2 \Psi / \partial z^2 = (k/\mu)(\partial^2 p / \partial z \partial x - \partial^2 p / \partial x \partial z)$$
$$+ k[(\partial p/\partial x)\partial(1/\mu)/\partial z - (\partial p/\partial z)\partial(1/\mu)/\partial x]$$
$$- k\,\partial(\gamma/\mu)/\partial x. \qquad (6.3.9)$$

The first term on the right of equation (6.3.9) is zero because p is single-valued and continuous, so we finally get

$$\nabla^2 \Psi = -k\partial(\gamma/\mu)/\partial x + k[(\partial p/\partial x)\partial(1/\mu)/\partial z$$
$$- (\partial p/\partial z)\partial(1/\mu)/\partial x]. \qquad (6.3.10)$$

Since the right sides of both equations (6.3.8) and (6.3.10) contain the unknown variable p, neither of these equations can be interpreted as a Poisson equation, so that advantage can not be taken of an integral solution for the dependent variable.

Continuous Variations in Fluid and Medium Properties. In general, the parameters k, ρ , and μ can vary continuously throughout the flow region. Assuming that the fluid is incompressible and the porous medium is isotropic and nondeformable, Darcy's law is given by equation (6.3.6) and continuity is given by equation (6.3.7). Combining these equations, we get

$$\nabla^2 p = - \partial \gamma / \partial z - (\mu/k) \nabla (k/\mu) \cdot (\nabla p + \rho \vec{g}). \qquad (6.3.11)$$

Equation (6.3.11) cannot be interpreted as a Poisson equation because p occurs in the right side of the equation. Thus the singularity theory of interface motion cannot be applied to this general case. Obviously, if we also consider storage effects and anisotropy of the medium, the flow equations become even more complicated. Analytical solutions to equation (6.3.11), or more complicated forms of the flow equation, can probably not be determined. However, the flow equations are generally of elliptic or parabolic type, for which numerical solutions employing finite difference or finite element techniques should be relatively easy to obtain.

Hydrodynamic Dispersion. The phenomenon of hydrodynamic dispersion occurs when the fluid flowing through a porous medium contains a variable concentration C of some tracer, such as dissolved salt. The tracer concentration can vary with space and time because of molecular diffusion as well as convection of the tracer through the irregular pore space of the medium. As a result of dispersion, a gradual transition zone will occur at the interface between two fluids of different tracer concentrations C_1 and C_2, across which the relative concentration $(C - C_1)/(C_2 - C_1)$ will vary between zero and unity. The fluid density can be related to the tracer concentration by an expression such as (Pinder and Cooper, 1970)

$$\rho = \rho_o + (1-E)\, C, \qquad (6.3.12)$$

so that the fluid density also varies continuously across the transition zone. Thus the pressure distribution, and then the specific discharge distribution, can be determined by methods similar to those presented in Section 6.2.

The tracer concentration C is given by the dispersion equation, which can be written (Bear, 1972)

$$D \nabla^2 C - (\vec{q}/\epsilon) \cdot \nabla C = \partial C/\partial t \qquad (6.3.13)$$

under the assumption that the dispersion coefficient D is a scalar which is constant in space and time. Because of the relationship (6.3.12) between the tracer concentration and the fluid density, equation (6.3.13) must be solved simultaneously with the appropriate flow equation. Note that if dispersion is neglected, D = 0 and equation (6.3.13) reduces to equation (6.2.13), which describes the convection of density in a flow system of continuous density variation in space. Pinder and Cooper (1970) have noted that equation (6.3.13) behaves somewhat as a hyperbolic equation when the convective term is relatively large (equation (6.2.13) is purely a first-order hyperbolic equation). Although numerical solutions of hyperbolic equations are subject to numerical instabilities, Pinder and Cooper (1970) have presented a solution to equation (6.3.13) based on the introduction of marker particles of variable tracer concentration, and the use of the method of characteristics to follow the motion of the marker particles.

In general, the dispersion coefficient is not a scalar, but a tensor related to the tortuosity tensor of the porous medium. The general dispersion equation can then be written (Bear, 1972)

$$\partial C/\partial t = \nabla\cdot(\underline{\underline{D}}\cdot\nabla C) - (\vec{q}/\epsilon)\cdot\nabla C, \qquad (6.3.14)$$

where the double underscore on the dispersion coefficient $\underline{\underline{D}}$ denotes a tensor quantity. Furthermore, as shown by Bear (1972),

the dispersion coefficient $\underline{\underline{D}}$ is a function of the average pore velocity $\vec{q}/\epsilon$. Although equation (6.3.14) is somewhat more complicated than equation (6.3.13), it should in principle be possible to solve both equations by the same numerical techniques.

REFERENCES

Bear, Jacob, Dynamics of Fluids in Porous Media, 764 pp., American Elsevier, New York, 1972.

Holley, Edward R., and Paul E. Saylor, Flow and mass transport resulting from deep well liquid waste disposal in Illinois, research proposal submitted to the Office of Water Resources Research, 32 pp., University of Illinois, Urbana, 1973.

Jacob, C. E., Flow of ground water, Chapter 5 in Engineering Hydraulics, edited by Hunter Rouse, pp. 321-386, John Wiley and Sons, New York, 1950.

Knudsen, W. C., Equations of fluid flow through porous media -- incompressible fluid of varying density, Journal of Geophysical Research, 67, 733-737, 1962.

Pinder, George F., and Hilton H. Cooper, Jr., A numerical technique for calculating the transient position of the salt-water front, Water Resources Research, 6, 875-882, 1970.

CHAPTER 7. CONCLUSIONS AND RECOMMENDATIONS

7.1 Summary

This report describes a computer technique for simulating the motion of an interface between two fluids of different densities in a porous medium. The computer technique is based on the vortex theory of interface motion outlined in Chapter 2. The vortex theory has an advantage over other approaches to the simulation of interface motion because the interface is not treated as a moving boundary. Instead, the interface is interpreted as a line of vortices which generate the fluid motion. The stream function satisfies a Poisson equation, whose solution can be written as a line integral over the length of the interface. The specific discharge components are also given as line integrals derived from the stream function. The evaluation of the line integrals gives the stream function and specific discharge at each point of the flow region. Boundary conditions are introduced by means of an auxiliary stream function which satisfies a Laplace equation. The position of the interface must be determined in order to evaluate the line integrals, but the interface does not have to be treated as a boundary because the stream function is continuous and single-valued throughout the flow region.

The computer model employing the vortex theory is outlined in Chapter 3. The model is based on approximating the

interface shape in order to provide for numerical evaluation of the line integrals. The interface is basically determined by a set of interface points, connected by linear segments. At the end of a finite time step, the interface points are moved to new positions according to the local fluid velocity, and connected line segments are fit to the new positions of the interface points. The Laplace equation for the auxiliary stream function is solved numerically by the standard point successive over-relaxation method.

The computer model has been formulated to simulate the rotation of an initially vertical interface between two fluids of different densities, which is referred to as the basic check problem. Chapter 4 presents some special techniques needed to treat the initial and boundary conditions for this problem. Theoretically, the initial interface is a vertical straight line. In the computer model, the initial instant has been chosen as a small time δt after zero, such that the endpoints of the interface have moved a very small distance along the horizontal boundaries. This is done in order to avoid infinite logarithmic singularities in the values of the specific discharge at the interface endpoints. The requirement that the fluid flow be strictly tangent to the horizontal boundaries is assured by introducing image interfaces reflected in the upper and lower boundaries of the flow region.

7.2 General Conclusions

Chapter 5 presents the results of the computer simulation of the basic check problem, and comparisons of those results with analytical and parallel-plate model studies of the same problem. There is generally very good agreement among the results of all three lines of investigation, with the computer model agreeing more closely with the analytical solutions than with the physical model. The discrepancies which do occur among the results of the three solution techniques can generally be explained on the basis of minor differences in the physical phenomena being modeled, and do not appear to indicate any serious inaccuracies in the results of the computer model.

A number of conclusions can be drawn from the results of this study:

(1) When the vortex theory of interface motion can be applied, it is preferable to other methods of simulating interface motion because the interface does not have to be treated as a moving boundary.

(2) The computer technique discussed in this report provides for study of the transient motion of an interface between two fluids in a porous medium. The technique has been used to simulate interface motion in the basic check problem, for which a complete analytical solution has only been obtained at the initial instant.

(3) The computer technique closely simulates the interface motion in the basic check problem. The applicability of the technique to problems of greater practical interest must await further investigation. However, the technique can potentially be a valuable tool for the study of problems of interface motion in porous media.

(4) The specific technique presented here is limited to simulation of the motion of a sharp interface between two incompressible fluids which differ only in their densities. The porous medium must be homogeneous, isotropic, and nondeformable, and the flow must exhibit two-dimensional Cartesian symmetry. However, the computer method based on the vortex theory can in principle be extended to include radially-symmetric flow in cylindrical coordinates, storage effects due to compressibility of the fluids and the medium, and motion of a gradual transition zone between the fluids.

(5) Such important effects as anisotropy and inhomogeneity of the porous medium, and differences in the viscosities of the fluids, cannot be treated by the vortex theory. Thus the advantage of an integral solution is lost in the study of problems involving these phenomena.

(6) In general, a numerical solution to the flow equation seems feasible, regardless of variations in the physical parameters. Such a solution can probably be carried out by either the finite-difference or finite-element method. However, because of their hyperbolic

nature, the equations of mass convection or dispersion may prove to be more difficult to solve.

7.3 Recommendations for Further Study

The present study represents a first step in the development of a general interface code based on the vortex theory of interface motion in a porous medium. Further development of such a general code will require additional study in the areas of improvement of the code, extensions of the theory, and applications.

The present formulation of the code can be improved in a number of ways:

(1) Certain statements in the code should be reprogrammed to minimize the effects of roundoff error.

(2) The lengths of the tangent line segments used in the interface fit should be made dependent upon the spacing of the interface points and the slopes of the tangent line segments.

(3) In the present version of the computer code, the routines for treating initial and bounary conditions are problem-dependent, and have been formulated only for the basic check problem. These routines should be generalized as much as possible, so that the code can be used to simulate other problems with a minimum of set-up effort.

Further study is needed to devise convenient methods for accomp lishing these improvements.

The present version of the interface code is limited in some respects, but can be extended to include phenomena not considered in the basic theory.

(1) The vortex theory of interface motion can be extended to include radial flow, storage effects due to compressibility of the fluids and the medium, and a gradual transition zone between the fluids. However, the inclusion of these phenomena in the computer code has yet to be done. Preliminary investigation indicates that the integrals needed to determine the fluid pressure in radial symmetry cannot be evaluated in closed form, although it should be possible to evaluate them by an approximate numerical method.

(2) The vortex theory cannot be applied if the porous medium is anisotropic or inhomogeneous, or if the viscosities of the fluids differ. Because of the importance of these phenomena in practical problems, methods for solving the flow equations incorporating them must be developed. Since the general flow equations are of either elliptic or parabolic form, there do not appear to be any major difficulties involved in their solution by standard numerical methods. However, further work is needed in the development of solution techniques for such problems.

(3) In addition to a flow equation, the description of the motion of an inhomogeneous fluid through a porous medium requires an equation of mass convection or hydrodynamic dispersion. Such equations can be difficult to solve because of their hyperbolic nature, although some success has been reported

in the numerical solution of the dispersion equation. Further study is needed into the numerical solution of such equations.

Ultimately, it is hoped that the computer model discussed in this report can be used in the study of practical problems of multiple-fluid flow in porous media. As mentioned previously, the vortex theory can only be applied to problems in which the viscosity difference between the fluids can be neglected. However, the assumption may not be valid unless the fluids involved are fresh water and sea water, such as in the problems of sea-water intrusion into a coastal fresh-water aquifer, and salt-water coning below an oceanic island. Significant differences in viscosity can occur between fresh and saline waters in continental aquifers, especially in deep, thick aquifers, where the effect of temperature on brine viscosity can be considerable. The present model is contemplated as a possible mode of investigation of liquid waste disposal into deep saline aquifers of the Illinois Basin, but its use may be precluded by the viscosity and temperature gradients observed in those aquifers. The computer model based on the vortex theory of interface motion should, however, be investigated further for its applicability to interface problems in coastal environments, where the viscosity differences can be neglected with greater confidence.

APPENDIX A. EVALUATION OF LINE INTEGRALS ALONG A LINEAR SEGMENT

A.1 Introduction

Suppose we wish to evaluate the line integrals for Ψ_1 and its derivatives along the line segment connecting the points (x_1, y_1) and (x_2, y_2). The slope of this line segment is

$$m = (y_2 - y_1) / (x_2 - x_1) . \tag{A.1.1}$$

Let the point (x_n, y_n) lie on this line segment. Then the equation of the segment is

$$\frac{y_o - y_n}{x_o - x_n} = m$$

or

$$y_o = y_n + m (x_o - x_n), \tag{A.1.2}$$

where (x_o, y_o) are the coordinates of any point lying on the line segment. From equation (A.1.2),

$$dy_o = m \, dx_o , \tag{A.1.3}$$

and

$$\begin{aligned} y - y_o &= y - y_n - m (x_o - x_n) \\ &= y - y_n + m x_n - m x_o \\ &= \alpha - m x_o , \end{aligned} \tag{A.1.4}$$

with

$$\alpha \equiv y - y_n + m x_n . \qquad \text{(A.1.5)}$$

Furthermore, by equation (A.1.4),

$$\begin{aligned} r^2 &\equiv (x - x_0)^2 + (y - y_0)^2 \\ &= (x - x_0)^2 + (\alpha - m x_0)^2 \\ &= (x^2 + \alpha^2) - 2(x + m\alpha) x_0 + (1 + m^2) x_0^2 \\ &= a + b x_0 + c x_0^2 , \end{aligned} \qquad \text{(A.1.6)}$$

with

$$a = x^2 + \alpha^2 \qquad \text{(A.1.7a)}$$

$$b = -2(x + m\alpha) \qquad \text{(A.1.7b)}$$

$$c = 1 + m^2 \qquad \text{(A.1.7c)}$$

The above expressions are valid for $0 \leq |m| < \infty$. For $|m| = \infty$, the equation of the line segment is $x_0 = x_n$. Then, defining

$$A = x - x_n , \qquad \text{(A.1.8)}$$

we have

$$x - x_0 = A \qquad \text{(A.1.9)}$$

and

$$\begin{aligned} r^2 &\equiv (x - x_0)^2 + (y - y_0)^2 \\ &= A^2 + (y - y_0)^2 . \end{aligned} \qquad \text{(A.1.10)}$$

A.2 Evaluation of $\int_{y_1}^{y_2} \ln\left[(x-x_0)^2 + (y-y_0)^2\right] dy_0$

Let

$$I_1 = \int_{y_1}^{y_2} \ln\left[(x-x_0)^2 + (y-y_0)^2\right] dy_0 \qquad \text{(A.2.1)}$$

By equations (A.1.3) and (A.1.6), we have

$$I_1 = \int_{x_1}^{x_2} m \ln\left(a + b x_0 + c x_0^2\right) dx_0 \qquad \text{(A.2.2)}$$

Now, by equations (A.1.7),

$$b^2 - 4ac = 4(x + m\alpha)^2 - 4(1+m^2)(x^2 + \alpha^2)$$

$$= -4(\alpha - mx)^2 < 0 \qquad \text{(A.2.3)}$$

Then, from any standard table of integrals (such as Selby, 1964), we find

$$I_1 = m\left\{(x_0 + \tfrac{b}{2c})\ln(a + bx_0 + cx_0^2) - 2x_0 + \frac{4ac-b^2}{c}\tan^{-1}\frac{2cx_0+b}{\sqrt{4ac-b^2}}\right\}_{x_0=x_1}^{x_2}$$

$$= m\left\{(x_2 + \tfrac{b}{2c})\ln(a + bx_2 + cx_2^2) - (x_1 + \tfrac{b}{2c})\ln(a + bx_1 + cx_1^2) - \right.$$

$$\left. -2x_2 + 2x_1 + \frac{2(\alpha - mx)}{c}\tan^{-1}\left[\frac{2cx_2+b}{2(\alpha-mx)}\right] - \frac{2(\alpha-mx)}{c}\tan^{-1}\left[\frac{2cx_1+b}{2(\alpha-mx)}\right]\right\}, \qquad \text{(A.2.4)}$$

applying equation (A.2.3).

From equations (A.1.7), we find

$$\frac{b}{2c} = \frac{-2(x+m\alpha)}{2(1+m^2)} = -\frac{x+m\alpha}{1+m^2}$$

Then, applying equation (A.1.5), we get

$$x_2 + b/2c = x_2 - (x+m\alpha)/(1+m^2)$$

$$= \frac{1}{1+m^2}\left\{(1+m^2)(x_2-x) - m\left[(y-y_n) - m(x-x_n)\right]\right\} \qquad \text{(A.2.5a)}$$

Similarly,

$$x_1 + b/2c = \frac{1}{1+m^2}\left\{(1+m^2)(x_1-x) - m\left[(y-y_n) - m(x-x_n)\right]\right\} \qquad \text{(A.2.5b)}$$

Also,

$$d + b x_2 + c x_2^2 = x^2 + \alpha^2 - 2(x+m\alpha)x_2 + (1+m^2)x_2^2$$

$$= (x-x_2)^2 + (\alpha - m x_2)^2$$

$$= (x-x_2)^2 + \left[(y-y_n) - m(x-x_n) + m(x-x_2)\right]^2, \qquad \text{(A.2.6a)}$$

applying equation (A.1.5). Similarly,

$$d + b x_1 + c x_1^2 = (x-x_1)^2 + \left[(y-y_n) - m(x-x_n) + m(x-x_1)\right]^2. \qquad \text{(A.2.6b)}$$

By equation (A.1.5),

$$2(\alpha - m x) = 2\left[(y-y_n + m x_n) - m x\right]$$

$$= 2\left[(y-y_n) - m(x-x_n)\right]$$

Then

$$\frac{2c x_2 + b}{2(\alpha - m x)} = \frac{2(1+m^2)x_2 - 2(x+m\alpha)}{2\left[(y-y_n) - m(x-x_n)\right]}$$

$$= \frac{(1+m^2)(x_2-x) - m\left[(y-y_n) - m(x-x_n)\right]}{(y-y_n) - m(x-x_n)} \qquad \text{(A.2.7a)}$$

Similarly,

$$\frac{2c x_1 + b}{2(\alpha - m x)} = \frac{(1+m^2)(x_1-x) - m\left[(y-y_n) - m(x-x_n)\right]}{(y-y_n) - m(x-x_n)} \qquad \text{(A.2.7b)}$$

Finally, applying equations (A.2.5) through (A.2.7), we get

$$I_1 = \frac{m}{1+m^2}\left\{(1+m^2)(x_2-x) - m[(y-y_n) - m(x-x_n)]\right\} \ln\left\{(x-x_2)^2 + [(y-y_n) - m(x-x_n) + m(x-x_2)]^2\right\} - \frac{m}{1+m^2}\left\{(1+m^2)(x_1-x) - m[(y-y_n) - m(x-x_n)]\right\} \ln\left\{(x-x_1)^2 + [(y-y_n) - m(x-x_n) + m(x-x_1)]^2\right\} - 2(x_2-x_1)m + \frac{2[(y-y_n) - m(x-x_n)]m}{1+m^2}\left\{\tan^{-1}\frac{(1+m^2)(x_2-x) - m[(y-y_n) - m(x-x_n)]}{(y-y_n) - m(x-x_n)} - \tan^{-1}\frac{(1+m^2)(x_1-x) - m[(y-y_n) - m(x-x_n)]}{(y-y_n) - m(x-x_n)}\right\} \qquad (A.2.8)$$

Equation (A.2.8) applies for $0 \le |m| < \infty$. For $m=0$, we get $I_1=0$. For $|m| = \infty$, applying equation (A.1.10), we get

$$I_1 = \int_{y_1}^{y_2} \ln\left[A^2 + (y-y_o)^2\right] dy_o \qquad (A.2.9)$$

Transforming the variable of integration in equation (A.2.9) by

$$u = y - y_o , \qquad (A.2.10)$$

we get $dy_o = -du$ and then

$$I_1 = -\int_{y-y_1}^{y-y_2} \ln(A^2+u^2)\, du$$

$$= \left[-u \ln(A^2+u^2) + 2u - 2A \tan^{-1}(u/A)\right]_{u=y-y_1}^{y-y_2}$$

$$= -(y-y_2)\ln\left[(x-x_n)^2 + (y-y_2)^2\right] + (y-y_1)\ln\left[(x-x_n)^2 + (y-y_1)^2\right] - 2(y_2-y_1) - 2(x-x_n)\left\{\tan^{-1}\frac{y-y_2}{x-x_n} - \tan^{-1}\frac{y-y_1}{x-x_n}\right\}, \qquad (A.2.11)$$

applying equation (A.1.8).

A.3 Evaluation of $\int_{Y_1}^{Y_2} \frac{(Y - Y_0)\, dY_0}{(X - X_0)^2 + (Y - Y_0)^2}$

Let

$$I_2 = \int_{Y_1}^{Y_2} \frac{(Y - Y_0)\, dY_0}{(X - X_0)^2 + (Y - Y_0)^2} \qquad (A.3.1)$$

By equations (A.1.3), (A.1.4), and (A.1.6), we have

$$I_2 = \int_{X_1}^{X_2} \frac{(\alpha - m X_0)\, m\, dX_0}{a + b X_0 + c X_0^2}$$

$$= m\alpha \int_{X_1}^{X_2} \frac{dX_0}{a + b X_0 + c X_0^2} - m^2 \int_{X_1}^{X_2} \frac{X_0\, dX_0}{a + b X_0 + c X_0^2} \qquad (A.3.2)$$

From a standard table of integrals, we find

$$\int_{X_1}^{X_2} \frac{X_0\, dX_0}{a + b X_0 + c X_0^2} = \frac{1}{2c} \ln(a + b X_0 + c X_0^2)\Big|_{X_1}^{X_2} - \frac{b}{2c} \int_{X_1}^{X_2} \frac{dX_0}{a + b X_0 + c X_0^2} \qquad (A.3.3)$$

Then equation (A.3.2) becomes

$$I_2 = -\frac{m^2}{2c} \ln \frac{a + b X_2 + c X_2^2}{a + b X_1 + c X_1^2} + \left(m\alpha + \frac{m^2 b}{2c}\right) \int_{X_1}^{X_2} \frac{dX_0}{a + b X_0 + c X_0^2} \qquad (A.3.4)$$

From equation (A.2.3), $4ac - b^2 = 4(\alpha - mx)^2 > 0$, so

$$\int_{X_1}^{X_2} \frac{dX_0}{a + b X_0 + c X_0^2} = \frac{2}{\sqrt{4ac - b^2}} \tan^{-1} \frac{2cX_0 + b}{\sqrt{4ac - b^2}}\Big|_{X_1}^{X_2}$$

$$= \frac{1}{\alpha - mx} \left\{ \tan^{-1} \frac{2cX_2 + b}{2(\alpha - mx)} - \tan^{-1} \frac{2cX_1 + b}{2(\alpha - mx)} \right\} \qquad (A.3.5)$$

Then equation (A.3.4) becomes

$$I_2 = -\frac{m^2}{2c} \ln \frac{a + b X_2 + c X_2^2}{a + b X_1 + c X_1^2} + \frac{m\alpha + \frac{m^2 b}{2c}}{\alpha - mx} \left[\tan^{-1} \frac{2cX_2 + b}{2(\alpha - mx)} - \right.$$

$$\left. - \tan^{-1} \frac{2cX_1 + b}{2(\alpha - mx)} \right] \qquad (A.3.6)$$

From equations (A.1.7), we have

$$m^2/2c = m^2/[2(1+m^2)], \tag{A.3.7}$$

and

$$\frac{m\alpha + m^2 b/2c}{\alpha - mx} = \frac{m(2c\alpha + mb)}{2c(\alpha - mx)}$$

$$= \frac{m(\alpha - mx)}{(1+m^2)(\alpha - mx)} = \frac{m}{1+m^2} \tag{A.3.8}$$

Thus, applying equations (A.3.7) and (A.3.8), as well as equations (A.2.6) and (A.2.7), equation (A.3.6) becomes

$$I_2 = -\frac{m^2}{2(1+m^2)} \ln \frac{(x-x_2)^2 + [(y-y_n) - m(x-x_n) + m(x-x_2)]^2}{(x-x_1)^2 + [(y-y_n) - m(x-x_n) + m(x-x_1)]^2} +$$

$$+ \frac{m}{1+m^2} \left\{ \tan^{-1} \frac{(1+m^2)(x_2-x) - m[(y-y_n) - m(x-x_n)]}{(y-y_n) - m(x-x_n)} - \right.$$

$$\left. - \tan^{-1} \frac{(1+m^2)(x_1-x) - m[(y-y_n) - m(x-x_n)]}{(y-y_n) - m(x-x_n)} \right\} \tag{A.3.9}$$

For m = 0, equation (A.3.9) gives $I_2 = 0$.

For $|m| = \infty$, applying equation (A.1.10), we get

$$I_2 = \int_{y_1}^{y_2} \frac{(y-y_0)\,dy_0}{A^2 + (y-y_0)^2} \tag{A.3.10}$$

Letting $u = y - y_0$, we get

$$I_2 = -\int_{y-y_1}^{y-y_2} \frac{u\,du}{A^2+u^2} = -\frac{1}{2}\int_{y-y_1}^{y-y_2} \frac{2u\,du}{A^2+u^2}$$

$$= -\frac{1}{2}\left[\ln(A^2+u^2)\right]_{y-y_1}^{y-y_2} = -\frac{1}{2}\ln\frac{(x-x_n)^2+(y-y_2)^2}{(x-x_n)^2+(y-y_1)^2} \tag{A.3.11}$$

A.4 Evaluation of $\int_{y_1}^{y_2} \frac{(x-x_0)\,dy_0}{(x-x_0)^2 + (y-y_0)^2}$

Let

$$I_3 = \int_{y_1}^{y_2} \frac{(x-x_0)\,dy_0}{(x-x_0)^2 + (y-y_0)^2} \qquad (A.4.1)$$

From equations (A.1.3) and (A.1.6), we get

$$I_3 = \int_{x_1}^{x_2} \frac{(x-x_0)\,m\,dx_0}{a + bx_0 + cx_0^2}$$

$$= mx \int_{x_1}^{x_2} \frac{dx_0}{a + bx_0 + cx_0^2} - m \int_{x_1}^{x_2} \frac{x_0\,dx_0}{a + bx_0 + cx_0^2} \qquad (A.4.2)$$

From equation (A.3.3), we get

$$I_3 = mx \int_{x_1}^{x_2} \frac{dx_0}{a + bx_0 + cx_0^2} - m\left[\frac{1}{2c} \ln \frac{a + bx_2 + cx_2^2}{a + bx_1 + cx_1^2} - \frac{b}{2c} \int_{x_1}^{x_2} \frac{dx_0}{a + bx_0 + cx_0^2}\right]$$

$$= -\frac{m}{2c} \ln \frac{a + bx_2 + cx_2^2}{a + bx_1 + cx_1^2} + \left(mx + \frac{mb}{2c}\right) \int_{x_1}^{x_2} \frac{dx_0}{a + bx_0 + cx_0^2} \qquad (A.4.3)$$

From equation (A.3.5), this becomes

$$I_3 = -\frac{m}{2c} \ln \frac{a + bx_2 + cx_2^2}{a + bx_1 + cx_1^2} + \frac{m(x + b/2c)}{\alpha - mx} \left\{\tan^{-1} \frac{2cx_2 + b}{2(\alpha - mx)} - \right.$$

$$\left. - \tan^{-1} \frac{2cx_1 + b}{2(\alpha - mx)}\right\} \qquad (A.4.4)$$

From equations (A.1.5) and (A.1.7),

$$\frac{m(x + b/2c)}{\alpha - mx} = \frac{m(2cx + b)}{2c(\alpha - mx)}$$

$$= \frac{-m^2(\alpha - mx)}{(1+m^2)(\alpha - mx)} = -\frac{m^2}{1 + m^2} \qquad (A.4.5)$$

Noting that the expressions in equation (A.4.4) are the same as those in equation (A.3.6), except for their coefficients, we get, from equation (A.3.9),

$$I_3 = -\frac{m}{2(1+m^2)} \ln \frac{(x-x_2)^2+[(y-y_n)-m(x-x_n)+m(x-x_2)]^2}{(x-x_1)^2+[(y-y_n)-m(x-x_n)+m(x-x_1)]^2} -$$

$$-\frac{m^2}{1+m^2}\left\{\tanh^{-1}\frac{(1+m^2)(x_2-x)-m[(y-y_n)-m(x-x_n)]}{(y-y_n)-m(x-x_n)} -\right.$$

$$\left.-\tanh^{-1}\frac{(1+m^2)(x_1-x)-m[(y-y_n)-m(x-x_n)]}{(y-y_n)-m(x-x_n)}\right\} \qquad \text{(A.4.5)}$$

For $m = 0$, equation (A.4.5) gives $I_3 = 0$.

For $|m| = \infty$, equations (A.1.9) and (A.1.10) give

$$I_3 = \int_{y_1}^{y_2} \frac{A\, dy_0}{A^2+(y-y_0)^2} \qquad \text{(A.4.6)}$$

Letting $u = y-y_0$, we get

$$I_3 = -A\int_{y-y_1}^{y-y_2} \frac{du}{A^2+u^2}$$

$$= -A\left[\frac{1}{A}\tanh^{-1}\frac{u}{A}\right]_{y-y_1}^{y-y_2}$$

$$= -\tanh^{-1}\frac{y-y_2}{x-x_n} + \tanh^{-1}\frac{y-y_1}{x-x_n} \qquad \text{(A.4.7)}$$

APPENDIX B. PARABOLIC SPLINE INTERFACE FIT

Consider the set of interface points (x_o^n, y_o^n), n = 1, 2, ... N (Fig. B.1). A polynomial spline fit to the interface points will result in an interface representation which exhibits continuity of slope at the interface points. We will consider a parabolic spline fit in this appendix; such a fit is quite easy to determine, and it might be possible to readily evaluate the line integrals along parabolic arcs (although this proves not to be the case, as seen in Appendix C). A cubic spline fit to a set of points is discussed in most standard texts on numerical analysis (for example, Gerald, 1970).

Let the points (x_o^n, y_o^n) and (x_o^{n+1}, y_o^{n+1}) be connected by the parabola

$$y_o = a_n (x_o - x_o^n)^2 + b_n (x_o - x_o^n) + c_n \qquad \text{(B.1)}$$

Each successive pair of points can be connected by such a parabola. Our problem is to determine the coefficients a_n, b_n, and c_n, n=1, 2, ..., N-1, subject to the condition that the two parabolic arcs meeting at the point (x_o^n, y_o^n) must have the same slope at that point.

The parabola (B.1) passes through the point (x_o^n, y_o^n), so that

$$y_o^n = a_n \cancel{(x_o^n - x_o^n)^2}^{\,0} + b_n \cancel{(x_o^n - x_o^n)}^{\,0} + c_n = c_n \qquad \text{(B.2)}$$

(B.1) also passes through the point (x_o^{n+1}, y_o^{n+1}), so

$$y_o^{n+1} = a_n (x_o^{n+1} - x_o^n)^2 + b_n (x_o^{n+1} - x_o^n) + c_n$$

$$= a_n h_n^2 + b_n h_n + y_o^n , \qquad \text{(B.3)}$$

with

$$h_n \equiv x_o^{n+1} - x_o^n . \qquad \text{(B.4)}$$

Equation (B.2) gives

$$c_n = y_o^n , \qquad \text{(B.5)}$$

while equation (B.3) gives

$$b_n = (y_o^{n+1} - y_o^n - a_n h_n^2)/h_n$$

$$= k_n/h_n - h_n a_n , \qquad \text{(B.6)}$$

with

$$k_n \equiv y_o^{n+1} - y_o^n . \qquad \text{(B.7)}$$

From equation (B.1), we find

$$y_o' = dy_o/dx_o = 2a_n (x_o - x_o^n) + b_n \qquad \text{(B.8)}$$

For segment n, $y_o' = 2a_n(x_o - x_o^n) + b_n$, while for segment n-1, $y_o' = 2a_{n-1}(x_o - x_o^{n-1}) + b_{n-1}$. Equating these slopes at (x_o^n, y_o^n), where these two segments meet, we get

$$2a_n (\cancel{x_o^n - x_o^n}^{\,0}) + b_n = 2a_{n-1}(x_o^n - x_o^{n-1}) + b_{n-1} ,$$

or

$$b_n = 2 a_{n-1} h_{n-1} + b_{n-1} \qquad \text{(B.9)}$$

Expressing b_n and b_{n-1} in equation (B.9) by equation (B.6), we get

$$k_n / h_n - h_n a_n = 2 a_{n-1} h_{n-1} + k_{n-1} / h_{n-1} - h_{n-1} a_{n-1} ,$$

or

$$h_{n-1} a_{n-1} + h_n a_n = k_n / h_n - k_{n-1} / h_{n-1} \qquad \text{(B.10)}$$

Equation (B.10) applies at each interior interface point, $n = 2, 3, \ldots, N-1$, giving N-2 equations for N-1 unknowns: a_n, $n = 1, 2, \ldots, N-1$. To obtain an additional equation, let the slope $y_0')_1$ at (x_0^1 , y_0^1) be given by linear extrapolation from the slopes at (x_0^2 , y_0^2) and (x_0^3 , y_0^3):

$$\frac{y_0')_3 - y_0')_2}{x_0^3 - x_0^2} = \frac{y_0')_2 - y_0')_1}{x_0^2 - x_0^1} ,$$

so

$$(2 a_2 h_2 + b_2 - b_2) / h_2 = (2 a_1 h_1 + b_1 - b_1) / h_1 ,$$

or

$$a_2 = a_1 \qquad \text{(B.11)}$$

The equations (B.10) and (B.11) can now be readily solved for all of the coefficients a_n. For n = 2, (B.10) gives

$$h_1 a_1 + h_2 a_2 = k_2/h_2 - k_1/h_1 .$$

Applying equation (B.11), this becomes

$$(h_1 + h_2) a_1 = k_2/h_2 - k_1/h_1 ,$$

or

$$a_1 = (k_2/h_2 - k_1/h_1)/(h_1 + h_2) \qquad \text{(B.12)}$$

Then $a_2 = a_1$, and, from equation (B.10),

$$a_n = (k_n/h_n - k_{n-1}/h_{n-1} - h_{n-1} a_{n-1})/h_n , \quad n = 3, 4, \ldots, N-1. \qquad \text{(B.13)}$$

Once the set of values of a_n have been determined, the values of b_n are given by equation (B.9). The values of c_n are given by equation (B.5). The values of all of the coefficients can be expressed in terms of the coordinates of the interface points (x_o^n , y_o^n) by applying equations (B.4) and (B.7).

Figure B.1. Parabolic spline interface fit.

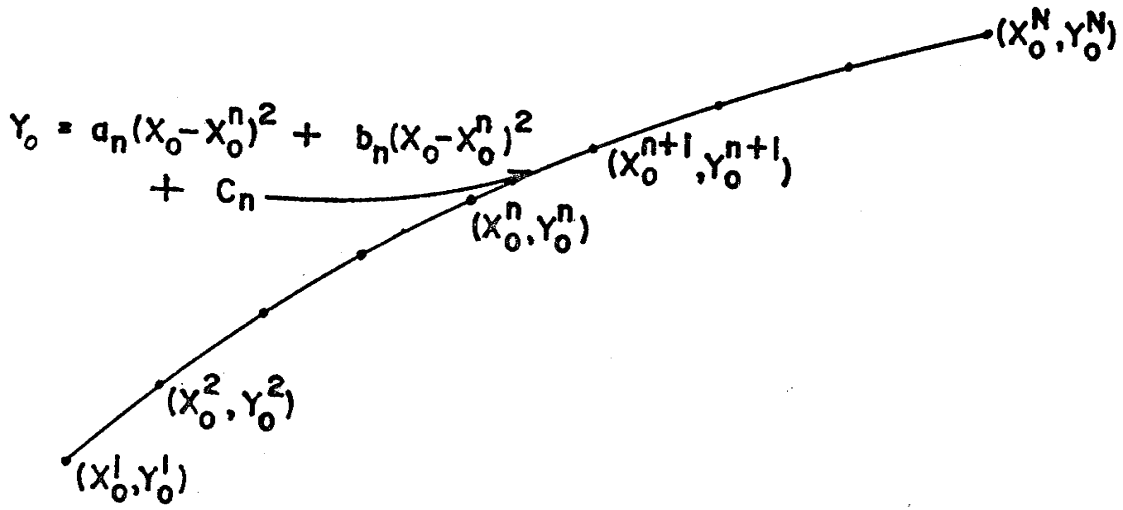
$Y_o = a_n(X_o - X_o^n)^2 + b_n(X_o - X_o^n)^2 + C_n$
(X_o^N, Y_o^N)
(X_o^{n+1}, Y_o^{n+1})
(X_o^n, Y_o^n)
(X_o^2, Y_o^2)
(X_o^1, Y_o^1)

APPENDIX C. EVALUATION OF LINE INTEGRALS ALONG A PARABOLIC ARC

C.1 Introduction

Suppose we wish to evaluate the line integrals for Ψ_1 and its derivatives along the curve

$$y_o - y_o^n = a_n (x_o - x_o^n)^2 + b_n (x_o - x_o^n) \qquad (C.1.1)$$

connecting the points (x_o^n , y_o^n) and (x_o^{n+1} , y_o^{n+1}). The coefficients a_n and b_n in equation (C.1.1) are presumed to be known from the parabolic spline fit described in Appendix B. From equation (C.1.1), we have

$$dy_o = [2 a_n (x_o - x_o^n) + b_n] dx_o \qquad (C.1.2)$$

and

$$y - y_o = y - y_o^n - a_n (x_o - x_o^n)^2 - b_n (x_o - x_o^n), \qquad (C.1.3)$$

Then

$$\begin{aligned} r^2 &\equiv (x - x_o)^2 + (y - y_o)^2 \\ &= [(x - x_o^n) - (x_o - x_o^n)]^2 + [(y - y_o^n) - a_n (x_o - x_o^n)^2 - b_n (x_o - x_o^n)]^2 \\ &= [(x - x_o^n)^2 + (y - y_o^n)^2] - 2[(x - x_o^n) + b_n (y - y_o^n)](x_o - x_o^n) + \\ &\quad + [1 + b_n^2 - 2 a_n (y - y_o^n)](x_o - x_o^n)^2 + 2 a_n b_n (x_o - x_o^n)^3 + \\ &\quad + a_n^2 (x_o - x_o^n)^4 \end{aligned} \qquad (C.1.4)$$

Now, define

$$A = (x - x_o^n)^2 + (y - y_o^n)^2 \tag{C.1.5a}$$

$$B = -2\left[(x - x_o^n) + b_n (y - y_o^n)\right] \tag{C.1.5b}$$

$$C = 1 + b_n^2 - 2 a_n (y - y_o^n) \tag{C.1.5c}$$

$$D = 2 a_n b_n \tag{C.1.5d}$$

$$E = a_n^2 \tag{C.1.5e}$$

to get

$$r^2 = A + B(x_o - x_o^n) + C(x_o - x_o^n)^2 + D(x_o - x_o^n)^3 + E(x_o - x_o^n)^4 \tag{C.1.6}$$

Applying equations (C.1.2), (C.1.3), and (C.1.6), we get

$$\Psi_1 \propto I_1 \equiv \int_{y_o^n}^{y_o^{n+1}} \ln r^2 \, dy_o$$

$$= \int_{x_o^n}^{x_o^{n+1}} \ln\left[A + B(x_o - x_o^n) + C(x_o - x_o^n)^2 + D(x_o - x_o^n)^3 + E(x_o - x_o^n)^4\right]\left[2 a_n (x_o - x_o^n) + b_n\right] dx_o \tag{C.1.7}$$

$$\partial\Psi_1/\partial y \propto I_2 \equiv \int_{y_o^n}^{y_o^{n+1}} \left[(y - y_o)/r^2\right] dy_o$$

$$= \int_{x_o^n}^{x_o^{n+1}} \frac{\left[(y - y_o^n) - a_n (x_o - x_o^n)^2 - b_n (x_o - x_o^n)\right]\left[2 a_n (x_o - x_o^n) + b_n\right] dx_o}{A + B(x_o - x_o^n) + C(x_o - x_o^n)^2 + D(x_o - x_o^n)^3 + E(x_o - x_o^n)^4} \tag{C.1.8}$$

We can write $x - x_o = x - x_o^n - (x_o - x_o^n)$, so that

$$\partial\Psi_1/\partial x \propto I_3 \equiv \int_{y_o^n}^{y_o^{n+1}} \left[(x - x_o)/r^2\right] dy_o$$

$$= \int_{x_o^n}^{x_o^{n+1}} \frac{\left[(x - x_o^n) - (x_o - x_o^n)\right]\left[2 a_n (x_o - x_o^n) + b_n\right] dx_o}{A + B(x_o - x_o^n) + C(x_o - x_o^n)^2 + D(x_o - x_o^n)^3 + E(x_o - x_o^n)^4} \tag{C.1.9}$$

Finally, by the change of variable $u=(x_0-x_0^n)$, equations (C.1.7) through (C.1.9) become

$$I_1=\int_0^{x_0^{n+1}-x_0^n}(2a_nu+b_n)\ln(A+Bu+Cu^2+Du^3+Eu^4)\,du \qquad (C.1.10)$$

$$I_2=\int_0^{x_0^{n+1}-x_0^n}\frac{(2a_nu+b_n)[(y-y_0^n)-b_nu-a_nu^2]\,du}{A+Bu+Cu^2+Du^3+Eu^4} \qquad (C.1.11)$$

$$I_3=\int_0^{x_0^{n+1}-x_0^n}\frac{[(x-x_0^n)-u][2a_nu+b_n]\,du}{A+Bu+Cu^2+Du^3+Eu^4} \qquad (C.1.12)$$

C.2 Linear Factors of $A + Bu + Cu^2 + Du^3 + Eu^4$

We can evaluate equations (C.1.10) through (C.1.12) if we know the linear factors of the quartic polynomial $A + Bu + Cu^2 + Du^3 + Eu^4$. The factors of a general quartic polynomial can be determined from formulas given in most standard books of mathematical formulas and tables. Let

$$A+Bu+Cu^2+Du^3+Eu^4 = E\left[u^4+(D/E)u^3+(C/E)u^3+(B/E)u+(A/E)\right]$$

$$= E\left[(u-\alpha_1)(u-\alpha_2)(u-\alpha_3)(u-\alpha_4)\right], \qquad (C.2.1)$$

where the α_i are the roots of the equation

$$u^4 + (D/E)u^3 + (C/E)u^2 + (B/E)u + A/E = 0. \qquad (C.2.2)$$

In equation (C.2.2), let $u = v - (D/4E)$, to obtain the reduced equation

$$v^4 + \left(\frac{CE-6D^2}{E^2}\right)v^2 + \left(\frac{16BE^2-8CDE+2D^3}{16E^3}\right)v +$$

$$+ \left(\frac{64AE^3-16BDE^2+4CD^2E-3D^4}{64E^4}\right) = 0 \qquad (C.2.3)$$

or

$$v^4 + av^2 + bv + c = 0, \qquad (C.2.4)$$

where

$$a = (CE-6D^2)/E^2 \qquad (C.2.5a)$$

$$b = (16BE^2-8CDE+2D^3)/16E^3 \qquad (C.2.5b)$$

$$c = (64AE^3 - 16BDE^2 + 4CD^2E - 3D^4)/64E^4 \qquad \text{(C.2.5c)}$$

The resolvent cubic equation associated with (C.2.4) is

$$w^3 + (a/2)w^2 + [(a^2 - 4c)/16]w - b^2/64 = 0. \qquad \text{(C.2.6)}$$

We now seek to determine the roots of the resolvent cubic equation (C.2.6). In equation (C.2.6), let

$$w = t - a/6, \qquad \text{(C.2.7)}$$

to obtain the normal form

$$t^3 + dt + e = 0, \qquad \text{(C.2.8)}$$

where

$$d = \frac{1}{3}\left[3\left(\frac{a^2 - 4c}{16}\right) - \frac{a^2}{4}\right] \qquad \text{(C.2.9a)}$$

and

$$e = \frac{1}{27}\left[\frac{a^3}{4} - 9\left(\frac{a}{2}\right)\left(\frac{a^2 - 4c}{16}\right) - 27\left(\frac{b^2}{64}\right)\right] \qquad \text{(C.2.9b)}$$

The solutions to equation (C.2.8) are

$$t_1 = F + G \qquad \text{(C.2.10a)}$$

$$t_2 = -(F+G)/2 + i\sqrt{3}(F-G)/2 \qquad \text{(C.2.10b)}$$

$$t_3 = -(F+G)/2 - i\sqrt{3}(F-G)/2 \qquad \text{(C.2.10c)}$$

where

$$F = \left[-\frac{e}{2} + \left(\frac{e^2}{4} + \frac{d^3}{27} \right)^{1/2} \right]^{1/3} \qquad \text{(C.2.11a)}$$

and

$$G = \left[-\frac{e}{2} - \left(\frac{e^2}{4} + \frac{d^3}{27} \right)^{1/2} \right]^{1/3} \qquad \text{(C.2.11b)}$$

From equations (C.2.7) and (C.2.10), the roots of the resolvent cubic equation (C.2.6) are

$$w_1 = t_1 - a/6 \qquad \text{(C.2.12a)}$$

$$w_2 = t_2 - a/6 \qquad \text{(C.2.12b)}$$

$$w_3 = t_3 - a/6 \qquad \text{(C.2.12c)}$$

Then the roots of the reduced quartic equation (C.2.4) are

$$v_1 = \sqrt{w_1} + \sqrt{w_2} + \sqrt{w_3} \qquad \text{(C.2.13a)}$$

$$v_2 = \sqrt{w_1} - \sqrt{w_2} - \sqrt{w_3} \qquad \text{(C.2.13b)}$$

$$v_3 = -\sqrt{w_1} + \sqrt{w_2} - \sqrt{w_3} \qquad \text{(C.2.13c)}$$

$$v_4 = -\sqrt{w_1} - \sqrt{w_2} + \sqrt{w_3}\,, \qquad \text{(C.2.13d)}$$

where the signs of the radicals $\sqrt{w_1}$, $\sqrt{w_2}$, and $\sqrt{w_3}$ must be be chosen such that

$$\sqrt{w_1}\,\sqrt{w_2}\,\sqrt{w_3} = -b/8 \qquad \text{(C.2.14)}$$

Finally, the roots of the equation (C.2.2) are

$$\alpha_1 = V_1 - (D/4E) \qquad \text{(C.2.15a)}$$

$$\alpha_2 = V_2 - (D/4E) \qquad \text{(C.2.15b)}$$

$$\alpha_3 = V_3 - (D/4E) \qquad \text{(C.2.15c)}$$

$$\alpha_4 = V_4 - (D/4E) \qquad \text{(C.2.15d)}$$

C.3 Evaluation of $I_1 \equiv \int_{y_0^n}^{y_0^{n+1}} \ln r^2 \, dy_0$

From equations (C.1.10) and (C.2.1), we have

$$I_1 = \int_0^{x_0^{n+1}-x_0^n} (2a_n u + b_n) \ln[E(u-\alpha_1)(u-\alpha_2)(u-\alpha_3)(u-\alpha_4)] \, du$$

$$= \int_0^{x_0^{n+1}-x_0^n} (2a_n u + b_n) \left[\ln E + \sum_{i=1}^{4} \ln(u-\alpha_i) \right] du$$

$$= \ln E \int_0^{x_0^{n+1}-x_0^n} (2a_n u + b_n) du + \sum_{i=1}^{4} \int_0^{x_0^{n+1}-x_0^n} (2a_n u + b_n) \ln(u-\alpha_i) du \qquad \text{(C.3.1)}$$

Now

$$\int_0^{x_0^{n+1}-x_0^n} (2a_n u + b_n) du = (a_n u^2 + b_n u) \Big|_0^{x_0^{n+1}-x_0^n}$$

$$= a_n (x_0^{n+1}-x_0^n)^2 + b_n (x_0^{n+1}-x_0^n) \qquad \text{(C.3.2)}$$

$$\int_0^{x_0^{n+1}-x_0^n} (2a_n u + b_n) \ln(u-\alpha_i) \, du =$$

$$= 2a_n \int_0^{x_0^{n+1}-x_0^n} u \ln(u-\alpha_i) du + b_n \int_0^{x_0^{n+1}-x_0^n} \ln(u-\alpha_i) \, du \qquad \text{(C.3.3)}$$

In equation (C.3.3), let $v = u - \alpha_i$ to get

$$\int_0^{x_0^{n+1}-x_0^n} (2a_n u + b_n) \ln(u-\alpha_i) \, du =$$

$$= 2a_n \int_{-\alpha_i}^{x_0^{n+1}-x_0^n-\alpha_i} (v+\alpha_i) \ln v \, dv + b_n \int_{-\alpha_i}^{x_0^{n+1}-x_0^n-\alpha_i} \ln v \, dv$$

$$= 2a_n \int_{-\alpha_i}^{x_0^{n+1}-x_0^n-\alpha_i} v \ln v \, dv + (2a_n\alpha_i + b_n) \int_{-\alpha_i}^{x_0^{n+1}-x_0^n-\alpha_i} \ln v \, dv$$

$$= 2a_n \left\{ v^2 \left[\tfrac{1}{2} \ln v - \tfrac{1}{4} \right] \right\}_{-\alpha_i}^{x_0^{n+1}-x_0^n-\alpha_i} + (2a_n\alpha_i + b_n) \left\{ v[\ln v - 1] \right\}_{-\alpha_i}^{x_0^{n+1}-x_0^n-\alpha_i}$$

$$= (x_0^{n+1}-x_0^n-\alpha_i)[a_n(x_0^{n+1}-x_0^n) + (a_n\alpha_i + b_n)] \ln(x_0^{n+1}-x_0^n-\alpha_i) +$$

$$+ \alpha_i(a_n\alpha_i + b_n) \ln(-\alpha_i) - \tfrac{1}{2} a_n (x_0^{n+1}-x_0^n)[(x_0^{n+1}-x_0^n) - 2\alpha_i] -$$

$$- (x_0^{n+1}-x_0^n)(2a_n\alpha_i + b_n) \qquad \text{(C.3.4)}$$

Combining equations (C.3.1), (C.3.2), and (C.3.4), we get

$$I_1 = \ln E\left\{(x_o^{n+1} - x_o^n)\left[a_n(x_o^{n+1} - x_o^n) + b_n\right]\right\} +$$

$$+ \sum_{i=1}^{4}\left\{(x_o^{n+1} - x_o^n - \alpha_i)\left[a_n(x_o^{n+1} - x_o^n) + (a_n\alpha_i + b_n)\right]\ln(x_o^{n+1} - x_o^n - \alpha_i) + \right.$$

$$+ \alpha_i(a_n\alpha_i + b_n)\ln(-\alpha_i) - \tfrac{1}{2}a_n(x_o^{n+1} - x_o^n)\left[(x_o^{n+1} - x_o^n) - 2\alpha_i\right] -$$

$$\left. - (x_o^{n+1} - x_o^n)(2a_n\alpha_i + b_n)\right\} \qquad \text{(C. 3. 5)}$$

C.4 Evaluation of $I_2 \equiv \int_{Y_o^n}^{Y_o^{n+1}} [(Y-Y_o)/r^2]\, dY_o$

From equations (C.1.11) and (C.2.1), we have

$$I_2 = \int_0^{X_o^{n+1} - X_o^n} \frac{(2a_n u + b_n)[(Y-Y_o^n) - b_n u - a_n u^2]\, du}{E(u-\alpha_1)(u-\alpha_2)(u-\alpha_3)(u-\alpha_4)} \qquad (C.4.1)$$

Equation (C.4.1) can be evaluated by applying the method of partial fractions. Let

$$\frac{(2a_n u + b_n)[(Y-Y_o^n) - b_n u - a_n u^2]}{(u-\alpha_1)(u-\alpha_2)(u-\alpha_3)(u-\alpha_4)} = \frac{R_1}{u-\alpha_1} + \frac{R_2}{u-\alpha_2} + \frac{R_3}{u-\alpha_3} + \frac{R_4}{u-\alpha_4},$$

or

$$(2a_n u + b_n)[(Y-Y_o^n) - b_n u - a_n u^2] = R_1(u-\alpha_2)(u-\alpha_3)(u-\alpha_4) + R_2(u-\alpha_1)(u-\alpha_3)(u-\alpha_4) + R_3(u-\alpha_1)(u-\alpha_2)(u-\alpha_4) + R_3(u-\alpha_1)(u-\alpha_2)(u-\alpha_3) \qquad (C.4.2)$$

Letting u take on the values α_i, i = 1, 2, 3, 4, in equation (C.4.2), we get

$$R_1 = \frac{(2a_n\alpha_1 + b_n)[(Y-Y_o^n) - b_n\alpha_1 - a_n\alpha_1^2]}{(\alpha_1-\alpha_2)(\alpha_1-\alpha_3)(\alpha_1-\alpha_4)} \qquad (C.4.3a)$$

$$R_2 = \frac{(2a_n\alpha_2 + b_n)[(Y-Y_o^n) - b_n\alpha_2 - a_n\alpha_2^2]}{(\alpha_2-\alpha_1)(\alpha_2-\alpha_3)(\alpha_2-\alpha_4)} \qquad (C.4.3b)$$

$$R_3 = \frac{(2a_n\alpha_3 + b_n)[(Y-Y_o^n) - b_n\alpha_3 - a_n\alpha_3^2]}{(\alpha_3-\alpha_1)(\alpha_3-\alpha_2)(\alpha_3-\alpha_4)} \qquad (C.4.3c)$$

$$R_4 = \frac{(2a_n\alpha_4 + b_n)[(Y-Y_o^n) - b_n\alpha_4 - a_n\alpha_4^2]}{(\alpha_4-\alpha_1)(\alpha_4-\alpha_2)(\alpha_4-\alpha_3)} \qquad (C.4.3d)$$

Then we can write equation (C.4.1) in the form

$$I_2 = \frac{1}{E}\sum_{i=1}^{4} R_i \int_0^{x_0^{n+1}-x_0^{n}} \frac{du}{u-\alpha_i}$$

$$= \frac{1}{E}\sum_{i=1}^{4} R_i \ln\left[\frac{\alpha_i - (x_0^{n+1}-x_0^{n})}{\alpha_i}\right] \qquad \text{(C.4.4)}$$

C.5 Evaluation of $I_3 \equiv \int_{Y_o^n}^{Y_o^{n+1}} [(x-x_o)/r^2]\, dy_o$

From equations (C.1.12) and (C.2.1), we have

$$I_3 = \int_0^{x_o^{n+1}-x_o^n} \frac{[(x-x_o^n)-u][2a_n u + b_n]\, du}{E[(u-\alpha_1)(u-\alpha_2)(u-\alpha_3)(u-\alpha_4)]} \qquad (C.5.1)$$

Equation (C.5.1) can also be evaluated by the method of partial fractions. Let

$$\frac{[(x-x_o^n)-u][2a_n u + b_n]}{(u-\alpha_1)(u-\alpha_2)(u-\alpha_3)(u-\alpha_4)} = \frac{S_1}{u-\alpha_1} + \frac{S_2}{u-\alpha_2} + \frac{S_3}{u-\alpha_3} + \frac{S_4}{u-\alpha_4}$$

or

$$[(x-x_o^n)-u][2a_n u + b_n] = S_1(u-\alpha_2)(u-\alpha_3)(u-\alpha_4) + S_2(u-\alpha_1)(u-\alpha_3)(u-\alpha_4) + S_3(u-\alpha_1)(u-\alpha_2)(u-\alpha_4) + S_4(u-\alpha_1)(u-\alpha_2)(u-\alpha_3) \qquad (C.5.2)$$

Letting u take on the values α_i , i=1, 2, 3, 4, in equation (C.5.2), we get

$$S_1 = \frac{[(x-x_o^n)-\alpha_1][2a_n\alpha_1 + b_n]}{(\alpha_1-\alpha_2)(\alpha_1-\alpha_3)(\alpha_1-\alpha_4)} \qquad (C.5.3a)$$

$$S_2 = \frac{[(x-x_o^n)-\alpha_2][2a_n\alpha_2 + b_n]}{(\alpha_2-\alpha_1)(\alpha_2-\alpha_3)(\alpha_2-\alpha_4)} \qquad (C.5.3b)$$

$$S_3 = \frac{[(x-x_o^n)-\alpha_3][2a_n\alpha_3 + b_n]}{(\alpha_3-\alpha_1)(\alpha_3-\alpha_2)(\alpha_3-\alpha_4)} \qquad (C.5.3c)$$

$$S_4 = \frac{[(x-x_o^n)-\alpha_4][2a_n\alpha_4 + b_n]}{(\alpha_4-\alpha_1)(\alpha_4-\alpha_2)(\alpha_4-\alpha_3)} \qquad (C.5.3d)$$

Then we can write equation (C.5.1) in the form

$$I_3 = \frac{1}{E} \sum_{i=1}^{4} S_i \int_0^{x_0^{n+1} - x_0^n} \frac{du}{u - \alpha_i}$$

$$= \frac{1}{E} \sum_{i=1}^{4} S_i \ln \left[\frac{\alpha_i - (x_0^{n+1} - x_0^n)}{\alpha_i} \right] \qquad \text{(C.5.4)}$$

APPENDIX D. THE SHEAR DISCONTINUITY IN THE SPECIFIC DISCHARGE AT A POINT ON THE INTERFACE

From equations (3.1.6) and (3.1.7), we can write the specific discharge components resulting from the line integrals along a straight line segment as

$$q_x)_1 = \frac{k(\gamma_2-\gamma_1)}{2\pi\mu}\int_{Y_1}^{Y_2}\frac{(y-y_0)\,dy_0}{(x-x_0)^2+(y-y_0)^2} \qquad (D.1)$$

$$q_y)_1 = -\frac{k(\gamma_2-\gamma_1)}{2\pi\mu}\int_{Y_1}^{Y_2}\frac{(x-x_0)\,dy_0}{(x-x_0)^2+(y-y_0)^2}\,, \qquad (D.2)$$

where y_1 and y_2 denote the y-coordinates of the endpoints of the line segment. As in Appendix A, we will assume that the line segment connects the points (x_1, y_1) and (x_2, y_2), passes through the point (x_n, y_n), and has slope m. Then, from Appendix A, we get

$$q_x)_1 = \frac{k(\gamma_2-\gamma_1)}{2\pi\mu}\left\{-\frac{m^2}{2(1+m^2)}\ln\frac{(x-x_2)^2+[(y-y_n)-m(x-x_n)+m(x-x_2)]^2}{(x-x_1)^2+[(y-y_n)-m(x-x_n)+m(x-x_1)]^2}+\right.$$
$$+\frac{m}{1+m^2}\left\{\tan^{-1}\frac{(1+m^2)(x_2-x)-m[(y-y_n)-m(x-x_n)]}{(y-y_n)-m(x-x_n)}-\right.$$
$$\left.\left.-\tan^{-1}\frac{(1+m^2)(x_1-x)-m[(y-y_n)-m(x-x_n)]}{(y-y_n)-m(x-x_n)}\right\}\right\} \qquad (D.3)$$

and

$$q_y)_1 = -\frac{k(\gamma_2-\gamma_1)}{2\pi\mu}\left\{-\frac{m^2}{2(1+m^2)}\ln\frac{(x-x_2)^2+[(y-y_n)-m(x-x_n)+m(x-x_2)]^2}{(x-x_1)^2+[(y-y_n)-m(x-x_n)+m(x-x_1)]^2}-\right.$$
$$-\frac{m^2}{1+m^2}\left\{\tan^{-1}\frac{(1+m^2)(x_2-x)-m[(y-y_n)-m(x-x_n)]}{(y-y_n)-m(x-x_n)}-\right.$$
$$\left.\left.-\tan^{-1}\frac{(1+m^2)(x_1-x)-m[(y-y_n)-m(x-x_n)]}{(y-y_n)-m(x-x_n)}\right\}\right\} \qquad (D.4)$$

We will confine our attention to the arctangent terms in equations (D.3) and (D.4). We first note that these terms are the same in both equations, differing only in their coefficients. Define

$$A = \tan^{-1}\frac{(1+m^2)(x_2-x) - mD}{D} - \tan^{-1}\frac{(1+m^2)(x_1-x) - mD}{D} \quad \text{(D.5)}$$

where

$$D = (y - y_n) - m(x - x_n). \quad \text{(D.6)}$$

We will now consider the behavior of A, given by equation (D.5), when the point (x, y), at which the expressions are to be evaluated, lies on the line segment. Since the line segment passes through the point (x_n, y_n) and has slope m, its equation is $y - y_n - m(x - x_n) = 0$. Thus, from equation (D.6), we must consider the vehavior of A when D = 0. We see from equation (D.5) that the arguments of the arctangent functions become infinite when D = 0. Furthermore, since $\tan^{-1}(+\infty) \neq \tan^{-1}(-\infty)$, we must consider both $\lim_{D \to 0+} A$ and $\lim_{D \to 0-} A$; that is, we must consider the behavior of A as the point (x, y) approaches a point on the line segment from the right and from the left.

Suppose that $m > 0$. Then, from Fig. D.1a, we see that $x < x_2$ and $x > x_1$. Thus we have

$$\lim_{D \to 0} [(1+m^2)(x_2 - x) - mD] > 0 \quad \text{(D.7a)}$$

and

$$\lim_{D\to 0} \left[(1+m^2)(X_1 - x) - m D\right] < 0. \qquad \text{(D.7b)}$$

Note that the limits in inequalities (D.7) are unique, regardless of whether $D \to 0+$ or $D \to 0-$. Hence, from equation (D.5), we get

$$\lim_{D\to 0+} A = \tan^{-1}(+\infty) - \tan^{-1}(-\infty)$$

$$= \pi/2 - (-\pi/2) = \pi, \quad m > 0 \qquad \text{(D.8a)}$$

$$\lim_{D\to 0-} A = \tan^{-1}(-\infty) - \tan^{-1}(+\infty)$$

$$= -\pi/2 - \pi/2 = -\pi, \quad m > 0 \qquad \text{(D.8b)}$$

Similarly, for $m < 0$, we have $x > x_2$ and $x < x_1$. Then

$$\lim_{D\to 0} \left[(1+m^2)(X_2 - x) - m D\right] < 0 \qquad \text{(D.9a)}$$

and

$$\lim_{D\to 0} \left[(1+m^2)(X_1 - x) - m D\right] > 0 \qquad \text{(D.9b)}$$

Hence

$$\lim_{D\to 0+} A = \tan^{-1}(-\infty) - \tan^{-1}(+\infty) = -\pi, \quad m < 0 \qquad \text{(D.10a)}$$

$$\lim_{D\to 0-} A = \tan^{-1}(+\infty) - \tan^{-1}(-\infty) = \pi, \quad m < 0 \qquad \text{(D.10b)}$$

Applying these results to equations (D.3) and (D.4), we find that the contributions to the specific discharge components from the arctangent terms, denoted by $q_{x)_1}^{*}$ and $q_{y)_1}^{*}$, are, for $m>0$,

$$\lim_{D\to 0+} q_{x)_1}^{*} = \left[k(Y_2 - Y_1)\, m / 2\pi\mu(1+m^2)\right](\pi) \qquad \text{(D.11a)}$$

$$\lim_{D\to 0-} q_x)_1^* = [k(\gamma_2-\gamma_1)m/2\pi\mu(1+m^2)](-\pi) \qquad \text{(D.11b)}$$

$$\lim_{D\to 0+} q_y)_1^* = [k(\gamma_2-\gamma_1)m^2/2\pi\mu(1+m^2)](\pi) \qquad \text{(D.12a)}$$

$$\lim_{D\to 0-} q_y)_1^* = [k(\gamma_2-\gamma_1)m^2/2\pi\mu(1+m^2)](-\pi) \qquad \text{(D.12b)}$$

Similarly, for $m < 0$,

$$\lim_{D\to 0+} q_x)_1^* = [k(\gamma_2-\gamma_1)m/2\pi\mu(1+m^2)](-\pi) \qquad \text{(D.13a)}$$

$$\lim_{D\to 0-} q_x)_1^* = [k(\gamma_2-\gamma_1)m/2\pi\mu(1+m^2)](\pi) \qquad \text{(D.13b)}$$

$$\lim_{D\to 0+} q_y)_1^* = [k(\gamma_2-\gamma_1)m^2/2\pi\mu(1+m^2)](-\pi) \qquad \text{(D.14a)}$$

$$\lim_{D\to 0-} q_y)_1^* = [k(\gamma_2-\gamma_1)m^2/2\pi\mu(1+m^2)](\pi) \qquad \text{(D.14b)}$$

The terms $q_x)_1^*$ and $q_y)_1^*$ give rise to a vector of length $q_1^* = \sqrt{[q_x)_1^*]^2+[q_y)_1^*]^2}$ and inclination $\alpha_1^* = \tan^{-1}[q_y)_1^*/q_x)_1^*]$. In each case considered above, we get

$$q_1^* = \left\{\left[\frac{k(\gamma_2-\gamma_1)m}{2\pi\mu(1+m^2)}\right]^2(\pm\pi)^2 + \left[\frac{k(\gamma_2-\gamma_1)m^2}{2\pi\mu(1+m^2)}\right]^2(\pm\pi)^2\right\}^{1/2}$$

$$= k(\gamma_2-\gamma_1)|m|\pi/2\pi\mu\sqrt{1+m^2}, \qquad \text{(D.15)}$$

while

$$\alpha_1^* = \tan^{-1}\left[\frac{k(\gamma_2-\gamma_1)m^2(\pm\pi)/2\pi\mu(1+m^2)}{k(\gamma_2-\gamma_1)m(\pm\pi)/2\pi\mu(1+m^2)}\right] = \tan^{-1}(m) \qquad \text{(D.16)}$$

Equations (D.15) and (D.16) are unique, regardless of whether $D \to 0+$ or $D \to 0-$. However, we also see from equations (D.11) through (D.14) that regardless of the sign of m, we have

Figure D.1. Relation between interface points for positive and negative slope of interface line segment.

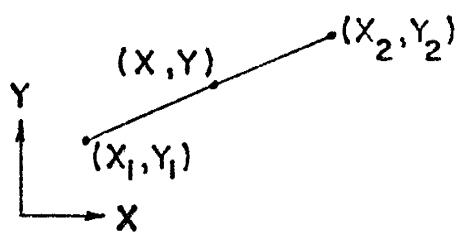

(a) $m > 0$

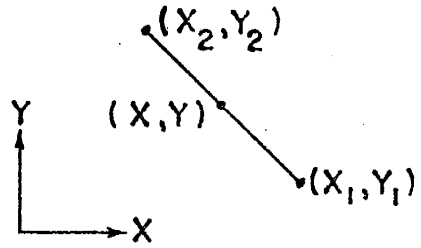

(b) $m < 0$

$$\lim_{D\to 0-} q_x)_1^* = - \lim_{D\to 0+} q_x)_1^* , \qquad \text{(D.17a)}$$

and

$$\lim_{D\to 0-} q_y)_1^* = - \lim_{D\to 0+} q_y)_1^* . \qquad \text{(D.17b)}$$

Thus, the contributions to the specific discharge vector from the inverse tangent terms, as $D \to 0+$ or $D \to 0-$, are vectors of the same magnitude and inclination, but are oppositely directed. Furthermore, from equation (D.16), we see that these vectors are parallel to the line segment. Finally, referring to equation (D.15), as well as equation (2.3.1) and the subsequent discussion, and noting that

$$|m| / \sqrt{1+m^2} = \sqrt{\tan^2\alpha / (1+\tan^2\alpha)} = \sin\alpha ,$$

where α is the angle of inclination of the interfacial line segment, we see that the magnitude of the shear discontinuity is proportional to the strength of the vortex located at the point $(x\ ,\ y)$ on the interface. Thus the specific discharge component at $(x\ ,\ y)$ given by $q_x)_1^*$ and $q_y)_1^*$ consists of a shear flow tangent to the interface, and proportional to the vortex strength at that point.

For m = 0, we see from Appendix A that $\partial\Psi_1/\partial x = \partial\Psi_1/\partial y = 0$. Furthermore, from equation (D.15), we have $q_1^* = 0$. Thus there is no shear discontinuity in the specific discharge at a point on a horizontal segment of the interface. However, if $|m| = \infty$, the shear discontinuity again appears. In this case, from equations (D.1), (D.2), (A.3.11), and (A.4.7), we have

$$q_x)_1 = \frac{k(\gamma_2-\gamma_1)}{4\pi\mu} \ln \frac{(x-x_n)^2+(y-y_1)^2}{(x-x_n)^2+(y-y_2)^2} \tag{D.18}$$

$$q_y)_1 = -\frac{k(\gamma_2-\gamma_1)}{2\pi\mu}\left[\tan^{-1}\left(\frac{y-y_1}{x-x_n}\right) - \tan^{-1}\left(\frac{y-y_2}{x-x_n}\right)\right] \tag{D.19}$$

The equation of the line segment is now $x=x_n$, so that $x - x_n \to 0$ in equations (D.18) and (D.19). The expression for $q_x)_1$ given by equation (D.18) exhibits no discontinuity as $x - x_n \to 0$, so we can say that

$$q_x)_1^* = 0 \tag{D.20}$$

However, since $y > y_1$ and $y < y_2$, equation (D.19) gives

$$\lim_{x-x_n \to 0+} q_y)_1^* = -\frac{k(\gamma_2-\gamma_1)}{2\pi\mu}\left[\tan^{-1}(+\infty) - \tan^{-1}(-\infty)\right]$$

$$= -\frac{k(\gamma_2-\gamma_1)}{2\pi\mu}(\pi) \tag{D.21a}$$

$$\lim_{x-x_n \to 0-} q_y)_1^* = -\frac{k(\gamma_2-\gamma_1)}{2\pi\mu}\left[\tan^{-1}(-\infty) - \tan^{-1}(+\infty)\right]$$

$$= -\frac{k(\gamma_2-\gamma_1)}{2\pi\mu}(-\pi) \tag{D.21b}$$

Thus, in either case, we have

$$q_1^* = \frac{k(\gamma_2-\gamma_1)}{2\pi\mu}(\pi) \tag{D.22a}$$

$$\alpha_1^* = \tan^{-1}\left[\frac{k(\gamma_2-\gamma_1)}{2\pi\mu}(\pm\pi)/0\right] = \pm\pi/2 \tag{D.22b}$$

Hence the specific discharge at the point (x, y) again consists of a shear flow tangent to the (vertical) interface, and proportional to the vortex strength at that point. (Note that

$$\lim_{m\to\infty} \frac{m^2}{1+m^2} = \lim_{m\to\infty} \frac{1}{1+1/m^2} = 1,$$

so that q_1^* is again proportional to the vortex strength discussed in Section 2.3.)

APPENDIX E. FINITE-DIFFERENCE APPROXIMATIONS TO THE DERIVATIVES OF A FUNCTION u(x, y)

Let a two-dimensional finite-difference mesh be defined by the lines

$$x_i = x_0 + (i-1)\Delta x, \quad i = 1, 2, \ldots, I \tag{E.1a}$$

$$y_j = y_0 + (j-1)\Delta y, \quad j = 1, 2, \ldots, J \tag{E.1b}$$

where (x_0, y_0) denotes the lower left-hand corner of the mesh (Fig. E.1). Let $u(x_i, y_j)$ be denoted by $u_{i,j}$. We seek to determine finite-difference approximations to the first and second derivatives of u(x, y) at the mesh points (x_i, y_j).

The Taylor series expansion of u(x, y) about the point (x_i, y_j) is

$$\begin{aligned} u(x,y) = u_{i,j} &+ (x-x_i)(\partial u/\partial x)_{i,j} + (y-y_j)(\partial u/\partial y)_{i,j} + \\ &+ \tfrac{1}{2}(x-x_i)^2(\partial^2 u/\partial x^2)_{i,j} + (x-x_i)(y-y_j)(\partial^2 u/\partial x\,\partial y)_{i,j} + \\ &+ \tfrac{1}{2}(y-y_j)^2(\partial^2 u/\partial y^2)_{i,j} + \tfrac{1}{6}(x-x_i)^3(\partial^3 u/\partial x^3)_{i,j} + \\ &+ \tfrac{1}{2}(x-x_i)^2(y-y_j)(\partial^3 u/\partial x^2\,\partial y)_{i,j} + \\ &+ \tfrac{1}{2}(x-x_i)(y-y_j)^2(\partial^3 u/\partial x\,\partial y^2)_{i,j} + \\ &+ \tfrac{1}{6}(y-y_j)^3(\partial^3 u/\partial y^3)_{i,j} + \ldots \end{aligned} \tag{E.2}$$

Evaluating equation (E.2) at the points (x_{i+1}, y_j), (x_{i-1}, y_j), (x_i, y_{j+1}), and (x_i, y_{j-1}), we get, respectively,

$$u_{i+1,j} = u_{i,j} + \Delta x (\partial u/\partial x)_{i,j} + \tfrac{1}{2}\Delta x^2 (\partial^2 u/\partial x^2)_{i,j} + \\ + \tfrac{1}{6}\Delta x^3 (\partial^3 u/\partial x^3)_{i,j} + O(\Delta x^4) \qquad \text{(E.3)}$$

$$u_{i-1,j} = u_{i,j} - \Delta x (\partial u/\partial x)_{i,j} + \tfrac{1}{2}\Delta x^2 (\partial^2 u/\partial x^2)_{i,j} - \\ - \tfrac{1}{6}\Delta x^3 (\partial^3 u/\partial x^3)_{i,j} + O(\Delta x^4) \qquad \text{(E.4)}$$

$$u_{i,j+1} = u_{i,j} + \Delta y (\partial u/\partial y)_{i,j} + \tfrac{1}{2}\Delta y^2 (\partial^2 u/\partial y^2)_{i,j} + \\ + \tfrac{1}{6}\Delta y^3 (\partial^3 u/\partial y^3)_{i,j} + O(\Delta y^4) \qquad \text{(E.5)}$$

$$u_{i,j-1} = u_{i,j} - \Delta y (\partial u/\partial y)_{i,j} + \tfrac{1}{2}\Delta y^2 (\partial^2 u/\partial y^2)_{i,j} - \\ - \tfrac{1}{6}\Delta y^3 (\partial^3 u/\partial y^3)_{i,j} + O(\Delta y^4) \qquad \text{(E.6)}$$

Dividing equations (E.3) and (E.4) by Δx, and (E.5) and (E.6) by Δy, and neglecting terms of first and higher order in Δx and Δy, we get first-order accurate approximations to $\partial u/\partial x$ and $\partial u/\partial y$:

$$\partial u/\partial x)_{i,j} \approx (u_{i+1,j} - u_{i,j})/\Delta x \qquad \text{(E.7)}$$

$$\partial u/\partial x)_{i,j} \approx (u_{i,j} - u_{i-1,j})/\Delta x \qquad \text{(E.8)}$$

$$\partial u/\partial y)_{i,j} \approx (u_{i,j+1} - u_{i,j})/\Delta y \qquad \text{(E.9)}$$

$$\partial u/\partial y)_{i,j} \approx (u_{i,j} - u_{i,j-1})/\Delta y \qquad \text{(E.10)}$$

Equations (E.7) and (E.9) are <u>forward</u> difference approximations, while (E.8) and (E.10) are <u>backward</u> difference approximations.

Figure E.1. Definition of finite-difference mesh.

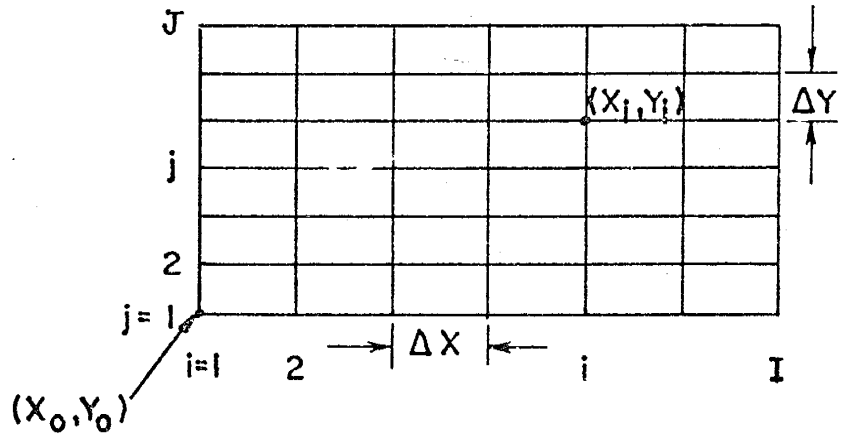
J
j
2
j= 1
i=1
2
ΔX
i
I
ΔY
(X_i, Y_j)
(X_0, Y_0)

Subtracting equation (E.4) from (E.3), we get

$$u_{i+1,j} - u_{i-1,j} = 2\Delta x\,(\partial u/\partial x)_{i,j} + O(\Delta x^3).$$

Dividing through by $2\Delta x$, and neglecting terms of second and higher order in Δx, we get a second-order accurate approximation to $\partial u/\partial x$:

$$\partial u/\partial x)_{i,j} \approx (u_{i+1,j} - u_{i-1,j})/2\Delta x \qquad \text{(E.11)}$$

Similarly, from equations (E.5) and (E.6), we get a second-order accurate approximation to $u/\ y$:

$$\partial u/\partial y)_{i,j} \approx (u_{i,j+1} - u_{i,j-1})/2\Delta y \qquad \text{(E.12)}$$

Equations (E.11) and (E.12) are <u>central</u> difference approximations.

Adding equations (E.3) and (E.4), we get

$$u_{i+1,j} + u_{i-1,j} = 2u_{i,j} + \Delta x^2(\partial^2 u/\partial x^2)_{i,j} + O(\Delta x^4)$$

Dividing through by Δx^2, and neglecting terms of second and higher order in Δx, we get the second-order accurate central difference approximation to $\partial^2 u/\partial x^2$:

$$\partial^2 u/\partial x^2)_{i,j} \approx (u_{i-1,j} - 2u_{i,j} + u_{i+1,j})/\Delta x^2 \qquad \text{(E.13)}$$

Similarly, from equations (E.5) and (E.6), we get the second-order accurate central difference approximation to $\partial^2 u/\partial y^2$:

$$\partial^2 u/\partial y^2)_{i,j} \approx (u_{i,j-1} - 2u_{i,j} + u_{i,j+1})/\Delta y^2 \qquad \text{(E.14)}$$

Evaluating equation (E.2) at the additional points (x_{i+1}, y_{j+1}), (x_{i-1}, y_{j-1}), (x_{i+1}, y_{j-1}), and (x_{i-1}, y_{j+1}), we get, respectively,

$$u_{i+1,j+1} = u_{i,j} + \Delta x (\partial u/\partial x)_{i,j} + \Delta y (\partial u/\partial y)_{i,j} + \tfrac{1}{2}\Delta x^2 (\partial^2 u/\partial x^2)_{i,j} + \\ + \Delta x \Delta y (\partial^2 u/\partial x \partial y)_{i,j} + \tfrac{1}{2}\Delta y^2 (\partial^2 u/\partial y^2)_{i,j} + O(\Delta x^3, \Delta y^3) \quad \text{(E.15)}$$

$$u_{i-1,j-1} = u_{i,j} - \Delta x (\partial u/\partial x)_{i,j} - \Delta y (\partial u/\partial y)_{i,j} + \tfrac{1}{2}\Delta x^2 (\partial^2 u/\partial x^2)_{i,j} + \\ + \Delta x \Delta y (\partial^2 u/\partial x \partial y)_{i,j} + \tfrac{1}{2}\Delta y^2 (\partial^2 u/\partial y^2)_{i,j} + O(\Delta x^3, \Delta y^3) \quad \text{(E.16)}$$

$$u_{i+1,j-1} = u_{i,j} + \Delta x (\partial u/\partial x)_{i,j} - \Delta y (\partial u/\partial y)_{i,j} + \tfrac{1}{2}\Delta x^2 (\partial^2 u/\partial x^2)_{i,j} - \\ - \Delta x \Delta y (\partial^2 u/\partial x \partial y)_{i,j} + \tfrac{1}{2}\Delta y^2 (\partial^2 u/\partial y^2)_{i,j} + O(\Delta x^3, \Delta y^3) \quad \text{(E.17)}$$

$$u_{i-1,j+1} = u_{i,j} - \Delta x (\partial u/\partial x)_{i,j} + \Delta y (\partial u/\partial y)_{i,j} + \tfrac{1}{2}\Delta x^2 (\partial^2 u/\partial x^2)_{i,j} - \\ - \Delta x \Delta y (\partial^2 u/\partial x \partial y)_{i,j} + \tfrac{1}{2}\Delta y^2 (\partial^2 u/\partial y^2)_{i,j} + O(\Delta x^3, \Delta y^3) \quad \text{(E.18)}$$

Then equation (E.15) plus (E.16) minus (E.17) minus (E.18) gives us

$$u_{i+1,j+1} - u_{i-1,j+1} - u_{i+1,j-1} + u_{i-1,j-1} =$$

$$= 4 \Delta x \Delta y (\partial^2 u/\partial x \partial y)_{i,j} + O(\Delta x^3, \Delta y^3)$$

Dividing through by $4\Delta x \Delta y$, and neglecting terms of second and higher order in Δx and Δy, we get a second-order accurate approximation to $\partial^2 u/\partial x \partial y$:

$$\left.\frac{\partial^2 u}{\partial x \partial y}\right)_{i,j} \approx \frac{u_{i+1,j+1} - u_{i-1,j+1} - u_{i+1,j-1} + u_{i-1,j-1}}{4 \Delta x \Delta y} \quad \text{(E.19)}$$

APPENDIX F. PSOR SOLUTION OF LAPLACE'S EQUATION

F.1 Iterative Solution of the Finite-Difference Equations

We wish to solve Laplace's equation

$$\nabla^2 u = 0, \tag{F.1.1}$$

subject to certain boundary conditions. We will assume that the boundary conditions consist of specifying u at boundary mesh points of a rectangular finite-difference mesh. Equation (F.1.1) can be easily written in finite difference form by applying equations (E.13) and (E.14) from Appendix E. Then we get

$$\begin{aligned}\nabla^2 u &= \partial^2 u/\partial x^2 + \partial^2 u/\partial y^2 \\ &\approx [u_{i-1,j} - 2u_{i,j} + u_{i+1,j}]/\Delta x^2 + \\ &\quad + [u_{i,j-1} - 2u_{i,j} + u_{i,j+1}]/\Delta y^2 = 0.\end{aligned} \tag{F.1.2}$$

Solving equation (F.1.2) for $u_{i,j}$, we get

$$u_{i,j} = \frac{\Delta y^2}{2(\Delta x^2+\Delta y^2)}\left[u_{i-1,j}+u_{i+1,j}\right] + \frac{\Delta x^2}{2(\Delta x^2+\Delta y^2)}\left[u_{i,j-1}+u_{i,j+1}\right] \tag{F.1.3}$$

Equation (F.1.3) can be used to derive an iterative scheme for determining $u_{i,j}$ at each mesh point. Add and subtract $u_{i,j}$ on the right-hand side of equation (F.1.3) to get

$$\begin{aligned}u_{i,j} = u_{i,j} + \Bigg\{&\frac{\Delta y^2}{2(\Delta x^2+\Delta y^2)}\left[u_{i-1,j} + u_{i+1,j}\right] + \\ &+ \frac{\Delta x^2}{2(\Delta x^2+\Delta y^2)}\left[u_{i,j-1} + u_{i,j+1}\right] - u_{i,j}\Bigg\}\end{aligned} \tag{F.1.4}$$

Denoting the k^{th} iterative value of $u_{i,j}$ by $u_{i,j}^{k}$, we can obtain an iterative scheme for solving for $u_{i,j}$ from equation (F.1.4) in the form

$$u_{i,j}^{k+1} = u_{i,j}^{k} + R_{i,j}^{k} \,, \qquad \text{(F.1.5)}$$

where

$$R_{i,j}^{k} = \left\{ \delta y^2 \left[u_{i-1,j}^{k+1} + u_{i+1,j}^{k} \right] + \delta x^2 \left[u_{i,j-1}^{k+1} + u_{i,j+1}^{k} \right] - \right.$$

$$\left. - 2(\delta x^2 + \delta y^2) u_{i,j}^{k} \right\} / 2(\delta x^2 + \delta y^2). \qquad \text{(F.1.6)}$$

Equation (F.1.5) is applied at each mesh point in succession for a given value of k. Then k is increased by unity and equation (F.1.5) is again applied at each mesh point in succession. This procedure continues until a desired degree of convergence is attained, as discussed below. Note that if each mesh row is swept from left to right, and the rows in turn are swept from bottom to top, then the quantities $u_{i-1,j}^{k+1}$ and $u_{i,j-1}^{k+1}$ in equation (F.1.6) are known at the present (k+1) iterative step, while the quantities $u_{i,j}^{k}$, $u_{i+1,j}^{k}$, and $u_{i,j+1}^{k}$ are known only at the preceding (k) iterative step (Fig. F.1.1). Equation (F.1.5) then gives $u_{i,j}^{k+1}$ at the present step, and we can proceed to the next mesh point.

The quantity $R_{i,j}^{k}$ defined by equation (F.1.6) is termed the k^{th} residual at point (x_i, y_j), and the iteration proceeds until the maximum residual, $\max_{i,j}\{R_{i,j}^{k}\}$, is less than some predefined small value (in principle, successive values of the residual at

any point should approach a limiting value of zero). The rate of convergence of the iterative scheme can be accelerated by multiplying the residual in equation (F.1.5) by a relaxation parameter ω, giving us

$$u_{i,j}^{k+1} = u_{i,j}^{k} + \omega R_{i,j}^{k} . \qquad \text{(F.1.7)}$$

Equation (F.1.7) defines the point successive over-relaxation (PSOR) iterative scheme which is used in the code. As shown in Section F.3, this iterative scheme is stable for $0 \leq \omega \leq 2$, although the maximum rate of convergence occurs for $1 \leq \omega \leq 2$; this point is illustrated in Section F.4, where we consider the estimation of the optimum relaxation parameter.

Figure F.1.1. Known values of $u_{i,j}$ at iteration k+1.

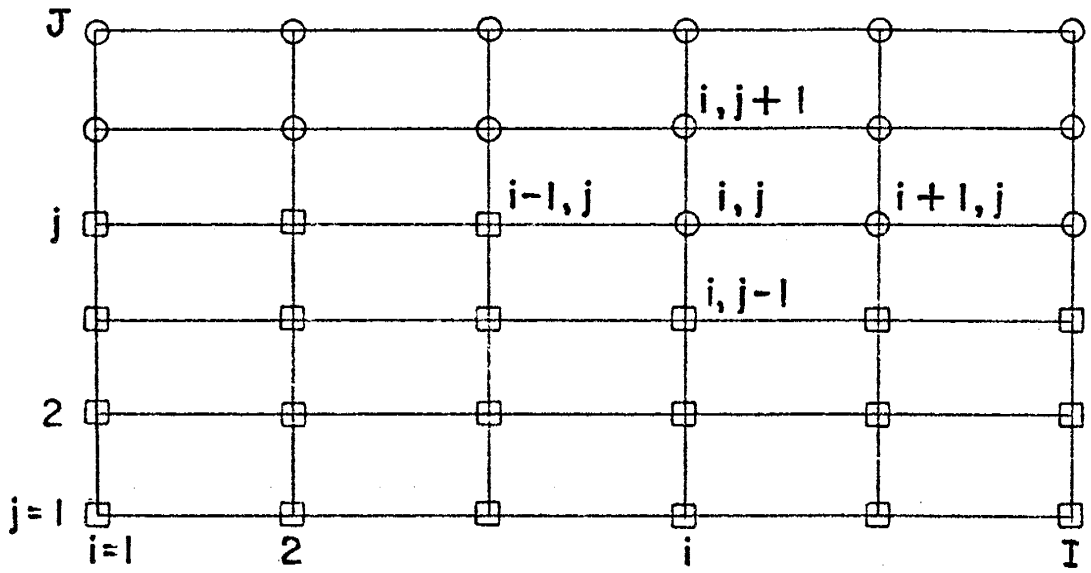

□ MESH POINTS AT WHICH $U_{i,j}^{k+1}$ HAS BEEN CALCULATED.

○ MESH POINTS AT WHICH $U_{i,j}^{k}$ ONLY IS KNOWN.

F.2 Truncation Error and Compatibility

The PSOR scheme described in Section F.1 is a technique of solution of the finite-difference equation (F.1.2). One measure of the accuracy of the finite-difference approximation is the degree of truncation error, which is defined as the difference between the original partial differential equation and its finite-difference approximation. The truncation error is a function of the mesh spacings Δx and Δy; if the the truncation error approaches zero as Δx and Δy approach zero, then the finite-difference approximation is said to be compatible with the partial differential equation.

From the Taylor series expansion of the function u(x, y) about the point (x_i, y_j), we have

$$\partial^2 u/\partial x^2)_{i,j} = (u_{i-1,j} - 2u_{i,j} + u_{i+1,j})/\Delta x^2 + O(\Delta x^2) \qquad \text{(F.2.1)}$$

and

$$\partial^2 u/\partial y^2)_{i,j} = (u_{i,j-1} - 2u_{i,j} + u_{i,j+1})/\Delta y^2 + O(\Delta y^2), \qquad \text{(F.2.2)}$$

where $0(\Delta x^2)$ represents terms which approach zero at least as rapidly as Δx^2 approaches zero. From equations (F.1.2), (F.2.1), and (F.2.2), the truncation error at the point (x_i, y_j) is given by

$$E_{i,j} = \partial^2 u/\partial x^2)_{i,j} + \partial^2 u/\partial y^2)_{i,j} - (u_{i-1,j} - 2u_{i,j} + u_{i+1,j})/\Delta x^2 -$$

$$-(u_{i,j-1} - 2u_{i,j} + u_{i,j+1})/\Delta y^2 = O(\Delta x^2) + O(\Delta y^2). \qquad \text{(F.2.3)}$$

Equation (F.2.3) shows that the truncation error does indeed

approach zero as Δx and Δy approach zero, so the finite-difference equation (F.1.2) is compatible with Laplace's equation (F.1.1).

F.3 Stability and Convergence of the Iterative Technique

The iterative technique outlined in Section F.1 is actually a procedure for solving a set of N simultaneous linear equations, of the form of equation (F.1.3), in the N unknowns $u_{i,j}$ (where N = IxJ). The set of simultaneous equations can be written in matrix form as

$$\bar{\bar{A}}\,\bar{u} = \bar{v}\,, \qquad (F.3.1)$$

where $\bar{u}$ is the column vector of unknowns and $\bar{\bar{A}}$ is the NxN matrix of coefficients of the $u_{i,j}$. The exact solution $\bar{u}^*$ is given by

$$\bar{u}^* = \bar{\bar{A}}^{-1}\,\bar{v}\,. \qquad (F.3.2)$$

The iterative procedure is begun by assuming a trial solution $\bar{u}^0$, and then finding a new trial solution $\bar{u}^1$ in the form

$$\bar{u}^1 = \bar{\bar{B}}\,\bar{u}^0 + \bar{z}\,. \qquad (F.3.3)$$

Successive trial solutions are then given by

$$\bar{u}^{k+1} = \bar{\bar{B}}\,\bar{u}^k + \bar{z}\,, \qquad (F.3.4)$$

where the superscript k on $\bar{u}$ denotes the k^{th} iteration. Convergence of the iterative technique requires that the sequence of vectors $\bar{u}^k$ approaches $\bar{u}^*$, and that iteration with $\bar{u}^*$ reproduces itself; i.e.,

$$\bar{u}^* = \bar{\bar{B}}\,\bar{u}^* + \bar{z}\,. \qquad (F.3.5)$$

At each step in the iteration, errors can be introduced through such things as round-off, depending upon the computing machine and solution algorithm being used. Defining the error vector at the k^{th} iteration by

$$\bar{e}^{\,k} = \bar{u}^{\,k} - \bar{u}^{\,*} ,$$

where the superscript k on $\bar{e}$ again denotes the k^{th} iteration, equations (F. 3.4) and (F. 3.5) give

$$\begin{aligned} \bar{e}^{\,k} &= \bar{\bar{B}}\,\bar{u}^{\,k-1} + \bar{z} - \bar{\bar{B}}\,\bar{u}^{\,*} - \bar{z} \\ &= \bar{\bar{B}}\,(\bar{u}^{\,k-1} - \bar{u}^{\,*}) = \bar{\bar{B}}\,\bar{e}^{\,k-1} ; \end{aligned} \qquad \text{(F. 3.6)}$$

i. e., the error vector satisfies the homogeneous form of the iteration equation. From equation (F. 3.6), we get

$$\bar{e}^{\,k} = \bar{\bar{B}}^{\,k}\,\bar{e}^{\,o} , \qquad \text{(F. 3.7)}$$

where the superscript k on $\bar{\bar{B}}$ here denotes the k^{th} power of $\bar{\bar{B}}$. Now we require that $\bar{u}^{\,k}$ approach $\bar{u}^{\,*}$, so that $\bar{e}^{\,k}$ must approach zero. If we denote the eigenvectors of $\bar{\bar{B}}$ by $\bar{\beta}_\ell$, and the corresponding eigenvalues by λ_ℓ , then it can be shown (Clark and Hansen, 1964) that the k^{th} iterate of the error vector is given by

$$\bar{e}^{\,k} = \sum_{\ell=1}^{\infty} \alpha_\ell \lambda_\ell^{\,k} \bar{\beta}_\ell , \qquad \text{(F. 3.8)}$$

where α_ℓ is a constant, and the superscript k on λ_ℓ denotes the k^{th} power. In order for $\bar{e}^{\,k}$ to vanish, it is necessary that

$$|\lambda_\ell| < 1, \quad \text{all } \ell. \tag{F.3.9}$$

Equation (F.3.9) expresses the stability condition for the iterative method.

Since the errors satisfy the iteration equation, equations (F.1.6) and (F.1.7) imply

$$e_{i,j}^{k+1} = e_{i,j}^{k} + \omega \left[\Delta y^2 (e_{i-1,j}^{k+1} + e_{i+1,j}^{k}) + \Delta x^2 (e_{i,j-1}^{k+1} + e_{i,j+1}^{k}) - \right.$$

$$\left. - 2(\Delta x^2 + \Delta y^2) e_{i,j}^{k} \right] / 2(\Delta x^2 + \Delta y^2), \tag{F.3.10}$$

where the superscripts on the $e_{i,j}$ denote iterations. If we assume $\Delta x = \Delta y$ (as is the case in the present form of the computer code), equation (F.3.10) can be simplified to

$$e_{i,j}^{k+1} = (1-\omega) e_{i,j}^{k} + \omega (e_{i-1,j}^{k+1} + e_{i+1,j}^{k} + e_{i,j-1}^{k+1} + e_{i,j+1}^{k})/4. \tag{F.3.11}$$

Following Frankel (1950), we assume that the error has a double sine series expansion over the indices m and n, with one component being

$$e_{i,j}^{k} = A^i \sin(m\pi i/I)\, B^j \sin(n\pi j/J), \tag{F.3.12}$$

where A and B are constants to be determined, and the superscripts on A and B denote powers. We also assume

$$e_{i,j}^{k+1} = \lambda_{m,n}\, e_{i,j}^{k}, \tag{F.3.13}$$

where $\lambda_{m,n}$ is an eigenvalue of the iteration matrix. Substituting equation (F.3.12) into equation (F.3.11), and applying equation (F.3.13), we get

$$\frac{\lambda_{m,n}}{A^i B^i} e^k_{i,j} = \lambda_{m,n}\left\{\frac{\omega}{4A}\sin\left(\frac{n\pi j}{J}\right)\left[\sin\left(\frac{m\pi i}{I}\right)\cos\left(\frac{m\pi}{I}\right) - \cos\left(\frac{m\pi i}{I}\right)\sin\left(\frac{m\pi}{I}\right)\right] + \right.$$

$$+ \frac{\omega}{4B}\sin\left(\frac{m\pi i}{I}\right)\left[\sin\left(\frac{n\pi j}{J}\right)\cos\left(\frac{n\pi}{J}\right) - \cos\left(\frac{n\pi j}{J}\right)\sin\left(\frac{n\pi}{J}\right)\right]\Big\} +$$

$$+(1-\omega)\sin\left(\frac{m\pi i}{I}\right)\sin\left(\frac{n\pi j}{J}\right) + \frac{\omega}{4}\left\{A\sin\left(\frac{n\pi j}{J}\right)\left[\sin\left(\frac{m\pi i}{I}\right)\cos\left(\frac{m\pi}{I}\right) + \right.\right.$$

$$\left.+\cos\left(\frac{m\pi i}{I}\right)\sin\left(\frac{m\pi}{I}\right)\right] + B\sin\left(\frac{m\pi i}{I}\right)\left[\sin\left(\frac{n\pi j}{J}\right)\cos\left(\frac{n\pi}{J}\right) + \right. \qquad \text{(F.3.14)}$$

$$\left.\left.+\cos\left(\frac{n\pi j}{J}\right)\sin\left(\frac{n\pi}{J}\right)\right]\right\}$$

Since the value of u is known exactly at the boundaries, the errors at the boundaries i = I and j = J must be zero. At i = I, $e^k_{I,j} = 0$, so equation (F.3.14) becomes

$$\frac{\omega}{4}\sin\left(\frac{n\pi j}{J}\right)\cos(m\pi)\sin\left(\frac{m\pi}{I}\right)\left[A - \frac{\lambda_{m,n}}{A}\right] = 0,$$

or

$$A^2 = \lambda_{m,n} . \qquad \text{(F.3.15)}$$

Similarly, at j = J, $e^k_{i,J} = 0$, and equation (F.3.14) gives

$$B^2 = \lambda_{m,n} . \qquad \text{(F.3.16)}$$

Substituting equations (F.3.15) and (F.3.16) into equation (F.3.14) and simplifying, we get

$$\lambda_{m,n} - \frac{\omega\sqrt{\lambda_{m,n}}}{2}\left[\cos\left(\frac{m\pi}{I}\right) + \cos\left(\frac{n\pi}{J}\right)\right] + (\omega - 1) = 0. \qquad \text{(F.3.17)}$$

Equation (F.3.17) can be viewed as a quadratic equation in $\sqrt{\lambda_{m,n}}$, with the solutions

$$\sqrt{\lambda_{m,n}} = \frac{\omega}{4}\left[\cos\left(\frac{m\pi}{I}\right) + \cos\left(\frac{n\pi}{J}\right)\right] \pm \pm \frac{1}{2}\sqrt{\frac{\omega^2}{4}\left[\cos\left(\frac{m\pi}{I}\right) + \cos\left(\frac{n\pi}{J}\right)\right]^2 - 4(\omega-1)} \qquad \text{(F.3.18)}$$

The maximum value of $\lambda_{m,n}$ will occur for m = n = 1, and the positive sign on the radical in equation (F.3.18). Thus we consider

$$\sqrt{\lambda_{1,1}} = \frac{\omega}{4}\left[\cos\left(\frac{\pi}{I}\right) + \cos\left(\frac{\pi}{J}\right)\right] + + \frac{1}{2}\sqrt{\frac{\omega^2}{4}\left[\cos\left(\frac{\pi}{I}\right) + \cos\left(\frac{\pi}{J}\right)\right]^2 - 4(\omega-1)}. \qquad \text{(F.3.19)}$$

In equation (F.3.19), let

$$t = \frac{1}{2}\left[\cos\left(\frac{\pi}{I}\right) + \cos\left(\frac{\pi}{J}\right)\right], \qquad \text{(F.3.20)}$$

to get

$$\sqrt{\lambda_{1,1}} = \frac{1}{2}\omega t + \frac{1}{2}\sqrt{\omega^2 t^2 - 4(\omega-1)}. \qquad \text{(F.3.21)}$$

We must consider two ranges of values of ω, depending on the sign of the argument of the square root function in equation (F.3.21). For $\omega^2 t^2 - 4(\omega - 1) \geq 0$, $\sqrt{\lambda_{1,1}}$ is real and

$$|\lambda_{1,1}| = \frac{1}{2}\left[\omega^2 t^2 - 2(\omega-1) + \omega t\sqrt{\omega^2 t^2 - 4(\omega-1)}\right]. \qquad \text{(F.3.22)}$$

From equation (F.3.20), we see that $t < 1$, so equation (F.3.22) implies

$$|\lambda_{1,1}| < \tfrac{1}{2}\left[\omega^2 - 2(\omega-1) + \omega\sqrt{(\omega-2)^2}\right] = (\omega-1)^2. \qquad \text{(F.3.23)}$$

For $\omega^2 t^2 - 4(\omega - 1) < 0$, $\sqrt{\lambda_{1,1}}$ is complex and

$$|\lambda_{1,1}| = \omega - 1; \qquad \text{(F.3.24)}$$

obviously, this condition can only occur for $\omega \geq 1$, because otherwise $|\lambda_{1,1}|$ would be negative, which is a contradiction. For $0 \leq \omega \leq 2$, equation (F.3.23) implies that

$$|\lambda_{1,1}| < 1. \qquad \text{(F.3.25a)}$$

Similarly, for $1 \leq \omega \leq 2$, equation (F.3.24) implies that

$$|\lambda_{1,1}| \leq 1. \qquad \text{(F.3.25b)}$$

Equations (F.3.25) show that the maximum eigenvalue of the PSOR iteration matrix satisfies the stability condition (F.3.9) for $0 \leq \omega \leq 2$, so that the iteration scheme is indeed stable. Richtmyer and Morton (1967) show that, in general, for a compatible finite-difference approximation to a linear partial differential equation with constant coefficients, stability implies that the solution of the finite-difference equations converges to the true solution of the partial differential equation. Since we have shown in Section F.2 that the finite-difference approximation (F.1.2) is compatible with Laplace's equation, we have now shown that the PSOR iterative scheme is stable and converges to the true solution of Laplace's equation.

F.4 Estimate of the Optimum Relaxation Parameter

The rate of convergence of the PSOR technique depends upon the value of the relaxation parameter ω . The rate of convergence can be measured by the magnitude of the largest eigenvalue $\lambda_{1,1}$ of the iteration matrix; the smaller $|\lambda_{1,1}|$ is, the faster will be the convergence. Thus the optimum relaxation parameter is that value of ω which minimizes $|\lambda_{1,1}|$ as given by equations (F.3.22) and (F.3.24).

For $\omega^2 t^2 - 4(\omega - 1) > 0$, equation (F.3.22) defines $|\lambda_{1,1}|$ as a decreasing function of ω . For $\omega^2 t^2 - 4(\omega - 1) < 0$, equation (F.3.24) defines $|\lambda_{1,1}|$ as an increasing function of ω . Thus the minimum value of $|\lambda_{1,1}|$ must occur for

$$\omega^2 t^2 - 4(\omega - 1) = 0, \qquad \text{(F.4.1)}$$

and the corresponding value of $|\lambda_{1,1}|$ is given by equation (F.3.24) as

$$|\lambda_{1,1}| = \omega - 1. \qquad \text{(F.4.2)}$$

The optimum value of ω , given by the smaller root of equation (F.4.1), is

$$\omega_{opt} = \frac{2 - 2\sqrt{1 - t^2}}{t^2} , \qquad \text{(F.4.3)}$$

and the corresponding minimum value of $|\lambda_{1,1}|$, given by equation (F.4.2), is

$$|\lambda_{1,1}|_{min} = \omega_{opt} - 1 . \qquad \text{(F.4.4)}$$

From equation (F.3.24) and the subsequent discussion, the optimum value of ω must be greater than or equal to unity.

The behavior of $|\lambda_{1,1}|$ as a function of ω can best be seen graphically. In the present version of the computer code for interface motion, I = 21 and J = 11; thus, from equation (F.3.20),

$$t = \tfrac{1}{2}\left[\cos\left(\frac{\pi}{21}\right) + \cos\left(\frac{\pi}{11}\right)\right] = 0.97416 . \quad \text{(F.4.5)}$$

Then, from equation (F.4.3), the optimum value of the relaxation parameter is

$$\omega_{opt} = \frac{2 - 2\sqrt{1 - t^2}}{t^2} = 1.6315 ;$$

from equation (F.4.4), the corresponding value of $|\lambda_{1,1}|$ is

$$|\lambda_{1,1}|_{min} = \omega_{opt} - 1 = 0.6315 .$$

The function given by equations (F.4.1) and (F.4.2), with the value of t given by equation (F.4.5), is shown in Figure F.4.1. The shape of that curve is typical of plots of $|\lambda|$ versus ω for the PSOR iterative scheme (e.g., see Clark and Hansen, 1964; Smith, 1965).

Figure F.4.1. The maximum eigenvalue of the iteration matrix as a function of the relaxation parameter.

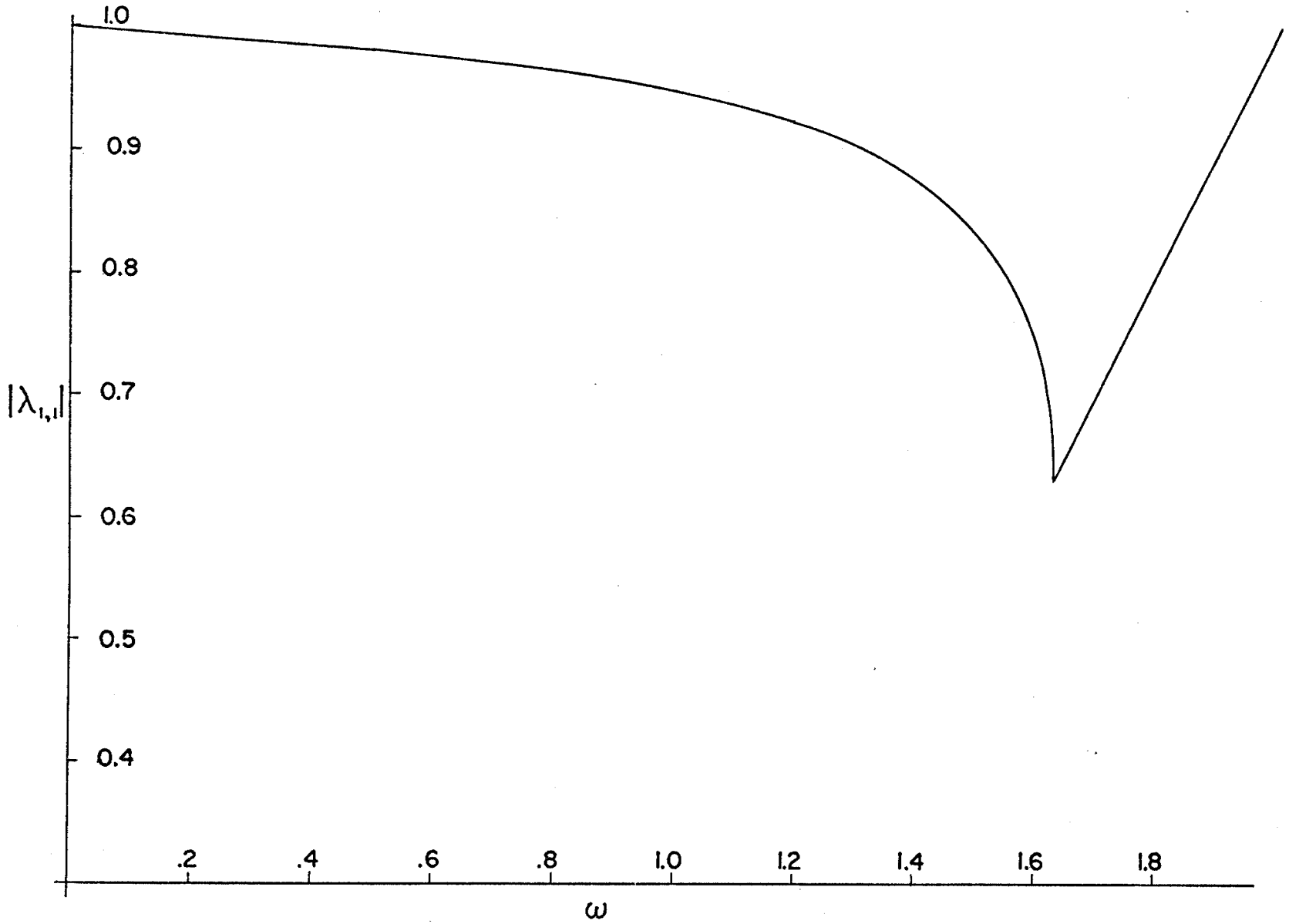
1.0
0.9
0.8
0.7
0.6
0.5
0.4
$|\lambda_{1,1}|$
.2
.4
.6
.8
1.0
1.2
1.4
1.6
1.8
ω

REFERENCES

Clark, Melville, Jr., and Kent F. Hansen, Numerical Methods of Reactor Analysis, 340 pp., Academic Press, New York, 1964.

Frankel, Stanley P., Convergence rates of iterative treatments of partial differential equations, Math. Tables and Aids to Computation (now known as Mathematics of Computation), 4, 65-75, 1950.

Richtmyer, Robert D., and K. W. Morton, Difference Methods for Initial-Value Problems, Second Edition, 405 pp., Interscience Publishers, New York, 1967.

Smith, G. D., Numerical Solution of Partial Differential Equations, 179 pp., Oxford University Press, New York, 1965.

APPENDIX G. THE COMPUTER PROGRAM FOR SIMULATING INTERFACE MOTION -- GENERAL DESCRIPTION

G.1 Introduction

The techniques described earlier for simulating interface motion have been programmed in FORTRAN IV for numerical evaluation by the IBM 360/44 digital computing system at New Mexico Tech. A listing of the computer program is given in Appendix H. The program consists of a MAIN routine, eleven subroutines, and a data deck, plus appropriate job control language. The MAIN routine serves principally to call the subroutines in the correct sequence, according to the flow chart given in Figure G.1.1. The routine also provides for calculation of $\Psi = \Psi_1 + \Psi_2$, $q_x = q_x)_1 + q_x)_2$, and $q_y = q_y)_1 + q_y)_2$; motion of interface points at the end of each time step; updating of time, time step, and cycle counter; and editing to determine if output has been requested during the current cycle or if the end of the simulation has been reached.

Data are transmitted between the MAIN routine and the various subroutines by way of a single COMMON block, which contains all of the major parameters which occur in the mathematical theory, as well as various control parameters. Descriptions of the parameters contained in the COMMON block are given in Table G.1.1.

Subsequent sections of this appendix give brief descriptions of the various subroutines, including flow charts for some of them, and descriptions of the input and output routines. Each subroutine is thoroughly documented by way of COMMENT statements, so detailed descriptions should not be necessary.

Figure G.1.1. Flow chart for MAIN routine.

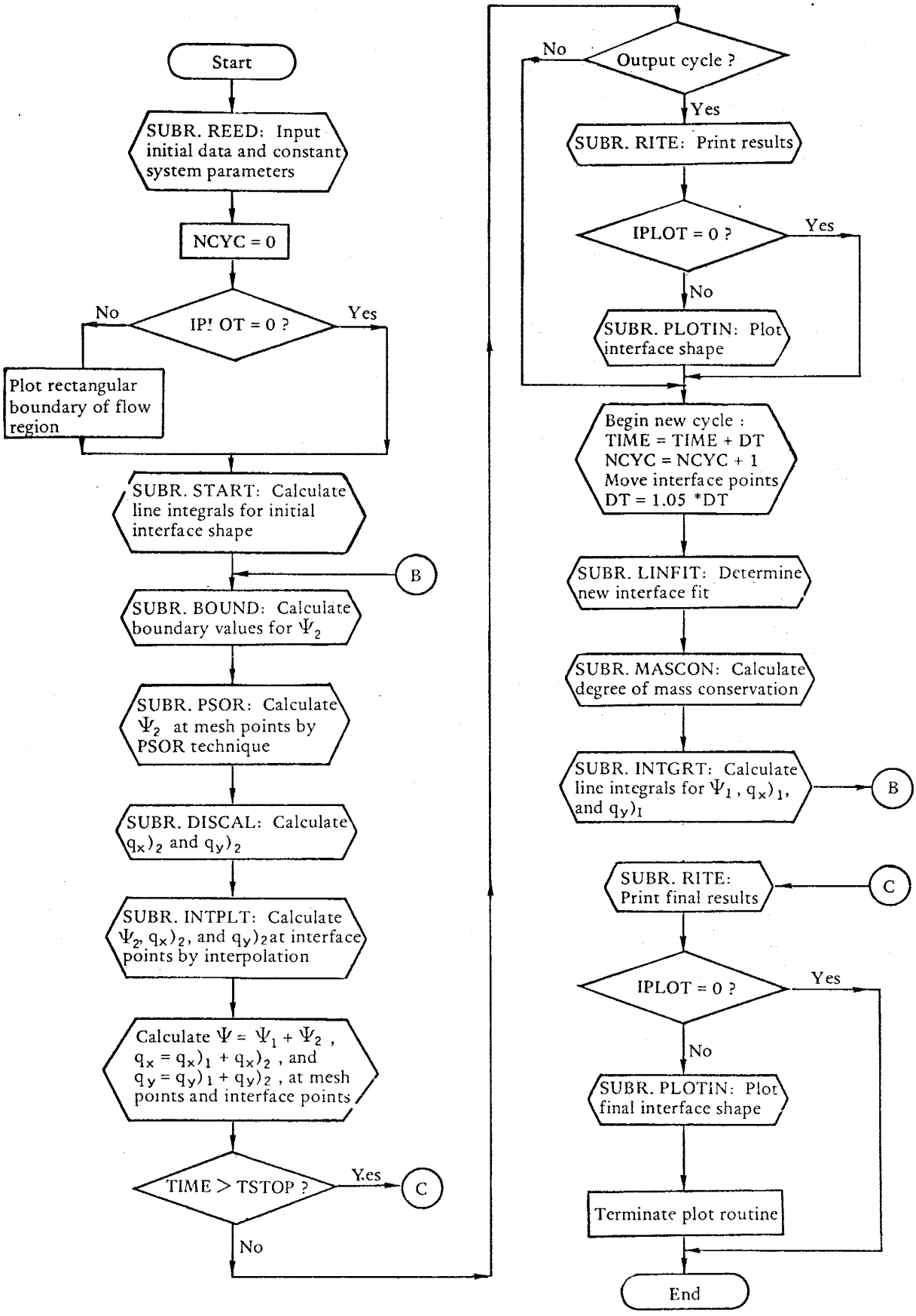
Start
SUBR. REED: Input initial data and constant system parameters
NCYC = 0
IPLOT = 0 ?
No
Yes
Plot rectangular boundary of flow region
SUBR. START: Calculate line integrals for initial interface shape
B
SUBR. BOUND: Calculate boundary values for Ψ_2
SUBR. PSOR: Calculate Ψ_2 at mesh points by PSOR technique
SUBR. DISCAL: Calculate $q_x)_2$ and $q_y)_2$
SUBR. INTPLT: Calculate Ψ_2, $q_x)_2$, and $q_y)_2$ at interface points by interpolation
Calculate $\Psi = \Psi_1 + \Psi_2$, $q_x = q_x)_1 + q_x)_2$, and $q_y = q_y)_1 + q_y)_2$, at mesh points and interface points
TIME > TSTOP ?
Yes
C
No
Output cycle ?
No
Yes
SUBR. RITE: Print results
IPLOT = 0 ?
Yes
No
SUBR. PLOTIN: Plot interface shape
Begin new cycle :
TIME = TIME + DT
NCYC = NCYC + 1
Move interface points
DT = 1.05 *DT
SUBR. LINFIT: Determine new interface fit
SUBR. MASCON: Calculate degree of mass conservation
SUBR. INTGRT: Calculate line integrals for Ψ_1, $q_x)_1$, and $q_y)_1$
B
SUBR. RITE: Print final results
C
IPLOT = 0 ?
Yes
No
SUBR. PLOTIN: Plot final interface shape
Terminate plot routine
End

Table G.1.1. Parameters contained in COMMON blocks.

FORTRAN symbol	Math. symbol	Description
IMX	I	Total mesh points in x-direction
JMX	J	Total mesh points in y-direction
NMAX	N	Total number of interface points
KMAX		Maximum number of iterations allowed
K	K	Number of iterations
IMAX, JMAX		Mesh coordinates of maximum residual
NREAD		Input device code
NPRINT		Output device code
NOUT		Results printed every NOUT cycles
NCYC	n	Cycle number
ZERO		0.0
ONE		1.0
TWO		2.0
THREE		3.0
FOUR		4.0
HALF		0.5
QUART		0.25
PI		$\pi = 3.14159265$
PERM	k	Permeability of medium
GAM1	γ_1	Specific weight of lighter fluid
GAM2	γ_2	Specific weight of heavier fluid
VIS	μ	Viscosity of fluids
CBND	c	Half-width of basic check problem
XIN		x-coordinate of initial vertical interface for basic check problem

FORTRAN symbol	Math. symbol	Description
DX	Δx	Mesh spacing in x-direction
DY	Δy	Mesh spacing in y-direction
RMAX		Maximum residual
OMEGA	ω	Relaxation parameter
EPS	ε	Convergence parameter
TIME	t	Time
DT	Δt	Time step
TSTOP		Maximum model time
PROPC		Proportionality constant for length of tangent line segment (inversely proportional to interface curvature)
AREAIN		Initial area of flow region occupied by heavier fluid
AREA		Area of flow region occupied by heavier fluid at any later time
ABSERR		Absolute error = AREAIN - AREA
RELERR		Relative error = ABSERR/AREAIN
XO(99)	x_o^n	Coordinates of interface points
YO(99)	y_o^n	
X1(99)	x_1^n	Coordinates of left endpoints of tangent line segments
Y1(99)	y_1^n	
X2(99)	x_2^n	Coordinates of right endpoints of tangent line segments
Y2(99)	y_2^n	
SLOPE(99)	σ_n	Slopes of tangent line segments
SLOPEC(99)	τ_n	Slopes of connecting line segments

FORTRAN symbol	Math. symbol	Description
PSI1N(99)	Ψ_1	Ψ_1 at interface points
VX(99)	$q_x)_1$	$q_x)_1$ at interface points
VY(99)	$q_y)_1$	$q_y)_1$ at interface points
PSI2N(99)	Ψ_2	Ψ_2 at interface points
U2N(99)	$q_x)_2$	$q_x)_2$ at interface points
V2N(99)	$q_y)_2$	$q_y)_2$ at interface points
X(40) Y(20)	x_i y_j	Coordinates of mesh points
PSI1(40,20)	Ψ_1	Ψ_1 at mesh points; total Ψ_1
U(40,20)	$q_x)_1$	$q_x)_1$ at mesh points; total q_x
V(40,20)	$q_y)_1$	$q_y)_1$ at mesh points; total q_y
PSI2(40,20)	Ψ_2	Ψ_2 at mesh points
U2(40,20)	$q_x)_2$	$q_x)_2$ at mesh points
V2(40,20)	$q_y)_2$	$q_y)_2$ at mesh points
IPLOT		Plot code, interface plotted if IPLOT $\neq$ 0

G.2 Subroutines

REED. Subroutine REED provides for input of initial data and system parameters, as well as calculation of the mesh point coordinates. The data are also output to the line printer so that they can be verified. The input/output procedures are discussed in greater detail in Section G.3.

START. Subroutine START provides for calculation of Ψ_1, $q_x)_1$, and $q_y)_1$ for the initial interface position. This routine is problem-dependent, and has been formulated for the basic check problem. The values of Ψ_1, $q_x)_1$, and $q_y)_1$ are determined from the formulas given in Section 3.3.

The initial interface fit is shown in Figure G.2.1. The interface fit consists of a single vertical line segment, connected to horizontal line segments at the boundaries. The interfacial segments are also reflected in both boundaries as image interfaces. The contributions to the line integrals from the horizontal interfacial segments are identically zero. Thus, the only contributions to the line integrals from the initial interface fit are from the vertical line segment, the two connecting segments, and their images.

Figure G.2.2 gives a flow chart of subroutine START.

Figure G.2.1. Initial interface fit in the computer model.

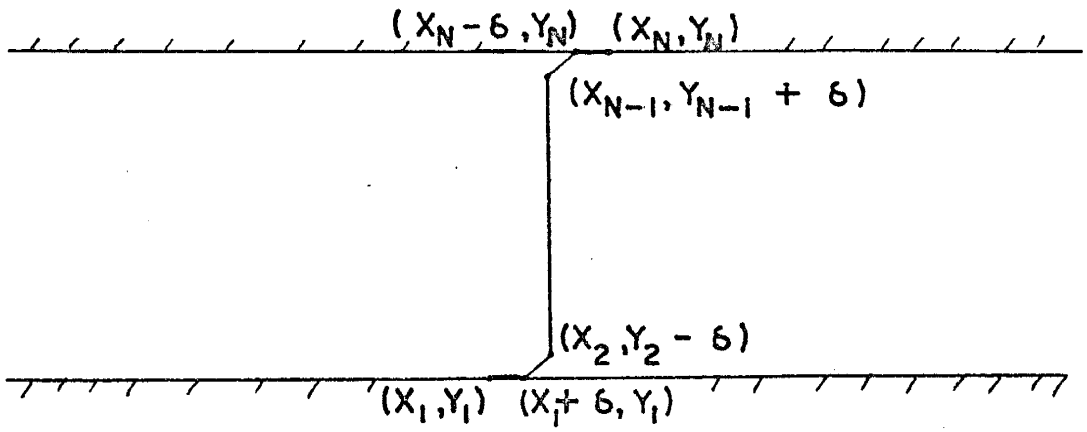
$(X_N - \delta, Y_N)$
(X_N, Y_N)
$(X_{N-1}, Y_{N-1} + \delta)$
$(X_2, Y_2 - \delta)$
(X_1, Y_1)
$(X_1 + \delta, Y_1)$

Figure G.2.2. Flow chart for subroutine START.

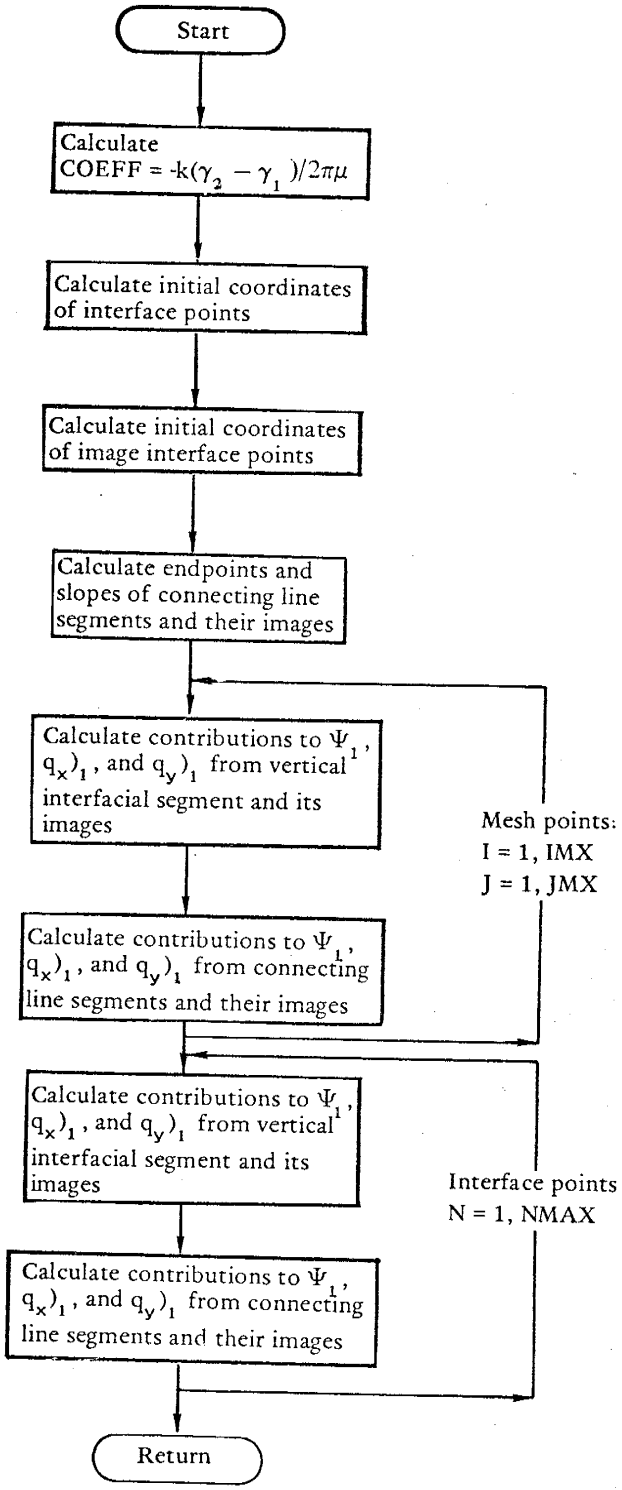
Start
Calculate COEFF = -k($\gamma_2 - \gamma_1$)/2$\pi\mu$
Calculate initial coordinates of interface points
Calculate initial coordinates of image interface points
Calculate endpoints and slopes of connecting line segments and their images
Calculate contributions to Ψ_1, $q_x)_1$, and $q_y)_1$ from vertical interfacial segment and its images
Calculate contributions to Ψ_1, $q_x)_1$, and $q_y)_1$ from connecting line segments and their images
Mesh points:
I = 1, IMX
J = 1, JMX
Calculate contributions to Ψ_1, $q_x)_1$, and $q_y)_1$ from vertical interfacial segment and its images
Calculate contributions to Ψ_1, $q_x)_1$, and $q_y)_1$ from connecting line segments and their images
Interface points
N = 1, NMAX
Return

INTGRT. Subroutine INTGRT provides for calculation of Ψ_1, $\eta(x)$, , and $\eta(y)$, at all mesh points and at all interface points. The line integrals are evaluated over the length of the interface, plus partial image interfaces. Only the first five interface points are reflected in the lower boundary, and the last five points reflected in the upper boundary. Figure G.2.3 is a flow chart for subroutine INTGRT.

BOUND. Subroutine BOUND determines boundary values for Ψ_2 from the physical boundary conditions of the problem under consideration. The boundary values determined are required by subroutine PSOR. This is a problem-dependent subroutine. The formulation presented here is for the basic check problem, for which $\Psi_2 = -\Psi_1$ at the boundary mesh points.

PSOR. Subroutine PSOR provides for calculation of Ψ_2 at each interior mesh point by the point successive over-relaxation method. Values of Ψ_2 at the boundary mesh points are given by subroutine BOUND, and are required by subroutine PSOR. The iteration proceeds until the maximum residual RMAX is less than a predefined tolerance $\mathcal{E}$, or the total number of iterations K is greater than or equal to a predefined maximum KMAX. Figure G.2.4 is a flow chart of subroutine PSOR.

Figure G.2.3. Flow chart for subroutine INTGRT.

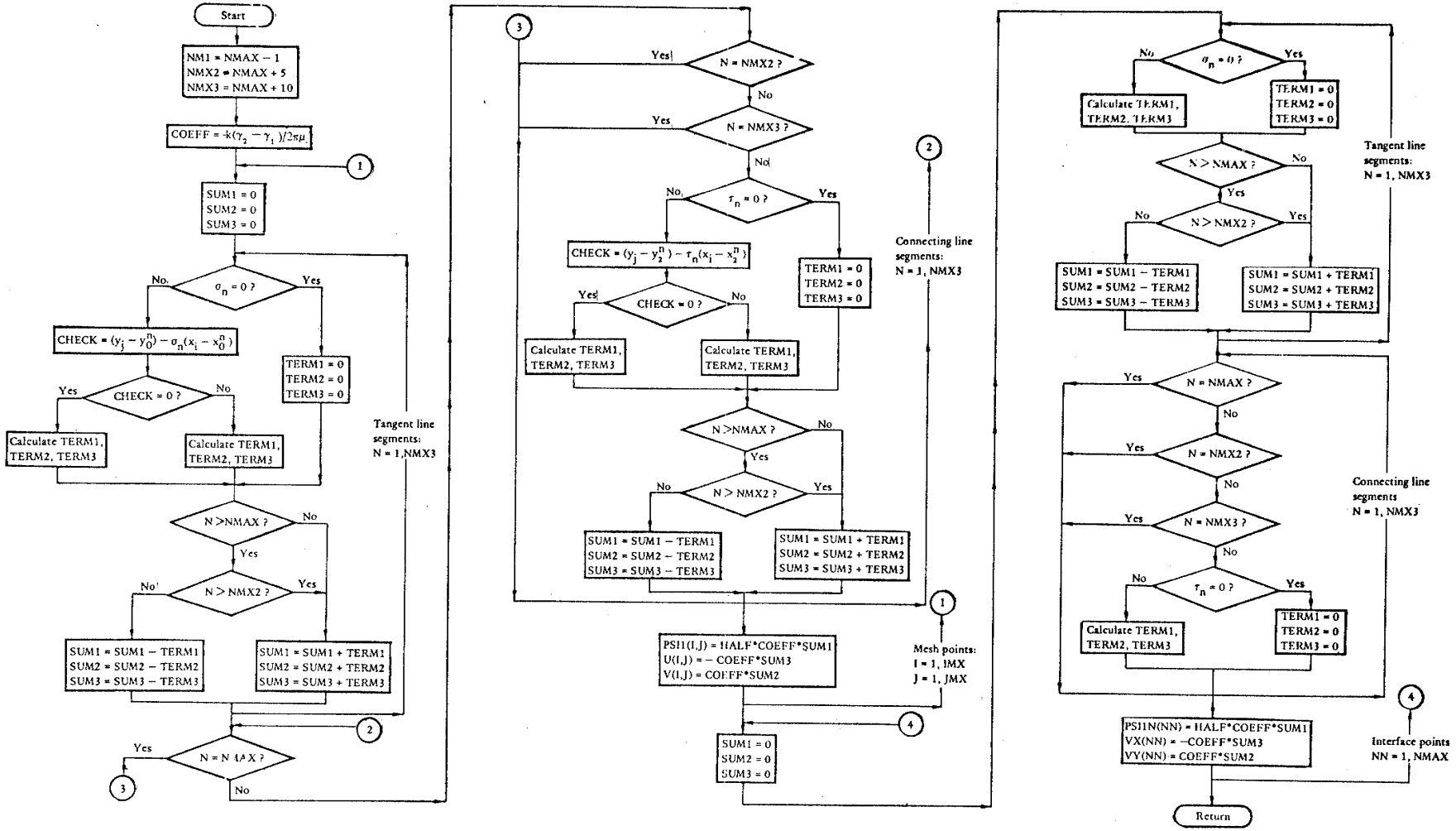
Start
NM1 = NMAX − 1
NMX2 = NMAX + 5
NMX3 = NMAX + 10
COEFF = k(γ2 − γ1)/2πμ
1
SUM1 = 0
SUM2 = 0
SUM3 = 0
σn = 0 ?
No
Yes
CHECK = (yj − y0n) − σn(xi − x0n)
TERM1 = 0
TERM2 = 0
TERM3 = 0
CHECK = 0 ?
Yes
No
Calculate TERM1, TERM2, TERM3
Calculate TERM1, TERM2, TERM3
N >NMAX ?
No
Yes
N > NMX2 ?
No
Yes
SUM1 = SUM1 − TERM1
SUM2 = SUM2 − TERM2
SUM3 = SUM3 − TERM3
SUM1 = SUM1 + TERM1
SUM2 = SUM2 + TERM2
SUM3 = SUM3 + TERM3
2
N = NMAX ?
Yes
3
No
Tangent line segments: N = 1, NMX3
3
Yes
N = NMX2 ?
No
Yes
N = NMX3 ?
No
τn = 0 ?
No
Yes
CHECK = (yj − y2n) − τn(xi − x2n)
TERM1 = 0
TERM2 = 0
TERM3 = 0
Yes
CHECK = 0 ?
No
Calculate TERM1, TERM2, TERM3
Calculate TERM1, TERM2, TERM3
N >NMAX ?
No
Yes
N > NMX2 ?
No
Yes
SUM1 = SUM1 − TERM1
SUM2 = SUM2 − TERM2
SUM3 = SUM3 − TERM3
SUM1 = SUM1 + TERM1
SUM2 = SUM2 + TERM2
SUM3 = SUM3 + TERM3
PSI1(I,J) = HALF*COEFF*SUM1
U(I,J) = − COEFF*SUM3
V(I,J) = COEFF*SUM2
1
Mesh points: I = 1, IMX J = 1, JMX
4
SUM1 = 0
SUM2 = 0
SUM3 = 0
2
Connecting line segments: N = 1, NMX3
σn = 0 ?
No
Yes
Calculate TERM1, TERM2, TERM3
TERM1 = 0
TERM2 = 0
TERM3 = 0
N > NMAX ?
No
Yes
N > NMX2 ?
No
Yes
SUM1 = SUM1 − TERM1
SUM2 = SUM2 − TERM2
SUM3 = SUM3 − TERM3
SUM1 = SUM1 + TERM1
SUM2 = SUM2 + TERM2
SUM3 = SUM3 + TERM3
Tangent line segments: N = 1, NMX3
N = NMAX ?
Yes
No
N = NMX2 ?
Yes
No
N = NMX3 ?
Yes
No
τn = 0 ?
No
Yes
Calculate TERM1, TERM2, TERM3
TERM1 = 0
TERM2 = 0
TERM3 = 0
Connecting line segments N = 1, NMX3
4
PSI1N(NN) = HALF*COEFF*SUM1
VX(NN) = −COEFF*SUM3
VY(NN) = COEFF*SUM2
Interface points NN = 1, NMAX
Return

Figure G.2.4. Flow chart for subroutine PSOR.

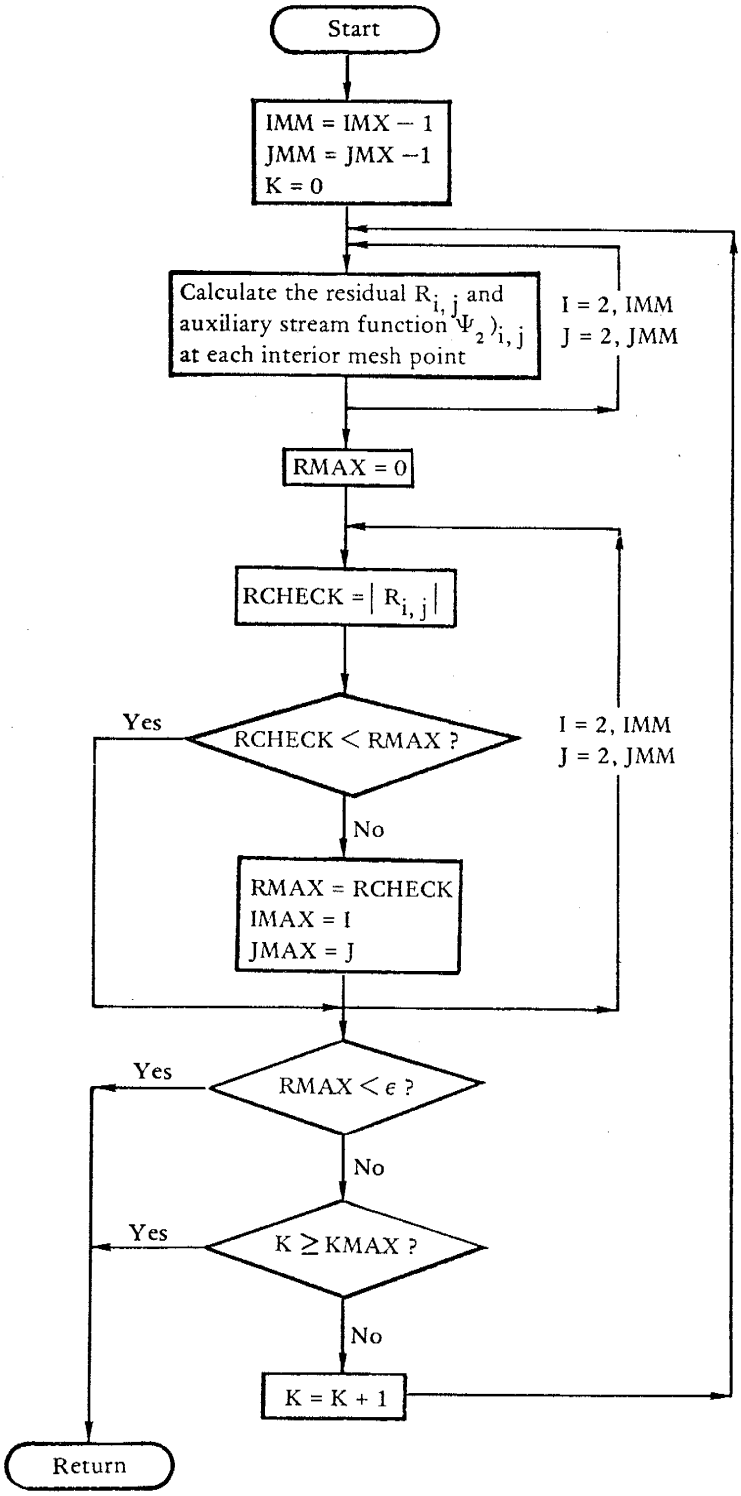
Start
IMM = IMX − 1
JMM = JMX −1
K = 0
Calculate the residual $R_{i,j}$ and auxiliary stream function $\Psi_2)_{i,j}$ at each interior mesh point
I = 2, IMM
J = 2, JMM
RMAX = 0
RCHECK = $|R_{i,j}|$
Yes
RCHECK < RMAX ?
I = 2, IMM
J = 2, JMM
No
RMAX = RCHECK
IMAX = I
JMAX = J
Yes
RMAX < ϵ ?
No
Yes
K ≥ KMAX ?
No
K = K + 1
Return

DISCAL. Subroutine DISCAL provides for calculation of finite-difference approximations to the derivatives of Ψ_2. The resulting values are the contributions to the specific discharge, $q_x)_2$ and $q_y)_2$, resulting from the physical boundary conditions. In subroutine DISCAL, $q_x)_2$ and $q_y)_2$ are calculated only at the mesh points, using the formulas of Section 3.5.

INTPLT. Subroutine INTPLT provides for interpolation between mesh-point values of Ψ_2, $q_x)_2$, and $q_y)_2$ in order to determine values of these quantities at the interface points. The subroutine makes use of the interpolation formulas presented in Section 3.6. Figure G.2.5 is a flow chart for subroutine INTPLT.

LINFIT. Subroutine LINFIT provides for calculations leading to a fit of connected line segments to the interface points. Given the coordinates of the interface points, the subroutine calculates the slopes and endpoints of the tangent line segments, and then the slopes of the connecting line segments.

The subroutine allows the lengths of each tangent line segment to be calculated separately, and placed in the array DELTA(N). However, maximum and minimum values of δ can also be provided. In the present formulation of the routine, DELMAX = DELMIN, so that all the DELTA(N) are equal.

Figure G.2.6 is a flow chart for subroutine LINFIT.

Figure G.2.5. Flow chart for subroutine INTPLT.

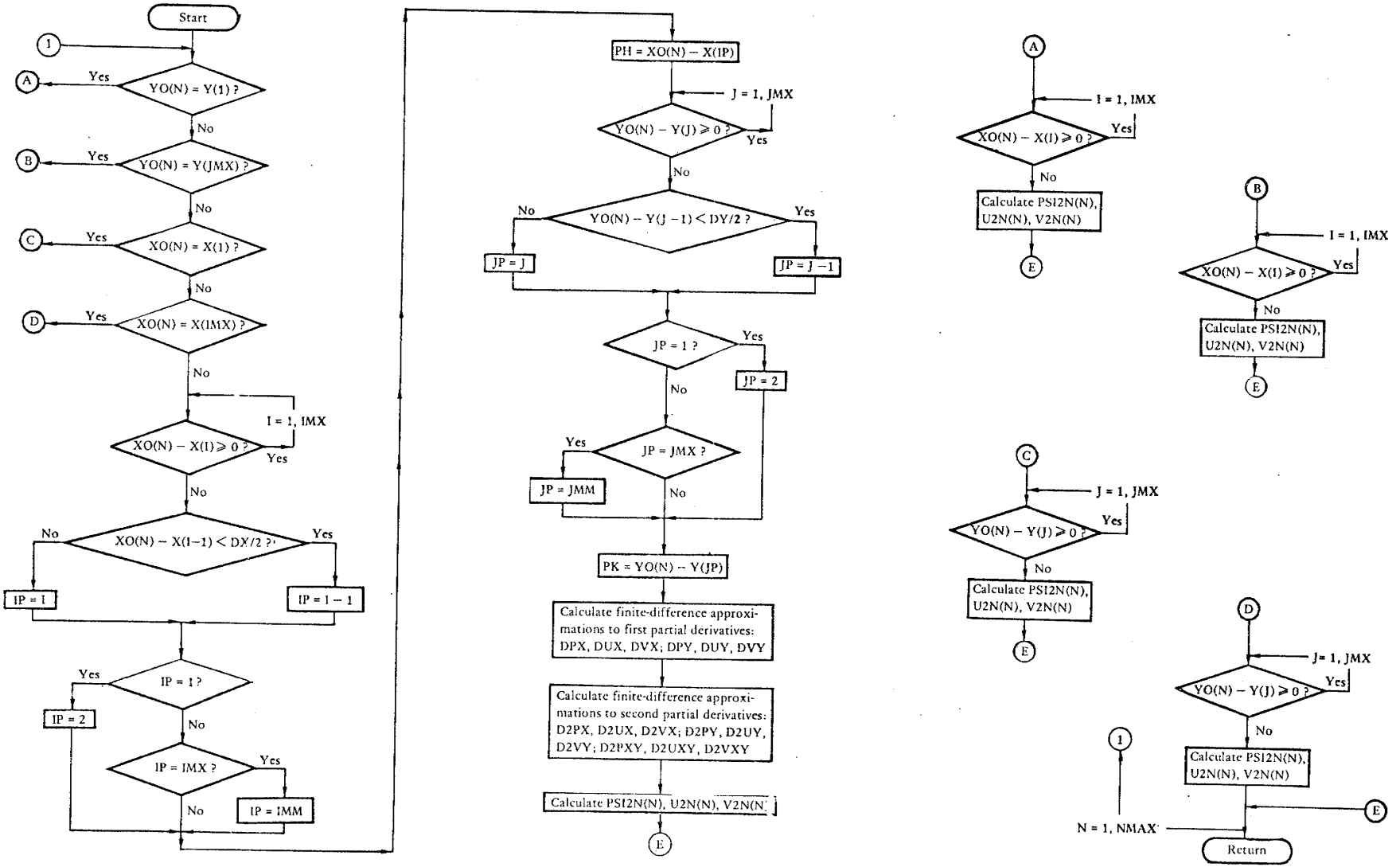
Start
1
A
Yes
YO(N) = Y(1) ?
No
B
Yes
YO(N) = Y(JMX) ?
No
C
Yes
XO(N) = X(1) ?
No
D
Yes
XO(N) = X(IMX) ?
No
I = 1, IMX
XO(N) − X(I) ⩾ 0 ?
Yes
No
No
XO(N) − X(I−1) < DX/2 ?
Yes
IP = I
IP = I − 1
Yes
IP = 1 ?
IP = 2
No
IP = IMX ?
Yes
No
IP = IMM
PH = XO(N) − X(IP)
J = 1, JMX
YO(N) − Y(J) ⩾ 0 ?
Yes
No
No
YO(N) − Y(J −1) < DY/2 ?
Yes
JP = J
JP = J −1
JP = 1 ?
Yes
JP = 2
No
Yes
JP = JMX ?
JP = JMM
No
PK = YO(N) − Y(JP)
Calculate finite-difference approxi-mations to first partial derivatives: DPX, DUX, DVX; DPY, DUY, DVY
Calculate finite-difference approxi-mations to second partial derivatives: D2PX, D2UX, D2VX; D2PY, D2UY, D2VY; D2PXY, D2UXY, D2VXY
Calculate PSI2N(N), U2N(N), V2N(N
E
A
I = 1, IMX
XO(N) − X(I) ⩾ 0 ?
Yes
No
Calculate PSI2N(N), U2N(N), V2N(N)
E
B
I = 1, IMX
XO(N) − X(I) ⩾ 0 ?
Yes
No
Calculate PSI2N(N), U2N(N), V2N(N)
E
C
J = 1, JMX
YO(N) − Y(J) ⩾ 0 ?
Yes
No
Calculate PSI2N(N), U2N(N), V2N(N)
E
D
J = 1, JMX
YO(N) − Y(J) ⩾ 0 ?
Yes
No
Calculate PSI2N(N), U2N(N), V2N(N)
E
1
N = 1, NMAX
Return

Figure G.2.6. Flow chart for subroutine LINFIT.

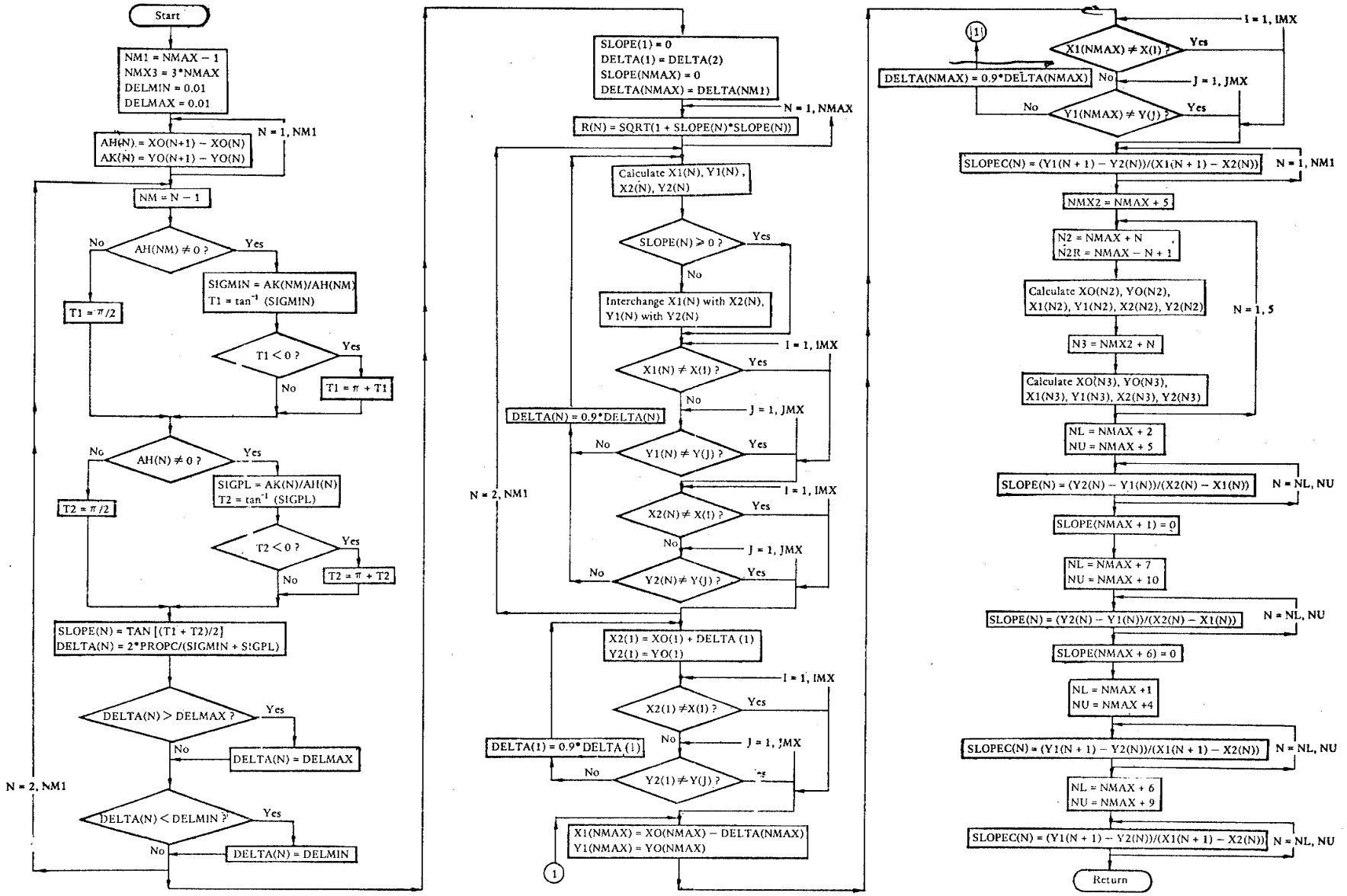
Start
NM1 = NMAX − 1
NMX3 = 3*NMAX
DELMIN = 0.01
DELMAX = 0.01
N = 1, NM1
AH(N) = XO(N+1) − XO(N)
AK(N) = YO(N+1) − YO(N)
NM = N − 1
No
AH(NM) ≠ 0 ?
Yes
SIGMIN = AK(NM)/AH(NM)
T1 = tan⁻¹ (SIGMIN)
T1 = π/2
T1 < 0 ?
Yes
No
T1 = π + T1
No
AH(N) ≠ 0 ?
Yes
SIGPL = AK(N)/AH(N)
T2 = tan⁻¹ (SIGPL)
T2 = π/2
T2 < 0 ?
Yes
No
T2 = π + T2
SLOPE(N) = TAN [(T1 + T2)/2]
DELTA(N) = 2*PROPC/(SIGMIN + SIGPL)
DELTA(N) > DELMAX ?
Yes
No
DELTA(N) = DELMAX
N = 2, NM1
DELTA(N) < DELMIN ?
Yes
No
DELTA(N) = DELMIN
SLOPE(1) = 0
DELTA(1) = DELTA(2)
SLOPE(NMAX) = 0
DELTA(NMAX) = DELTA(NM1)
N = 1, NMAX
R(N) = SQRT(1 + SLOPE(N)*SLOPE(N))
Calculate X1(N), Y1(N), X2(N), Y2(N)
SLOPE(N) ⩾ 0 ?
Yes
No
Interchange X1(N) with X2(N), Y1(N) with Y2(N)
I = 1, IMX
X1(N) ≠ X(I) ?
Yes
No
DELTA(N) = 0.9*DELTA(N)
J = 1, JMX
No
Y1(N) ≠ Y(J) ?
Yes
N = 2, NM1
I = 1, IMX
X2(N) ≠ X(1) ?
Yes
No
J = 1, JMX
No
Y2(N) ≠ Y(J) ?
Yes
X2(1) = XO(1) + DELTA (1)
Y2(1) = YO(1)
I = 1, IMX
X2(1) ≠ X(I) ?
Yes
No
DELTA(1) = 0.9*DELTA (1)
J = 1, JMX
No
Y2(1) ≠ Y(J) ?
Yes
X1(NMAX) = XO(NMAX) − DELTA(NMAX)
Y1(NMAX) = YO(NMAX)
1
1
I = 1, IMX
X1(NMAX) ≠ X(I) ?
Yes
DELTA(NMAX) = 0.9*DELTA(NMAX)
No
J = 1, JMX
No
Y1(NMAX) ≠ Y(J) ?
Yes
SLOPEC(N) = (Y1(N + 1) − Y2(N))/(X1(N + 1) − X2(N))
N = 1, NM1
NMX2 = NMAX + 5
N2 = NMAX + N
N2R = NMAX − N + 1
Calculate XO(N2), YO(N2), X1(N2), Y1(N2), X2(N2), Y2(N2)
N = 1, 5
N3 = NMX2 + N
Calculate XO(N3), YO(N3), X1(N3), Y1(N3), X2(N3), Y2(N3)
NL = NMAX + 2
NU = NMAX + 5
SLOPE(N) = (Y2(N) − Y1(N))/(X2(N) − X1(N))
N = NL, NU
SLOPE(NMAX + 1) = 0
NL = NMAX + 7
NU = NMAX + 10
SLOPE(N) = (Y2(N) − Y1(N))/(X2(N) − X1(N))
N = NL, NU
SLOPE(NMAX + 6) = 0
NL = NMAX +1
NU = NMAX +4
SLOPEC(N) = (Y1(N + 1) − Y2(N))/(X1(N + 1) − X2(N))
N = NL, NU
NL = NMAX + 6
NU = NMAX + 9
SLOPEC(N) = (Y1(N + 1) − Y2(N))/(X1(N + 1) − X2(N))
N = NL, NU
Return

MASCON. Subroutine MASCON provides for calculation of the degree of mass conservation maintained by the code. This subroutine is problem-dependent, and has been formulated for the basic check problem. The routine calculates the area of the flow region occupied by the heavier fluid by integrating the interface fit, and then compares that area with the initial area occupied by the heavier fluid.

RITE. Subroutine RITE provides for output, to the line printer, of coordinates of interface points (including image interface points) and values of Ψ, q_x, and q_y at the interface points and at the mesh points. The input/output procedures are discussed in greater detail in Section G. 3.

PLOTIN. Subroutine PLOTIN provides for automatic plotting of the interface with a CalComp digital incremental drum plotter. The routine causes each interface point to be plotted, as well as straight line segments connecting adjacent interface points. The routine is basically a simple call of the standard CalComp LINE subroutine.

G. 3 Input/Output Procedures

Input. Initial data and system parameters are input to the program in subroutine REED. The data are input from a deck of punched cards, or from a card-image tape or disk file. The arrangement of the data on the punched cards is given below. These data are identified in Table G.1.1.

Card 1, Format 20A4

Cols. 1-80. HEAD(I), I = 1, 20. This is a heading which can be used to identify the problem being studied.

Card 2, Format 1X, I5

Col. 1. Blank

Cols. 2-5. IPLOT, I5.

Card 3, Format 2X, 5I5

Cols. 1-2. Blank

Cols. 3-7. IMX, I5

Cols. 8-12. JMX, I5

Cols. 13-17. NMAX, I5

Cols. 18-22. KMAX, I5

Cols. 23-27. NOUT, I5

Card 4, Format 2X, 4F10.4

Cols. 1-2. Blank

Cols. 3-12. PERM, F10.4

Cols. 13-22. GAM1, F10.4

Cols. 23-32. GAM2, F10.4

Cols. 33-42. VIS, F10.4

Card 5, Format 2X, 4F10.4

Cols. 1-2. Blank

Cols. 3-12. X(1), F10.4

Cols. 13-22. Y(1), F10.4

Cols. 23-32. DX, F10.4

Cols. 33-42. DY, F10.4

Card 6, Format 2X, 3F10.4

Cols. 1-2. Blank

Cols. 3-12. OMEGA, F10.4

Cols. 13-22. EPS, F10.4

Cols. 23-32. PROPC, F10.4

Card 7, Format 2X, 3F10.4

Cols. 1-2. Blank

Cols. 3-12. TIME, F10.4

Cols. 13-22. DT, F10.4

Cols. 23-32. TSTOP, F10.4

Card 8, Format 2X, 2F10.4

Cols. 1-2. Blank

Cols. 3-12. CBND, F10.4

Cols. 13-22. XIN, F10.4

Card 9, and additional cards as needed, Format 8F10.4

Cols. 1-10, XO(1), F10.4

Cols. 11-20. YO(1), F10.4

Cols. 21-30. XO(2), F10.4

Cols. 31-40, YO(2), F10.4

etc.

In the present version of the computer program, which is formulated for the basic check problem, the initial coordinates of the interface points, XO(N) and YO(N), are generated in subroutine START. Thus the data cards for these parameters are left blank, and read as zeroes in subroutine REED.

Output. Some kind of output can be generated by MAIN, REED, RITE, and PLOTIN. If plotting of the interface is requested by specifying IPLOT $\neq$ 0, MAIN generates a rectangular plot of the boundaries of the flow region, and PLOTIN generates plots of the interface at the initial time and subsequently every NOUT cycles. Output to the line printer is generated by subroutines REED and RITE; only this output will be discussed in detail here.

Subroutine REED provides for input of initial data and system parameters, and calculation of mesh point coordinates. In addition, the routine provides for output of those same data so that they may be verified. The data, which are identified in Table G.1.1, appear on the first page of the printed output in the following order:

Line 1: The heading "INPUT DATA"

Line 2: A heading, contained in the array HEAD(20), which identifies the problem being studied.

Line 3: IMX, JMX, NMAX, KMAX, NOUT

LINE 4: PERM, GAM1, GAM2, VIS

Line 5: OMEGA, EPS, PROPC

Line 6: TIME, DT, TSTOP

Line 7: CBND, XIN

Lines 8-17: XO(N), YO(N). All of these values are zero for the formulation of the basic check problem.

Lines 18-21: X(I)

Lines 22-23: Y(J)

Figure G. 3.1 is a reproduction of the first page of printer output.

Subroutine RITE provides for output of various calculated data every NOUT cycles. The data are generally printed as tables of values at each interface point or at each mesh point. For the basic check problem, with NMAX = 32, the data are printed in the following order:

Line 1: TIME, NCYC

Lines 2-33: XO(N), YO(N). Coordinates of principal interface points.

Lines 34-65: XO(N), YO(N). Coordinates of upper image interface points.

Lines 66-97: XO(N), YO(N). Coordinates of lower image interface points.

Lines 98-129: PSI1N(N), VX(N), VY(N). Stream function and specific discharge components at interface points.

Lines 130-133: PSI1(I, 1)
Lines 134-137: PSI1(I, 2)
...
Lines 170-173: PSI1(I, 11)
} Values of stream function at mesh points

Lines 174-177: U(I, 1)
...
Lines 214-217: U(I, 11)
} Values of q_x at mesh points

Lines 218-221: V(I, 11)
...
Lines 258-261: V(I, 11)
} Values of q_y at mesh points

Line 262: K

Line 263: RMAX, IMAX, JMAX

Line 264: AREAIN, AREA

Line 265: ABSERR, RELERR

Figure G.3.2 is a reproduction of printer output produced by subroutine RITE.

Figure G.3.1. The first page of printer output, showing input data and system parameters.

INPUT DATA

```
   BASIC CHECK PROB., NONITERATIVE, PSOR, OMEGA=1.3, CONST. TIME STEP
22   11   32   50    5
 0.0008    1.2300    1.4000    0.0050
 1.3000    0.0001    0.2500
 0.0       5.0000   50.0000
 7.5000    0.0
      0.0         0.0         0.0         0.0         0.0         0.0         0.0         0.0
 0.0         0.0         0.0         0.0         0.0         0.0         0.0         0.0
 0.0         0.0         0.0         0.0         0.0         0.0         0.0         0.0
 0.0         0.0         0.0         0.0         0.0         0.0         0.0         0.0
 0.0         0.0         0.0         0.0         0.0         0.0         0.0         0.0
 0.0         0.0         0.0         0.0         0.0         0.0         0.0         0.0
 0.0         0.0         0.0         0.0         0.0         0.0         0.0         0.0
 0.0         0.0         0.0         0.0         0.0         0.0         0.0         0.0
     -15.7500   -14.2500   -12.7500   -11.2500    -9.7500    -8.2500    -6.7500    -5.2500
-3.7500    -2.2500    -0.7500     0.7500     2.2500     3.7500     5.2500     6.7500
 8.2500     9.7500    11.2500    12.7500    14.2500    15.7500
      -7.5000    -6.0000    -4.5000    -3.0000    -1.5000     0.0        1.5000     3.0000
 4.5000     6.0000     7.5000
```

Figure G. 3.2. Sample printer output produced by subroutine RITE.

(a) Coordinates of principal interface points.

```
        TIME =      0.0       NCYC =       0
-0.0100       -7.5000
 0.0          -7.3661
 0.0          -7.2321
 0.0          -6.6964
 0.0          -6.1607
 0.0          -5.6250
 0.0          -5.0893
 0.0          -4.5536
 0.0          -4.0179
 0.0          -3.4821
 0.0          -2.9464
 0.0          -2.4107
 0.0          -1.8750
 0.0          -1.3393
 0.0          -0.8036
 0.0          -0.2678
 0.0           0.2679
 0.0           0.8036
 0.0           1.3393
 0.0           1.8750
 0.0           2.4107
 0.0           2.9464
 0.0           3.4822
 0.0           4.0179
 0.0           4.5536
 0.0           5.0893
 0.0           5.6250
 0.0           6.1607
 0.0           6.6964
 0.0           7.2321
 0.0           7.3661
 0.0100        7.5000
```

(b) Coordinates of upper image interface points.

0.0100	7.5000
0.0	7.6339
0.0	7.7679
0.0	8.3036
0.0	8.8393
0.0	9.3750
0.0	9.9107
0.0	10.4464
0.0	10.9821
0.0	11.5178
0.0	12.0536
0.0	12.5893
0.0	13.1250
0.0	13.6607
0.0	14.1964
0.0	14.7321
0.0	15.2678
0.0	15.8036
0.0	16.3393
0.0	16.8750
0.0	17.4107
0.0	17.9464
0.0	18.4821
0.0	19.0178
0.0	19.5536
0.0	20.0893
0.0	20.6250
0.0	21.1607
0.0	21.6964
0.0	22.2321
0.0	22.3661
-0.0100	22.5000

(c) Coordinates of lower image interface points.

-0.0100	-7.5000
0.0	-7.6339
0.0	-7.7679
0.0	-8.3036
0.0	-8.8393
0.0	-9.3750
0.0	-9.9107
0.0	-10.4464
0.0	-10.9821
0.0	-11.5179
0.0	-12.0536
0.0	-12.5893
0.0	-13.1250
0.0	-13.6607
0.0	-14.1964
0.0	-14.7322
0.0	-15.2679
0.0	-15.8036
0.0	-16.3393
0.0	-16.8750
0.0	-17.4107
0.0	-17.9464
0.0	-18.4821
0.0	-19.0179
0.0	-19.5536
0.0	-20.0893
0.0	-20.6250
0.0	-21.1607
0.0	-21.6964
0.0	-22.2321
0.0	-22.3661
0.0100	-22.5000

(d) Values of Ψ, q_x, and q_y at interface points.

-0.0000	-0.0652	0.0
0.0061	-0.0372	-0.0003
0.0107	-0.0312	-0.0000
0.0243	-0.0216	-0.0000
0.0346	-0.0171	-0.0000
0.0429	-0.0141	-0.0000
0.0499	-0.0119	-0.0000
0.0557	-0.0100	-0.0000
0.0607	-0.0084	-0.0000
0.0648	-0.0070	-0.0000
0.0683	-0.0058	-0.0000
0.0710	-0.0046	-0.0000
0.0732	-0.0035	-0.0000
0.0748	-0.0025	-0.0000
0.0759	-0.0015	-0.0000
0.0764	-0.0005	-0.0000
0.0764	0.0005	-0.0000
0.0758	0.0015	-0.0000
0.0747	0.0025	-0.0000
0.0731	0.0036	-0.0000
0.0709	0.0047	-0.0000
0.0681	0.0058	-0.0000
0.0646	0.0071	-0.0000
0.0605	0.0084	-0.0000
0.0556	0.0100	-0.0000
0.0497	0.0118	-0.0000
0.0428	0.0141	-0.0000
0.0345	0.0171	-0.0000
0.0243	0.0216	-0.0000
0.0106	0.0311	0.0000
0.0061	0.0371	0.0003
-0.0000	0.0651	0.0

(e) Values of Ψ at mesh points.

```
     0.0         0.0         0.0         0.0         0.0         0.0         0.0
0.0         0.0         0.0         0.0         0.0         0.0         0.0
0.0         0.0         0.0         0.0         0.0         0.0         0.0
0.0
     0.0         0.0007      0.0014      0.0023      0.0033      0.0047      0.0065
0.0091      0.0127      0.0184      0.0287      0.0287      0.0184      0.0126
0.0089      0.0064      0.0046      0.0032      0.0022      0.0013      0.0006
0.0
     0.0         0.0013      0.0027      0.0043      0.0063      0.0089      0.0123
0.0170      0.0235      0.0329      0.0470      0.0469      0.0328      0.0233
0.0167      0.0121      0.0086      0.0061      0.0041      0.0025      0.0012
0.0
     0.0         0.0018      0.0037      0.0059      0.0086      0.0121      0.0168
0.0229      0.0314      0.0429      0.0584      0.0583      0.0427      0.0311
0.0227      0.0164      0.0118      0.0083      0.0056      0.0035      0.0016
0.0
     0.0         0.0021      0.0043      0.0069      0.0101      0.0142      0.0195
0.0266      0.0361      0.0486      0.0648      0.0647      0.0484      0.0358
0.0263      0.0191      0.0138      0.0097      0.0066      0.0041      0.0019
0.0
     0.0         0.0022      0.0045      0.0072      0.0106      0.0148      0.0204
0.0278      0.0376      0.0504      0.0668      0.0667      0.0502      0.0373
0.0275      0.0201      0.0144      0.0102      0.0069      0.0043      0.0020
0.0
     0.0         0.0021      0.0043      0.0068      0.0100      0.0141      0.0194
0.0265      0.0359      0.0484      0.0646      0.0646      0.0483      0.0357
0.0262      0.0191      0.0137      0.0097      0.0065      0.0040      0.0019
0.0
     0.0         0.0017      0.0036      0.0058      0.0085      0.0120      0.0166
0.0228      0.0312      0.0427      0.0582      0.0582      0.0426      0.0310
0.0225      0.0163      0.0117      0.0082      0.0056      0.0034      0.0016
0.0
     0.0         0.0013      0.0026      0.0042      0.0062      0.0087      0.0121
0.0168      0.0233      0.0327      0.0468      0.0467      0.0327      0.0232
0.0166      0.0119      0.0085      0.0060      0.0040      0.0025      0.0012
0.0
     0.0         0.0007      0.0014      0.0022      0.0032      0.0046      0.0064
0.0089      0.0126      0.0183      0.0285      0.0285      0.0182      0.0125
0.0088      0.0063      0.0045      0.0031      0.0021      0.0013      0.0006
0.0
     0.0         0.0         0.0         0.0         0.0         0.0         0.0
0.0         0.0         0.0         0.0         0.0         0.0         0.0
0.0         0.0         0.0         0.0         0.0         0.0         0.0
0.0
```

(f) Values of q_x at mesh points.

```
     -0.0000    -0.0005    -0.0010    -0.0016    -0.0023    -0.0033    -0.0045
-0.0063    -0.0088    -0.0130    -0.0224    -0.0223    -0.0129    -0.0088
-0.0062    -0.0044    -0.0032    -0.0022    -0.0015    -0.0009    -0.0005
-0.0000
     -0.0000    -0.0004    -0.0009    -0.0015    -0.0021    -0.0030    -0.0042
-0.0058    -0.0080    -0.0112    -0.0152    -0.0152    -0.0112    -0.0079
-0.0057    -0.0041    -0.0029    -0.0021    -0.0014    -0.0009    -0.0004
-0.0000
     -0.0000    -0.0004    -0.0008    -0.0012    -0.0018    -0.0025    -0.0035
-0.0047    -0.0063    -0.0081    -0.0096    -0.0096    -0.0081    -0.0062
-0.0046    -0.0034    -0.0024    -0.0017    -0.0012    -0.0007    -0.0003
-0.0000
     -0.0000    -0.0003    -0.0005    -0.0009    -0.0013    -0.0018    -0.0024
-0.0032    -0.0042    -0.0052    -0.0058    -0.0058    -0.0051    -0.0042
-0.0032    -0.0024    -0.0017    -0.0012    -0.0008    -0.0005    -0.0003
-0.0000
     -0.0000    -0.0001    -0.0003    -0.0004    -0.0007    -0.0009    -0.0012
-0.0016    -0.0021    -0.0025    -0.0027    -0.0027    -0.0025    -0.0021
-0.0016    -0.0012    -0.0009    -0.0006    -0.0004    -0.0003    -0.0001
-0.0000
     -0.0000     0.0000     0.0000     0.0000     0.0000     0.0000     0.0000
 0.0000     0.0000     0.0000     0.0000     0.0000     0.0000     0.0000
 0.0000     0.0000     0.0000     0.0000     0.0000     0.0000     0.0000
 0.0000
      0.0000     0.0001     0.0003     0.0005     0.0007     0.0010     0.0013
 0.0017     0.0021     0.0025     0.0028     0.0028     0.0025     0.0021
 0.0017     0.0013     0.0009     0.0007     0.0005     0.0003     0.0001
 0.0000
      0.0000     0.0003     0.0006     0.0009     0.0013     0.0018     0.0025
 0.0033     0.0042     0.0052     0.0058     0.0058     0.0052     0.0042
 0.0032     0.0024     0.0018     0.0012     0.0008     0.0005     0.0003
 0.0000
      0.0000     0.0004     0.0008     0.0012     0.0018     0.0025     0.0034
 0.0047     0.0063     0.0081     0.0096     0.0096     0.0081     0.0062
 0.0046     0.0034     0.0024     0.0017     0.0012     0.0007     0.0003
 0.0000
      0.0000     0.0004     0.0009     0.0014     0.0021     0.0030     0.0041
 0.0057     0.0079     0.0111     0.0151     0.0151     0.0111     0.0079
 0.0056     0.0040     0.0029     0.0020     0.0014     0.0009     0.0004
 0.0000
      0.0000     0.0005     0.0010     0.0015     0.0023     0.0032     0.0044
 0.0062     0.0087     0.0129     0.0223     0.0223     0.0129     0.0087
 0.0061     0.0044     0.0031     0.0022     0.0015     0.0009     0.0005
 0.0000
```

(g) Values of q_y at mesh points.

```
     -0.0000    -0.0000    -0.0000    -0.0000    -0.0000    -0.0000    -0.0000
-0.0000    -0.0000    -0.0000    -0.0000     0.0000     0.0000     0.0000
 0.0000     0.0000     0.0000     0.0000    -0.0000     0.0000     0.0000
 0.0000
      0.0004     0.0005     0.0005     0.0006     0.0008     0.0010     0.0014
 0.0020     0.0030     0.0049     0.0095    -0.0095    -0.0049    -0.0030
-0.0020    -0.0014    -0.0010    -0.0008    -0.0006    -0.0005    -0.0004
-0.0004
      0.0008     0.0009     0.0010     0.0012     0.0015     0.0020     0.0026
 0.0036     0.0052     0.0076     0.0113    -0.0114    -0.0076    -0.0052
-0.0037    -0.0027    -0.0020    -0.0015    -0.0012    -0.0009    -0.0008
-0.0007
      0.0011     0.0012     0.0014     0.0016     0.0020     0.0027     0.0035
 0.0048     0.0065     0.0089     0.0119    -0.0120    -0.0090    -0.0066
-0.0048    -0.0036    -0.0027    -0.0020    -0.0016    -0.0013    -0.0011
-0.0010
      0.0013     0.0014     0.0016     0.0019     0.0024     0.0031     0.0041
 0.0054     0.0072     0.0095     0.0122    -0.0122    -0.0096    -0.0073
-0.0055    -0.0041    -0.0031    -0.0024    -0.0019    -0.0015    -0.0013
-0.0012
      0.0013     0.0015     0.0017     0.0020     0.0025     0.0032     0.0043
 0.0057     0.0075     0.0097     0.0122    -0.0123    -0.0097    -0.0075
-0.0057    -0.0043    -0.0032    -0.0025    -0.0019    -0.0016    -0.0014
-0.0012
      0.0012     0.0014     0.0016     0.0019     0.0024     0.0031     0.0041
 0.0054     0.0072     0.0095     0.0122    -0.0122    -0.0096    -0.0073
-0.0055    -0.0041    -0.0031    -0.0024    -0.0019    -0.0015    -0.0013
-0.0011
      0.0010     0.0012     0.0013     0.0016     0.0020     0.0026     0.0035
 0.0048     0.0065     0.0089     0.0119    -0.0120    -0.0089    -0.0066
-0.0048    -0.0036    -0.0027    -0.0020    -0.0016    -0.0013    -0.0011
-0.0010
      0.0007     0.0009     0.0010     0.0012     0.0015     0.0019     0.0026
 0.0036     0.0052     0.0076     0.0113    -0.0114    -0.0076    -0.0052
-0.0037    -0.0026    -0.0019    -0.0015    -0.0011    -0.0009    -0.0008
-0.0007
      0.0004     0.0004     0.0005     0.0006     0.0008     0.0010     0.0014
 0.0020     0.0030     0.0049     0.0095    -0.0095    -0.0049    -0.0030
-0.0020    -0.0014    -0.0010    -0.0008    -0.0006    -0.0005    -0.0004
-0.0004
     -0.0000    -0.0000    -0.0000    -0.0000    -0.0000    -0.0000    -0.0000
-0.0000    -0.0000    -0.0000    -0.0000     0.0000     0.0000     0.0000
 0.0000     0.0000     0.0000     0.0000    -0.0000     0.0000     0.0000
-0.0000
```

(h) Miscellaneous information.

50 ITERATIONS

MAXIMUM RESIDUAL = 0.0001AT I = 9 J = 5

INITIAL AREA = 0.0 AREA = 0.0

ABSOLUTE ERROR = 0.0 RELATIVE ERROR = 0.0

APPENDIX H. THE COMPUTER PROGRAM FOR SIMULATING INTERFACE MOTION -- PROGRAM LISTING

Figure H.1 is a reproduction of the line printer listing of the FORTRAN IV program which has been developed for simulating interface motion through a porous medium. This formulation of the program is specialized to treat the basic check problem discussed previously.

Figure H.1. Listing of the computer program.

INTERFACE CODE, BASIC CHECK PROBLEM

```
C     ************************************
C        INTER1 EFFECTS CALCULATION OF TWO-FLUID INTERFACE MOTION
C     IN POROUS MEDIA, ACCORDING TO THE VORTEX THEORY OF G. DE
C     JOSSELIN DE JONG.  THIS IS VERSION ONE, AND IS SPECIALIZED
C     TO SOLVE THE BASIC CHECK PROBLEM.
C
      COMMON
     1   IMX,JMX,NMAX,KMAX,K,IMAX,JMAX,NREAD,NPRINT,NOUT,NCYC,
     2   ZERO,ONE,TWO,THREE,FOUR,HALF,QUART,PI,
     3   PERM,GAM1,GAM2,VIS,CBND,XIN,DX,DY,RMAX,OMEGA,EPS,TIME,DT,TSTOP,
     4   PROPC,AREAIN,AREA,ABSERR,RELERR,
     5   X0(99),Y0(99),X1(99),Y1(99),X2(99),Y2(99),
     6   SLOPE(99),SLOPEC(99),PSI1N(99),VX(99),VY(99),
     7   PSI2N(99),U2N(99),V2N(99),X(40),Y(20),
     8   PSI1(40,20),U(40,20),V(40,20),PSI2(40,20),U2(40,20),V2(40,20)
      COMMON /IN/ IPLOT
C
      NREAD=5
      NPRINT=6
C
      ZERO=0.0
      ONE=1.0
      TWO=2.0
      THREE=3.0
      FOUR=4.0
      HALF=0.5
      QUART=0.25
      PI=3.14159265
C
C        INPUT INITIAL DATA
C
      CALL REED
      NCYC=0
      IF(IPLOT .EQ. 0) GO TO 15
      CALL PLOT(5.,-11.,-3)
      CALL PLOT(0.,.5,-3)
       CALL PLOT(20.,0.,2)
      CALL PLOT(20.,10.,2)
      CALL PLOT(0.,10.,2)
      CALL PLOT(0.,0.,2)
   15 CONTINUE
C
C        CALCULATE LINE INTEGRALS FOR INITIAL INTERFACE SHAPE
C
      CALL START
      GO TO 50
C
   20 CONTINUE
```

```
C
C          CALCULATE LINE INTEGRALS
C
      CALL INTGRT
C
C          CALCULATE PSI2 AND ITS DERIVATIVES
C
   50 CONTINUE
      CALL BOUND
      CALL PSOR
      CALL DISCAL
      CALL INTPLT
C
C          CALCULATE PSI AND THE DISCHARGE COMPONENTS
C
C
      DO 60 J=1,JMX
      DO 60 I=1,IMX
      PSI1(I,J)=PSI1(I,J)+PSI2(I,J)
      U(I,J)=U(I,J)+U2(I,J)
      V(I,J)=V(I,J)+V2(I,J)
   60 CONTINUE
C
      DO 70 N=1,NMAX
      PSI1N(N)=PSI1N(N)+PSI2N(N)
      VX(N)=VX(N)+U2N(N)
      VY(N)=VY(N)+V2N(N)
   70 CONTINUE
                          VY(1)=ZERO
                          VY(NMAX)=ZERO
C
C          EDIT
C
      IF(TIME .GT. TSTOP) GO TO 100
      IF((NCYC-NCYC/NOUT*NOUT) .NE. 0) GO TO 80
      CALL RITE
      IF(IPLOT .EQ. 0) GO TO 75
      CALL PLOTIN
   75 CONTINUE
   80 CONTINUE
C
C          BEGIN NEW CYCLE
C
      TIME=TIME+DT
      NCYC=NCYC+1
      DO 90 N=1,NMAX
      XO(N)=XO(N)+DT*VX(N)
      YO(N)=YO(N)+DT*VY(N)
```

```
   90 CONTINUE
      DT=1.05*DT
C
C        DETERMINE NEW INTERFACE FIT
C
      CALL LINFIT
C
C        CALCULATE DEGREE OF MASS CONSERVATION
C
      CALL MASCON
      GO TO 20
C
  100 CONTINUE
      CALL RITE
      IF(IPLOT .EQ. 0) GO TO 102
      CALL PLOTIN
  102 CONTINUE
C
      IF(IPLOT .EQ. 0) GO TO 105
      CALL PLOT(20.,-11.,999)
  105 CONTINUE
      CALL EXIT
      END
      SUBROUTINE REED
C     **********************************
C
C        REED EFFECTS INPUT AND ECHO OF INITIAL DATA AND
C     SYSTEM CONSTANTS.
C
      COMMON
     1    IMX,JMX,NMAX,KMAX,K,IMAX,JMAX,NREAD,NPRINT,NOUT,NCYC,
     2    ZERO,ONE,TWO,THREE,FOUR,HALF,QUART,PI,
     3    PERM,GAM1,GAM2,VIS,CBND,XIN,DX,DY,RMAX,OMEGA,EPS,TIME,DT,TSTOP,
     4    PROPC,AREAIN,AREA,ABSERR,RELERR,
     5    X0(99),Y0(99),X1(99),Y1(99),X2(99),Y2(99),
     6    SLOPE(99),SLOPEC(99),PSI1N(99),VX(99),VY(99),
     7    PSI2N(99),U2N(99),V2N(99),X(40),Y(20),
     8    PSI1(40,20),U(40,20),V(40,20),PSI2(40,20),U2(40,20),V2(40,20)
      COMMON /IN/ IPLOT
C
      DIMENSION HEAD(20)
C
      READ(NREAD,500) (HEAD(I), I=1,20)
      READ(NREAD,600) IPLOT
      READ(NREAD,100) IMX,JMX,NMAX,KMAX,NOUT
      READ(NREAD,150) PERM,GAM1,GAM2,VIS
      READ(NREAD,150) X(1),Y(1),DX,DY
      READ(NREAD,250) OMEGA,EPS,PROPC
```

```
      READ(NREAD,250) TIME,DT,TSTOP
      READ(NREAD,300) CBND,XIN
      READ(NREAD,350)(XO(N),YO(N),N=1,NMAX)
C
      DO 10 I=2,IMX
      X(I)=X(I-1)+DX
   10 CONTINUE
C
      DO 20 J=2,JMX
      Y(J)=Y(J-1)+DY
   20 CONTINUE
C
      WRITE(NPRINT,50)
   50 FORMAT(1H1,////////,20X,10HINPUT DATA)
C
      WRITE(NPRINT,505) (HEAD(I), I=1,20)
        WRITE(NPRINT,101) IMX,JMX,NMAX,KMAX,NOUT
      WRITE(NPRINT,151) PERM,GAM1,GAM2,VIS
      WRITE(NPRINT,251) OMEGA,EPS,PROPC
      WRITE(NPRINT,251) TIME,DT,TSTOP
      WRITE(NPRINT,301) CBND,XIN
      WRITE(NPRINT,400)(XO(N),YO(N),N=1,NMAX)
      WRITE(NPRINT,400) (X(I),I=1,IMX)
      WRITE(NPRINT,400) (Y(J),J=1,JMX)
C
  100 FORMAT(2X,5I5)
  101 FORMAT(20X,5I5)
  150 FORMAT(2X,4F10.4)
  151 FORMAT(20X,4F10.4)
  250 FORMAT(2X,3F10.4)
  251 FORMAT(20X,3F10.4)
  300 FORMAT(2X,2F10.4)
  301 FORMAT(20X, 2F10.4)
  350 FORMAT(8F10.4)
  400 FORMAT(25X,8(1X,F10.4)/(F30.4,7(1X,F10.4)))
  500 FORMAT(20A4)
  505 FORMAT(///25X,20A4)
  600 FORMAT(1X,I5)
C
      RETURN
      END
      SUBROUTINE START
C     **********************************************
C
C        START CALCULATES PSI1, QX, AND QY FOR THE INITIAL
C     INTERFACE POSITION
C
C        START IS PROBLEM-DEPENDENT.  THE FOLLOWING ROUTINE
```

```
C      IS FOR THE BASIC CHECK PROBLEM.  IF THE INITIAL INTER-
C      FACE HAS NO VERTICAL SWGMENTS, AND IS HORIZONTAL AT
C      THE BOUNDARIES, START IS NOT NEEDED, EXCEPT POSSIBLY
C      TO CALCULATE THE INITIAL COORDINATES OF THE INTERFACE
C      POINTS.
C
C         CBND IS THE HALF-WIDTH OF THE BASIC CHECK PROBLEM.
C      XIN IS THE X-COORDINATE OF THE INITIAL VERTICAL INTER-
C      FACE OF THE BASIC CHECK PROBLEM.  SEE SUBROUTINE INTGRT
C      FOR THE DEFINITIONS OF THE OTHER VARIABLES USED HERE.
C
       COMMON
      1    IMX,JMX,NMAX,KMAX,K,IMAX,JMAX,NREAD,NPRINT,NOUT,NCYC,
      2    ZERO,ONE,TWO,THREE,FOUR,HALF,QUART,PI,
      3    PERM,GAM1,GAM2,VIS,CBND,XIN,DX,DY,RMAX,OMEGA,EPS,TIME,DT,TSTOP,
      4    PROPC,AREAIN,AREA,ABSERR,RELERR,
      5    X0(99),Y0(99),X1(99),Y1(99),X2(99),Y2(99),
      6    SLOPE(99),SLOPEC(99),PSI1N(99),VX(99),VY(99),
      7    PSI2N(99),U2N(99),V2N(99),X(40),Y(20),
      8    PSI1(40,20),U(40,20),V(40,20),PSI2(40,20),U2(40,20),V2(40,20)
C
       NM1=NMAX-1
       NMX3=3*NMAX
       COEFF=-HALF*PERM*(GAM2-GAM1)/(PI*VIS)
C
C         CALCULATE INITIAL COORDINATES OF INTERFACE POINTS
C
       DELTA=0.005
C
       X0(1)=XIN-TWO*DELTA
       Y0(1)=-CBND
       X0(NMAX)=XIN+TWO*DELTA
       Y0(NMAX)=CBND
       NM2=NMAX-2
       NM3=NMAX-3
       NM4=NMAX-4
       ANM=NM4
       DYN=(Y0(NMAX)-Y0(1))/ANM
       X0(2)=XIN
       Y0(2)=-CBND+QUART*DYN
       X0(3)=XIN
       Y0(3)=-CBND+HALF*DYN
       X0(NM1)=XIN
       Y0(NM1)=CBND-QUART*DYN
       X0(NM2)=XIN
       Y0(NM2)=CBND-HALF*DYN
       DO 10 N=4,NM3
       X0(N)=XIN
```

```
      YO(N)=YO(N-1)+DYN
   10 CONTINUE
      DO 20 N=1,NMAX
      N2=NMAX+N
      N2R=NMAX-N+1
      XO(N2)=XO(N2R)
      YO(N2)=TWO*YO(NMAX)-YO(N2R)
      N3=2*NMAX+N
      XO(N3)=XO(N)
      YO(N3)=TWO*YO(1)-YO(N)
   20 CONTINUE
C
C        CALCULATE ENDPOINTS AND SLOPES OF CONNECTING LINE SEG-
C     MENTS AT ENDS OF INTERFACE
C
      X2(1)=XO(1)+DELTA
      Y2(1)=YO(1)
      X1(2)=XO(2)
      Y1(2)=YO(2)-DELTA
      SLOPEC(1)=(Y1(2)-Y2(1))/(X1(2)-X2(1))
C
      X2(NM1)=XO(NM1)
      Y2(NM1)=YO(NM1)+DELTA
      X1(NMAX)=XO(NMAX)-DELTA
      Y1(NMAX)=YO(NMAX)
      SLOPEC(NM1)=(Y1(NMAX)-Y2(NM1))/(X1(NMAX)-X2(NM1))
      X2(NMAX+1)=XO(NMAX+1)-DELTA
      Y2(NMAX+1)=YO(NMAX+1)
      X1(NMAX+2)=XO(NMAX+2)
      Y1(NMAX+2)=YO(NMAX+2)-DELTA
      SLOPEC(NMAX+1)=(Y1(NMAX+2)-Y2(NMAX+1))/(X1(NMAX+2)-X2(NMAX+1))
      X2(2*NMAX-1)=XO(2*NMAX-1)
      Y2(2*NMAX-1)=YO(2*NMAX-1)+DELTA
      X1(2*NMAX)=XO(2*NMAX)+DELTA
      Y1(2*NMAX)=YO(2*NMAX)
      SLOPEC(2*NMAX-1)=(Y1(2*NMAX)-Y2(2*NMAX-1))/(X1(2*NMAX)-
     1      X2(2*NMAX-1))
      X2(2*NMAX+1)=XO(2*NMAX+1)+DELTA
      Y2(2*NMAX+1)=YO(2*NMAX+1)
      X1(2*NMAX+2)=XO(2*NMAX+2)
      Y1(2*NMAX+2)=YO(2*NMAX+2)+DELTA
      SLOPEC(2*NMAX+1)=(Y1(2*NMAX+2)-Y2(2*NMAX+1))/
     1      (X1(2*NMAX+2)-X2(2*NMAX+1))
      X2(3*NMAX-1)=XO(3*NMAX-1)
      Y2(3*NMAX-1)=YO(3*NMAX-1)-DELTA
      X1(3*NMAX)=XO(3*NMAX)-DELTA
      Y1(3*NMAX)=YO(3*NMAX)
      SLOPEC(3*NMAX-1)=(Y1(3*NMAX)-Y2(3*NMAX-1))/
```

```
     1      (X1(3*NMAX)-X2(3*NMAX-1))
C
C          CALCULATE PSI1, U, AND V AT MESH POINTS
C
C
      DO 100 I=1,IMX
      DO 100 J=1,JMX
      SUM1=ZERO
      SUM2=ZERO
      SUM3=ZERO
      DXIN=XIN-X(I)
      DXSQ=DXIN*DXIN
      DO 30 L=1,3
      GO TO (21,22,23), L
   21 DY1=Y2(NM1)-Y(J)
      DY2=Y1(2)-Y(J)
      GO TO 24
   22 DY1=Y2(2*NMAX-1)-Y(J)
      DY2=Y1(NMAX+2)-Y(J)
      GO TO 24
   23 DY1=Y1(2*NMAX+2)-Y(J)
      DY2=Y2(3*NMAX-1)-Y(J)
   24 DY1SQ=DY1*DY1
      DY2SQ=DY2*DY2
      ARG1=DXSQ+DY1SQ
      ARG2=DXSQ+DY2SQ
      ARG3=DY1/DXIN
      ARG4=DY2/DXIN
      F1=ALOG(ARG1)
      F2=ALOG(ARG2)
      F3= ATAN(ARG4)- ATAN(ARG3)
      GO TO (25,26,27), L
   25 SUM1=SUM1+DY1*F1-DY2*F2-TWO*(Y2(NM1)-Y1(2)+DXIN*F3)
      SUM2=SUM2+F3
      SUM3=SUM3+HALF*(F2-F1)
      GO TO 28
   26 SUM1=SUM1-DY1*F1+DY2*F2+TWO*(Y2(2*NMAX-1)-Y1(NMAX+2)+DXIN*F3)
      SUM2=SUM2-F3
      SUM3=SUM3-HALF*(F2-F1)
      GO TO 28
   27 SUM1=SUM1-DY1*F1+DY2*F2+TWO*(Y1(2*NMAX+2)-Y2(3*NMAX-1)+DXIN*F3)
      SUM2=SUM2-F3
      SUM3=SUM3-HALF*(F2-F1)
   28 CONTINUE
   30 CONTINUE
      DO 50 L=1,6
      GO TO (31,32,33,34,35,36), L
   31 N=1
```

```
      GO TO 40
   32 N=NM1
      GO TO 40
   33 N=NMAX+1
      GO TO 40
   34 N=2*NMAX-1
      GO TO 40
   35 N=2*NMAX+1
      GO TO 40
   36 N=3*NMAX-1
   40 CONTINUE
      CHECK=Y(J)-Y2(N)-SLOPEC(N)*(X(I)-X2(N))
      DELX1=X1(N+1)-X(I)
      DELX2=X2(N)-X(I)
      DELXX=X1(N+1)-X2(N)
      DELY2=Y(J)-Y2(N)
C
      F1=ONE+SLOPEC(N)*SLOPEC(N)
      F2=SLOPEC(N)/F1
      F3=SLOPEC(N)*F2
      F4=SLOPEC(N)*DELX2
      F5=SLOPEC(N)*DELX1
      F6=CHECK-F4
      F7=CHECK-F5
      F8=F3*CHECK
      F9=F2*CHECK
C
      ARG1=DELX1*DELX1+F7*F7
      ARG2=DELX2*DELX2+DELY2*DELY2
      ARG3=-(F1*DELX1-SLOPEC(N)*CHECK)/CHECK
      ARG4=(DELX2-SLOPEC(N)*DELY2)/CHECK
C
      F10= ATAN(ARG3)+ ATAN(ARG4)
      F11=ALOG(ARG1)
      F12=ALOG(ARG2)
C
      TERM1=(F5-F8)*F11+F2*(SLOPEC(N)*DELY2-DELX2)*F12
     1    -TWO*(SLOPEC(N)*DELXX+F2*CHECK*F10)
      F13=HALF*(F12-F11)
      TERM2=F2*F13+F3*F10
      TERM3=F3*F13-F2*F10
C
      IF(L .GE. 3) GO TO 45
   42 CONTINUE
      SUM1=SUM1+TERM1
      SUM2=SUM2+TERM2
      SUM3=SUM3+TERM3
      GO TO 50
```

```
   45 CONTINUE
      IF(L .GE. 5) GO TO 42
      SUM1=SUM1-TERM1
      SUM2=SUM2-TERM2
      SUM3=SUM3-TERM3
   50 CONTINUE
C
      PSI1(I,J)=HALF*COEFF*SUM1
      U(I,J)=-COEFF*SUM3
      V(I,J)=COEFF*SUM2
  100 CONTINUE
C
C        CALCULATE PSI1, VX, AND VY AT INTERFACE POINTS
C
      DO 200 NN=1,NMAX
      SUM1=ZERO
      SUM2=ZERO
      SUM3=ZERO
      DO 120 L=1,3
      GO TO (102,104,106), L
  102 DY1=Y2(NM1)-Y0(NN)
      DY2=Y1(2)-Y0(NN)
      GO TO 110
  104 DY1=Y2(2*NMAX-1)-Y0(NN)
      DY2=Y1(NMAX+2)-Y0(NN)
      GO TO 110
  106 DY1=Y1(2*NMAX+2)-Y0(NN)
      DY2=Y2(3*NMAX-1)-Y0(NN)
  110 CONTINUE
      DY1SQ=DY1*DY1
      DY2SQ=DY2*DY2
      F1=ALOG(DY1SQ)
      F2=ALOG(DY2SQ)
      GO TO (112,114,116), L
  112 SUM1=SUM1+DY1*F1-DY2*F2-TWO*(Y2(NM1)-Y1(2))
      SUM2=SUM2
      SUM3=SUM3+HALF*(F2-F1)
      GO TO 120
  114 SUM1=SUM1-DY1*F1+DY2*F2+TWO*(Y2(2*NMAX-1)-Y1(NMAX+2))
      SUM2=SUM2
      SUM3=SUM3-HALF*(F2-F1)
      GO TO 120
  116 SUM1=SUM1-DY1*F1+DY2*F2+TWO*(Y1(2*NMAX+2)-Y2(3*NMAX-1))
      SUM2=SUM2
      SUM3=SUM3-HALF*(F2-F1)
  120 CONTINUE
      DO 150 L=1,6
      GO TO (121, 122,123,124,125,126), L
```

```
  121 N=1
      GO TO 130
  122 N=NM1
      GO TO 130
  123 N=NMAX+1
      GO TO 130
  124 N=2*NMAX-1
      GO TO 130
  125 N=2*NMAX+1
      GO TO 130
  126 N=3*NMAX-1
  130 CONTINUE
      CHECK=YO(NN)-Y2(N)-SLOPEC(N)*(XO(NN)-X2(N))
      DELX1=X1(N+1)-XO(NN)
      DELX2=X2(N)-XO(NN)
      DELXX=X1(N+1)-X2(N)
      DELY2=YO(NN)-Y2(N)
C
      F1=ONE+SLOPEC(N)*SLOPEC(N)
      F2=SLOPEC(N)/F1
      F3=SLOPEC(N)*F2
      F4=SLOPEC(N)*DELX2
      F5=SLOPEC(N)*DELX1
      F6=CHECK-F4
      F7=CHECK-F5
      F8=F3*CHECK
      F9=F2*CHECK
C
      ARG1=DELX1*DELX1+F7*F7
      ARG2=DELX2*DELX2+DELY2*DELY2
      ARG3=-(F1*DELX1-SLOPEC(N)*CHECK)/CHECK
      ARG4=(DELX2-SLOPEC(N)*DELY2)/CHECK
C
      F10= ATAN(ARG3)+ ATAN(ARG4)
      F11=ALOG(ARG1)
      F12=ALOG(ARG2)
C
      TERM1=(F5-F8)*F11+F2*(SLOPEC(N)*DELY2-DELX2)*F12
     1    -TWO*(SLOPEC(N)*DELXX+F2*CHECK*F10)
      F13=HALF*(F12-F11)
      TERM2=F2*F13+F3*F10
      TERM3=F3*F13-F2*F10
      IF(L .GE. 3) GO TO 135
  132 CONTINUE
      SUM1=SUM1+TERM1
      SUM2=SUM2+TERM2
      SUM3=SUM3+TERM3
      GO TO 150
```

```
  135 CONTINUE
      IF(L .GE. 5) GO TO 132
      SUM1=SUM1-TERM1
      SUM2=SUM2-TERM2
      SUM3=SUM3-TERM3
  150 CONTINUE
C
      PSI1N(NN)=HALF*COEFF*SUM1
      VX(NN)=-COEFF*SUM3
      VY(NN)=COEFF*SUM2
  200 CONTINUE
C
      RETURN
      END
      SUBROUTINE INTGRT
C     ***********************************
C
C        INTGRT PROVIDES EVALUATION OF THE LINE INTEGRALS
C     ALONG THE INTERFACE IN ORDER TO DETERMINE PSI1 AND
C     THE COMPONENTS OF THE SPECIFIC DISCHARGE AT EACH
C     MESH POINT AND AT EACH INTERFACE POINT.
C
C        INPUT DATA **
C     XO(N), YO(N) -- COORDINATES OF THE INTERFACE POINTS
C     NMAX         -- TOTAL NUMBER OF INTERFACE POINTS
C     X1(N), Y1(N), -- COORDINATES OF LEFT ENDPOINT OF TAN-
C           GENT LINE SEGMENT AT XO(N), YO(N)
C     X2(N), Y2(N) -- COORDINATES OF RIGHT ENDPOINT OF
C           TANGENT LINE SEGMENT AT XO(N), YO(N)
C     SLOPE(N)     -- SLOPE OF TANGENT LINE SEGMENT AT
C           XO(N), YO(N)
C     SLOPEC(N)    -- SLOPE OF LINE SEGMENT CONNECTING
C           POINTS X2(N), Y2(N) AND X1(N+1), Y1(N+1)
C     X(I), Y(J)   -- COORDINATES OF MESH POINTS
C     IMX          -- TOTAL MESH POINTS IN X-DIRECTION
C     JMX          -- TOTAL MESH POINTS IN Y-DIRECTION
C     PERM         -- PERMEABILITY OF THE MEDIUM
C     GAM1, GAM2   -- SPECIFIC WEIGHTS OF THE TWO FLUIDS
C     VIS          -- (EQUAL) VISCOSITY OF THE TWO FLUIDS
C     PI           -- CONSTANT PI=3.14159265
C
C        OUTPUT DATA **
C     PSI1(I,J) -- VALUE OF PSI1 AT X(I), Y(J)
C     U(I,J)    -- VORTEX CONTRIBUTION TO QX AT X(I), Y(J)
C     V(I,J)    -- VORTEX CONTRIBUTION TO QY AT X(I), Y(J)
C     PSI1N(N)  -- VALUE OF PSI1 AT XO(N), YO(N)
C     VX(N)     -- VORTEX CONTRIBUTION TO QX AT XO(N), YO(N)
C     VY(N)     -- VORTEX CONTRIBUTION TO QY AT XO(N), YO(N)
```

```
C
C          NOTE -- QX AND QY ARE COMPONENTS OF SPECIFIC DIS-
C                  CHARGE AND MUST BE DIVIDED BY THE POROSITY
C                  TO GIVE THE LOCAL AVERAGE VELOCITY, WHICH
C                  GOVERNS THE INTERFACE MOTION.
C
C          OTHER VARIABLES **
C       TERM1 -- INTEGRAL OVER ONE LINE SEGMENT IN CALCULA-
C              TION OF PSI1 OR PSI1N
C       TERM2 -- INTEGRAL OVER ONE LINE SEGMENT IN CALCULA-
C              TION OF U OR VX
C       TERM3 -- INTEGRAL OVER ONE LINE SEGMENT IN CALCULA-
C              TION OF V OR VY
C       SUM1  -- SUMMATION OF TERM1
C       SUM2  -- SUMMATION OF TERM2
C       SUM3  -- SUMMATION OF TERM3
C       COEFF -- MULTIPLIED BY SUM1, SUM2, SUM3 TO
C              OBTAIN PROPER VALUES OF STREAM FUNCTION AND
C              SPECIFIC DISCHARGE COMPONENTS.
C
C          NOTE -- EXPRESSIONS LIKE DELX1, F1, AND ARG1 ARE
C                  INTRODUCED TO AVOID THEIR DUPLICATE CALCU-
C                  LATION
C
      COMMON
     1    IMX,JMX,NMAX,KMAX,K,IMAX,JMAX,NREAD,NPRINT,NOUT,NCYC,
     2    ZERO,ONE,TWO,THREE,FOUR,HALF,QUART,PI,
     3    PERM,GAM1,GAM2,VIS,CBND,XIN,DX,DY,RMAX,OMEGA,EPS,TIME,DT,TSTOP,
     4    PROPC,AREAIN,AREA,ABSERR,RELERR,
     5    X0(99),Y0(99),X1(99),Y1(99),X2(99),Y2(99),
     6    SLOPE(99),SLOPEC(99),PSI1N(99),VX(99),VY(99),
     7    PSI2N(99),U2N(99),V2N(99),X(40),Y(20),
     8    PSI1(40,20),U(40,20),V(40,20),PSI2(40,20),U2(40,20),V2(40,20)
C
      NM1=NMAX-1
      NMX2=NMAX+5
      NMX3=NMAX+10
C
C          CALCULATE COEFF
C
      COEFF=-HALF*PERM*(GAM2-GAM1)/(PI*VIS)
C
C          CALCULATE PSI1, U, AND V AT EACH MESH POINT
C
      DO 100 I=1,IMX
      DO 100 J=1,JMX
C
C               SUM INTEGRALS OVER TANGENT LINE SEGMENTS
```

```
C
      SUM1=ZERO
      SUM2=ZERO
      SUM3=ZERO
C
C         CALCULATE INTEGRAL OVER NTH LINE SEGMENT
C
      DO 50 N=1,NMX3
C
C            CHECK FOR ZERO SLOPE
C
      IF(SLOPE(N).EQ.ZERO) GO TO 45
C
C            CALCULATION FOR NONZERO SLOPE
C
      CHECK=Y(J)-YO(N)-SLOPE(N)*(X(I)-XO(N))
C
      DELX1=X1(N)-X(I)
      DELX2=X2(N)-X(I)
      DELXX=X2(N)-X1(N)
C
      F1=ONE+SLOPE(N)*SLOPE(N)
      F2=SLOPE(N)/F1
      F3=SLOPE(N)*F2
   10                 CONTINUE
C
C         CHECK FOR X(I), Y(J) LYING ON LINE SEGMENT
C
      IF(CHECK.EQ.ZERO) GO TO 30
C
C         X(I), Y(J) NOT ON LINE SEGMENT
C
      F4=SLOPE(N)*DELX2
      F5=SLOPE(N)*DELX1
      F6=CHECK-F4
      F7=CHECK-F5
      F8=F3*CHECK
      F9=F1/CHECK
   12                 CONTINUE
C
      ARG1=DELX2*DELX2+F6*F6
      ARG2=DELX1*DELX1+F7*F7
      ARG3=SLOPE(N)-F9*DELX2
      ARG4=SLOPE(N)-F9*DELX1
   14                 CONTINUE
C
C            CALCULATE TERM1, TERM2, TERM3
C
```

```
      F10= ATAN(ARG3)- ATAN(ARG4)
      F11=ALOG(ARG1)
      F12=ALOG(ARG2)
   16                 CONTINUE
C
      TERM1=(F4-F8)*F11-(F5-F8)*F12-TWO*(SLOPE(N)*DELXX
     1      +F2*CHECK*F10)
C
      F13=HALF*(F12-F11)
   18                 CONTINUE
C
      TERM2=F2*F13+F3*F10
   20                 CONTINUE
C
      TERM3=F3*F13-F2*F10
C
      GO TO 48
C
C        X(I), Y(J) LIES ON LINE SEGMENT
C
   30 CONTINUE
C
      DX1SQ=DELX1*DELX1
      DX2SQ=DELX2*DELX2
C
      F4=DX2SQ/DX1SQ
      F5=HALF*ALOG(F4)
C
C             CALCULATE TERM1, TERM2, TERM3
C
      TERM1=SLOPE(N)*(DELX2*ALOG(F1*DX2SQ)-DELX1*ALOG(F1*DX1SQ)
     1      -TWO*DELXX)
C
      TERM2=-F2*F5
C
      TERM3=-F3*F5
C
      GO TO 48
C
C               CALCULATION FOR ZERO SLOPE. ALL INTEGRALS ZERO.
C
   45 CONTINUE
C
      TERM1=ZERO
      TERM2=ZERO
      TERM3=ZERO
C
C        SUM ALL TERMS
```

```
C
   48 CONTINUE
      IF(N .GT. NMAX) GO TO 49
   47 CONTINUE
      SUM1=SUM1+TERM1
      SUM2=SUM2+TERM2
      SUM3=SUM3+TERM3
      GO TO 50
   49 CONTINUE
      IF(N .GT. NMX2) GO TO 47
      SUM1=SUM1-TERM1
      SUM2=SUM2-TERM2
      SUM3=SUM3-TERM3
C
   50 CONTINUE
C
C        CALCULATE INTEGRAL OVER NTH CONNECTING LINE SEGMENT
C
      DO 90 N=1,NMX3
      IF(N .EQ. NMAX) GO TO 90
      IF(N .EQ. NMX2) GO TO 90
      IF(N .EQ. NMX3) GO TO 90
C
C              CHECK FOR ZERO SLOPE
C
      IF(SLOPEC(N).EQ. ZERO) GO TO 85
C
C              CALCULATION FOR NONZERO SLOPE
C
      CHECK=Y(J)-Y2(N)-SLOPEC(N)*(X(I)-X2(N))
C
      DELX1=X1(N+1)-X(I)
      DELX2=X2(N)-X(I)
      DELXX=X1(N+1)-X2(N)
      DELY2=Y(J)-Y2(N)
C
      F1=ONE+SLOPEC(N)*SLOPEC(N)
      F2=SLOPEC(N)/F1
      F3=SLOPEC(N)*F2
      F4=SLOPEC(N)*DELX2
      F5=SLOPEC(N)*DELX1
   52               CONTINUE
C
C        CHECK FOR X(I), Y(J) LYING ON LINE SEGMENT
C
      IF(CHECK.EQ.ZERO) GO TO 70
C
C        X(I), Y(J) NOT ON LINE SEGMENT
```

```
C
      F6=CHECK-F4
      F7=CHECK-F5
      F8=F3*CHECK
      F9=F2*CHECK
   54                 CONTINUE
C
      ARG1=DELX1*DELX1+F7*F7
      ARG2=DELX2*DELX2+DELY2*DELY2
      ARG3=-(F1*DELX1-SLOPEC(N)*CHECK)/CHECK
      ARG4=(DELX2-SLOPEC(N)*DELY2)/CHECK
   56                 CONTINUE
C
      F10= ATAN(ARG3)+ ATAN(ARG4)
      F11=ALOG(ARG1)
      F12=ALOG(ARG2)
   58                 CONTINUE
C
C                CALCULATE TERM1, TERM2, TERM3
C
      TERM1=(F5-F8)*F11+F2*(SLOPEC(N)*DELY2-DELX2)*F12
     1       -TWO*(SLOPEC(N)*DELXX+F2*CHECK*F10)
C
   60                 CONTINUE
      F13=HALF*(F12-F11)
C
      TERM2=F2*F13+F3*F10
C
      TERM3=F3*F13-F2*F10
C
      GO TO 88
C
C          X(I), Y(J) LIES ON LINE SEGMENT
C
   70 CONTINUE
C
      ARG1=F1*DELX1*DELX1
      ARG2=DELX2*DELX2+DELY2*DELY2
C
      F6=ALOG(ARG1)
      F7=ALOG(ARG2)
C
C          CALCULATE TERM1, TERM2, TERM3
C
      TERM1=F5*F6-F4*F7-TWO*SLOPEC(N)*DELXX
C
      F8=HALF*(F7-F6)
C
```

```
      TERM2=F2*F8
C
      TERM3=F3*F8
C
      GO TO 88
C
C           CALCULATION FOR ZERO SLOPE. ALL INTEGRALS ZERO.
C
   85 CONTINUE
      TERM1=ZERO
      TERM2=ZERO
      TERM3=ZERO
C
C         SUM ALL TERMS
C
   88 CONTINUE
      IF(N .GT. NMAX) GO TO 89
C
   87 CONTINUE
      SUM1=SUM1+TERM1
      SUM2=SUM2+TERM2
      SUM3=SUM3+TERM3
      GO TO 90
   89 CONTINUE
      IF(N .GT. NMX2) GO TO 87
      SUM1=SUM1-TERM1
      SUM2=SUM2-TERM2
      SUM3=SUM3-TERM3
C
   90 CONTINUE
C
C         CALCULATE PSI1, U, AND V
C
      PSI1(I,J)=HALF*COEFF*SUM1
      U(I,J)=-COEFF*SUM3
      V(I,J)=COEFF*SUM2
C
  100 CONTINUE
C
C         CALCULATE PSI1N, VX, AND VY AT EACH INTERFACE POINT
C
      DO 200 NN=1,NMAX
C
C              SUM INTEGRALS OVER TANGENT LINE SEGMENTS
C
      SUM1=ZERO
      SUM2=ZERO
      SUM3=ZERO
```

```
C
C          CALCULATE INTEGRAL OVER NTH TANGENT LINE SEGMENT
C
      DO 150 N=1,NMX3
C
C                CHECK FOR ZERO SLOPE
C
      IF(SLOPE(N).NE. ZERO) GO TO 120
C
C                CALCULATION FOR ZERO SLOPE
C
      TERM1=ZERO
      TERM2=ZERO
      TERM3=ZERO
      GO TO 140
C
C                CALCULATION FOR NONZERO SLOPE
C
  120 CONTINUE
C
      F1=ONE+SLOPE(N)*SLOPE(N)
      F2=SLOPE(N)/F1
      F3=SLOPE(N)*F2
C
      DELX1=X1(N)-XO(NN)
      DELX2=X2(N)-XO(NN)
      DELXX=X2(N)-X1(N)
C
      DX1SQ=DELX1*DELX1
      DX2SQ=DELX2*DELX2
C
      F4=DX2SQ/DX1SQ
      F5=HALF*ALOG(F4)
C
      TERM1=SLOPE(N)*(DELX2*ALOG(F1*DX2SQ)-DELX1*ALOG(F1*DX1SQ)
     1       -TWO*DELXX)
      TERM2=-F2*F5
      TERM3=-F3*F5
C
C          SUM ALL TERMS
C
  140 CONTINUE
      IF(N .GT. NMAX) GO TO 145
  142 CONTINUE
      SUM1=SUM1+TERM1
      SUM2=SUM2+TERM2
      SUM3=SUM3+TERM3
      GO TO 150
```

```
  145 CONTINUE
      IF(N .GT. NMX2) GO TO 142
      SUM1=SUM1-TERM1
      SUM2=SUM2-TERM2
      SUM3=SUM3-TERM3
C
  150 CONTINUE
C
C        CALCULATE INTEGRAL OVER NTH CONNECTING LINE SEGMENT
C
      DO 190 N=1,NMX3
      IF(N .EQ. NMAX) GO TO 190
      IF(N .EQ. NMX2) GO TO 190
      IF(N .EQ. NMX3) GO TO 190
C
C              CHECK FOR ZERO SLOPE
C
      IF(SLOPEC(N).NE.ZERO) GO TO 170
C
C              CALCULATION FOR ZERO SLOPE
C
      TERM1=ZERO
      TERM2=ZERO
      TERM3=ZERO
      GO TO 180
C
C              CALCULATION FOR NONZERO SLOPE
C
  170 CONTINUE
C
      CHECK=YO(NN)-Y2(N)-SLOPEC(N)*(XO(NN)-X2(N))
C
      DELX1=X1(N+1)-XO(NN)
      DELX2=X2(N)-XO(NN)
      DELXX=X1(N+1)-X2(N)
      DELY2=YO(NN)-Y2(N)
C
      F1=ONE+SLOPEC(N)*SLOPEC(N)
      F2=SLOPEC(N)/F1
      F3=F2*SLOPEC(N)
      F4=SLOPEC(N)*DELX2
      F5=SLOPEC(N)*DELX1
      F6=CHECK-F4
      F7=CHECK-F5
      F8=F3*CHECK
      F9=F2*CHECK
C
      ARG1=DELX1*DELX1+F7*F7
```

```
      ARG2=DELX2*DELX2+DELY2*DELY2
      ARG3=-(F1*DELX1-SLOPEC(N)*CHECK)/CHECK
      ARG4=(DELX2-SLOPEC(N)*DELY2)/CHECK
C
      F10= ATAN(ARG3)+ ATAN(ARG4)
      F11=ALOG(ARG1)
      F12=ALOG(ARG2)
C
      TERM1=(F5-F8)*F11+F2*(SLOPEC(N)*DELY2-DELX2)*F12
     1       -TWO*(SLOPEC(N)*DELXX+F2*CHECK*F10)
C
      F13=HALF*(F12-F11)
C
      TERM2=F2*F13+F3*F10
      TERM3=F3*F13-F2*F10
C
C         SUM ALL TERMS
C
  180 CONTINUE
      IF(N .GT. NMAX) GO TO 185
  182 CONTINUE
      SUM1=SUM1+TERM1
      SUM2=SUM2+TERM2
      SUM3=SUM3+TERM3
      GO TO 190
  185 CONTINUE
      IF(N .GT. NMX2) GO TO 182
      SUM1=SUM1-TERM1
      SUM2=SUM2-TERM2
      SUM3=SUM3-TERM3
C
  190 CONTINUE
C
C         CALCULATE PSI1N, VX, AND VY
C
      PSI1N(NN)=HALF*COEFF*SUM1
      VX(NN)=-COEFF*SUM3
      VY(NN)=COEFF*SUM2
C
  200 CONTINUE
C
      RETURN
      END
      SUBROUTINE BOUND
C     ********************************************
C
C         BOUND DETERMINES BOUNDARY VALUES FOR PSI2 FROM THE
C     PHYSICAL BOUNDARY CONDITIONS OF THE PROBLEM UNDER CON-
```

```
C      SIDERATION.  THE BOUNDARY VALUES DETERMINED ARE REQUIRED
C      BY SUBROUTINE PSOR.
C         THIS IS A PROBLEM-DEPENDENT SUBROUTINE.
C
C         THE FOLLOWING ROUTINE IS FOR THE BASIC CHECK PROBLEM,
C      FOR WHICH PSI2=-PSI1 ON THE BOUNDARIES OF A RECTANGULAR
C      REGION.
C
       COMMON
      1    IMX,JMX,NMAX,KMAX,K,IMAX,JMAX,NREAD,NPRINT,NOUT,NCYC,
      2    ZERO,ONE,TWO,THREE,FOUR,HALF,QUART,PI,
      3    PERM,GAM1,GAM2,VIS,CBND,XIN,DX,DY,RMAX,OMEGA,EPS,TIME,DT,TSTOP,
      4    PROPC,AREAIN,AREA,ABSERR,RELERR,
      5    X0(99),Y0(99),X1(99),Y1(99),X2(99),Y2(99),
      6    SLOPE(99),SLOPEC(99),PSI1N(99),VX(99),VY(99),
      7    PSI2N(99),U2N(99),V2N(99),X(40),Y(20),
      8    PSI1(40,20),U(40,20),V(40,20),PSI2(40,20),U2(40,20),V2(40,20)
C
       DO 10 I=1,IMX
       PSI2(I,1)=-PSI1(I,1)
       PSI2(I,JMX)=-PSI1(I,JMX)
   10 CONTINUE
C
       DO 20 J=1,JMX
       PSI2(1,J)=-PSI1(1,J)
       PSI2(IMX,J)=-PSI1(IMX,J)
   20 CONTINUE
C
       RETURN
       END
       SUBROUTINE PSOR
C      ***********************************
C
C         PSOR CALCULATES PSI2 AT EACH MESH POINT BY THE POINT
C      SUCCESSIVE OVERRELAXATION (PSOR) METHOD, GIVEN THE VALUES
C      OF PSI2 ON THE BOUNDARIES OF A RECTANGULAR REGION.  THESE
C      BOUNDARY VALUES ARE DETERMINED BY SUBROUTINE BOUND.
C
C         INPUT DATA **
C      PSI2(I,1), PSI2(I,JMX) -- BOUNDARY VALUES OF PSI2 ON
C            LOWER AND UPPER BOUNDARIES, RESPECTIVELY
C      PSI2(1,J), PSI2(IMX,J) -- BOUNDARY VALUES OF PSI2 ON
C            LEFT AND RIGHT BOUNDARIES, RESPECTIVELY
C      OMEGA -- RELAXATION PARAMETER
C      EPS -- CONVERGENCE PARAMETER
C      IMX -- TOTAL MESH POINTS IN X-DIRECTION
C      JMX -- TOTAL MESH POINTS IN Y-DIRECTION
C      KMAX -- MAXIMUM NUMBER OF ITERATIONS ALLOWED
```

```
C       DX -- MESH SPACING IN X-DIRECTION
C       DY -- MESH SPACING IN Y-DIRECTION
C
C          OUTPUT DATA **
C       PSI2(I,J) -- VALUES OF PSI2 AT EACH MESH POINT
C       K -- TOTAL NUMBER OF ITERATIONS
C
C          OTHER VARIABLES **
C       R(I,J) -- ARRAY OF RESIDUALS
C       RMAX -- MAXIMUM RESIDUAL
C       IMAX, JMAX -- LOCATION OF MAXIMUM RESIDUAL
C
C          NOTE -- FOR THE ZEROTH ITERATE, THE VALUES OF PSI2(I,J)
C       ARE THOSE FOR THE PRECEDING TIME STEP
C
        COMMON
       1   IMX,JMX,NMAX,KMAX,K,IMAX,JMAX,NREAD,NPRINT,NOUT,NCYC,
       2   ZERO,ONE,TWO,THREE,FOUR,HALF,QUART,PI,
       3   PERM,GAM1,GAM2,VIS,CBND,XIN,DX,DY,RMAX,OMEGA,EPS,TIME,DT,TSTOP,
       4   PROPC,AREAIN,AREA,ABSERR,RELERR,
       5   X0(99),Y0(99),X1(99),Y1(99),X2(99),Y2(99),
       6   SLOPE(99),SLOPEC(99),PSI1N(99),VX(99),VY(99),
       7   PSI2N(99),U2N(99),V2N(99),X(40),Y(20),
       8   PSI1(40,20),U(40,20),V(40,20),PSI2(40,20),U2(40,20),V2(40,20)
C
        DIMENSION R(40,40)
C
        IMM=IMX-1
        JMM=JMX-1
        K=0
C
        DXSQ=DX*DX
        DYSQ=DY*DY
        FACTOR=TWO*(DXSQ+DYSQ)
C
C          CALCULATE ARRAY OF RESIDUALS AND KTH ITERATE OF
C               PSI2(I,J)
C
   50 CONTINUE
C
        DO 100 J=2,JMM
        DO 100 I=2,IMM
C
        R(I,J)=(DYSQ*(PSI2(I+1,J)+PSI2(I-1,J))+DXSQ*(PSI2(I,J+1)
       1   +PSI2(I,J-1))-FACTOR*PSI2(I,J))/FACTOR
C
        PSI2(I,J)=PSI2(I,J)+OMEGA*R(I,J)
C
```

```
  100 CONTINUE
C
C        DETERMINE MAXIMUM RESIDUAL, RMAX
C
      RMAX=ZERO
      DO 150 J=2,JMM
      DO 150 I=2,IMM
      RCHECK= ABS(R(I,J))
      IF(RCHECK .LT. RMAX) GO TO 150
      RMAX=RCHECK
      IMAX=I
      JMAX=J
  150 CONTINUE
C
C        CHECK FOR CONVERGENCE
C
      IF(RMAX .LE. EPS) GO TO 200
C
C        CHECK IF MAXIMUM NUMBER OF ITERATIONS HAS BEEN
C     REACHED.  IF SO, RMAX, IMAX, AND JMAX WILL BE OUTPUT.
C
      IF(K .GE. KMAX) GO TO 200
C
C        IF NOT, INCREMENT ITERATION COUNTER AND ITERATE
C
      K=K+1
      GO TO 50
C
  200 CONTINUE
C
      RETURN
      END
      SUBROUTINE DISCAL
C     **********************************
C
C        DISCAL PROVIDES CALCULATION OF THE SPECIFIC DISCHARGE
C     COMPONENTS AT THE MESH POINTS, DUE ONLY TO PSI2.  THESE
C     VALUES MUST BE ADDED TO U(I,J) AND V(I,J), DETERMINED IN
C     SUBROUTINE INTGRT, IN ORDER TO OBTAIN THE TOTAL SPECIFIC
C     DISCHARGE COMPONENTS AT THE MESH POINTS.
C
C        INPUT DATA **
C     PSI2(I,J) -- VALUES OF SECOND STREAM FUNCTION AT MESH
C           POINTS
C     DX -- MESH SPACING IN X-DIRECTION
C     DY -- MESH SPACING IN Y-DIRECTION
C     IMX -- TOTAL MESH POINTS IN X-DIRECTION
C     JMX -- TOTAL MESH POINTS IN Y-DIRECTION
```

```
C
C          OUTPUT DATA **
C       U2(I,J), V2(I,J) -- SPECIFIC DISCHARGE COMPONENTS AT
C             MESH POINTS
C
C          OTHER VARIABLES **
C       RDX -- RECIPROCAL OF DX
C       RDY -- RECIPROCAL OF DY
C
        COMMON
       1    IMX,JMX,NMAX,KMAX,K,IMAX,JMAX,NREAD,NPRINT,NOUT,NCYC,
       2    ZERO,ONE,TWO,THREE,FOUR,HALF,QUART,PI,
       3    PERM,GAM1,GAM2,VIS,CBND,XIN,DX,DY,RMAX,OMEGA,EPS,TIME,DT,TSTOP,
       4    PROPC,AREAIN,AREA,ABSERR,RELERR,
       5    X0(99),Y0(99),X1(99),Y1(99),X2(99),Y2(99),
       6    SLOPE(99),SLOPEC(99),PSI1N(99),VX(99),VY(99),
       7    PSI2N(99),U2N(99),V2N(99),X(40),Y(20),
       *    PSI1(40,20),U(40,20),V(40,20),PSI2(40,20),U2(40,20),V2(40,20)
C
        IMM=IMX-1
        JMM=JMX-1
C
        RDX=ONE/DX
        RDY=ONE/DY
C
C          INTERIOR MESH POINTS
C
        DO 50 J=2,JMM
        DO 50 I=2,IMM
C
        U2(I,J)=HALF*(PSI2(I,J-1)-PSI2(I,J+1))*RDY
C
        V2(I,J)=HALF*(PSI2(I+1,J)-PSI2(I-1,J))*RDX
C
   50 CONTINUE
C
C          BOUNDARY POINTS
C
        U2(1,1)=(PSI2(1,1)-PSI2(1,2))*RDY
        V2(1,1)=(PSI2(2,1)-PSI2(1,1))*RDX
C
        U2(IMX,1)=(PSI2(IMX,1)-PSI2(IMX,2))*RDY
        V2(IMX,1)=(PSI2(IMX,1)-PSI2(IMM,1))*RDX
C
        DO 60 J=2,JMM
        U2(1,J)=HALF*(PSI2(1,J-1)-PSI2(1,J+1))*RDY
        V2(1,J)=(PSI2(2,J)-PSI2(1,J))*RDX
C
```

```
      U2(IMX,J)=HALF*(PSI2(IMX,J-1)-PSI2(IMX,J+1))*RDY
      V2(IMX,J)=(PSI2(IMX,J)-PSI2(IMM,J))*RDX
   60 CONTINUE
C
      U2(1,JMX)=(PSI2(1,JMM)-PSI2(1,JMX))*RDY
      V2(1,JMX)=(PSI2(2,JMX)-PSI2(1,JMX))*RDX
C
      U2(IMX,JMX)=(PSI2(IMX,JMM)-PSI2(IMX,JMX))*RDY
      V2(IMX,JMX)=(PSI2(IMX,JMX)-PSI2(IMM,JMX))*RDX
C
      DO 70 I=2,IMM
      U2(I,1)=(PSI2(I,1)-PSI2(I,2))*RDY
      V2(I,1)=HALF*(PSI2(I+1,1)-PSI2(I-1,1))*RDX
C
      U2(I,JMX)=(PSI2(I,JMM)-PSI2(I,JMX))*RDY
      V2(I,JMX)=HALF*(PSI2(I+1,JMX)-PSI2(I-1,JMX))*RDX
   70 CONTINUE
C
      RETURN
      END
      SUBROUTINE INTPLT
C     ************************************
C
C        INTPLT INTERPOLATES BETWEEN VALUES OF PSI2(I,J),
C     U2(I,J), AND V2(I,J) TO DETERMINE VALUES OF PSI2, U2,
C     AND V2 AT THE INTERFACE POINTS.
C
C        INPUT DATA **
C     XO(N), YO(N) -- COORDINATES OF NTH INTERFACE POINT
C     PSI2(I,J) -- VALUES OF PSI2 AT MESH POINTS
C     U2(I,J) -- VALUES OF X-COMPONENT OF SPECIFIC DISCHARGE,
C           DETERMINED FROM PSI2, AT MESH POINTS
C     V2(I,J) -- VALUES OF Y-COMPONENT OF SPECIFIC DISCHARGE,
C           DETERMINED FROM PSI2, AT MESH POINTS
C     X(I), Y(J) -- COORDINATES OF MESH POINT
C     DX -- MESH SPACING IN X-DIRECTION
C     DY -- MESH SPACING IN Y-DIRECTION
C     NMAX -- TOTAL NUMBER OF INTERFACE POINTS
C     IMX -- TOTAL MESH POINTS IN X-DIRECTION
C     JMX -- TOTAL MESH POINTS IN Y-DIRECTION
C
C        OUTPUT DATA **
C     PSI2N(N) -- VALUE OF PSI2 AT INTERFACE POINT N
C     U2N(N) -- VALUE OF U2 AT INTERFACE POINT N
C     V2N(N) -- VALUE OF V2 AT INTERFACE POINT N
C
C        OTHER VARIABLES **
C     IP, JP -- COORDINATES OF MESH POINT NEAREST XO(N), YO(N)
```

```
C      PH -- X-DISTANCE BETWEEN INTERFACE POINT AND NEAREST
C            MESH POINT
C      PK -- Y-DISTANCE BETWEEN INTERFACE POINT AND NEAREST
C            MESH POINT
C      DPX, DUX, DVX -- PARTIAL DERIVATIVES OF PSI2, U2, AND
C            V2 WITH RESPECT TO X
C      DPY, DUY, DVY -- PARTIAL DERIVATIVES WITH RESPECT TO Y
C      D2PX, D2UX, D2VX -- SECOND PARTIALS WITH RESPECT TO X
C      D2PY, D2UY, D2VY -- SECOND PARTIALS WITH RESPECT TO Y
C      D2PXY, D2UXY, D2VXY -- SECOND PARTIALS WITH RESPECT
C            TO X AND Y
C
       COMMON
      1    IMX,JMX,NMAX,KMAX,K,IMAX,JMAX,NREAD,NPRINT,NOUT,NCYC,
      2    ZERO,ONE,TWO,THREE,FOUR,HALF,QUART,PI,
      3    PERM,GAM1,GAM2,VIS,CBND,XIN,DX,DY,RMAX,OMEGA,EPS,TIME,DT,TSTOP,
      4    PROPC,AREAIN,AREA,ABSERR,RELERR,
      5    X0(99),Y0(99),X1(99),Y1(99),X2(99),Y2(99),
      6    SLOPE(99),SLOPEC(99),PSI1N(99),VX(99),VY(99),
      7    PSI2N(99),U2N(99),V2N(99),X(40),Y(20),
      8    PSI1(40,20),U(40,20),V(40,20),PSI2(40,20),U2(40,20),V2(40,20)
C
       IMM=IMX-1
       JMM=JMX-1
C
       DO 900 N=1,NMAX
C
C         CHECK IF INTERFACE POINT LIES ON BOUNDARY.  IF SO,
C      SIMPLE LINEAR INTERPOLATION IS USED ALONG THE BOUNDARY.
C
       IF(Y0(N) .EQ. Y(1)) GO TO 500
       IF(Y0(N) .EQ. Y(JMX)) GO TO 600
       IF(X0(N) .EQ. X(1)) GO TO 700
       IF(X0(N) .EQ. X(IMX)) GO TO 800
C
C         LOCATE MESH POINT NEAREST INTERFACE POINT
C
       DO 10 I=1,IMX
       DELX=X0(N)-X(I)
       IF(DELX .LT. ZERO) GO TO 15
   10  CONTINUE
   15  CONTINUE
C
       CHECK=HALF*DX
       DELX=X0(N) - X(I-1)
C
       IF(DELX .LT. CHECK) GO TO 20
       IP=I
```

```
      GO TO 25
   20 CONTINUE
      IP=I-1
   25 CONTINUE
C
C        CHECK IF NEAREST MESH POINT IS A BOUNDARY POINT.  IF SO,
C     THE INTERPOLATION FORMULAS ARE CENTERED AT THE FIRST INTERIOR
C     MESH POINT NORMAL TO THE BOUNDARY.
C
      IF(IP .EQ. 1) GO TO 30
      IF(IP .EQ. IMX) GO TO 35
      GO TO 40
C
   30 CONTINUE
      IP=2
      GO TO 40
C
   35 CONTINUE
      IP=IMM
   40 CONTINUE
C
C        CALCULATE PH
C
      PH=XO(N)-X(IP)
C
      DO 50 J=1,JMX
      DELY=YO(N)-Y(J)
      IF(DELY .LT. ZERO) GO TO 55
   50 CONTINUE
   55 CONTINUE
C
      CHECK=HALF*DY
      DELY=YO(N)-Y(J-1)
C
      IF(DELY .LT.CHECK) GO TO 60
      JP=J
      GO TO 65
   60 CONTINUE
      JP=J-1
   65 CONTINUE
C
C        CHECK IF NEAREST MESH POINT IS A BOUNDARY POINT
C
      IF(JP .EQ. 1) GO TO 70
      IF(JP .EQ. JMX) GO TO 75
      GO TO 80
C
   70 CONTINUE
```

```
      JP=2
      GO TO 80
C
   75 CONTINUE
      JP=JMM
   80 CONTINUE
C
C        CALCULATE PK
C
      PK=YO(N)-Y(JP)
C
C        CALCULATE FINITE-DIFFERENCE APPROXIMATIONS TO PARTIAL
C           DERIVATIVES
C
      IPM=IP-1
      IPP=IP+1
      JPM=JP-1
      JPP=JP+1
C
      HDX=HALF/DX
      DPX=HDX*(PSI2(IPP,JP)-PSI2(IPM,JP))
      DUX=HDX*(U2(IPP,JP)-U2(IPM,JP))
      DVX=HDX*(V2(IPP,JP)-V2(IPM,JP))
C
      HDY=HALF/DY
      DPY=HDY*(PSI2(IP,JPP)-PSI2(IP,JPM))
      DUY=HDY*(U2(IP,JPP)-U2(IP,JPM))
      DVY=HDY*(V2(IP,JPP)-V2(IP,JPM))
C
      RDX=ONE/(DX*DX)
      D2PX=(PSI2(IPM,JP)-TWO*PSI2(IP,JP)+PSI2(IPP,JP))*RDX
      D2UX=(U2(IPM,JP)-TWO*U2(IP,JP)+U2(IPP,JP))*RDX
      D2VX=(V2(IPM,JP)-TWO*V2(IP,JP)+V2(IPP,JP))*RDX
C
      RDY=ONE/(DY*DY)
      D2PY=(PSI2(IP,JPM)-TWO*PSI2(IP,JP)+PSI2(IP,JPP))*RDY
      D2UY=(U2(IP,JPM)-TWO*U2(IP,JP)+U2(IP,JPP))*RDY
      D2VY=(V2(IP,JPM)-TWO*V2(IP,JP)+V2(IP,JPP))*RDY
C
      RDXY=QUART/(DX*DY)
      D2PXY=(PSI2(IPP,JPP)-PSI2(IPM,JPP)-PSI2(IPP,JPM)
     1   +PSI2(IPM,JPM))*RDXY
      D2UXY=(U2(IPP,JPP)-U2(IPM,JPP)-U2(IPP,JPM)+U2(IPM,JPM))*RDXY
      D2VXY=(V2(IPP,JPP)-V2(IPM,JPP)-V2(IPP,JPM)+V2(IPM,JPM))*RDXY
C
C        CALCULATE INTERPOLATED VALUES OF PSI2, U2, AND V2
C
      PHSQ=HALF*PH*PH
```

```
      PKSQ=HALF*PK*PK
      PHPK=PH*PK
C
      PSI2N(N)=PSI2(IP,JP)+PH*DPX+PK*DPY+PHSQ*D2PX+PHPK*D2PXY
     1    +PKSQ*D2PY
      U2N(N)=U2(IP,JP)+PH*DUX+PK*DUY+PHSQ*D2UX+PHPK*D2UXY+PKSQ*D2UY
      V2N(N)=V2(IP,JP)+PH*DVX+PK*DVY+PHSQ*D2VX+PHPK*D2VXY+PKSQ*D2VY
C
      GO TO 900
C
C        INTERPOLATION FOR INTERFACE POINT LYING ON THE BOUNDARY
C
C             LOWER BOUNDARY
C
  500 CONTINUE
      DO 550 I=1,IMX
      DELX1=XO(N)-X(I)
      IF(DELX1 .LT. ZERO) GO TO 560
  550 CONTINUE
  560 CONTINUE
C
      DELX1=-DELX1
      DELX2=XO(N)-X(I-1)
      IM=I-1
C
      PSI2N(N)=(DELX1*PSI2(IM,1)+DELX2*PSI2(I,1))/DX
      U2N(N)=(DELX1*U2(IM,1)+DELX2*U2(I,1))/DX
      V2N(N)=(DELX1*V2(IM,1)+DELX2*V2(I,1))/DX
C
      GO TO 900
C
C             UPPER BOUNDARY
C
  600 CONTINUE
      DO 650 I=1,IMX
      DELX1=XO(N)-X(I)
      IF(DELX1 .LT. ZERO) GO TO 660
  650 CONTINUE
  660 CONTINUE
C
      DELX1=-DELX1
      DELX2=XO(N)-X(I-1)
      IM=I-1
C
      PSI2N(N)=(DELX1*PSI2(IM,JMX)+DELX2*PSI2(I,JMX))/DX
      U2N(N)=(DELX1*U2(IM,JMX)+DELX2*U2(I,JMX))/DX
      V2N(N)=(DELX1*V2(IM,JMX)+DELX2*V2(I,JMX))/DX
C
```

```
      GO TO 900
C
C           LEFT BOUNDARY
C
  700 CONTINUE
      DO 750 J=1,JMX
      DELY1=YO(N)-Y(J)
      IF(DELY1 .LT. ZERO) GO TO 760
  750 CONTINUE
  760 CONTINUE
C
      DELY1=-DELY1
      DELY2=YO(N)-Y(J-1)
      JM=J-1
C
      PSI2N(N)=(DELY1*PSI2(1,JM)+DELY2*PSI2(1,J))/DY
      U2N(N)=(DELY1*U2(1,JM)+DELY2*U2(1,J))/DY
      V2N(N)=(DELY1*V2(1,JM)+DELY2*V2(1,J))/DY
C
      GO TO 900
C
C           RIGHT BOUNDARY
C
  800 CONTINUE
      DO 850 J=1,JMX
      DELY1=YO(N)-Y(J)
      IF(DELY1 .LT. ZERO) GO TO 860
  850 CONTINUE
  860 CONTINUE
C
      DELY1=-DELY1
      DELY2=YO(N)-Y(J-1)
      JM=J-1
C
      PSI2N(N)=(DELY1*PSI2(IMX,JM)+DELY2*PSI2(IMX,J))/DY
      U2N(N)=(DELY1*U2(IMX,JM)+DELY2*U2(IMX,J))/DY
      V2N(N)=(DELY1*V2(IMX,JM)+DELY2*V2(IMX,J))/DY
C
  900 CONTINUE
C
      RETURN
      END
      SUBROUTINE LINFIT
C     ********************************
C
C        LINFIT PROVIDES AN INTERFACE FIT ACCORDING
C     TO THE MODIFIED LINE SEGMENT SCHEME.
C
```

```
C          INPUT DATA **
C       XO(N), YO(N) -- COORDINATES OF THE INTERFACE POINTS
C       NMAX         -- TOTAL NUMBER OF INTERFACE POINTS,
C             LESS THAN OR EQUAL TO 50
C       PROPC        -- PROPORTIONALITY CONSTANT FOR DETER-
C             MINING DELTA FROM CURVATURE OF INTERFACE.
C
C          OUTPUT DATA **
C       X1(N), Y1(N) -- COORDINATES OF LEFT ENDPOINT OF TAN-
C             GENT LINE SEGMENT AT XO(N), YO(N)
C       X2(N), Y2(N) -- COORDINATES OF RIGHT ENDPOINT OF TAN-
C             GENT LINE SEGMENT AT XO(N), YO(N)
C       SLOPE(N)     -- SLOPE OF TANGENT LINE SEGMENT AT
C             XO(N), YO(N)
C       SLOPEC(N)    -- SLOPE OF LINE SEGMENT CONNECTING
C             POINTS X2(N), Y2(N) AND X1(N+1), Y1(N+1)
C       DELTA -- HALF-LENGTH OF TANGENT LINE SEGMENT
C             AT INTERFACE POINT XO(N), YO(N)
C
C          OTHER VARIABLES **
C             INTRODUCED TO SIMPLIFY CALCULATIONS
C       AH(N)=XO(N+1)-XO(N)
C       AK(N)=YO(N+1)-YO(N)
C       NM1=NMAX-1
C       NM2=NMAX-2
C       R(N) -- SQUARE ROOT OF ONE PLUS SLOPE(N) SQUARED,
C       RN1=DELTA/R(N)
C       RN2=SLOPE(N)*RN1
C       RECR -- RECIPROCAL OF R(N)
C       RECR1 -- RECIPROCAL OF R(N+1)
C
C
      COMMON
     1    IMX,JMX,NMAX,KMAX,K,IMAX,JMAX,NREAD,NPRINT,NOUT,NCYC,
     2    ZERO,ONE,TWO,THREE,FOUR,HALF,QUART,PI,
     3    PERM,GAM1,GAM2,VIS,CBND,XIN,DX,DY,RMAX,OMEGA,EPS,TIME,DT,TSTOP,
     4    PROPC,AREAIN,AREA,ABSERR,RELERR,
     5    XO(99),YO(99),X1(99),Y1(99),X2(99),Y2(99),
     6    SLOPE(99),SLOPEC(99),PSI1N(99),VX(99),VY(99),
     7    PSI2N(99),U2N(99),V2N(99),X(40),Y(20),
     8    PSI1(40,20),U(40,20),V(40,20),PSI2(40,20),U2(40,20),V2(40,20)
      DIMENSION AH(50), AK(50), R(50), DELTA(50)
      NM1=NMAX-1
      NMX3=3*NMAX
C
C          SET MINIMUM AND MAXIMUM VALUES FOR DELTA
C
      DELMIN=0.01
```

```
      DELMAX=0.01
C
C        CALCULATE INCREMENTS OF X AND Y
C
      DO 10 N=1,NM1
      AH(N)=XO(N+1)-XO(N)
      AK(N)=YO(N+1)-YO(N)
   10 CONTINUE
      DO 50 N=2,NM1
C
C        CALCULATE SLOPE OF LEFT LINE SEGMENT AT
C     INTERFACE POINT
C
      NM=N-1
      IF(AH(NM) .NE. ZERO) GO TO 20
      T1=.5*PI
      GO TO 25
   20 CONTINUE
      SIGMIN=AK(NM)/AH(NM)
      T1= ATAN(SIGMIN)
      IF(T1 .LT. ZERO) T1=PI+T1
   25 CONTINUE
C
C        CALCULATE SLOPE OF RIGHT LINE SEGMENT AT
C     INTERFACE POINT
C
      IF(AH(N) .NE. ZERO)GO TO 30
      T2=.5*PI
      GO TO 35
   30 CONTINUE
      SIGPL=AK(N)/AH(N)
      T2= ATAN(SIGPL)
      IF(T2 .LT. ZERO) T2=PI+T2
   35 CONTINUE
C
C        CALCULATE SLOPE AND HALF-LENGTH DELTA
C     OF TANGENT LINE SEGMENT AT INTERFACE
C     POINT N
C
      SLOPE(N)= TAN(HALF*(T1+T2))
      DELTA(N)=TWO*PROPC/(SIGMIN+SIGPL)
      IF(DELTA(N) .GT. DELMAX) DELTA(N)=DELMAX
      IF(DELTA(N) .LT. DELMIN) DELTA(N)=DELMIN
   50 CONTINUE
C
C        CALCULATE SLOPE AND DELTA AT INTERFACE
C     END POINTS
C
```

```
      SLOPE(1)=ZERO
      DELTA(1)=DELTA(2)
      SLOPE(NMAX)=ZERO
      DELTA(NMAX)=DELTA(NM1)
      DO 65 N=1,NMAX
      R(N)= SQRT(ONE+SLOPE(N)*SLOPE(N))
   65 CONTINUE
      DO 70 N=2,NM1
  101 CONTINUE
C
C        CALCULATE COORDINATES OF END POINTS
C     OF EACH TANGENT LINE SEGMENT
C
      RN1=DELTA(N)/R(N)
      RN2=SLOPE(N)*RN1
      X1(N)=XO(N)-RN1
      Y1(N)=YO(N)-RN2
      X2(N)=XO(N)+RN1
      Y2(N)=YO(N)+RN2
      IF(SLOPE(N) .GE. ZERO) GO TO 102
      T1=X1(N)
      T2=Y1(N)
      X1(N)=X2(N)
      Y1(N)=Y2(N)
      X2(N)=T1
      Y2(N)=T2
  102 CONTINUE
C
C        CHECK IF EITHER END POINT OF TANGENT LINE
C     SEGMENT COINCIDES WITH A MESH POINT.  IF SO,
C     DELTA=0.9*DELTA.
C
      DO 120 I=1,IMX
      IF(X1(N) .NE. X(I)) GO TO 120
      DO 110 J=1,JMX
      IF(Y1(N) .NE. Y(J)) GO TO 110
      DELTA(N)=0.9*DELTA(N)
      GO TO 101
  110 CONTINUE
  120 CONTINUE
      DO 140 I=1,IMX
      IF(X2(N) .NE. X(I)) GO TO 140
      DO 130 J=1,JMX
      IF(Y2(N) .NE. Y(J)) GO TO 130
      DELTA(N)=0.9*DELTA(N)
      GO TO 101
  130 CONTINUE
  140 CONTINUE
```

```
   70 CONTINUE
   71 CONTINUE
      X2(1)=XO(1)+DELTA(1)
      Y2(1)=YO(1)
      DO 74 I=1,IMX
      IF(X2(1) .NE. X(I)) GO TO 74
      DO 72 J=1,JMX
      IF(Y2(1) .NE. Y(J)) GO TO 72
      DELTA(1)=0.9*DELTA(1)
      GO TO 71
   72 CONTINUE
   74 CONTINUE
   75 CONTINUE
      X1(NMAX)=XO(NMAX)-DELTA(NMAX)
      Y1(NMAX)=YO(NMAX)
      DO 78 I=1,IMX
      IF(X1(NMAX) .NE. X(I)) GO TO 78
      DO 76 J=1,JMX
      IF(Y1(NMAX) .NE. Y(J)) GO TO 76
      DELTA(NMAX)=0.9*DELTA(NMAX)
      GO TO 75
   76 CONTINUE
   78 CONTINUE
C
C        CALCULATE SLOPES OF CONNECTING LINE
C     SEGMENTS
C
      DO 80 N=1,NM1
      SLOPEC(N)=(Y1(N+1)-Y2(N))/(X1(N+1)-X2(N))
   80 CONTINUE
      TYN=TWO*YO(NMAX)
      TY1=TWO*YO(1)
      NMX2=NMAX+5
C
C        CALCULATE INTERFACE POINTS AND END POINTS
C     OF TANGENT LINE SEGMENTS FOR IMAGE INTERFACES
C
      DO 200 N=1,5
      N2=NMAX+N
      N2R=NMAX-N+1
      XO(N2)=XO(N2R)
      YO(N2)=TYN-YO(N2R)
      X1(N2)=X2(N2R)
      Y1(N2)=TYN-Y2(N2R)
      X2(N2)=X1(N2R)
      Y2(N2)=TYN-Y1(N2R)
      N3=NMX2+N
      XO(N3)=XO(N)
```

```
      Y0(N3)=TY1-Y0(N)
      X1(N3)=X1(N)
      Y1(N3)=TY1-Y1(N)
      X2(N3)=X2(N)
      Y2(N3)=TY1-Y2(N)
  200 CONTINUE
C
C        CALCULATE SLOPES OF LINE SEGMENTS ALONG
C     IMAGE INTERFACES
C
      NL=NMAX+2
      NU=NMAX+5
      DO 300 N=NL,NU
      SLOPE(N)=(Y2(N)-Y1(N))/(X2(N)-X1(N))
  300 CONTINUE
      SLOPE(NMAX+1)=ZERO
      NL=NMAX+7
      NU=NMAX+10
      DO 350 N=NL,NU
      SLOPE(N)=(Y2(N)-Y1(N))/(X2(N)-X1(N))
  350 CONTINUE
      SLOPE(NMAX+6)=ZERO
      NL=NMAX+1
      NU=NMAX+4
      DO 450 N=NL,NU
      SLOPEC(N)=(Y1(N+1)-Y2(N))/(X1(N+1)-X2(N))
  450 CONTINUE
      NL=NMAX+6
      NU=NMAX+9
      DO 500 N=NL,NU
      SLOPEC(N)=(Y1(N+1)-Y2(N))/(X1(N+1)-X2(N))
  500 CONTINUE
      RETURN
      END
      SUBROUTINE MASCON
C     **********************************
C
C        MASCON PROVIDES A CALCULATION OF THE DEGREE OF MASS
C     CONSERVATION MAINTAINED BY THE CODE.
C
C        MASCON IS PROBLEM-DEPENDENT.  THE FOLLOWING ROUTINE
C     IS VALID ONLY FOR THE BASIC CHECK PROBLEM.
C
C        INPUT DATA **
C     X0(N), Y0(N) -- COORDINATES OF INTERFACE POINTS
C     X1(N), Y1(N) -- COORDINATES OF LEFT ENDPOINT OF TANGENT
C           LINE SEGMENT
C     X2(N), Y2(N) -- COORDINATES OF RIGHT ENDPOINT OF TAN-
```

```
C            GENT LINE SEGMENT
C     NMAX -- TOTAL NUMBER OF INTERFACE POINTS
C     CBND -- HALF-WIDTH OF BASIC CHECK PROBLEM
C     SLOPE(N) -- SLOPE OF NTH TANGENT LINE SEGMENT
C     SLOPEC(N) -- SLOPE OF NTH CONNECTING LINE SEGMENT
C
C        OUTPUT DATA **
C     AREAIN -- INITIAL SALT-WATER AREA
C     AREA -- SALT-WATER AREA AT ANY LATER TIME
C     ABSERR -- ABSOLUTE ERROR, AREAIN-AREA
C     RELERR -- RELATIVE AREA, (AREAIN-AREA)/AREAIN
C
      COMMON
     1    IMX,JMX,NMAX,KMAX,K,IMAX,JMAX,NREAD,NPRINT,NOUT,NCYC,
     2    ZERO,ONE,TWO,THREE,FOUR,HALF,QUART,PI,
     3    PERM,GAM1,GAM2,VIS,CBND,XIN,DX,DY,RMAX,OMEGA,EPS,TIME,DT,TSTOP,
     4    PROPC,AREAIN,AREA,ABSERR,RELERR,
     5    XO(99),YO(99),X1(99),Y1(99),X2(99),Y2(99),
     6    SLOPE(99),SLOPEC(99),PSI1N(99),VX(99),VY(99),
     7    PSI2N(99),U2N(99),V2N(99),X(40),Y(20),
     8    PSI1(40,20),U(40,20),V(40,20),PSI2(40,20),U2(40,20),V2(40,20)
C
      NM1=NMAX-1
      SUM=ZERO
      DO 50 N=1,NM1
      TERM=(XO(N+1)-XO(N))*(HALF*(YO(N+1)+YO(N))-YO(1))
      SUM=SUM+TERM
   50 CONTINUE
      AREAIN=TWO*CBND*X(IMX)
      AREA=SUM+TWO*CBND*(X(IMX)-XO(NMAX))
      ABSERR=AREAIN-AREA
      RELERR=ABSERR/AREAIN
      RETURN
      END
      SUBROUTINE RITE
C     **********************************
C
C        RITE EFFECTS OUTPUT OF TIME, CYCLE NUMBER, INTERFACE
C     POINT COORDINATES, PSI, QX, AND QY, ITERATION CONVERGENCE
C     DATA, AND MASS CONSERVATION DATA.
C
      COMMON
     1    IMX,JMX,NMAX,KMAX,K,IMAX,JMAX,NREAD,NPRINT,NOUT,NCYC,
     2    ZERO,ONE,TWO,THREE,FOUR,HALF,QUART,PI,
     3    PERM,GAM1,GAM2,VIS,CBND,XIN,DX,DY,RMAX,OMEGA,EPS,TIME,DT,TSTOP,
     4    PROPC,AREAIN,AREA,ABSERR,RELERR,
     5    XO(99),YO(99),X1(99),Y1(99),X2(99),Y2(99),
     6    SLOPE(99),SLOPEC(99),PSI1N(99),VX(99),VY(99),
```

```
     7   PSI2N(99),U2N(99),V2N(99),X(40),Y(20),
     8   PSI1(40,20),U(40,20),V(40,20),PSI2(40,20),U2(40,20),V2(40,20)
C
    5 FORMAT(1H1,///////)
      WRITE(NPRINT,10) TIME, NCYC
   10 FORMAT(1H1,////////,20X,7HTIME = ,F10.4,9H  NCYC = ,I5)
C
      NMX2=NMAX*2
      NMX3=3*NMAX
      DO 20 N=1,NMAX
      WRITE(NPRINT,15) XO(N), YO(N)
   15 FORMAT(10X,2(F10.4,2X))
   20 CONTINUE
C
      WRITE(NPRINT,5)
      N1=NMAX+1
      DO 21 N=N1,NMX2
   21 WRITE(NPRINT,15) XO(N), YO(N)
      WRITE(NPRINT,5)
      N1=NMX2+1
      DO 22 N=N1,NMX3
   22 WRITE(NPRINT,15) XO(N), YO(N)
      WRITE(NPRINT,5)
      DO 30 N=1,NMAX
      WRITE(NPRINT,25) PSI1N(N), VX(N), VY(N)
   25 FORMAT(10X, 3(F10.4,2X))
   30 CONTINUE
      WRITE(NPRINT,5)
C
      DO 40 J=1,JMX
      WRITE(NPRINT,35) (PSI1(I,J), I=1,IMX)
   35 FORMAT(25X,7(F10.4,1X)/(F30.4,6(1X,F10.4)))
   40 CONTINUE
      WRITE(NPRINT,5)
C
      DO 50 J=1,JMX
      WRITE(NPRINT,35) (U(I,J), I=1,IMX)
   50 CONTINUE
      WRITE(NPRINT,5)
C
      DO 60 J=1,JMX
      WRITE(NPRINT,35) (V(I,J), I=1,IMX)
   60 CONTINUE
      WRITE(NPRINT,5)
C
      WRITE(NPRINT,70) K,RMAX,IMAX,JMAX
   70 FORMAT(//10X,I5,12H  ITERATIONS,//15X,20HMAXIMUM RESIDUAL =   ,
     1    F10.4,7HAT I = ,I5,6H  J = ,I5)
```

```
C
      WRITE(NPRINT,80) AREAIN,AREA,ABSERR,RELERR
   80 FORMAT(//15X,15HINITIAL AREA = ,F10.4,9H  AREA = ,F10.4,
     1      //20X,17HABSOLUTE ERROR = ,E11.4,
     2      19H  RELATIVE ERROR = , E11.4)
C
      RETURN
      END
      SUBROUTINE PLOTIN
C     ***********************************
C
C        PLOTIN PROVIDES FOR PLOTTING OF THE
C     INTERFACE WITH A CALCOMP DIGITAL INCREMENTAL
C     DRUM PLOTTER.  THE ROUTINE PROVIDES FOR
C     PLOTTING OF STRAIGHT LINE SEGMENTS CONNECTING
C     ADJACENT INTERFACE POINTS, USING THE
C     STANDARD CALCOMP LINE SUBROUTINE.
C
      COMMON
     1    IMX,JMX,NMAX,KMAX,K,IMAX,JMAX,NREAD,NPRINT,NOUT,NCYC,
     2    ZERO,ONE,TWO,THREE,FOUR,HALF,QUART,PI,
     3    PERM,GAM1,GAM2,VIS,CBND,XIN,DX,DY,RMAX,OMEGA,EPS,TIME,DT,TSTOP,
     4    PROPC,AREAIN,AREA,ABSERR,RELERR,
     5    X0(99),Y0(99),X1(99),Y1(99),X2(99),Y2(99),
     6    SLOPE(99),SLOPEC(99),PSI1N(99),VX(99),VY(99),
     7    PSI2N(99),U2N(99),V2N(99),X(40),Y(20),
     8    PSI1(40,20),U(40,20),V(40,20),PSI2(40,20),U2(40,20),V2(40,20)
      DIMENSION XPLOT(100), YPLOT(100)
      DO 100 N=1,NMAX
      XPLOT(N)=X0(N)
      YPLOT(N)=Y0(N)
  100 CONTINUE
      XPLOT(NMAX+1)=-15.75
      XPLOT(NMAX+2)=1.575
      YPLOT(NMAX+1)=-7.5
      YPLOT(NMAX+2)=1.5
      JSYM=11
      CALL LINE(XPLOT,YPLOT,NMAX,1,1,JSYM)
      RETURN
      END
```

This dissertation is accepted on behalf of the faculty of the Institute by the following committee:

Gerard-Wolfgang Groß
Adviser

Frank W. Tuttle

Merle E. Hanson

May 7, 1973
Date